OPTICAL SCIENCE CONSULTANTS
P.O. Box 388, Yorba Linda, California 92686 ■ Phone: (714) 524-3622

Report No. DR-041

ANALYSIS OF APERTURE AVERAGING MEASUREMENTS

David L. Fried
Optical Science Consultants
P. O. Box 388
Yorba Linda, California 92686

March 1975

Final Report, 2 June 1974 - 2 March 1975

Prepared for

GODDARD SPACE FLIGHT CENTER
Greenbelt, Maryland 20771

1. Report No.	2. Government Accession No.	3. Recipient's Catalog No.

4. Title and Subtitle	5. Report Date
ANALYSIS OF APERTURE AVERAGING MEASUREMENTS	March 1975
	6. Performing Organization Code
7. Author(s) David L. Fried	8. Performing Organization Report No. DR-041
9. Performing Organization Name and Address Optical Science Consultants P. O. Box 388 Yorba Linda, California 92686	10. Work Unit No.
	11. Contract or Grant No. NAS5-20537
12. Sponsoring Agency Name and Address Goddard Space Flight Center Greenbelt, Maryland 20771 Technical Monitor - Jack L. Bufton	13. Type of Report and Period Covered Final Report 2 June 74 - 2 March 75
	14. Sponsoring Agency Code

15. Supplementary Notes

16. Abstract

This report is concerned with the analysis of laser scintillation data obtained by the NASA Goddard Space Flight Center balloon flight #5 from White Sands Missile Range on 19 October 1973. The principal objective of the analysis in this report is to relate the measurement data, taken with various size receiver apertures, to predictions of aperture averaging theory. On the basis of this study, it is concluded that the data is in reasonable agreement with theory. The following parameters are assigned to the vertical distribution of the strength of turbulence during the period of the measurements (daytime), for $\lambda = 0.633\ \mu m$, and the source at the zenith; the aperture averaging length is $d_0 = 0.125$ m, and the log-amplitude variance is $\sigma_\ell^2 = 0.084$ nepers^2. This corresponds to a normalized point intensity variance of 0.40.

In the course of the work reported here, it has been necessary to extend the previous results on aperture averaging to account for the effect of a central obscuration. This is presented in App. A.

17. Key Words (Selected by Author(s))	18. Distribution Statement
Aperture Averaging, Scintillation, Turbulence, Laser Communications.	

19. Security Classif. (of this report)	20. Security Classif. (of this page)	21. No. of Pages	22. Price*
Unclassified	Unclassified	127	

ABSTRACT

This report is concerned with the analysis of laser scintillation data obtained by the NASA Goddard Space Flight Center balloon flight #5 from White Sands Missile Range on 19 October 1973. The principal objective of the analysis in this report is to relate the measurement data, taken with various size receiver apertures, to predictions of aperture averaging theory. On the basis of this study, it is concluded that the data is in reasonable agreement with theory. The following parameters are assigned to the vertical distribution of the strength of turbulence during the period of the measurements (daytime), for $\lambda = 0.633$ μm , and the source at the zenith; the aperture averaging length, is $d_o = 0.125$ m , and the log-amplitude variance is $\sigma_\ell^2 = 0.084$ nepers^2 . This corresponds to a normalized point intensity variance of 0.40 .

In the course of the work reported here, it has been necessary to extend the previous results on aperture averaging to account for the effect of a central obscuration. This work is presented in Appendix A .

CONTENTS

LIST OF ILLUSTRATIONS

LIST OF TABLES

1. Introduction

It is well known that atmospheric turbulence will cause the strength of an optical signal to fluctuate. The reliability of an optical communications channel will be influenced by such signal fluctuation -- the fades producing more disadvantages than will be compensated by the anomalous signal enhancements. For a small diameter receiver, operating in the visible, the signal fluctuations can be very significant. Fortunately, if a large diameter receiver is used, not only is a greater average signal power collected, but also the relative magnitude of the signal fluctuations is reduced. This effect is referred to as aperture averaging. In the recent past, NASA-Goddard Space Flight Center has conducted experimental work in this area,[1] and Optical Science Consultants, under funding from NASA-Goddard Space Flight Center, has carried out theoretical analysis of aperture averaging.[2] In this report, we shall be concerned with establishing a relationship between these two efforts, i. e., between theory and experimentation. The primary emphasis of the work we shall be reporting here will be on the experimental aspects of the program. First, however, we shall review the pertinent features of scintillation and aperture averaging theory.

1.1 Scintillation Theory

The basic theory associated with scintillation was originally developed by Tatarski[3,4] and has recently been reviewed by Lawrence and Strobher.[5] For the purposes of this report, we shall rely on these and a few other references, and here we shall only quote without derivation the most pertinent general aspects of scintillation theory.

We start by noting the ubiquity of the log-normal distribution in optical scintillation due to atmospheric turbulence. Tatarski appears to have been the first to predict that the logarithm of the amplitude of a scintillating wave would follow a normal distribution. He also presented

experimental evidence for this. The fact that the amplitude follows a log-normal distribution implies, of course, that the intensity also does so.

At one time, it was believed that the signal collected by a large aperture, being the sum of the almost independent random intensities at various points in the aperture, would have a normal distribution by virtue of the central limit theorem. However, it was observed[6] that such signals actually appeared to follow a log-normal distribution, and subsequently a theoretical explanation for this fact was obtained by Mitchel.[7] We presently expect that all turbulence-induced scintillation signals will be log-normally distributed, no matter how large the collector aperture -- and, in fact, there has been no serious experimental evidence to the contrary.

The log-normal distribution for signal strength, S (i.e., optical power) is characterized by three parameters. These are $\overline{S}$, the mean signal power, $\overline{L}$, the mean value of the log-signal power, and σ_L^2, the variance of the log-amplitude. Here the instantaneous random signal power, S, is related to the instantaneous random log-signal power, L, by the equation

$$S = \overline{S} \exp (L) \quad . \tag{1}$$

Making use of the fact that the ensemble average of the exponential of a gaussian random variable, with zero mean, is equal to the exponential of one-half the variance, i.e.,

$$\langle \exp (x) \rangle = \exp \left(\tfrac{1}{2} \langle x^2 \rangle \right) \quad , \tag{2}$$

where x is a gaussian random variable with zero mean, it follows that

$$\overline{L} = - \tfrac{1}{2} \sigma_L^2 \quad . \tag{3}$$

Obviously, then, there are really only two independent parameters characterizing the log-normally distributed signal power, namely, $\overline{S}$ and σ_L^2 . It can be shown from Eq.'s (2) and (3) that the signal power variance, σ_S^2 , can be written as

$$\sigma_S^2 = \overline{S}^2 [\exp(\sigma_L^2) - 1] \quad , \tag{4}$$

and inversely that

$$\sigma_L^2 = \ell n \left(\frac{\sigma_S^2}{\overline{S}^2} + 1 \right) \quad . \tag{5}$$

The extent of the scintillation fluctuations is governed by the variance of the logarithm of the signal power. For a very small aperture collector (which in essence is making measurements of the optical power density at a point), the logarithm of the signal power, L , can be related to the logarithm of the field amplitude as

$$L = 2\ell \quad , \tag{6}$$

so that the log-amplitude variance, σ_ℓ^2 , can be written as

$$\sigma_\ell^2 = \tfrac{1}{4} \sigma_L^2 \quad . \tag{7}$$

Analysis of optical propagation through turbulence has established that the log-amplitude variance can be written as

$$\sigma_\ell^2 = 0.56\, k^{7/6} \int_{\text{Path}} ds\, C_N^2\, Q_1(s, L)\, (L-s)^{5/6} \quad , \tag{8}$$

where the integration is over the propagation path, with s running from 0 at the source to L at the place where the optical power density is measured.

The refractive-index structure constant, C_N^2 , is allowed to vary along the propagation path in accordance with whatever geophysical considerations apply. The optical wave number is given by $k = 2\pi/\lambda$. According to whether the source is a point source or an infinite plane wave source, the value of Q_1 is

$$Q_1(s, L) = \begin{cases} 1 & , \text{ for an infinite plane wave source} \\ (s/L)^{5/6} & , \text{ for a point source} \end{cases} . \quad (9)$$

For propagation from some high altitude H to the ground, at a zenith angle θ (so that $H = L \cos\theta$) , Eq. (8) can be recast in the form

$$\sigma_\ell^2 = (\cos\theta)^{11/6} (\sigma_\ell^2)_{zenith} , \quad (10)$$

where

$$(\sigma_\ell^2)_{zenith} = 0.56\, k^{7/6} \int_0^H dh\, C_N^2\, Q_1(H-h, H)\, h^{5/6} . \quad (11)$$

The point we particularly wish to note here is that one can explicitly define a zenith viewing log-amplitude variance, $(\sigma_\ell^2)_{zenith}$, and that the log-amplitude variance for viewing at a zenith angle $\theta \neq 0$ is proportional to this variance and depends on the 11/6-power of the cosine of the zenith angle. Similarly, the variance of the logarithm of the signal power, σ_L^2 also depends on the 11/6-power of the cosine of the zenith angle. We can write

$$\sigma_L^2 = (\cos\theta)^{11/6} (\sigma_L^2)_{zenith} , \quad (12)$$

where

$$(\sigma_L^2)_{zenith} = 4\, (\sigma_\ell^2)_{zenith} . \quad (13)$$

1.2 Aperture Averaging

Because the signal power fluctuations measured at different points (at the same time) are not perfectly correlated, the fluctuation of the total signal power collected by a large receiver aperture will, in a percentage-wise sense, be less than that of the signal collected by a small aperture. The key point here is the distance in which the decorrelation becomes significant, and the nature of the decrease in correlation. These two matters will determine the degree of aperture averaging achieved by a given size aperture.

It is convenient to define aperture averaging in terms of the ratio of the normalized signal power variance for an aperture of diameter D to the normalized signal power variance for a very small aperture. Using the notation of a subscript zero to denote measurements with a very small aperture diameter, we note first of all that in accordance with Eq. (4)

$$(\sigma_s^2)_0 = \overline{S}_0^2 \{\exp[(\sigma_L^2)_0] - 1\} \quad . \tag{14}$$

The aperture averaging factor, $\circledH$, is explicitly defined by the relationship

$$\frac{\sigma_s^2}{\overline{S}^2} = \circledH \frac{(\sigma_s^2)_0}{\overline{S}_0^2} \quad . \tag{15}$$

At one time, it was thought[8] that for large aperture diameters the aperture averaging factor would be inversely proportional to the aperture area, i.e., to the number of independently scintillating regions that existed within the aperture. The correlation length (i.e., the distance in which the decorrelation becomes significant) would be a dimension characteristic of the size of each of these independently scintillating regions. More recently

it has been recognized[2,9] that the existence of long range negative correlation of scintillation forces a modification of this rather simple line of reasoning. (The existence of long-range negative correlation of scintillation is to be associated with the fact that turbulence does not destroy, i.e., absorb, optical power, but merely redistributes it. Optical energy that "disappears" in one region must show up somewhere else. Because of the nature of the turbulence scattering mechanism, some of this redistribution involves rather large displacements of the energy. Hence, the long-range negative correlation.) The current theory for aperture averaging predicts that the normalized variation of total signal power collected by a circular aperture of diameter D will vary as the 7/3-power of the diameter for large diameter apertures.

The constant of proportionality for this dependence, which we denote by d_o, has the dimensions of length, and has been shown[2] to be given by the expression

$$d_o = 2.399\, k^{-1/2} \left\{ \frac{\int_{\text{Path}} ds\, C_N^2\, Q_2(s, L)(L-s)^2}{\int_{\text{Path}} ds\, C_N^2\, Q_1(s, L)(L-s)^{5/6}} \right\}^{3/7} , \qquad (16)$$

where the symbols have the same meaning as in Eq. (8), with Q_1 as defined by Eq. (9). Q_2 is defined by the equation

$$Q_2(s, L) = \begin{cases} 1 & , \text{ for an infinite plane wave source,} \\ (s/L)^{-1/3} & , \text{ for a point source} \end{cases} . \qquad (17)$$

If we cast this result in terms values for viewing in the direction of the zenith rather than at a zenith angle θ, for a source at altitude H (where $H = L \cos \theta$), we get

$$d_o = (d_o)_{zenith} (\cos \theta)^{-1/2} \quad , \tag{18}$$

where $(d_o)_{zenith}$ is the value of d_o for zenith viewing. Its value is given by the expression

$$(d_o)_{zenith} = 2.399\, k^{-1/2} \left\{ \frac{\int_o^H dh\, C_N^2\, Q_2(H-h, H)\, h^2}{\int_o^H dh\, C_N^2\, Q_1(H-h, H)\, h^{5/6}} \right\}^{3/7} \quad . \tag{19}$$

With this expression for the length d_o, the aperture averaging factor, Θ, for a circular clear aperture of diameter D has been shown to be[2]

$$\Theta = [1 + (D/d_o)^{7/6} + (D/d_o)^{7/3}]^{-1} \quad . \tag{20}$$

If the aperture has a central obscuration of diameter d, then it is shown in Appendix A that the aperture averaging factor has the form

$$\tilde{\Theta} = \frac{D^2}{D^2 - d^2} \left\{ \frac{1}{\left[1 + \left(\frac{D}{d_o}\right)^{7/6} + \left(\frac{D}{d_o}\right)^{7/3}\right]} + \frac{d^2/D^2}{\left[1 + \left(\frac{d}{d_o}\right)^{7/6} + \left(\frac{d}{d_o}\right)^{7/3}\right]} \right\} \quad . \tag{21}$$

I. 3 Optical Communications Considerations

Analysis of the effect of log-normally distributed fluctuations of optical signal strength on the error rate of a photon detecting (i. e., photon counting) intensity receiver where the noise is the Poisson shot noise of the signal shows that a given log-intensity variance can be equated with an equivalent reduction in the average signal power, for a given bit-error-rate. In Fig. 1 we show representative results[10] for such losses as a function of the logarithm of the signal power variance. As can be seen, the effects

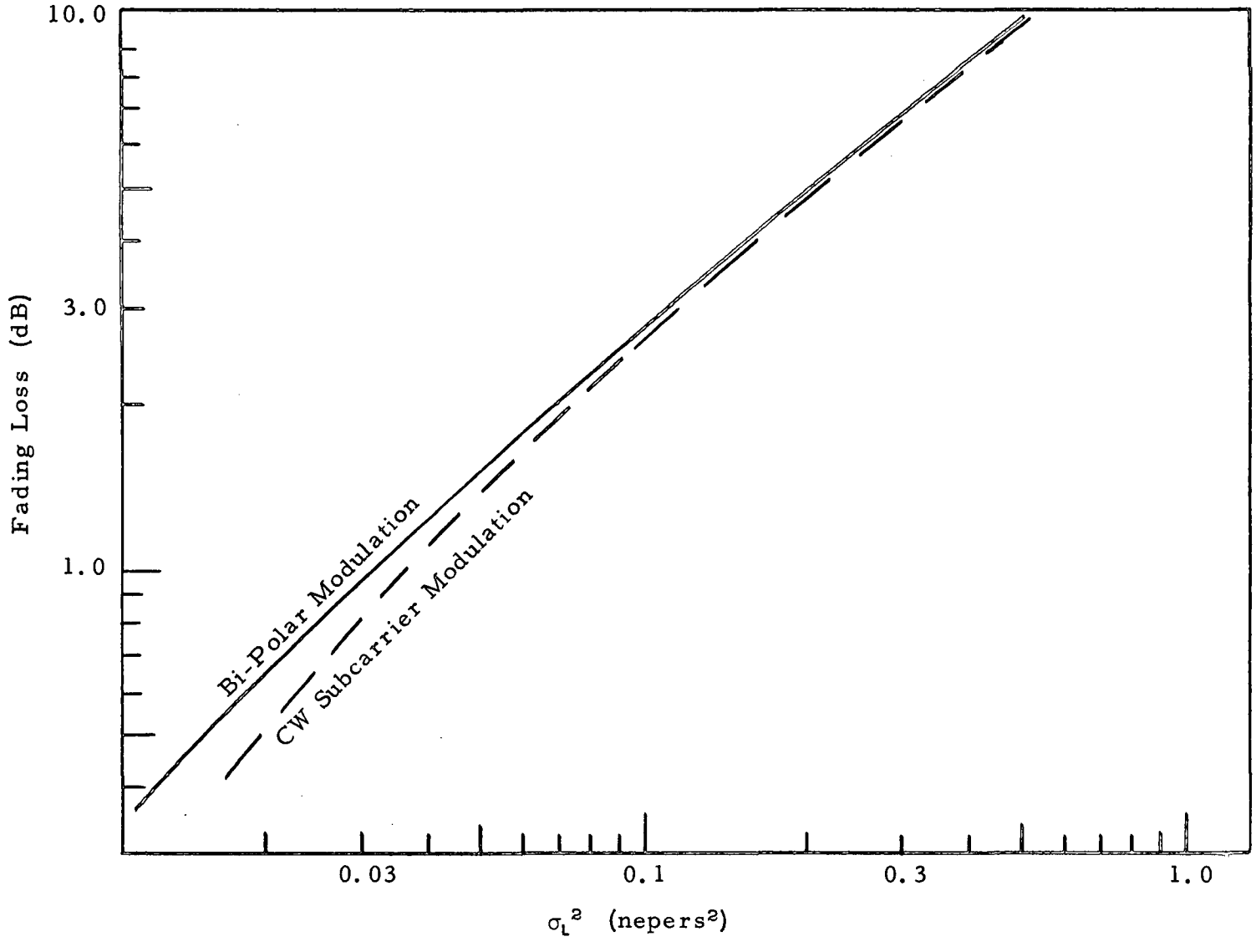

Figure 1. Fading Loss as a Function of Log-Signal Power Variance. Results shown are for log-normal fading for the two indicated types of modulation. Zero background level is assumed. The loss is calculated on the basis of the additional power required to maintain a bit error rate of $1:10^7$.

are potentially significant. It is in the context of such results as these that the matter of aperture averaging becomes significant, as a basis for reducing the signal fluctuations.

It is in relation to this sort of consideration that the NASA-Goddard Space Flight Center balloon flight laser scintillation measurement program described in Reference 1 has its significance. In this report, we are principally concerned with examining the experimental data obtained in that flight test program to obtain a check of the aperture averaging results presented above. In the next section, we shall review the general nature of the flight measurements. In the sections after that we shall examine the data in detail.

2. Flight Test Program - General Description

During October 1973, NASA-Goddard Space Flight Center personnel, supported by personnel from the Air Force Cambridge Research Laboratory, conducted a series of balloon flights at the U. S. Army White Sands Missile Range for the purpose of gathering data of atmospheric turbulence and its effect on laser beam propagation.[1] In this report, we shall be concerned with the analysis of optical scintillation data gathered on Flight #5. In particular, we shall be concerned with the down-link scintillation data, involving a He-Ne laser transmitter in the balloon and an adjustable aperture receiver on the ground. Data was gathered over a time span of about three (3) hours.

This flight for the purpose of gathering data on optical effects was supported by thermosonde balloon Flight #7 to provide data on the vertical distribution of turbulence during this time period. Unfortunately, because of unidentified problems presumed to be associated with solar heating of the thermosonde,* the measurements of the atmospheric turbulence

* Previous successful thermosonde measurements of C_N^2 were conducted during night time hours, so there was no problem of solar illumination heating of the micro-temperature sensors.

refractive-index structure constant, C_N^2 , appear to be unreliable. This C_N^2 data is examined in Appendix B. It has not seemed practical to attempt to directly relate it to the optical measurements which we shall be considering in the body of this report.

In this section, we shall describe the general nature of the experimental equipment and of data taken, as well as providing a description of the flight profile. Detailed examination of the measurement data, per se, will be deferred to subsequent sections.

2.1 Equipment Description

The basic electro-optical equipment utilized in generating the data we shall be considering here consists of two parts, the ground-based telescope receiver portion, and the balloon payload laser transmitter portion. In addition to the ability to perform their basic functions of reception and transmission, each unit had the ability to track the other unit, so that fairly narrow fields-of-view and transmitter beamwidths could be utilized. This required the ground-based receiver to also function as a transmitter, sending out a beacon signal to the balloon which the balloon unit could track.

The balloon payload transmitter utilized a 1.5 mW He-Ne laser operating at $\lambda = 633$ nm . The transmitted laser beam had a beam spread of 20 mrad, while the transmitter rms tracking jitter associated with its ability to track the laser beacon was of the order of 0.5 mrad . Using available theory for the statistics of laser beam fade induced by pointing jitter,[11] we see that if we consider the laser beam to have a gaussian intensity profile with a 10 mrad one-sigma spread, then the normalized rms fluctuations associated with the pointing jitter will only be

$$\text{RMS Jitter Scintillation} = \left[\int_0^\infty dI \left(\frac{I - I_o}{I_o} \right)^2 \text{Prob}\,(I) \right]^{1/2}$$

$$= \left[\int_0^\infty dI \left(\frac{I - I_o}{I_o} \right)^2 \mu\, (I/I_o)^\mu / I \right]^{1/2} , \qquad (21)$$

where μ is the ratio of the beam spread (10 mrad) to the rms pointing jitter (0.5 mrad) all squared, so $\mu = 400$. Evaluation of Eq. (21) yields

$$\text{RMS Jitter Scintillation} = [(1 + 2/\mu)^{-1} - 2(1 + 1/\mu)^{-1} + 1]^{1/2} \quad , \tag{22}$$

which for large values of μ is approximately given by

$$\text{RMS Jitter Scintillation} \approx (2\,\mu^{-2})^{1/2} \quad . \tag{23}$$

In this case, with $\mu = 400$, the rms scintillation due to transmitter pointing jitter will only be 0.353% , a clearly miniscule effect. Even if the rms jitter were ten times as large, i.e., 5 mrad , transmitter pointing jitter would only be 3.53% , still a minor quantity. We may therefore conclude that the laser transmitter was adequately stabilized so that it can be considered to be a stable source.

With the very large beam spread of $\pm$ 10 mrad, we may further conclude that the beam may adequately be characterized as a point source. This follows from consideration of the fact that atmospheric turbulence over the propagation path would not be expected to result, on the one hand, in any difference in the received average power at the receiver if additional laser power were added at the wings of the beam, and on the other hand, in any reduction in the average received power if energy were removed from near the wings of the transmitted beam.

The ground based laser receiver was a 0.76 m (i.e., 30 inch) diameter telescope with an optical detection apparatus with an intermediate focal plane that limited the receiver field-of-view to 0.5 mrad. Past the field stop, it was possible to insert various size iris diaphragms into the signal beam so as to in effect reduce the signal collection aperture to various sizes. It was possible to set the effective aperture size to

correspond to circular clear apertures of 0.04 m , 0.08 m , 0.16 m , and 0.32 m . In addition, the iris diaphragm could be set to correspond to a 0.64 m circular aperture or to a 0.76 m circular aperture, but each with a 0.20 m diameter concentric circular obscuration.

The received signals were detected by a photomultiplier and recorded for later data reduction. Data reduction was done by standard laboratory equipment and digital computer, with no special characteristics that need be mentioned here.

2.2 Balloon Flight Log

Balloon flight #5 was released at approximately 08:30 MST from the White Sands Missile Range on 19 October 1973. The balloon altitude and the zenith angle from the line-of-sight from the ground station to the balloon are shown in Fig. 2, together with an indication of the periods when the balloon-borne laser transmitter was operating. To provide a quick basis for calculation of the balloon altitude and the zenith angle of the line-of-sight at any time during the flight, we have made use of linear interpolation of the data listed in Table 1.

2.3 Data Run Log

During the course of flight #5, a set of 76 separate signal recording runs was carried out. All of these runs were connected with measurement of the scintillation of the 633 μm laser beam from the balloon-borne transmitter. The basic measurements were made with the ground-based receiver looking at the laser transmitter, but some of the data runs, called background runs, were made with the receiver pointed a small distance away from the laser transmitter so that data on only the background was recorded. Background runs were made close enough in time to the scintillation runs that a background run was available as a reference for almost all of the scintillation runs. The effective receiver aperture size setting was varied from

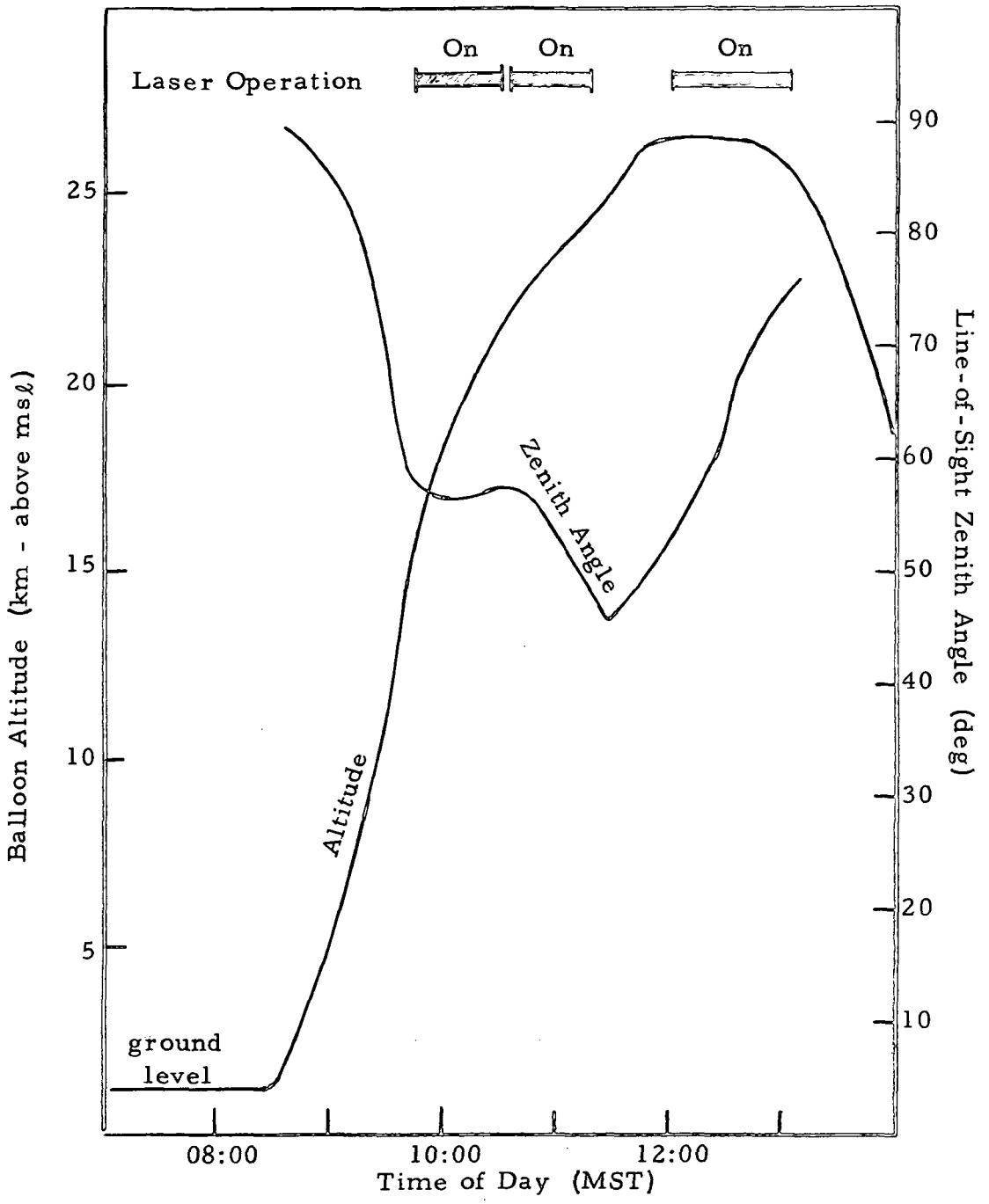

Figure 2. Flight Profile for Balloon Flight #5

Table 1

Balloon Flight Profile During Laser Operation

Time (MST)	Altitude (m)	Zenith Angle (deg)
10:00	18,245	56.56
10:15	20,045	56.57
10:30	21,580	57.19
10:45	22,615	56.78
11:00	23,465	53.13
11:15	24,150	49.34
11:30	25,070	45.52
11:45	26,080	48.66
12:00	26,420	52.72
12:15	26,455	56.21
12:30	26,420	62.39
12:45	26,325	69.70
13:00	25,790	74.24
13:15	24,910	76.87

run to run at the discretion of the experimenter, but the associated background run was always carried out with the same aperture setting. Moreover, in the analog-to-digital conversion process (which was used in conditioning all of the scintillation data we shall be considering) though the converter gain setting was varied in accordance with the average signal strength, the same gain setting was used for the analog-to-digital conversion of the associated background data run.

In Table 2, we provide a log of each of the data runs. The table indicates the time of the data run, the duration, the type of run (i.e., whether it was a scintillation run or a background run), the effective aperture diameter setting, and the background run number associated with each scintillation run. (We note that the central obscuration aperture settings, i.e., 0.76 m diameter with 0.20 m diameter obscuration, and the 0.64 m diameter with 0.20 m diameter central obscuration, are referred to merely as 0.76 diameter and 0.64 m diameter settings, respectively.) It will be seen from a study of the data in Table 2 that there was no applicable background run for certain of the scintillation runs. Because of the absence of this reference data, these runs could not be used in our data analysis.

By making use of the data in Table 1, we were able to obtain an altitude, zenith angle, and range to be associated with the start time of each data run listed in Table 2. In Table 3, we show the values of these quantities for each scintillation run for which we had a useable associated background run.

Table 2

Data Run Log

Data Run Number	Start Time (MST)	Duration (sec)	Type	Aperture Diameter (m)	Associated Background Run Number
1	10:01:58	20	Scint	0.76	7
2	10:03:05	15	Scint	0.76	7
3	10:08:28	22	Scint	0.08	6
4	10:11:10	20	Scint	0.04	5
5	10:11:45	10	Back	0.04	Self
6	10:12:30	10	Back	0.08	Self
7	10:13:40	10	Back	0.76	Self
8	10:14:15	15	Scint	0.76	7
9	10:15:20	15	Scint	0.76	7
10	10:16:30	20	Scint	0.76	7
11	10:19:32	15	Scint	0.64	None
12	10:21:30	16	Scint	0.08	15
13	10:22:12	20	Scint	0.08	15
14	10:24:54	18	Scint	0.08	15
15	10:25:30	20	Back	0.08	Self
16	10:28:45	20	Back	0.16	Self
17	10:29:25	15	Scint	0.16	16
18	10:46:30	20	Scint	0.16	73
19	10:31:00	30	Scint	0.16	21
20	10:31:49	27	Scint	0.16	21
21	10:32:30	18	Back	0.16	Self
22	10:43:00	16	Back	0.16	Self
23	10:47:05	25	Scint	0.16	22
24	10:48:08	24	Scint	0.16	22
25	10:49:30	10	Back	0.08	Self

Table 2 (Continued)

Data Run Number	Start Time (MST)	Duration (sec)	Type	Aperture Diameter (m)	Associated Background Run Number
26	10:52:28	30	Scint	0.08	None
27	10:53:40	24	Scint	0.04	28
28	10:54:30	12	Back	0.04	Self
29	10:59:10	20	Scint	0.76	36
30	10:59:55	25	Scint	0.76	36
31	11:01:58	14	Scint	0.32	32
32	11:03:05	10	Back	0.32	Self
33	11:04:14	12	Scint	0.32	34
34	11:04:45	10	Back	0.32	Self
35	11:05:10	10	Back	0.32	Self
36	11:06:00	24	Back	0.76	Self
37	12:02:00	19	Back	0.76	Self
38	12:04:14	10	Scint	0.76	37
39	12:05:26	08	Scint	0.76	74
40	12:08:20	07	Scint	0.32	None
41	12:09:05	12	Scint	0.32	None
42	12:11:38	05	Scint	0.16	43
43	12:14:50	10	Back	0.16	Self
44	12:22:10	10	Back	0.76	Self
45	12:25:00	10	Back	0.76	Self
46	12:26:32	21	Scint	0.76	45
47	12:27:50	25	Scint	0.76	45
48	12:30:20	40	Scint	0.32	50
49	12:31:00	50	Scint	0.32	50
50	12:32:20	10	Back	0.32	Self
51	12:32:55	15	Back	0.08	Self
52	12:33:50	40	Scint	0.08	51

Table 2 (Continued)

Data Run Number	Start Time (MST)	Duration (sec)	Type	Aperture Diameter (m)	Associated Background Run Number
53	12:35:25	30	Scint	0.16	55
54	12:37:05	40	Scint	0.16	55
55	12:38:05	17	Back	0.16	Self
56	12:39:00	15	Back	0.32	Self
57	12:39:45	20	Scint	0.32	56
58	12:40:26	16	Scint	0.32	56
59	12:42:40	32	Scint	0.76	60
60	12:44:30	05	Back	0.76	Self
61	12:45:06	30	Scint	0.76	60
62	12:47:00	30	Scint	0.76	63
63	12:50:10	10	Back	0.76	Self
64	12:51:30	30	Scint	0.76	65
65	12:53:00	20	Back	0.76	Self
66	12:55:10	60	Scint	0.76	68
67	12:56:55	60	Scint	0.76	68
68	12:58:40	15	Back	0.76	Self
69	12:59:10	60	Scint	0.76	68
70	13:02:15	45	Scint	0.76	68
71	13:06:25	35	Scint	0.76	72
72	13:07:40	40	Back	0.76	Self
73	10:44:00	16	Back	0.76	Self
74	12:22:10	10	Back	0.76	Self
75	12:59:10	50	Scint	0.76	72
76	13:02:15	58	Scint	0.76	72

Table 3

Flight Parameters for the Useable

Scintillation Data Runs

Run Number	Altitude (m)	Zenith Angle (deg)	Range (m)
1	18,481	56.56	33,538
2	18,615	56.56	33,782
3	19,261	56.57	34,958
4	19,585	56.57	35,547
8	19,955	56.57	36,221
9	20,079	56.58	36,460
10	20,199	56.63	36,724
12	20,710	56.84	37,861
13	20,782	56.87	38,022
14	21,058	56.98	38,643
17	21,520	57.17	39,690
18	22,700	56.41	41,036
19	21,649	57.16	39,924
20	21,705	57.14	40,004
23	22,733	56.27	40,943
24	22,793	56.02	40,778
27	23,106	54.67	39,957
29	23,418	53.33	39,215
30	23,460	53.15	39,119
31	23,555	52.63	38,810
33	23,658	52.06	38,479
38	26,430	53.70	44,649
39	26,433	53.98	44,953
42	26,447	55.42	46,606

Table 3 (Continued) Page 2

Run Number	Altitude (m)	Zenith Angle (deg)	Range (m)
46	26,428	60.96	54,446
47	26,425	61.50	55,375
48	26,418	62.55	57,313
49	26,414	62.88	57,938
52	26,398	64.26	60,775
53	26,386	65.03	62,503
54	26,375	65.84	64,446
57	26,358	67.14	67,854
58	26,354	67.47	68,791
59	26,340	68.56	72,069
61	26,321	69.73	75,976
62	26,254	70.30	77,902
64	26,093	71.67	82,958
66	25,962	72.78	87,684
67	25,900	73.31	90,166
69	25,820	73.99	93,603
70	25,658	74.63	96,831
71	25,414	75.36	100,584
75	25,820	73.99	93,603
76	25,658	74.63	96,831

3. Background Data Runs

A total of 25 background runs were carried out. For each of these runs, a 100-level probability density histogram, $p(x)$, was prepared. Using this, it was a straightforward matter to calculate the associated mean,

$$\bar{x} = \sum_i p(x_i)\, x_i \quad , \tag{24}$$

variance (or second central moment)

$$\sigma^2 = \sum_i p(x_i)\, (x_i - \bar{x})^2 \quad , \tag{25}$$

third central moment,

$$\mu_3 = \sum_i p(x_i)\, (x_i - \bar{x})^3 \quad , \tag{26}$$

and fourth central moment,

$$\mu_4 = \sum_i p(x_i)\, (x_i - \bar{x})^4 \quad . \tag{27}$$

In Table 4, we list each of these runs together with the four leading moments.

3.1 Expected Gaussian Distribution Moments

Based on the approximation that there are a very large number of background photoelectrons detected during each measurement interval, we can approximate the expected Poisson distribution of the photoelectron count by a gaussian distribution. This implies that the skewness and curtosis of the measured distribution should both vanish. We recall that

the skewness of a distribution is the ratio of the third moment to the three-halfs power of the variance, i.e.,

$$\gamma_{Sk} = \mu_3/(\sigma^2)^{3/2} \quad , \tag{28}$$

and the curtosis of a distribution is the ratio of the fourth central moment to the square of the second, minus three, i.e.,

$$\gamma_{Cur} = [\mu_4/(\sigma^2)^2 - 3] \quad . \tag{29}$$

In Table 5, we list the calculated skewness and curtosis of the 25 background data run distributions of Table 4. We see from a study of the data in Table 5 that only a very few of the background data runs have probability distributions whose skewness and curtosis appear to be in general agreement with the hypothesis that the distribution is gaussian.

3.2 Data Contamination and Reliability

The results shown by our study of the data in Table 5, as stated in the preceding paragraph, raise the concern that our background data runs may have been significantly contaminated by noise and/or that there may be some problem in the data channel (i.e., the photomultiplier, amplifier, recorder, digitizer, or other element) that might make our entire data set of questionable value. To make certain that this was not the case, we have plotted the cumulative probability distribution for each of these background data runs on normal distribution scale graphs.* These plots are shown in Fig.'s 3 to 27.

---

* On such a graph, the cumulative probability distribution for a gaussian random function will plot as a straight line.

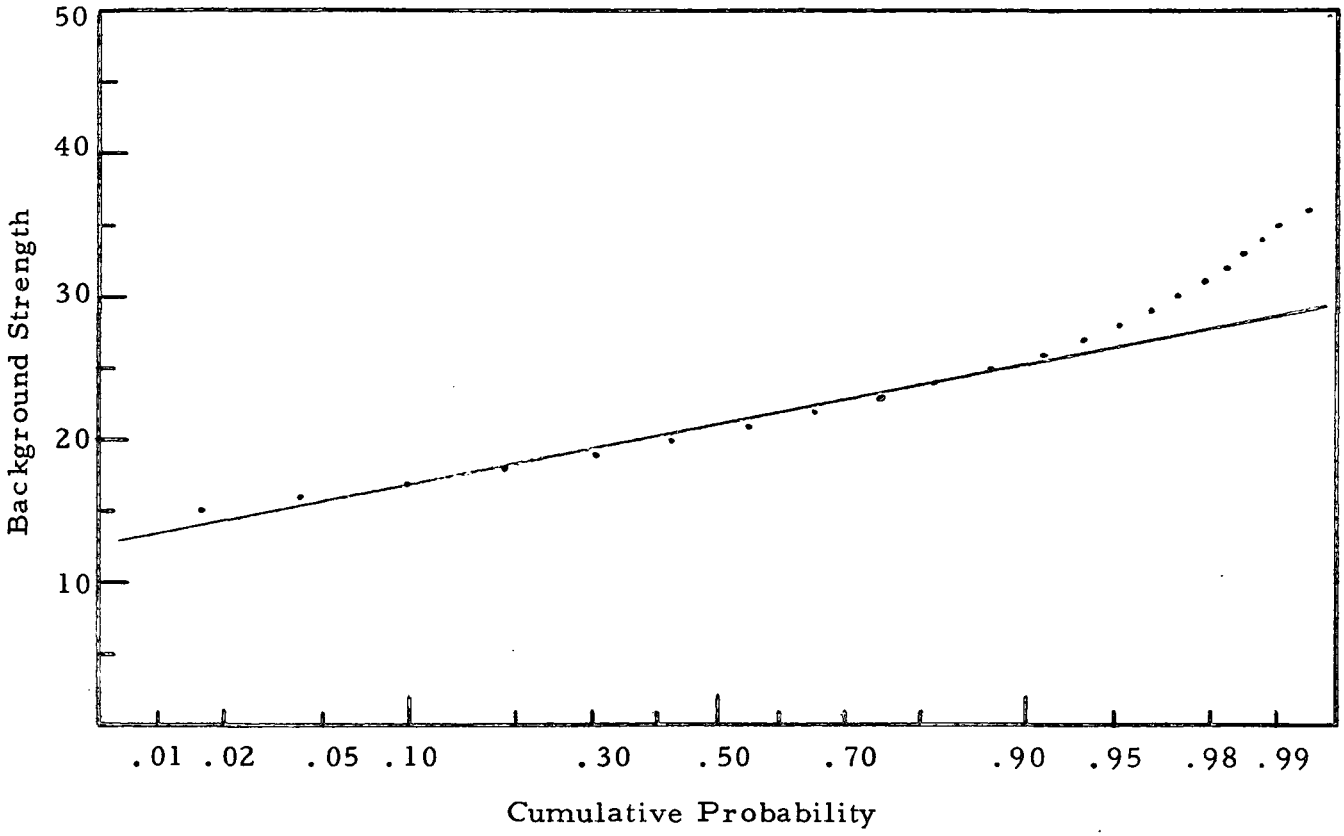

Figure 3. Background Probability Distribution for Run #5

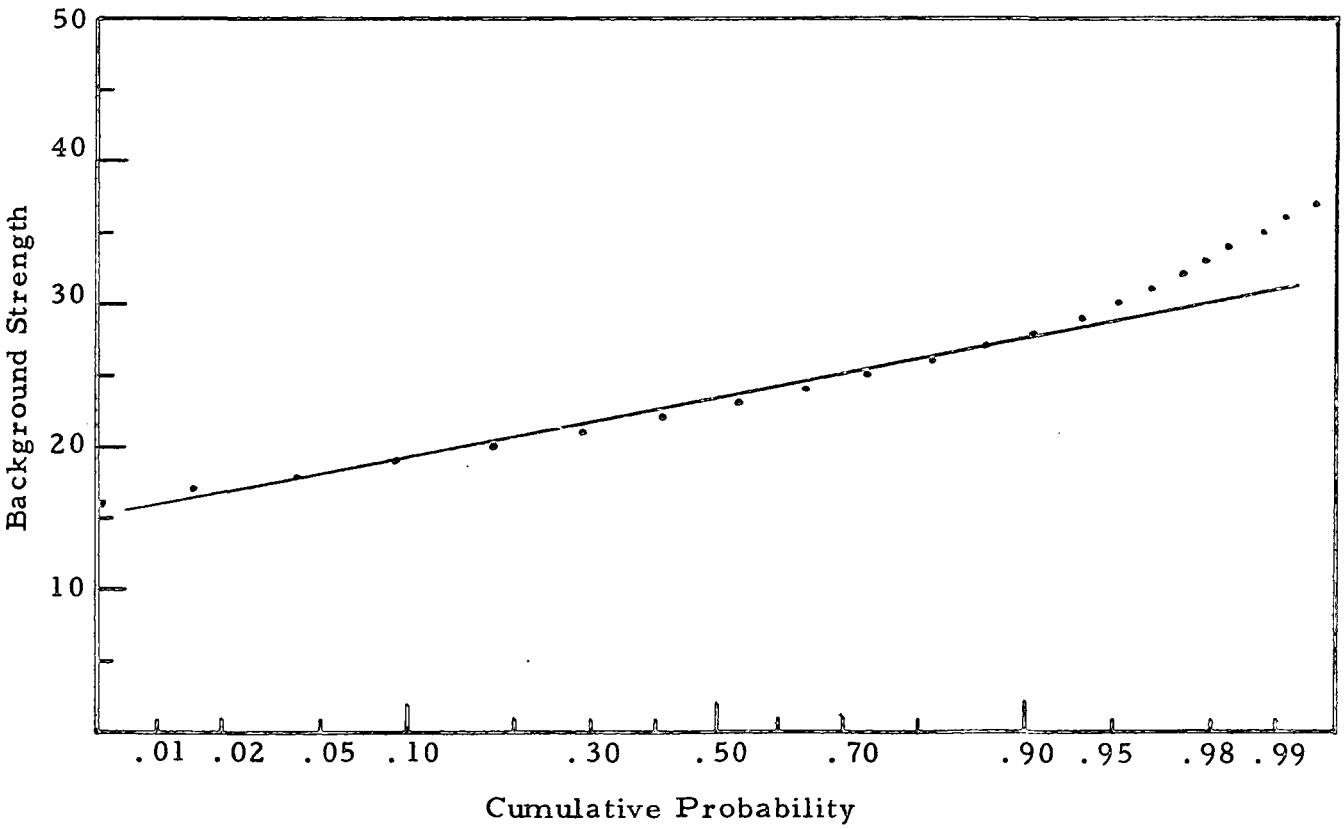

Figure 4. Background Probability Distribution for Run #6

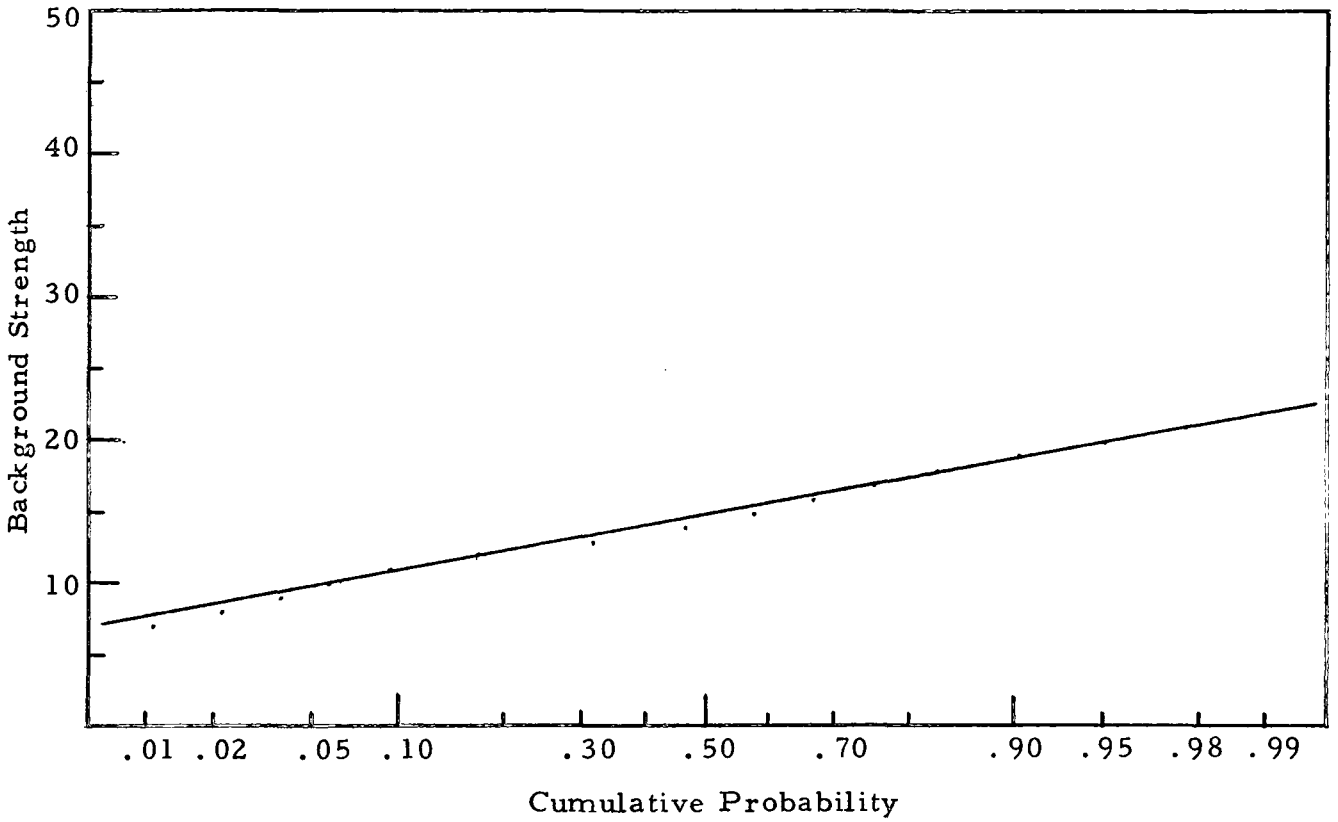

Figure 5. Background Probability Distribution for Run #7

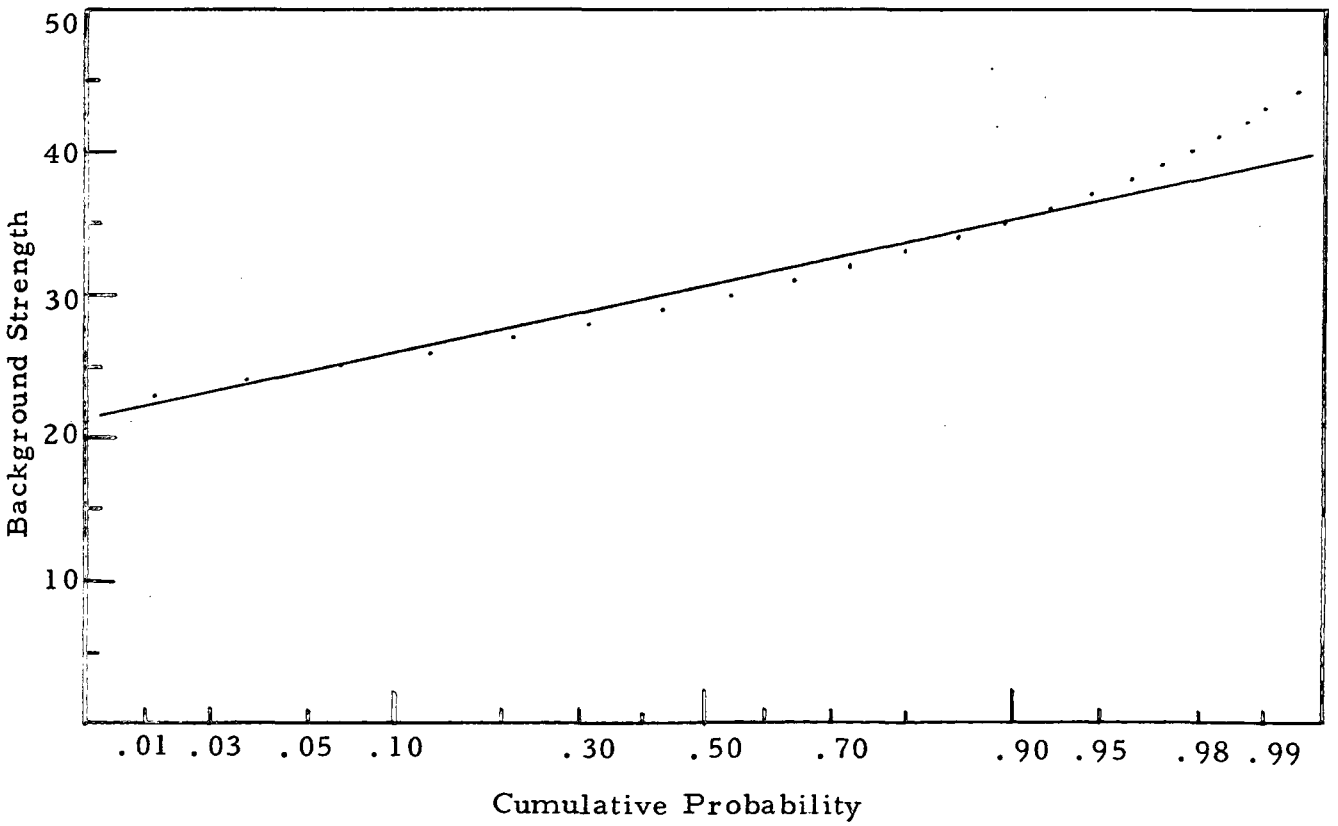

Figure 6. Background Probability Distribution for Run #15.

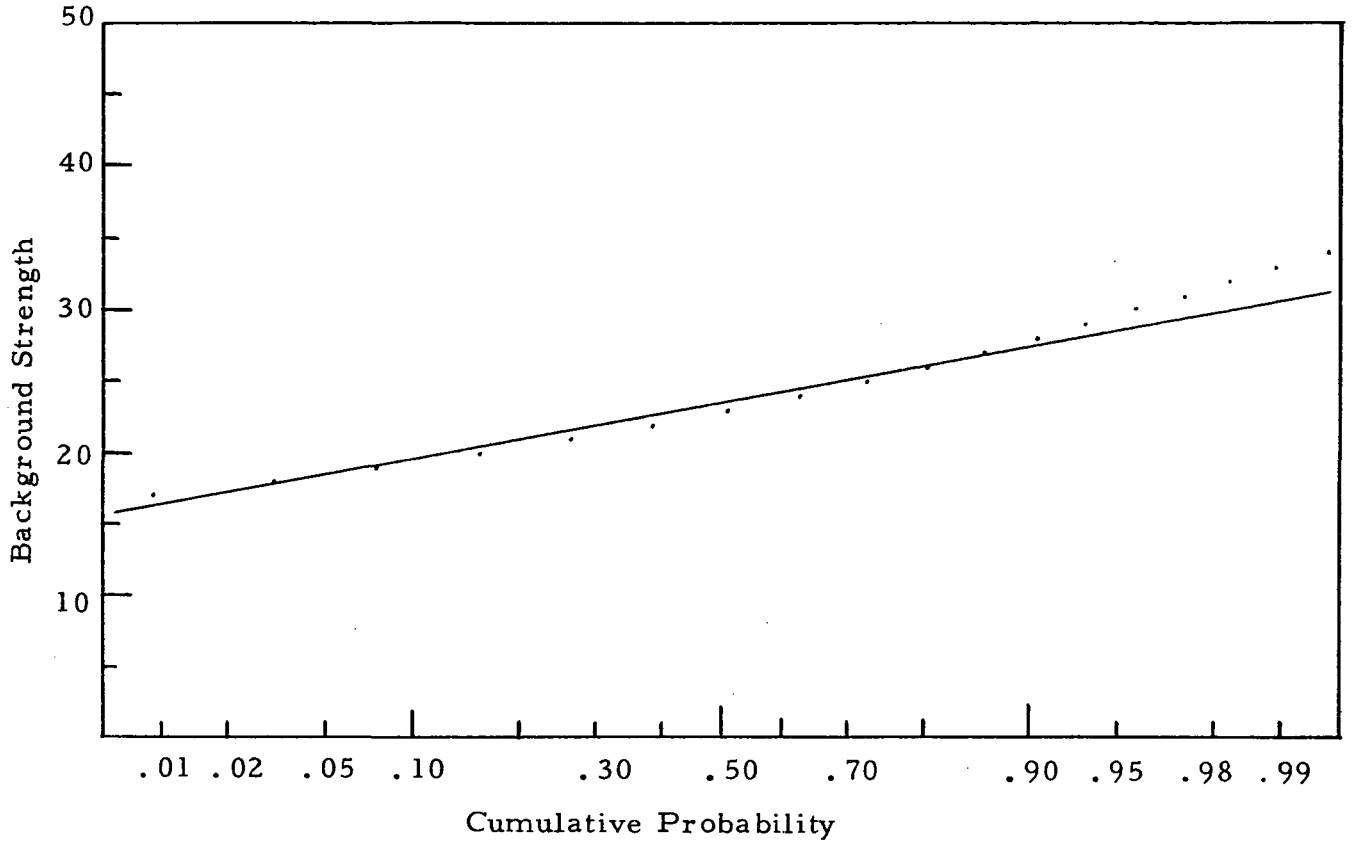

Figure 7. Background Probability Distribution for Run #16.

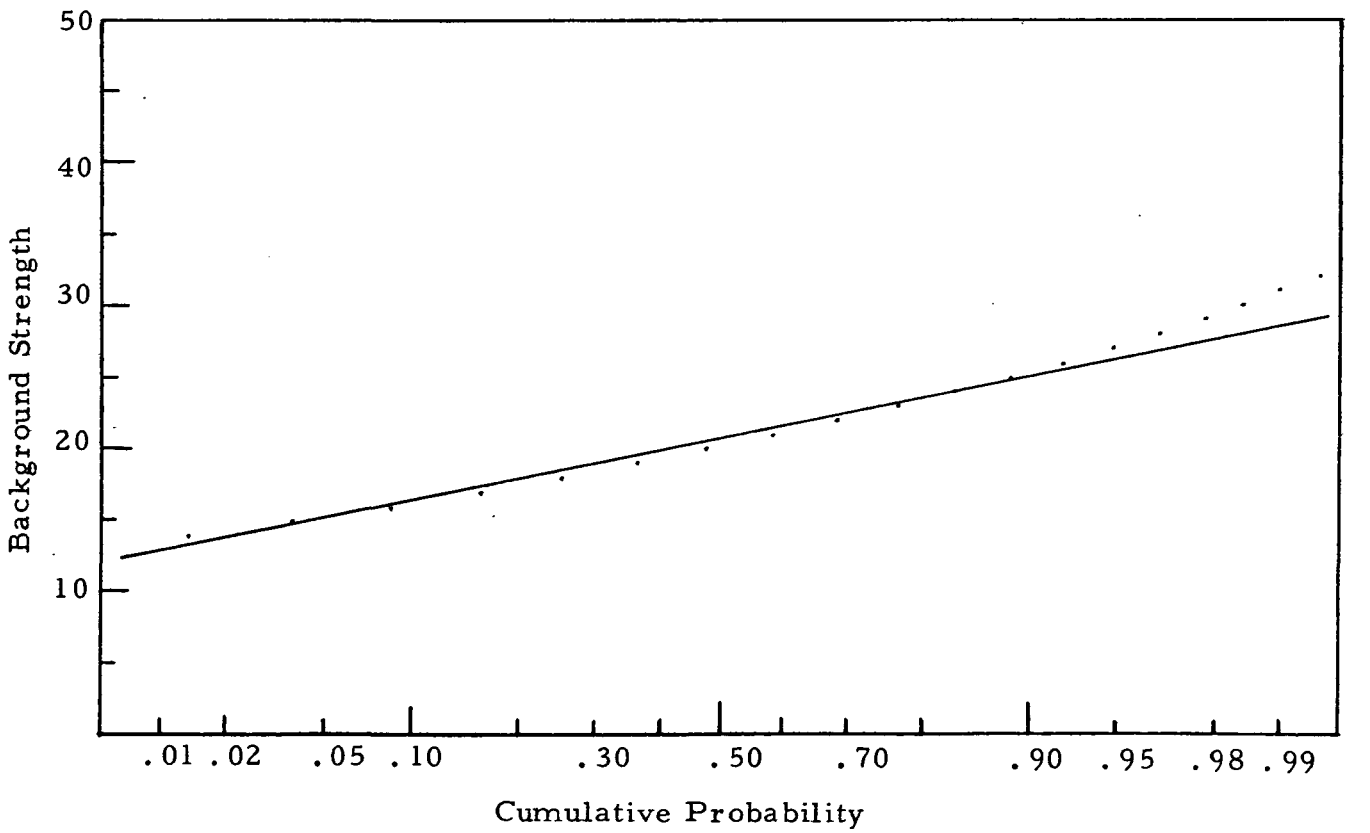

Figure 8. Background Probability Distribution for Run #21.

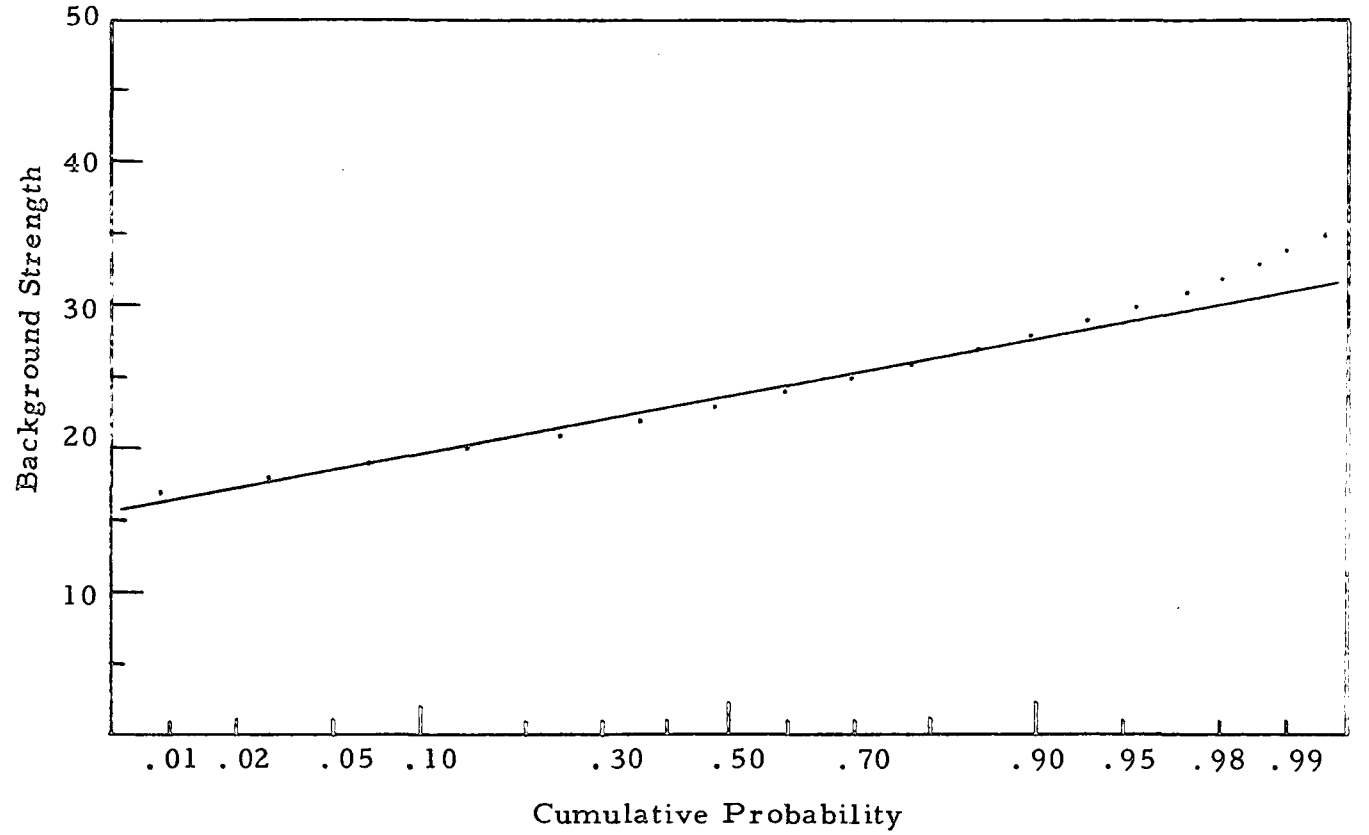

Figure 9. Background Probability Distribution for Run #22.

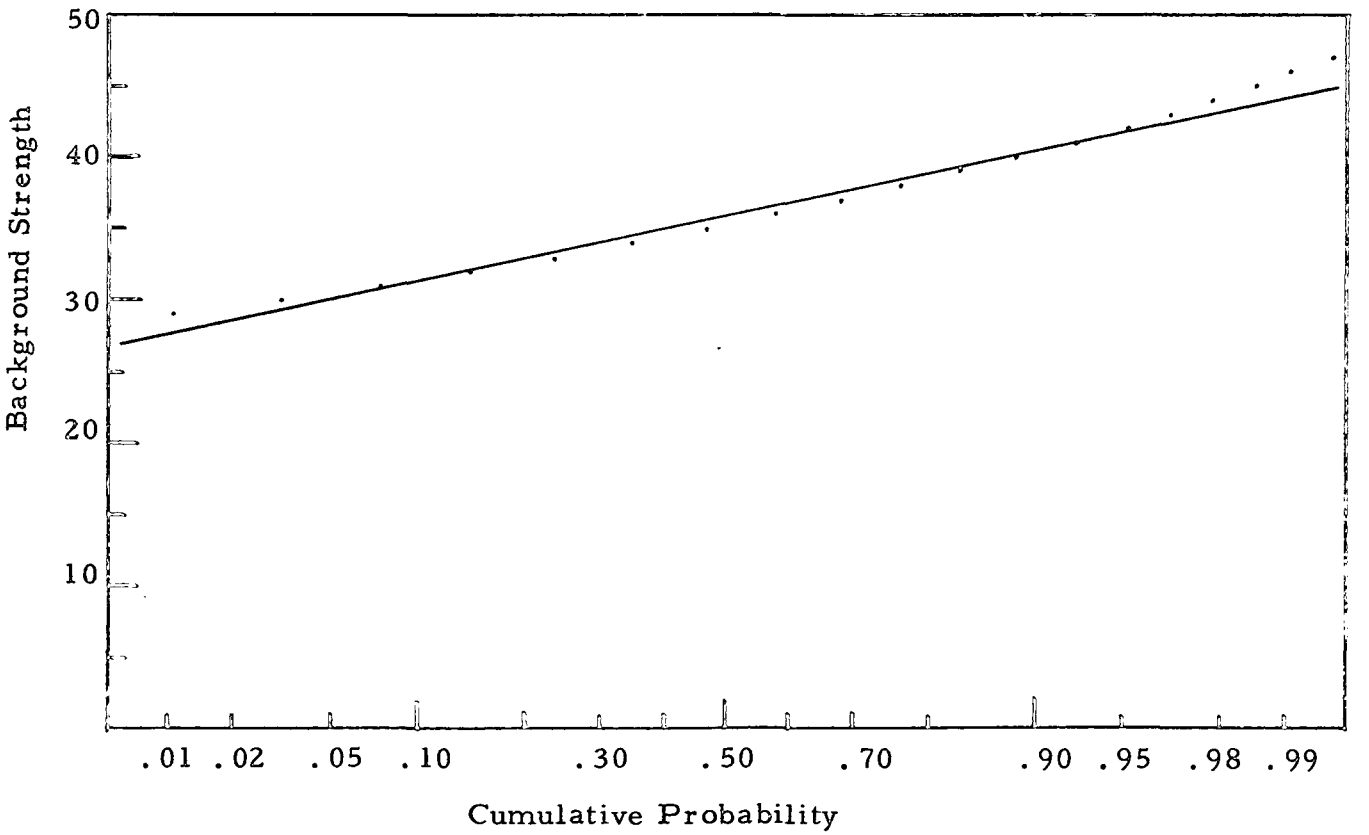

Figure 10. Background Probability Distribution for Run #28.

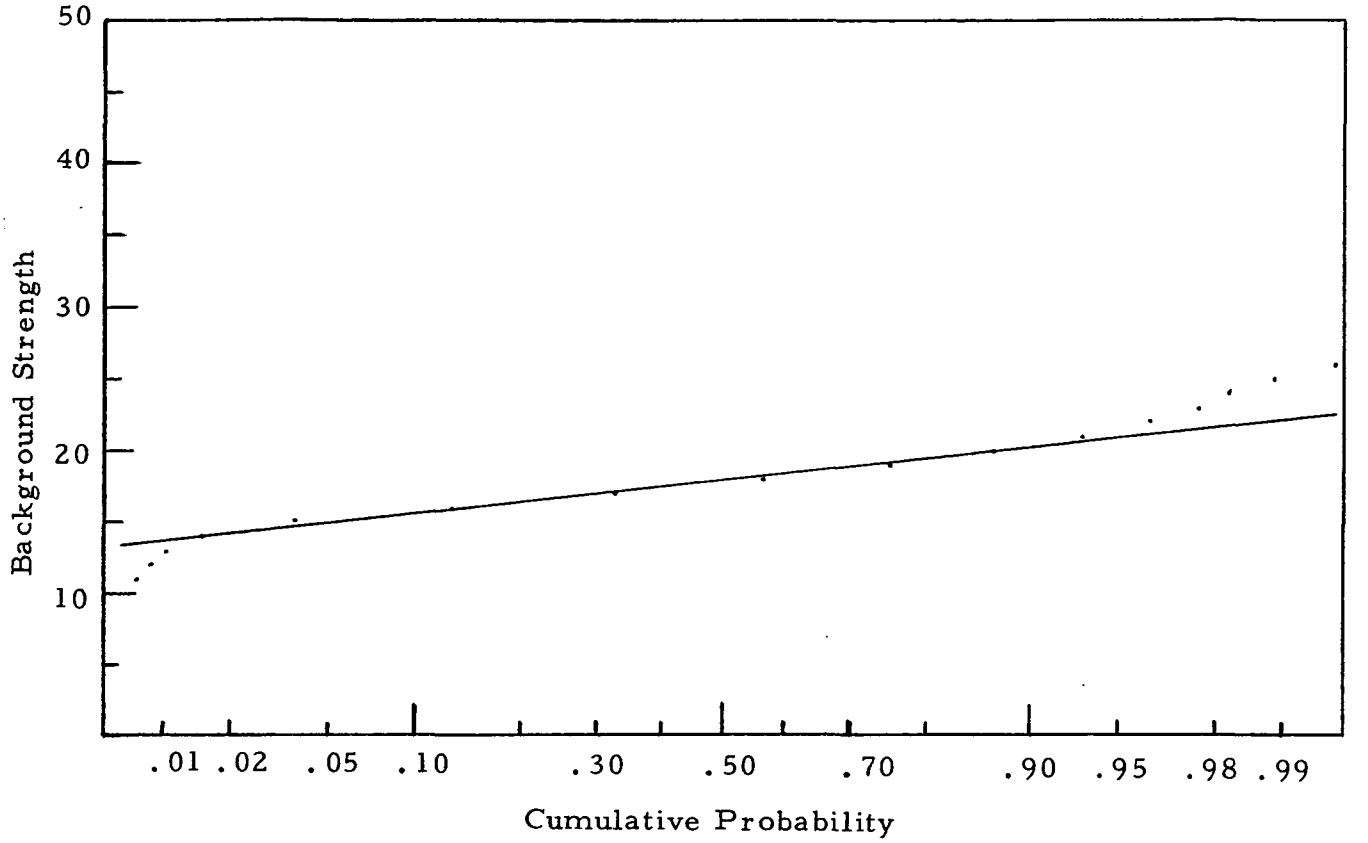

Figure 11. Background Probability Distribution for Run #32.

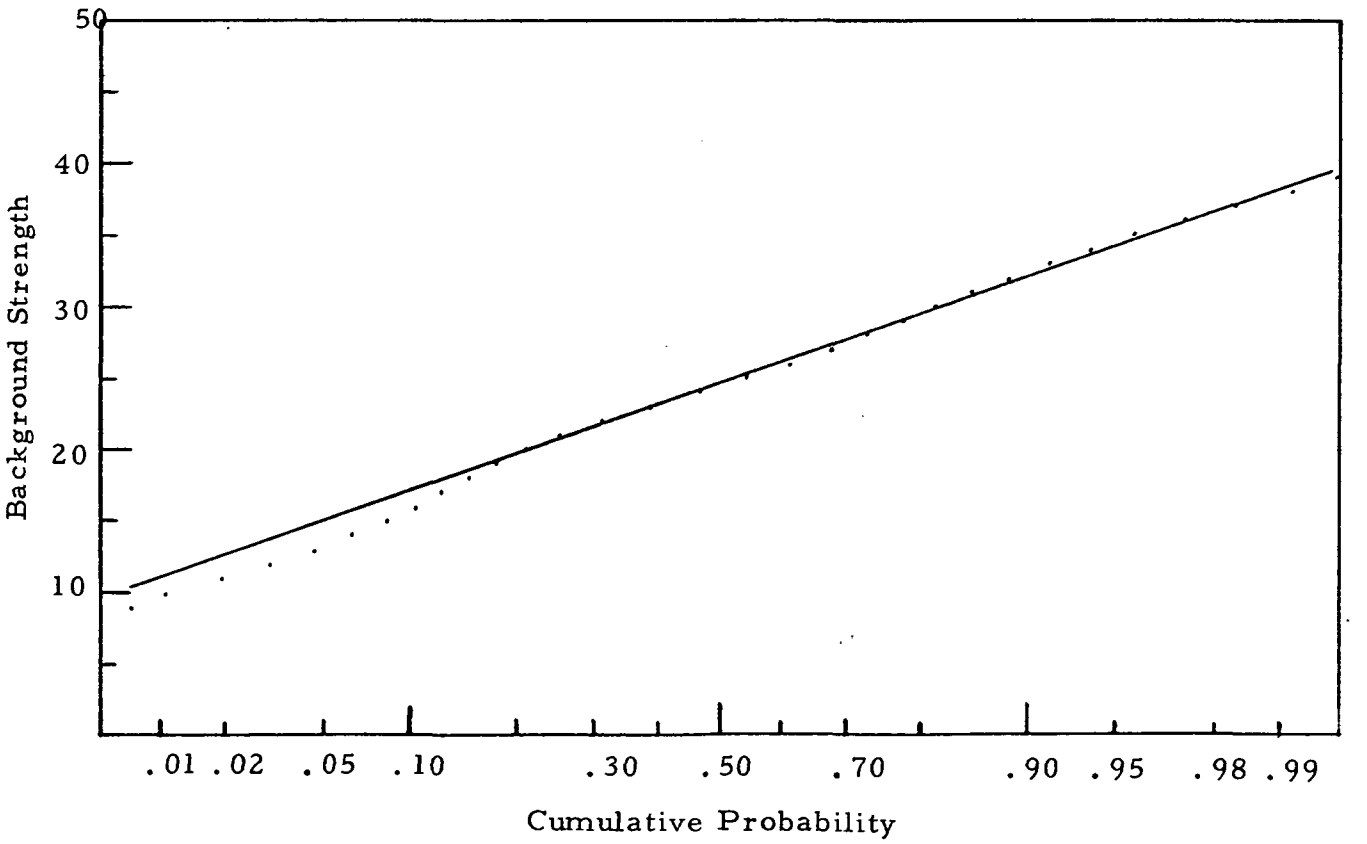

Figure 12. Background Probability Distribution for Run #34.

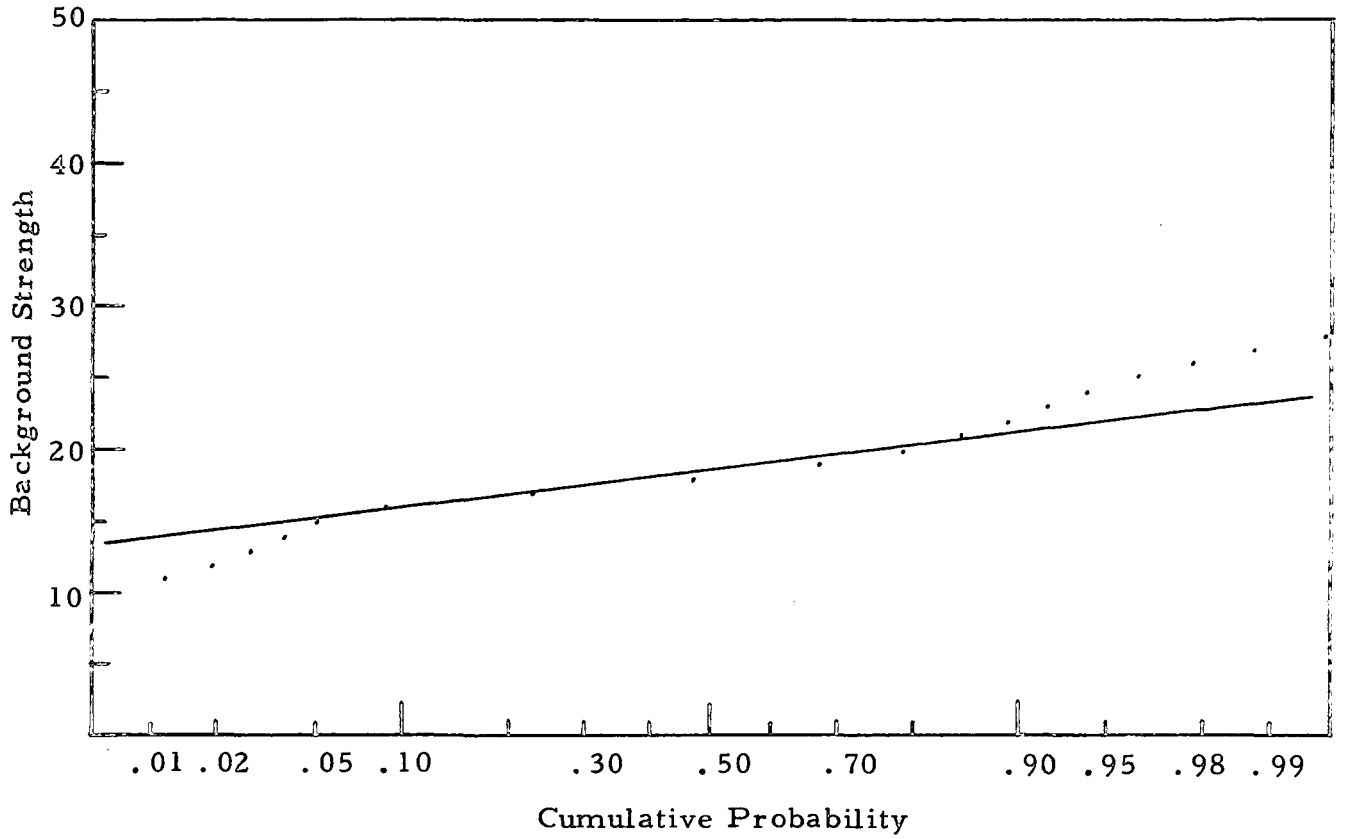

Figure 13. Background Probability Distribution for Run #36.

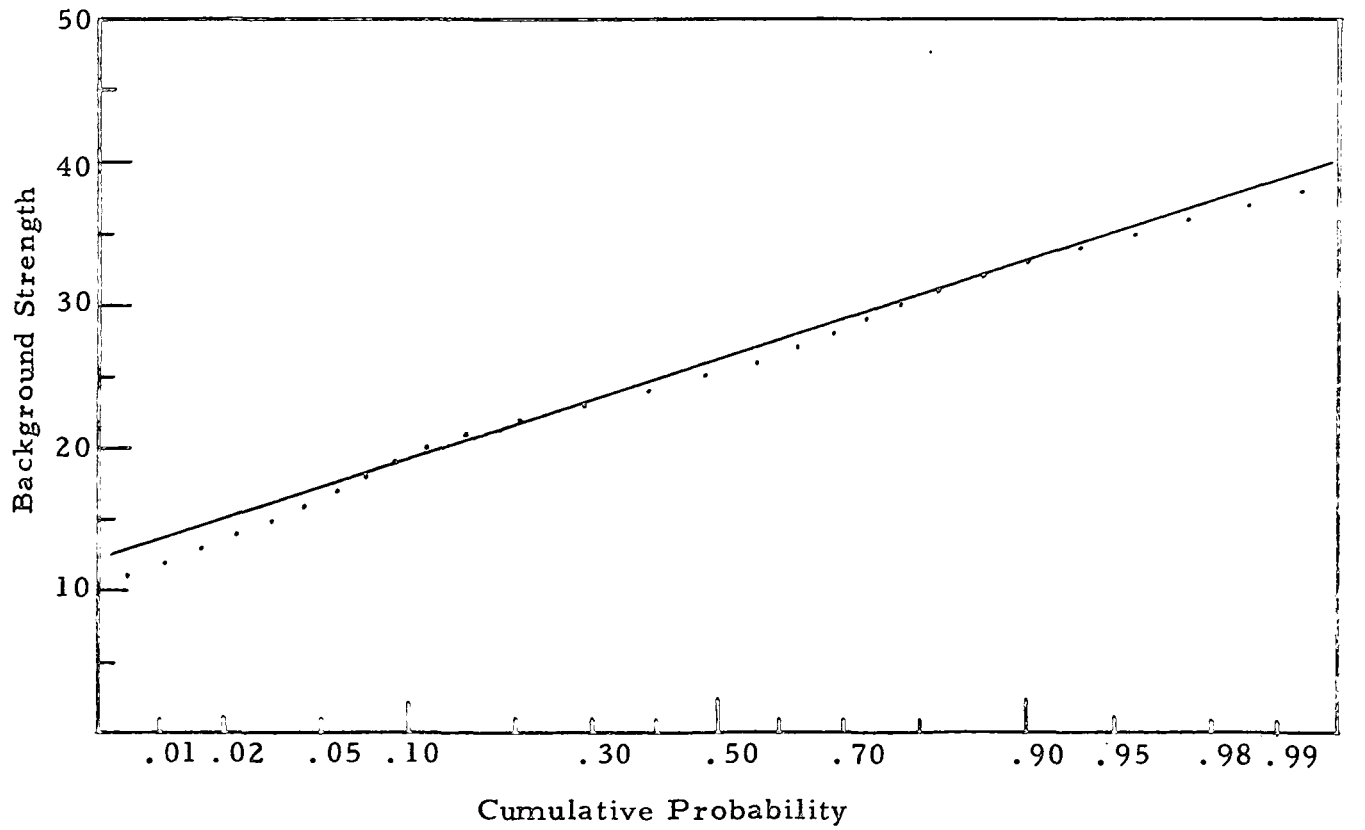

Figure 14. Background Probability Distribution for Run #37.

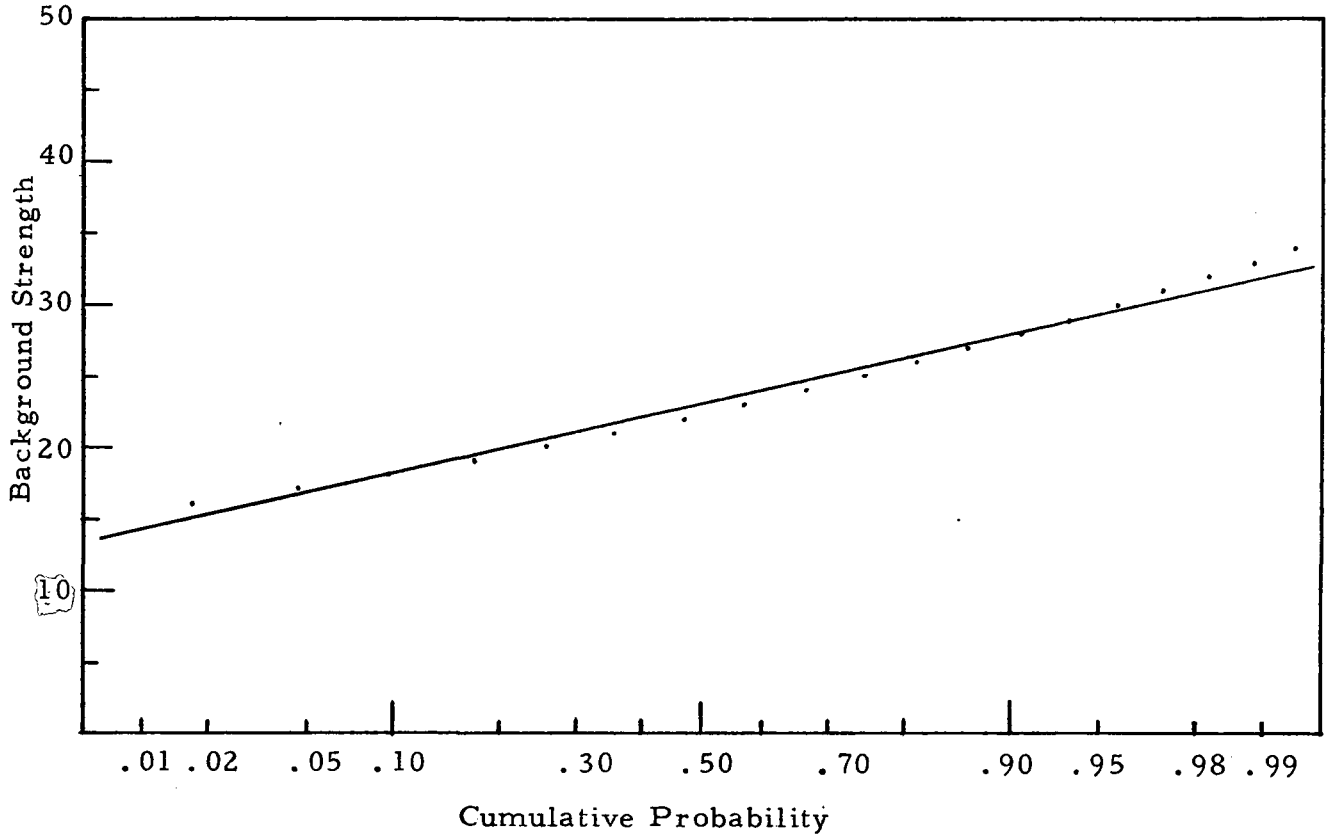

Figure 15. Background Probability Distribution for Run #43.

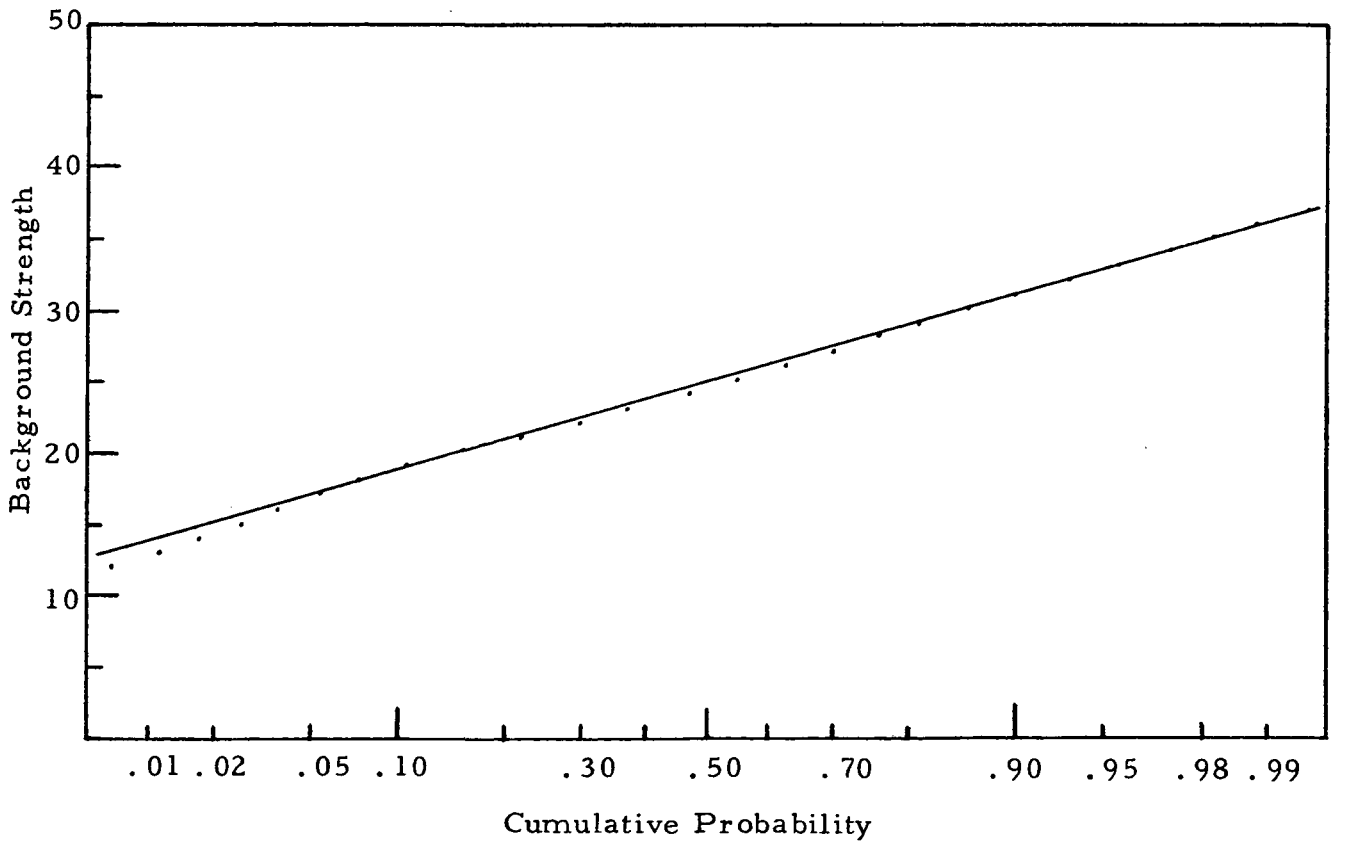

Figure 16. Background Probability Distribution for Run #45.

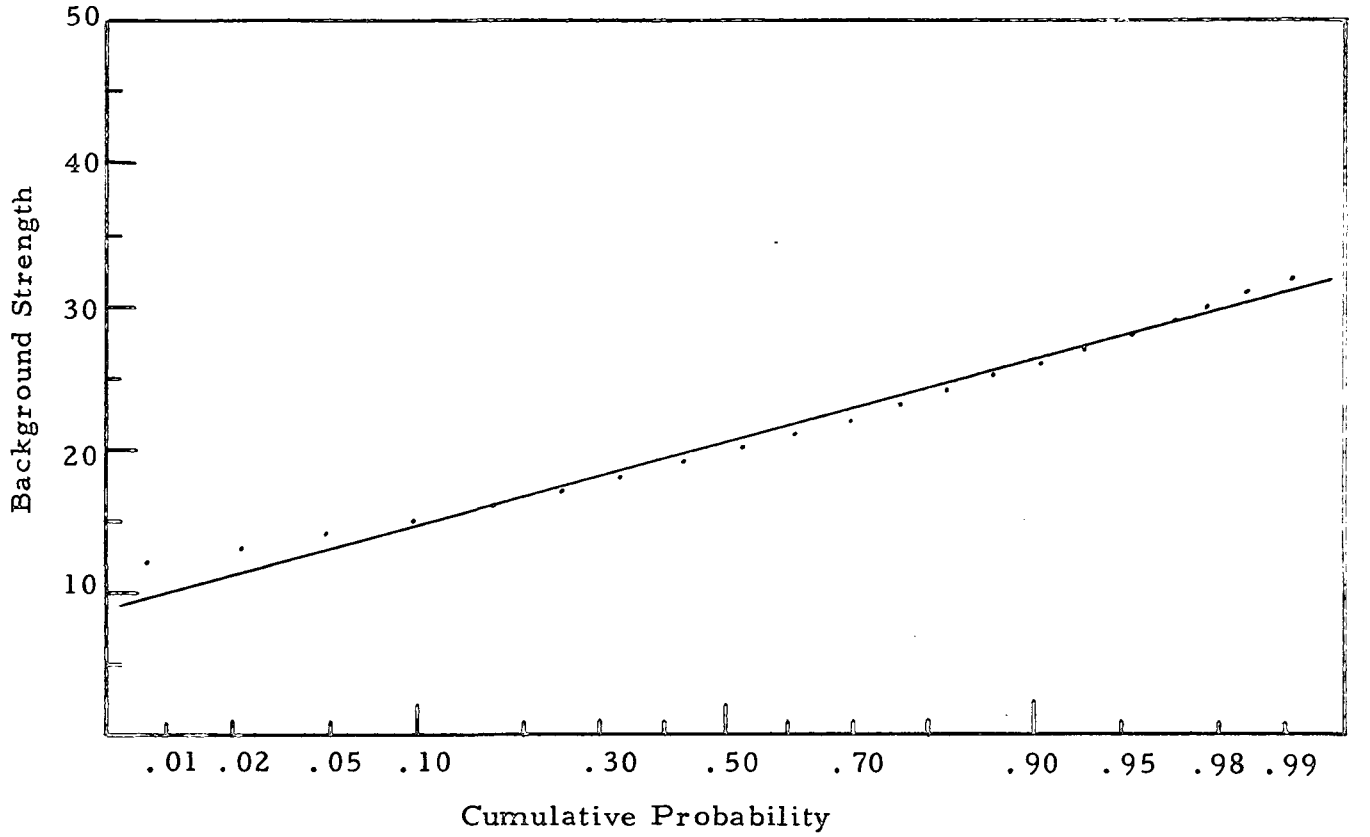

Figure 17. Background Probability Distribution for Run #50.

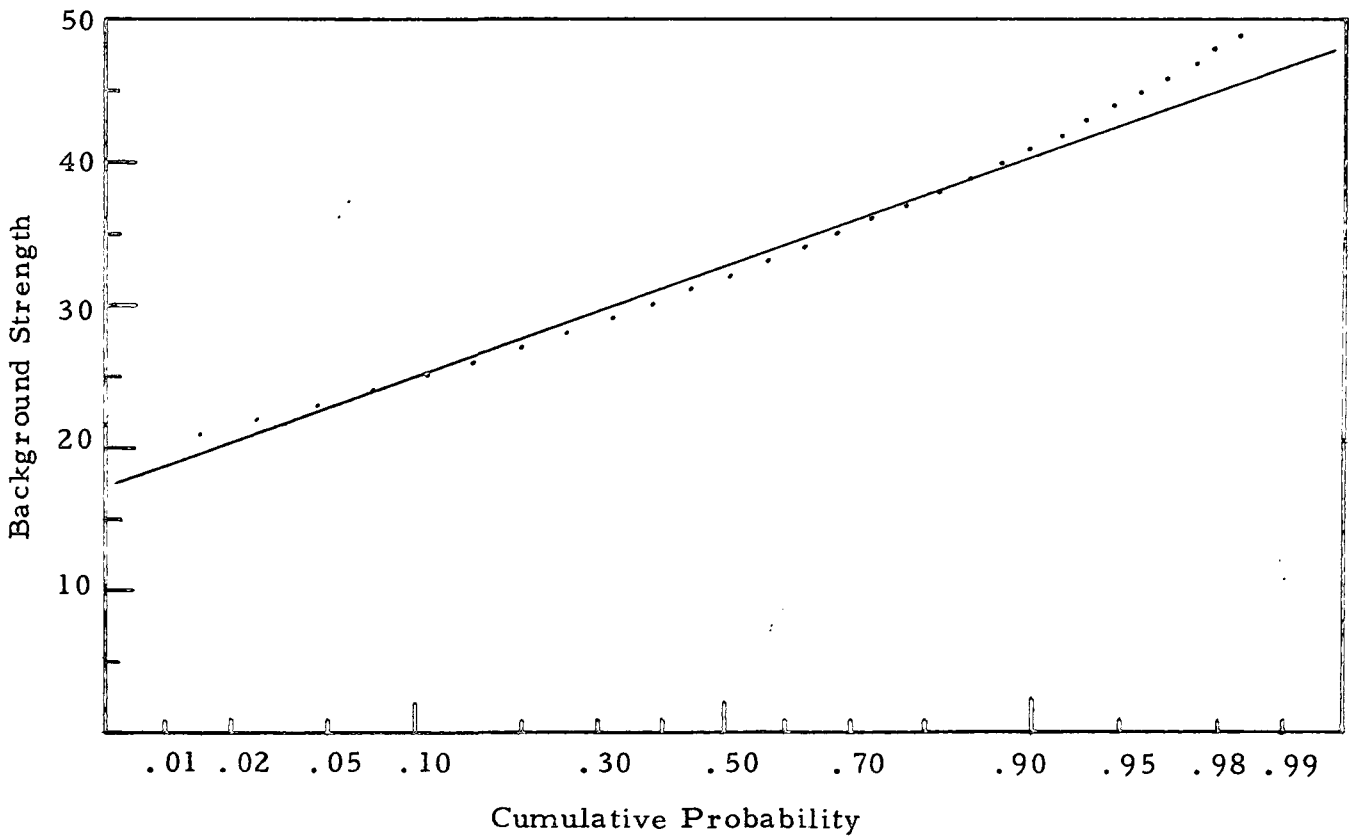

Figure 18. Background Probability Distribution for Run #51.

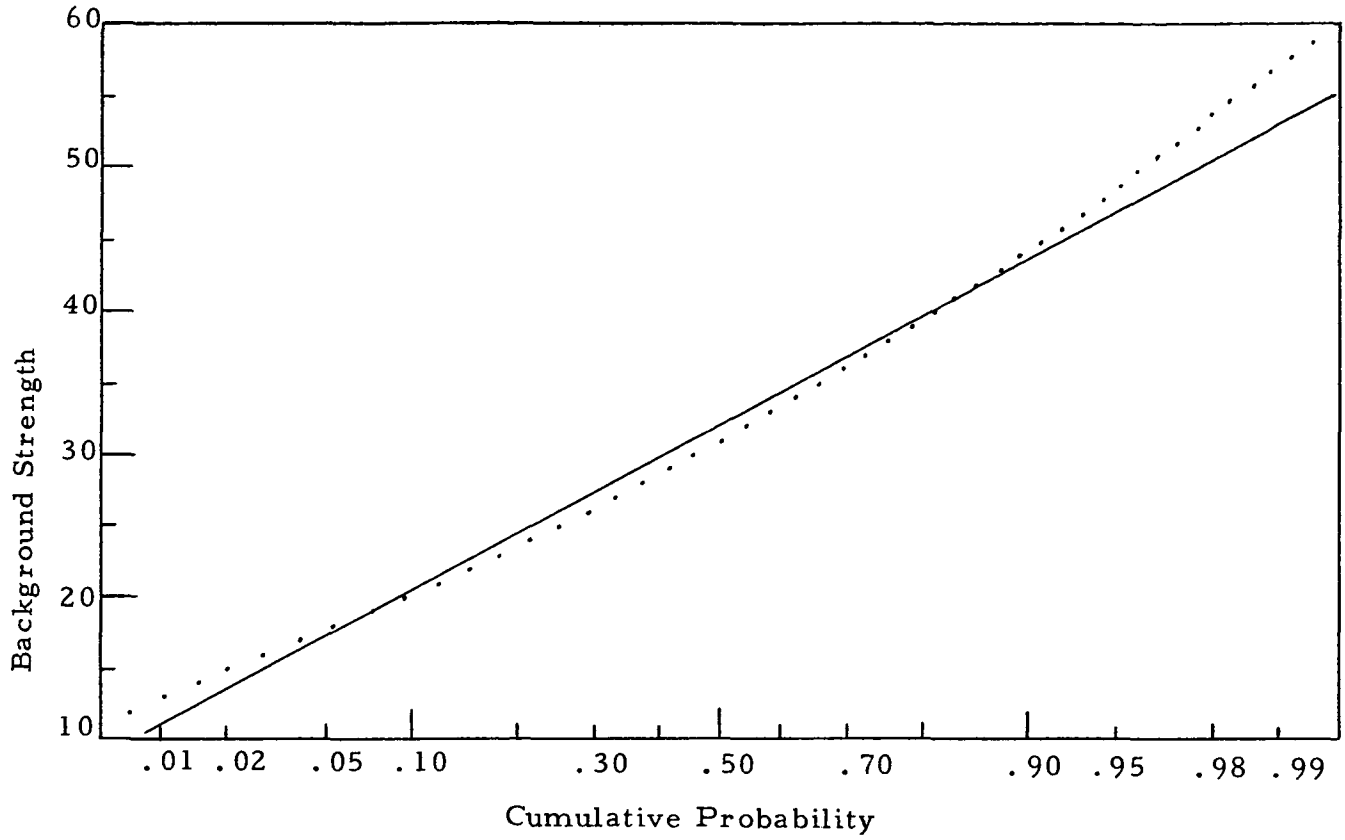

Figure 19. Background Probability Distribution for Run #55.

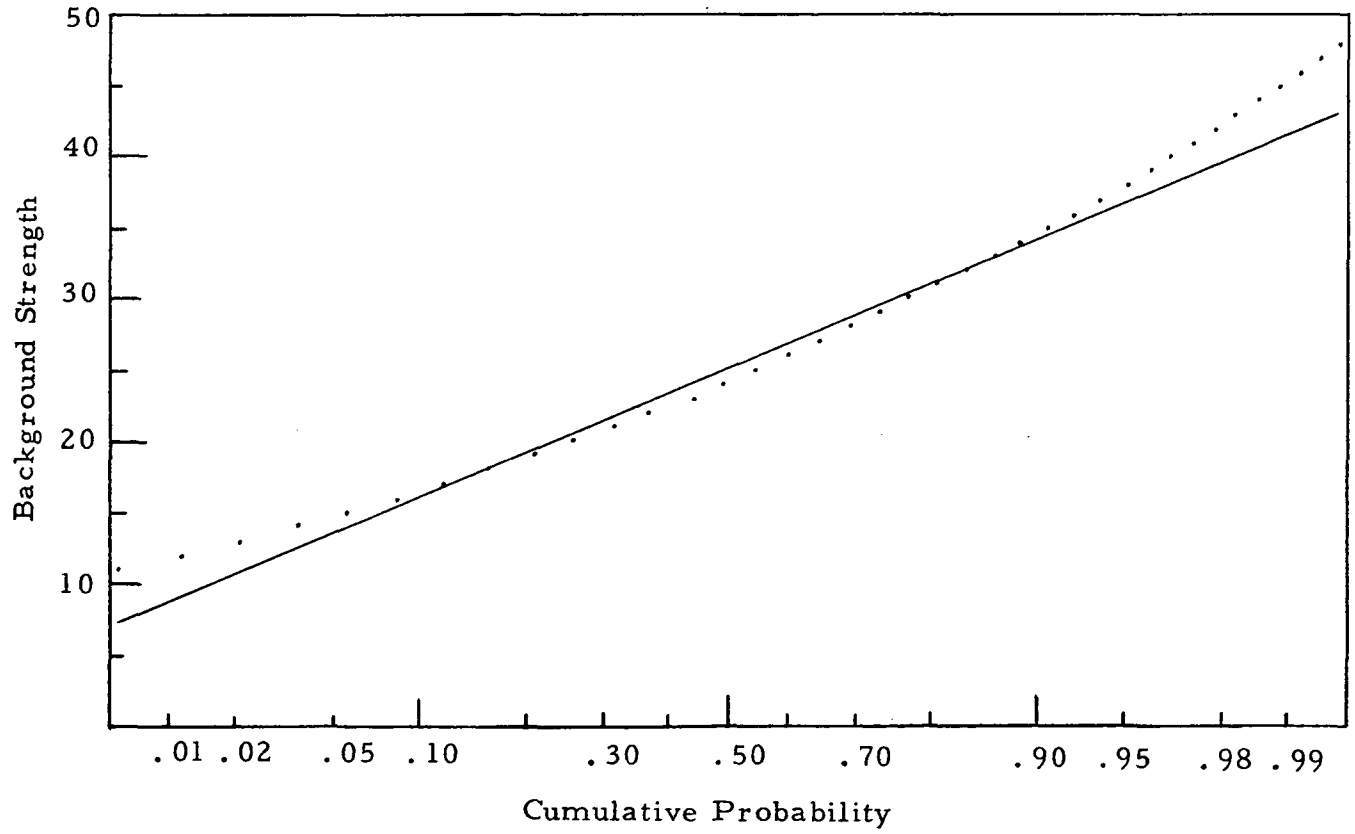

Figure 20. Background Probability Distribution for Run #56.

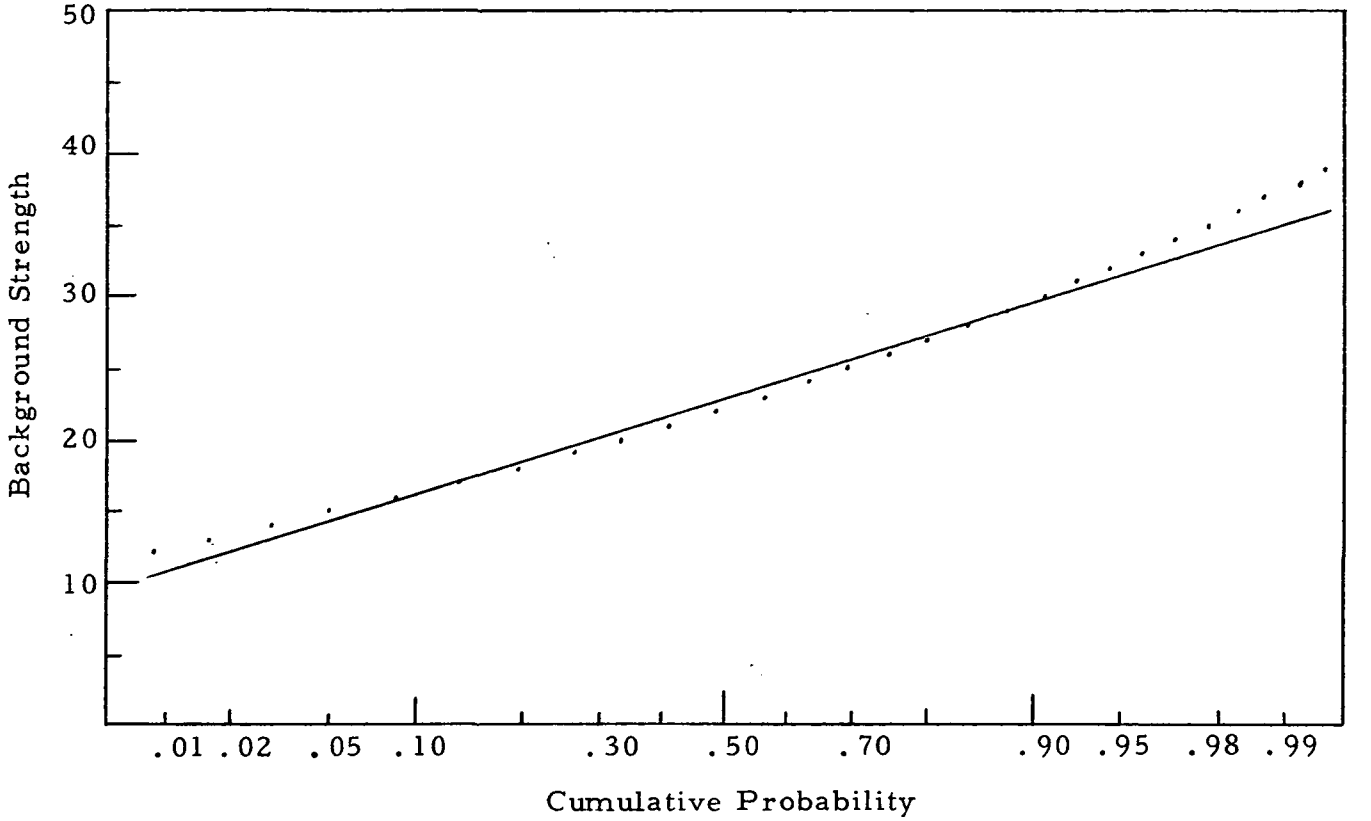

Figure 21. Background Probability Distribution for Run #60.

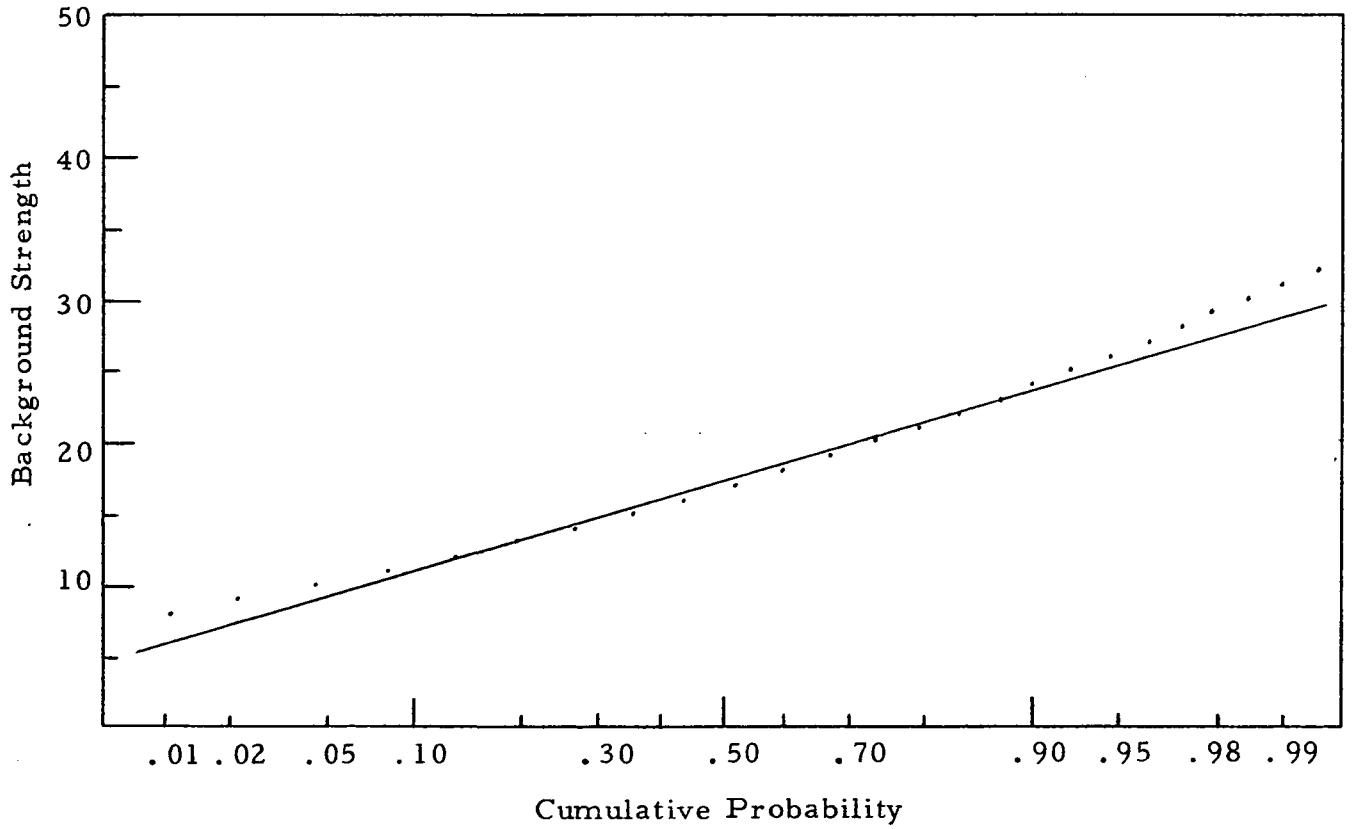

Figure 22. Background Probability Distribution for Run #63.

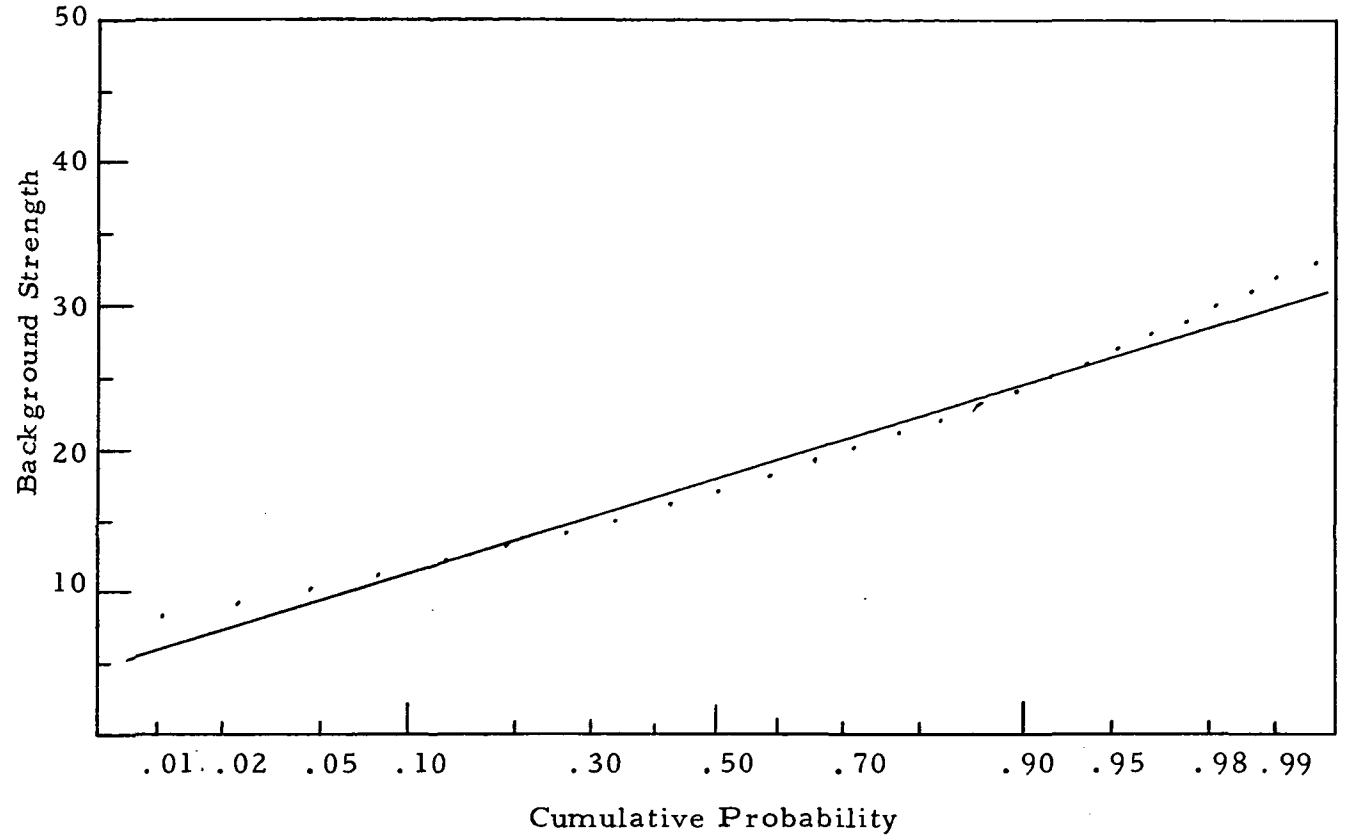

Figure 23. Background Probability Distribution for Run #65.

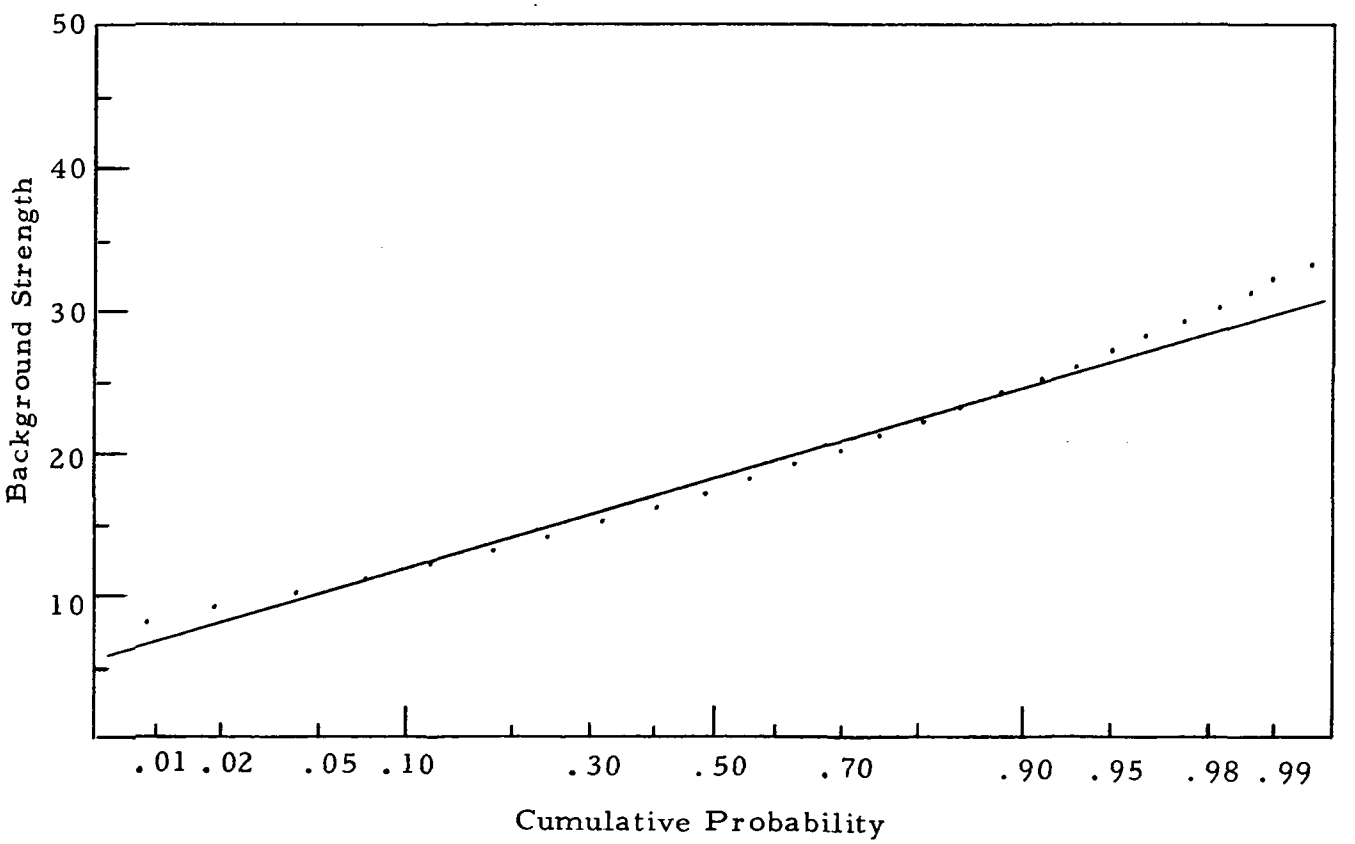

Figure 24. Background Probability Distribution for Run #68.

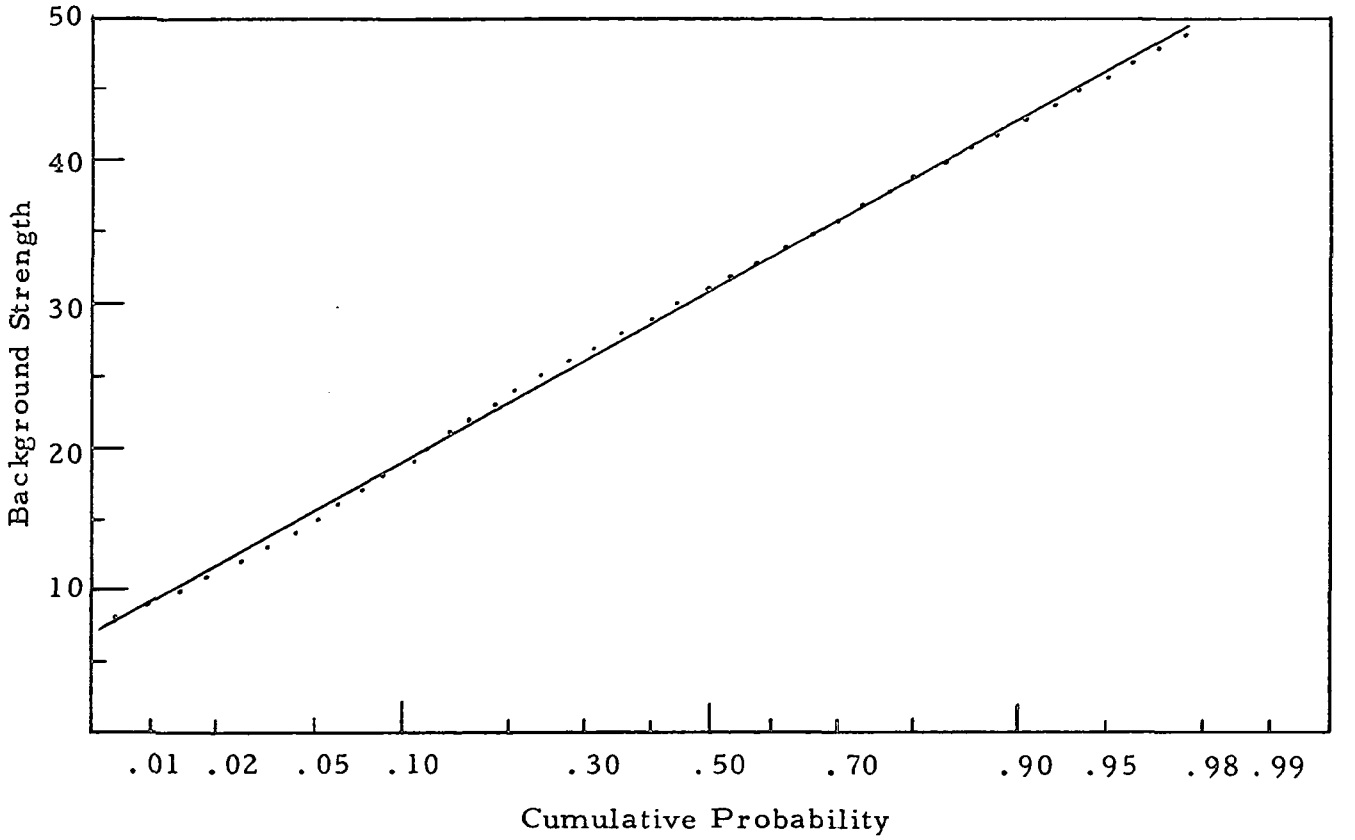

Figure 25. Background Probability Distribution for Run #72.

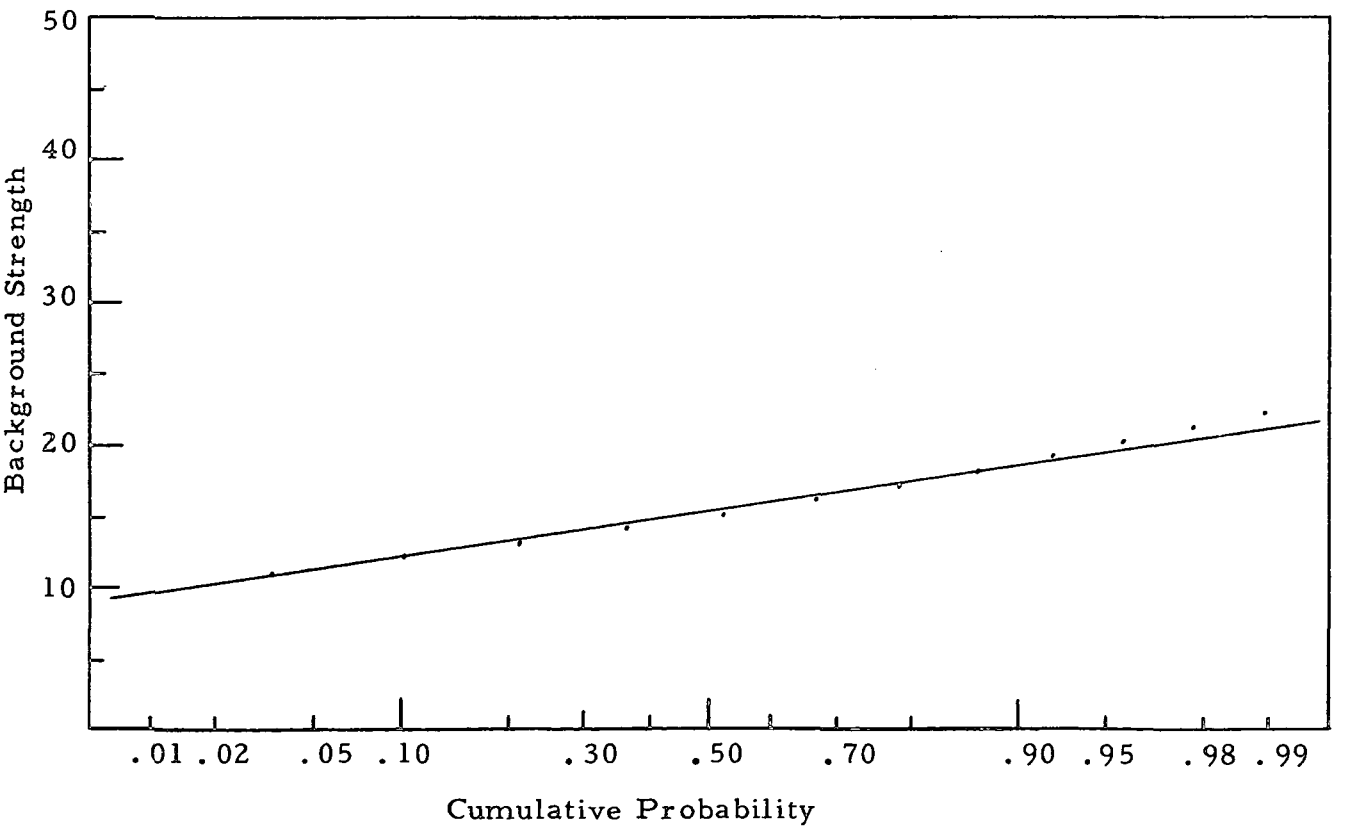

Figure 26. Background Probability Distribution for Run #73.

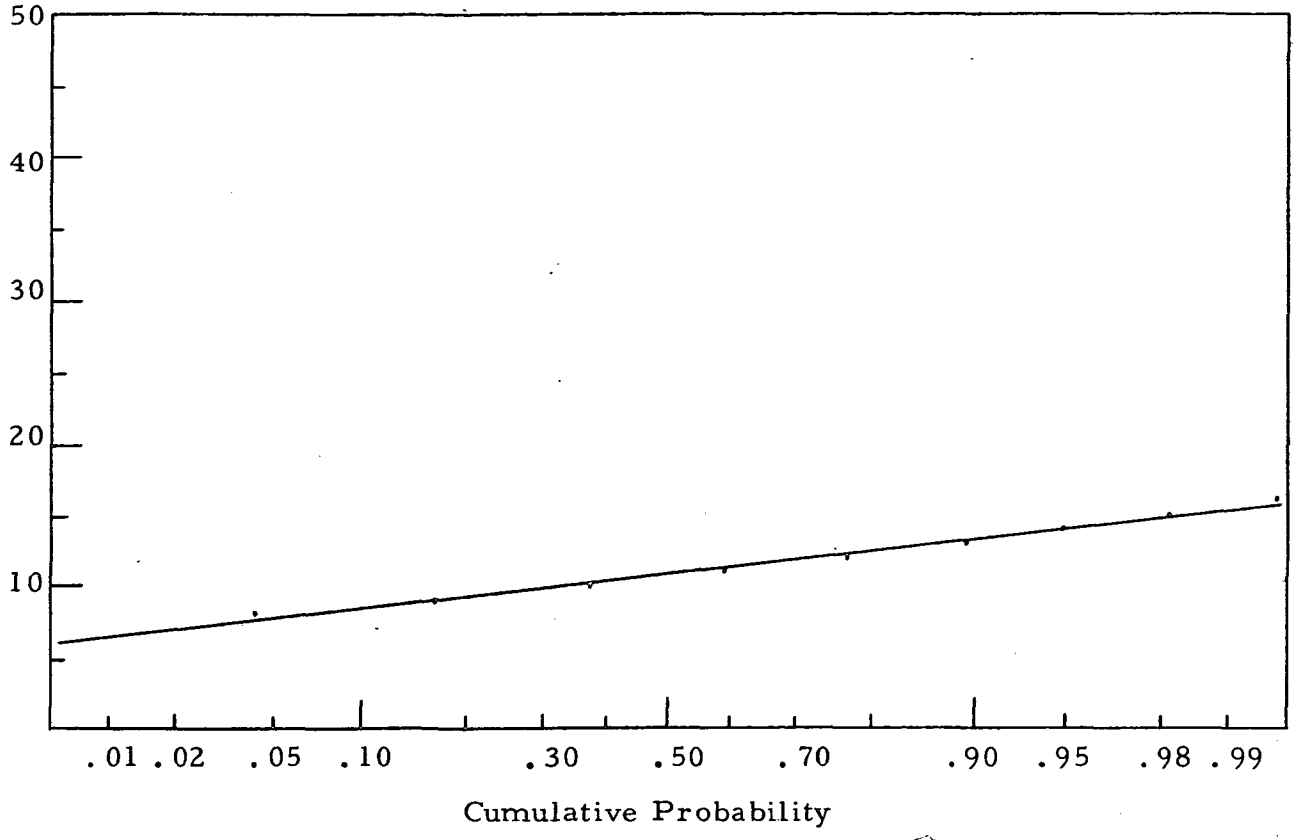

Figure 27. Background Probability Distribution for Run #74.

Table 4

Background Run Measured Moments

Run Number	Aperture Diameter (m)	Mean	Central Moments		
			Second	Third	Fourth
5	0.04	21.64	14.29	64.50	1160.
6	0.08	23.71	13.77	53.32	964.2
7	0.76	15.19	10.17	2.286	313.3
15	0.08	30.62	15.74	55.25	1141.
16	0.16	23.80	11.58	26.53	468.8
21	0.16	21.08	13.70	40.24	906.6
22	0.16	24.07	12.37	36.61	721.4
28	0.04	36.13	12.59	26.85	560.7
32	0.32	18.44	4.871	4.444	183.4
34	0.32	24.91	37.95	-38.37	4253.
36	0.76	19.06	8.056	13.59	338.8
37	0.76	26.24	28.45	-13.78	26.23
43	0.16	23.18	14.72	32.71	741.9
45	0.76	25.03	23.09	5.639	1706.
50	0.32	20.64	17.90	42.26	1407.
51	0.08	33.02	41.51	166.3	6033.
55	0.16	32.27	90.74	402.5	26770.
56	0.32	25.57	52.55	303.3	12710.
60	0.76	23.20	28.42	83.59	2725.
63	0.76	17.83	24.18	69.39	19.63
65	0.76	17.98	25.87	81.87	2334.
68	0.76	18.26	25.91	74.17	2238.
72	0.76	31.59	84.72	-67.62	21260.
73	0.76	15.59	6.585	8.996	142.8
74	0.76	11.25	3.261	2.919	33.59

Table 5

Background Run Measured Skewness and Curtosis

Run Number	Diameter (m)	Skewness	Curtosis
5	0.04	1.194	2.681
6	0.08	1.043	2.085
7	0.76	0.07048	0.02913
15	0.08	0.8848	1.605
16	0.16	0.6732	0.4960
21	0.16	0.7936	1.830
22	0.16	0.8415	1.715
28	0.04	0.6010	0.5374
32	0.32	0.4134	4.730
34	0.32	-0.1641	-0.04694
36	0.76	0.5943	2.220
37	0.76	-0.09081	-2.968
43	0.16	0.5792	0.4240
45	0.76	0.05082	0.2000
50	0.32	0.5580	0.2677
51	0.08	0.6218	0.5013
55	0.16	0.4657	0.2513
56	0.32	0.7962	1.603
60	0.76	0.5517	0.3738
63	0.76	0.5836	-2.966
65	0.76	0.6222	0.4875
68	0.76	0.5624	0.3337
72	0.76	-0.08672	-0.03796
73	0.76	0.5234	0.2932
74	0.76	0.4957	0.1587

By noting the way in which the cumulative distribution plot deviated from a straight line, it is possible to gain some insight into the apparent degree of contamination of the data. We see from a study of these figures that in the range of 0.1 to 0.9 cumulative probability, the distributions appear to be fairly well characterized by a straight line, corresponding to some gaussian distribution. Apparently the data corruption is limited to the extremes, with the central region seeming to be relatively unaffected. We expect the distortions of the extremes of the distribution to affect the higher moments before it affects the first two moments, i.e., the mean and variance, thus allowing for the possibility that we could rely on the mean and variance, although as Table 5 indicates, the third and fourth moments must be considered suspect. To see whether or not this was the case, i.e., that we could rely on the mean and variance values computed for each of the background data runs, we have extracted a mean and variance for the straight line gaussian drawn on each of the figures, i.e., Fig.'s 3 to 27, to match the data in the 0.1 to 0.9 cumulative probability range, and compared these straight-line-fit mean and variance to the mean and variance calculated directly from the full probability density. In Table 6, we show these values organized to facilitate comparison. As can be seen, the comparison is quite good, indicating that the factors that affected the data probably did not significantly affect the calculated mean and variance of each background run. Accordingly, we have felt justified in using these mean and variance values in the next section in the reduction of the scintillation run data.*

---

* It is significant to note that had we used the straight-line-fit mean and variance rather than the values calculated from the full distribution in our reduction of the scintillation data, the effects on the final results would have been legligible.

Table 6

Background Data Runs, Mean and Variance

Run Number	Diameter (m)	Measured		Straight-Line Fit	
		Mean	Variance	Mean	Variance
5	0.04	21.64	14.29	21.15	10.48
6	0.08	23.71	13.77	23.45	10.99
7	0.76	15.19	10.17	14.85	9.493
15	0.08	30.62	15.74	30.60	12.87
16	0.16	23.80	11.58	23.60	9.255
21	0.16	21.08	13.70	20.75	10.99
22	0.16	24.07	12.37	23.80	9.735
28	0.04	36.13	12.59	35.80	12.87
32	0.32	18.44	4.871	17.90	2.945
34	0.32	24.91	37.95	24.65	33.77
36	0.76	19.06	8.056	18.55	3.956
37	0.76	26.24	28.45	26.10	28.97
43	0.16	23.18	14.72	23.10	14.61
45	0.76	25.03	23.09	24.85	22.27
50	0.32	20.64	17.90	20.45	20.12
51	0.08	33.02	41.51	32.60	36.07
55	0.16	32.27	90.74	32.05	81.17
56	0.32	25.57	52.55	25.15	48.74
60	0.76	23.20	28.42	22.85	27.72
63	0.76	17.83	24.18	17.25	23.77
65	0.76	17.98	25.87	17.70	26.50
68	0.76	18.26	25.91	18.05	23.01
72	0.76	31.59	84.72	30.95	86.89
73	0.76	15.59	6.585	15.15	5.660
74	0.76	11.25	3.261	10.80	3.505

4. Scintillation Measurements

The data recorded during each scintillation run was processed to produce a 100-level probability density histogram. From this probability density, the mean, variance (or second central moment), the third central moment, and the fourth central moment have all been calculated in accordance with Eq.'s (24)-(27). In Table 7 we show these results. We recognize that this data does not represent scintillation alone. It also includes the effects of background and background noise, the moments of which can be estimated from the corresponding background runs. The match between the scintillation run and the background run is as indicated in the last column of Table 2.

4.1 Reduced Scintillation Data

The equations relating the actual scintillation moments to the measured background and measured scintillation moments can be derived as follows. Consider two random variables, x_B and x_S, corresponding to background and scintillation, and

$$x_T = x_B + x_S \quad . \tag{30}$$

x_B is the random variable whose statistics govern the data taken in a background run, and x_T is the random variable whose statistics govern the data taken in a scintillation run. In Tables 4 and 7, we have the measured four leading moments of x_B and x_T. We wish to determine the four leading moments of x_S. As a matter of definition, we note that the four leading moments of x_B are

$$\bar{x}_B = \langle x_B \rangle \quad , \tag{31}$$

$$\sigma_B^2 = \langle (x_B - \bar{x}_B)^2 \rangle \quad , \tag{32}$$

$$\mu_{3,B} = \langle (x_B - \bar{x}_B)^3 \rangle \quad , \tag{33}$$

$$\mu_{4,B} = \langle (x_B - \bar{x}_B)^4 \rangle \quad , \tag{34}$$

Table 7

Scintillation Run Measured Moments

Run Number	Diameter (m)	Mean	Central Moments		
			Second	Third	Fourth
1	0.76	42.37	117.9	808.3	51970.
2	0.76	38.17	135.5	953.2	60790.
3	0.08	34.54	117.8	1314.	64510.
4	0.04	24.70	29.90	115.1	3904.
8	0.76	40.10	141.6	2159.	120100.
9	0.76	38.79	99.36	395.3	28680.
10	0.76	34.33	66.44	325.8	16120.
12	0.08	43.06	140.3	984.7	70520.
13	0.08	40.17	110.4	796.8	47600.
14	0.08	38.42	84.93	483.1	27420.
17	0.16	40.73	133.1	1087.	63110.
18	0.16	28.04	105.9	1242.	55500.
19	0.16	37.32	136.0	1223.	69770.
20	0.16	39.24	168.3	1697.	104200.
23	0.16	38.44	144.0	1870.	95560.
24	0.16	39.82	142.9	1625.	86690.
27	0.04	38.59	29.99	200.7	4886.
29	0.76	44.05	132.8	889.7	58330.
30	0.76	44.56	147.4	1091.	72150.
31	0.32	33.32	70.32	440.4	18920.
33	0.32	46.00	128.8	808.2	58240.
38	0.76	40.22	149.8	842.3	63760.
39	0.76	43.29	169.1	328.7	80300.
42	0.16	39.83	137.3	853.3	59210.
46	0.76	47.11	150.0	700.9	66380.

Table 7 (Continued)

Run Number	Diameter (m)	Mean	Central Moments		
			Second	Third	Fourth
47	0.76	46.22	117.1	669.3	48570.
48	0.32	34.20	123.1	976.3	54670.
49	0.32	33.61	119.0	1059.	56890.
52	0.08	35.59	61.45	354.2	13930.
53	0.16	36.13	151.7	1636.	95290.
54	0.16	36.87	162.5	1794.	106300.
57	0.32	36.59	172.2	1735.	107400.
58	0.32	35.62	157.0	1386.	85470.
59	0.76	41.23	169.5	1056.	89290.
61	0.76	42.09	170.9	1157.	95370.
62	0.76	34.80	150.3	1135.	80710.
64	0.76	38.70	174.1	1036.	92350.
66	0.76	32.18	144.3	1144.	69590.
67	0.76	31.19	131.0	989.9	58600.
69	0.76	28.39	113.4	1029.	53830.
70	0.76	28.81	115.0	902.7	46350.
71	0.76	39.02	137.7	371.0	59000.
75	0.76	40.41	97.04	648.6	35460.
76	0.76	40.49	93.97	623.6	31100.

the four leading moments of x_T are

$$\bar{x}_T = \langle x_T \rangle \quad , \tag{35}$$

$$\sigma_T^2 = \langle (x_T - \bar{x}_T)^2 \rangle \quad , \tag{36}$$

$$\mu_{3,T} = \langle (x_T - \bar{x}_T)^3 \rangle \quad , \tag{37}$$

$$\mu_{4,T} = \langle (x_T - \bar{x}_T)^4 \rangle \quad , \tag{38}$$

and the four leading moments of x_S are

$$\bar{x}_S = \langle x_S \rangle \quad , \tag{39}$$

$$\sigma_S^2 = \langle (x_S - \bar{x}_S)^2 \rangle \quad , \tag{40}$$

$$\mu_{3,S} = \langle (x_S - \bar{x}_S)^3 \rangle \quad , \tag{41}$$

$$\mu_{4,S} = \langle (x_S - \bar{x}_S)^4 \rangle \quad . \tag{42}$$

It is these last four quantities which we wish to calculate from values of the preceding eight quantities as given in Tables 4 and 7. [In Eq.'s (31) to (42), the angle brackets $\langle\ \rangle$, denote an ensemble average.]

It follows from Eq.'s (30) and (35) that

$$\begin{aligned} \bar{x}_T &= \langle x_B + x_S \rangle \\ &= \langle x_B \rangle + \langle x_S \rangle \quad . \end{aligned} \tag{43}$$

Making use of Eq.'s (35) and (39),

$$\bar{x}_T = \bar{x}_B + \bar{x}_S \quad , \tag{44}$$

and solving for $\bar{x}_S$, we get

$$\bar{x}_S = \bar{x}_T - \bar{x}_B \quad . \tag{45}$$

From Eq.'s (36), (30), and (44), we obtain the result that

$$\begin{aligned} \sigma_T^2 &= \langle [x_B + x_S - (\bar{x}_B + \bar{x}_S)]^2 \rangle \\ &= \langle [(x_B - \bar{x}_B) + (x_S - \bar{x}_S)]^2 \rangle \\ &= \langle (x_B - \bar{x}_B)^2 \rangle + 2 \langle (x_B - \bar{x}_B)(x_S - \bar{x}_S) \rangle + \langle (x_S - \bar{x}_S)^2 \rangle \quad . \end{aligned} \tag{46}$$

If we make use of Eq.'s (32) and (40) and note that x_B and x_S are independent random variables so that $\langle (x_B - \bar{x}_B)(x_S - \bar{x}_S) \rangle$ must vanish, we can recast Eq. (46) in the form

$$\sigma_T^2 = \sigma_B^2 + \sigma_S^2 \quad , \tag{47}$$

so that

$$\sigma_S^2 = \sigma_T^2 - \sigma_B^2 \quad . \tag{48}$$

From Eq.'s (37), (30), and (44), we obtain the result that

$$\begin{aligned} \mu_{3,T} &= \langle [x_B + x_S - (\bar{x}_B + \bar{x}_S)]^3 \rangle \\ &= \langle [(x_B - \bar{x}_B) + (x_S - \bar{x}_S)]^3 \rangle \\ &= \langle (x_B - \bar{x}_B)^3 \rangle + 3 \langle x_B - \bar{x}_B)^2 (x_S - \bar{x}_S) \rangle \\ &\quad + 3 \langle (x_B - \bar{x}_B)(x_S - \bar{x}_S)^2 \rangle + \langle (x_S - \bar{x}_S)^3 \rangle \quad . \end{aligned} \tag{49}$$

Now making use of the fact that x_B and x_S are independent random variables, we see that $\langle (x_B - \bar{x}_B)^2 (x_S - \bar{x}_S) \rangle$ and $\langle (x_B - \bar{x}_B)(x_S - \bar{x}_S)^2 \rangle$ must

vanish, so that Eq. (49) can be rewritten as

$$\mu_{3,T} = \langle (x_B - \bar{x}_B)^3 \rangle + \langle (x_S - \bar{x}_S)^3 \rangle \quad . \tag{50}$$

Using Eq.'s (33) and (41), we see that Eq. (50) can be recast in the form

$$\mu_{3,S} = \mu_{3,T} - \mu_{3,B} \quad . \tag{51}$$

To obtain an expression for $\mu_{4,S}$, we start with Eq. (38) and substitute Eq.'s (30) and (44), to yield

$$\begin{aligned} \mu_{4,T} &= \langle [x_B + x_S - (\bar{x}_B + \bar{x}_S)]^4 \rangle \\ &= \langle [(x_B - \bar{x}_B) + (x_S - \bar{x}_S)]^4 \rangle \\ &= \langle (x_B - \bar{x}_B)^4 \rangle + 4 \langle (x_B - \bar{x}_B)^3 (x_S - \bar{x}_S) \rangle + 6 \langle (x_B - \bar{x}_B)(x_S - \bar{x}_S) \rangle \\ &\quad + 4 \langle (x_B - \bar{x}_B)(x_S - \bar{x}_S)^3 \rangle \quad . \end{aligned} \tag{52}$$

Now if we again take note of the fact that x_B and x_S are independent random variables, we see that $\langle (x_B - \bar{x}_B)^3 (x_S - \bar{x}_S) \rangle$ and $\langle (x_B - \bar{x}_B)(x_S - \bar{x}_S)^3 \rangle$ vanish, while $\langle (x_B - \bar{x}_B)^2 (x_S - \bar{x}_S)^2 \rangle$ can, with the help of Eq.'s (32) and (40), be rewritten as

$$\begin{aligned} \langle (x_B - \bar{x}_B)^2 (x_S - \bar{x}_S)^2 \rangle &= \langle (x_B - \bar{x}_B)^2 \rangle \langle (x_S - \bar{x}_S)^2 \rangle \\ &= \sigma_B^2 \, \sigma_S^2 \quad . \end{aligned} \tag{53}$$

This, together with Eq.'s (34) and (42), allows us to rewrite Eq. (52) as

$$\mu_{4,T} = \mu_{4,B} + 6 \, \sigma_B^2 \, \sigma_S^2 + \mu_{4,S} \quad . \tag{54}$$

Solving for $\mu_{4,S}$, we get

$$\mu_{4,S} = \mu_{4,T} - \mu_{4,B} - 6 \, \sigma_B^2 \, \sigma_S^2 \quad . \tag{55}$$

Making use of Eq.'s (45), (48), (51), and (55), we have been able to calculate the four leading moments of the scintillation with background effects extracted. Starting with the data in Tables 4 and 7, and using these equations, we have generated the results shown in Table 8. The values in Table 8 represent, in a sense, the basic scintillation measurement values which we plan to use to compare measurement with theory. Actually, however, it is more convenient to work with the normalized moments, i.e., the central moments divided by the appropriate powers of the mean. We define the normalized second, third, and fourth central moments of the scintillation as

$$\Sigma = \sigma_s^2/(\overline{x}_s)^2 \quad , \tag{56}$$

$$M_3 = \mu_{3,s}/(\overline{x}_s)^3 \quad , \tag{57}$$

and

$$M_4 = \mu_{4,s}/(\overline{x}_s)^4 \quad , \tag{58}$$

respectively. In Table 9, we show the values of these normalized central moments as calculated from the data in Table 8. It is these values which we shall actually use in our comparison of measurement data with theory.

4.2 Comparison With Log-Normal Hypothesis

As noted earlier, we expect the laser beam scintillation to manifest a log-normal probability distribution. To test this hypothesis and, as in Section 3.2, to see if the data is significantly contaminated by non-propagation effects, we shall calculate the expected values of the normalized third and fourth moments from the normalized second moment, and compare these calculated values with the measurement values given in Table 9.

To obtain the expressions we shall need to calculate the normalized third and fourth central moments from the normalized second central moment, we proceed by considering a random variable x, distributed according to a

Table 8

Scintillation Run Moments With Background Effects Extracted

Run Number	Diameter (m)	Mean	Central Moments		
			Second	Third	Fourth
1	0.76	27.18	107.7	806.0	45080.
2	0.76	22.98	125.3	950.9	52830.
3	0.08	10.83	104.0	1261.	54950.
4	0.04	3.06	15.61	90.6	1406.
8	0.76	24.91	131.4	2157.	111800.
9	0.76	23.60	89.19	393.0	22920.
10	0.76	19.14	56.27	323.5	12370.
12	0.08	12.44	124.6	929.5	57620.
13	0.08	9.55	94.66	741.6	37520.
14	0.08	7.80	69.19	427.9	19740.
17	0.16	16.93	121.5	1060.	54200.
18	0.16	12.45	99.32	1233.	51433.
19	0.16	16.24	122.3	1183.	58810.
20	0.16	18.16	154.6	1657.	90590.
23	0.16	14.37	131.6	1833.	65070.
24	0.16	15.75	130.5	1588.	76280.
27	0.04	2.46	17.4	173.9	3011.
29	0.76	24.99	124.7	876.1	51960.
30	0.76	25.50	139.3	1077.	65080.
31	0.32	14.88	65.45	436.0	16820.
33	0.32	21.09	90.85	846.6	33300.
38	0.76	13.98	121.4	856.1	40420.
39	0.76	32.04	165.8	325.8	77020.
42	0.16	16.65	122.6	820.6	47640.
46	0.76	22.08	126.9	695.3	47090.

Table 8 (Continued) Page 2

Run Number	Diameter (m)	Mean	Central Moments		
			Second	Third	Fourth
47	0.76	21.19	94.01	663.7	33840.
48	0.32	13.56	105.2	934.0	42320.
49	0.32	12.97	101.1	1017.	44980.
52	0.08	2.57	19.94	187.9	2931.
53	0.16	3.86	60.96	1234.	35330.
54	0.16	4.60	71.76	1392.	40460.
57	0.32	11.02	119.7	1432.	56960.
58	0.32	10.05	104.5	1083.	39830.
59	0.76	18.03	141.1	972.4	62510.
61	0.76	18.89	142.5	1073.	68350.
62	0.76	16.97	126.1	1066.	60450.
64	0.76	20.72	148.2	954.1	67010.
66	0.76	13.92	118.4	1070.	48950.
67	0.76	12.93	105.1	915.7	40020.
69	0.76	10.13	87.49	954.8	37990.
70	0.76	10.55	89.09	828.5	30260.
71	0.76	7.43	52.98	438.6	10810.
75	0.76	8.82	12.32	716.2	7937.
76	0.76	8.90	9.25	691.2	5138.

Table 9

Scintillation Run Normalized Central Moments With Background Effects Extracted

Run Number	Diameter (m)	Normalized Central Moments		
		Second	Third	Fourth
1	0.76	0.1458	0.04014	0.08261
2	0.76	0.2373	0.07836	0.1894
3	0.08	0.8870	0.9925	3.994
4	0.04	1.667	3.162	16.03
8	0.76	0.2118	0.1395	0.2903
9	0.76	0.1601	0.02990	0.07390
10	0.76	0.1536	0.04614	0.09220
12	0.08	0.8049	0.4828	2.406
13	0.08	1.040	0.8514	4.511
14	0.08	1.137	0.9016	5.334
17	0.16	0.4240	0.2185	0.6597
18	0.16	0.6407	0.6389	2.141
19	0.16	0.4637	0.2761	0.8455
20	0.16	0.4688	0.2766	0.8329
23	0.16	0.6374	0.6179	1.995
24	0.16	0.5262	0.4066	1.240
27	0.04	2.875	11.68	82.22
29	0.76	0.1998	0.05614	0.1332
30	0.76	0.2143	0.06498	0.1539
31	0.32	0.2956	0.1323	0.3432
33	0.32	0.2043	0.09025	0.1683
38	0.76	0.6209	0.3133	1.058
39	0.76	0.1615	0.009904	0.07309
42	0.16	0.4422	0.1778	0.6199
46	0.76	0.2603	0.06459	0.1981

Table 9 (Continued)

Run Number	Diameter (m)	Normalized Central Moments		
		Second	Third	Fourth
47	0.76	0.2094	0.06975	0.1678
48	0.32	0.5721	0.3746	1.252
49	0.32	0.6010	0.4660	1.590
52	0.08	3.019	11.07	67.18
53	0.16	4.091	21.45	159.1
54	0.16	3.391	14.30	90.37
57	0.32	0.9853	1.070	3.863
58	0.32	1.034	1.067	3.904
59	0.76	0.4340	0.1659	0.5915
61	0.76	0.3993	0.1592	0.5368
62	0.76	0.4379	0.2180	0.7289
64	0.76	0.3453	0.1073	0.3636
66	0.76	0.6110	0.3966	1.304
67	0.76	0.6286	0.4236	1.432
69	0.76	0.8526	0.9185	3.608
70	0.76	0.8004	0.7056	2.443
71	0.76	0.9597	1.069	3.547
75	0.76	0.1584	1.044	1.312
76	0.76	0.1168	0.9805	0.8189

log-normal distribution. If we define the random variable L by the relationship

$$L = \ell n\,(x/\bar{x}) \quad , \tag{59}$$

where

$$\bar{x} = \langle x \rangle \quad , \tag{60}$$

so that

$$x = \bar{x} \exp\,(L) \quad , \tag{61}$$

then L is a gaussian random variable.

We note first that if we substitute Eq. (61) into Eq. (60) and make use of the fact that for χ a gaussian random variable

$$\langle \exp\,(\chi) \rangle = \exp\,[-\langle \chi \rangle]\, \exp\,[\tfrac{1}{2} \langle (\chi - \bar{\chi})^2 \rangle] \quad , \tag{62}$$

(which can be demonstrated by carrying out the ensemble average as an integration of the exponential times a gaussian probability density weighting), then it follows that

$$\begin{aligned} 1 &= \langle \exp\,(L) \rangle \\ &= \exp\,(\bar{L} + \tfrac{1}{2}\, \sigma_L{}^2) \quad , \end{aligned} \tag{63}$$

so that

$$\bar{L} = -\tfrac{1}{2}\, \sigma_L{}^2 \quad . \tag{64}$$

Here

$$\bar{L} = \langle L \rangle \tag{65}$$

and

$$\sigma_L{}^2 = \langle (L - \bar{L})^2 \rangle \quad . \tag{66}$$

The normalized second central moment of x can be written as

$$\Sigma_x = \langle (x - \bar{x})^2 \rangle / \bar{x}^2$$
$$= \langle [\exp(L) - 1]^2 \rangle$$
$$= \langle \exp(2L) \rangle - 2 \langle \exp(L) \rangle + 1 \quad . \tag{67}$$

Making use of Eq.'s (62) and (64), we see that

$$\langle \exp(2L) \rangle = \exp(2\bar{L}) \exp(2\sigma_L^2)$$
$$= \exp(\sigma_L^2) \quad , \tag{68}$$

while

$$\langle \exp(L) \rangle = \exp(\bar{L}) \exp(\tfrac{1}{2}\sigma_L^2)$$
$$= 1 \quad . \tag{69}$$

Making use of Eq.'s (68) and (69), we can rewrite Eq. (67) as

$$\Sigma_x = \exp(\sigma_L^2) - 1 \quad , \tag{70}$$

so that

$$\exp(\sigma_L^2) = \Sigma_x + 1 \quad . \tag{71}$$

The normalized third central moment of x can be written as

$$M_{3,x} = \langle (x - \bar{x})^3 \rangle / \bar{x}^3$$
$$= \langle [\exp(L) - 1]^3 \rangle$$
$$= \langle \exp(3L) \rangle - 3 \langle \exp(2L) \rangle + 3 \langle \exp(L) \rangle - 1 \quad . \tag{72}$$

Making use of Eq.'s (62) and (64), we can write

$$\langle \exp(3L) \rangle = \exp(3\bar{L}) \exp(4.5\sigma_L^2)$$
$$= \exp(3\sigma_L^2) \quad . \tag{73}$$

If we substitute Eq.'s (68), (69), and (73) into Eq. (72), we get

$$M_{3,x} = \exp(3\sigma_L^2) - 3\exp(\sigma_L^2) + 2 \quad , \tag{74}$$

and now making use of Eq. (71), we can cast this result in the form

$$\begin{aligned} M_{3,x} &= (\Sigma_x + 1)^3 - 3(\Sigma_x + 1) + 2 \\ &= (\Sigma_x)^3 + 3(\Sigma_x)^2 + 3(\Sigma_x) + 1 - 3(\Sigma_x) - 3 + 2 \\ &= (\Sigma_x)^3 + 3(\Sigma_x)^2 \quad . \end{aligned} \tag{75}$$

Eq. (75) represents the desired relationship between the normalized second central moment and the normalized third central moment for a log-normal random variable.

The normalized fourth central moment of x can be written as

$$\begin{aligned} M_{4,x} &= \langle (x - \bar{x})^4 \rangle / \bar{x}^4 \\ &= \langle [\exp(L) - 1]^4 \rangle \\ &= \langle \exp(4L) \rangle - 4\langle \exp(3L) \rangle + 6\langle \exp(2L) \rangle \\ &\qquad - 4\langle \exp(L) \rangle + 1 \quad . \end{aligned} \tag{76}$$

Making use of Eq.'s (62) and (64), we can write

$$\begin{aligned} \langle \exp(4L) \rangle &= \exp(4\bar{L}) \exp(8\sigma_L^2) \\ &= \exp(6\sigma_L^2) \quad . \end{aligned} \tag{77}$$

If we substitute Eq.'s (68), (69), (73), and (77) into Eq. (76), we get

$$M_{4,x} = \exp(6\sigma_L^2) - 4\exp(3\sigma_L^2) + 6\exp(\sigma_L^2) - 3 \quad , \tag{78}$$

and now making use of Eq. (71), we can cast this result in the form

$$M_{4,x} = (\Sigma_x + 1)^6 - 4\,(\Sigma_x + 1)^3 + 6\,(\Sigma_x + 1) - 3$$

$$= (\Sigma_x)^6 + 6\,(\Sigma_x)^5 + 15(\Sigma_x)^4 + 20(\Sigma_x)^3 + 15(\Sigma_x)^2 + 6(\Sigma_x) + 1$$

$$- 4\,[(\Sigma_x)^3 + 3(\Sigma_x)^2 + 3(\Sigma_x) + 1] + 6\,[(\Sigma_x) + 1] - 3$$

$$= (\Sigma_x)^6 + 6(\Sigma_x)^5 + 15(\Sigma_x)^4 + 16(\Sigma_x)^3 + 3(\Sigma_x)^2 \quad . \qquad (79)$$

Eq. (79) represents the desired relationship between the normalized second central moment and the normalized fourth central moment for a log-normal random variable.

Making use of Eq.'s (75) and (79), we have used the normalized second central moments of the scintillation runs to calculate expected normalized third and fourth central moments based on the assumption that the scintillation data has a perfect log-normal distribution. These calculated values, along with the actual measured values as given in Table 9, are shown in Table 10. From a comparison between the actual measured normalized third and fourth central moments with the values calculated based on the log-normal hypothesis as shown in Table 10, we can see that the scintillation signal apparently can not be categorized as accurately following a log-normal distribution.

As before in the examination of the background data, we consider that the problem is possibly due to the inability of the data channel to properly handle the extremum values. This could be due to data channel introduced noise at the low end, or to saturation or infrequent spiking noise at the high end. In any case, we should be able to see such effects from an examination of a plot of the cumulative probability density. In Fig.'s 28 to 71, we have plotted the cumulative probability distribution for each of the 44 scintillation data runs on log-normal probability paper. (The signal magnitude is plotted on a logarithmic scale and the cumulative probability

Table 10

Comparison of Measured and Computed Normalized Third and Fourth Central Moments for Scintillation Runs

Run Number	Diameter (m)	Normalized Central Moments			
		Measured		Computed	
		Third	Fourth	Third	Fourth
1	0.76	0.04014	0.08261	0.06690	0.1206
2	0.76	0.07836	0.1894	0.1823	0.4352
3	0.08	0.9925	3.994	3.058	26.59
4	0.04	3.162	16.03	12.97	297.1
8	0.76	0.1395	0.2903	0.1441	0.3195
9	0.76	0.02990	0.07390	0.08104	0.1531
10	0.76	0.04614	0.09220	0.07440	0.1376
12	0.08	0.4828	2.406	2.465	18.88
13	0.08	0.8514	4.511	4.350	47.01
14	0.08	0.9016	5.334	5.351	66.08
17	0.16	0.2185	0.6597	0.6155	2.331
18	0.16	0.6389	2.141	1.495	8.686
19	0.16	0.2761	0.8455	0.7448	3.073
20	0.16	0.2766	0.8329	0.7623	3.179
23	0.16	0.6179	1.995	1.478	8.538
24	0.16	0.4066	1.240	0.9763	4.575
27	0.04	11.68	82.22	48.57	3174.
29	0.76	0.05614	0.1332	0.1277	0.2731
30	0.76	0.06498	0.1539	0.1476	0.3297
31	0.32	0.1323	0.3432	0.2880	0.8041
33	0.32	0.09025	0.1683	0.1337	0.2898
38	0.76	0.3133	1.058	1.396	7.827
39	0.76	0.009904	0.07309	0.08251	0.1566
42	0.16	0.1778	0.6199	0.6730	2.652

Table 10 (Continued) Page 2

Run Number	Diameter (m)	Normalized Central Moments			
		Measured		Computed	
		Third	Fourth	Third	Fourth
46	0.76	0.06459	0.1981	0.2209	0.5619
47	0.76	0.06975	0.1678	0.1407	0.3100
48	0.32	0.3746	1.252	1.169	5.989
49	0.32	0.4660	1.590	1.301	7.031
52	0.08	11.07	67.18	54.86	3975.
53	0.16	21.45	159.1	118.7	16920.
54	0.16	14.30	90.37	73.51	6855.
57	0.32	1.070	3.863	3.869	38.83
58	0.32	1.067	3.904	4.314	46.38
59	0.76	0.1659	0.5915	0.6468	2.504
61	0.76	0.1592	0.5368	0.5420	1.943
62	0.76	0.2180	0.7289	0.6594	2.575
64	0.76	0.1073	0.3636	0.3988	1.260
66	0.76	0.3966	1.304	1.348	7.423
67	0.76	0.4236	1.432	1.434	8.151
69	0.76	0.9185	3.608	2.800	23.11
70	0.76	0.7056	2.443	2.435	18.52
71	0.76	1.069	3.547	3.647	35.30
75	0.76	1.044	1.312	0.07922	0.1488
76	0.76	0.9805	0.8189	0.04250	0.06931

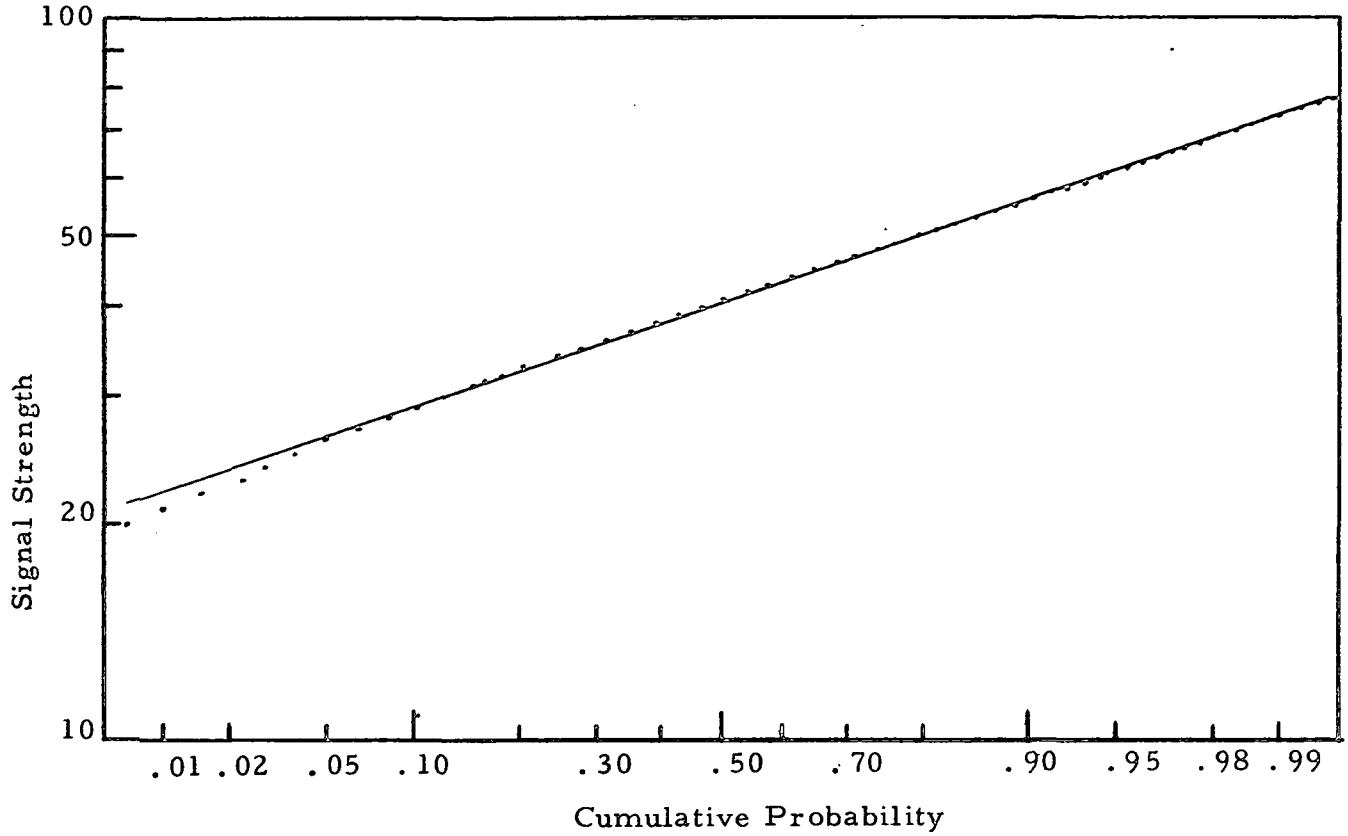

Figure 28. Signal Probability Distribution for Run #1.

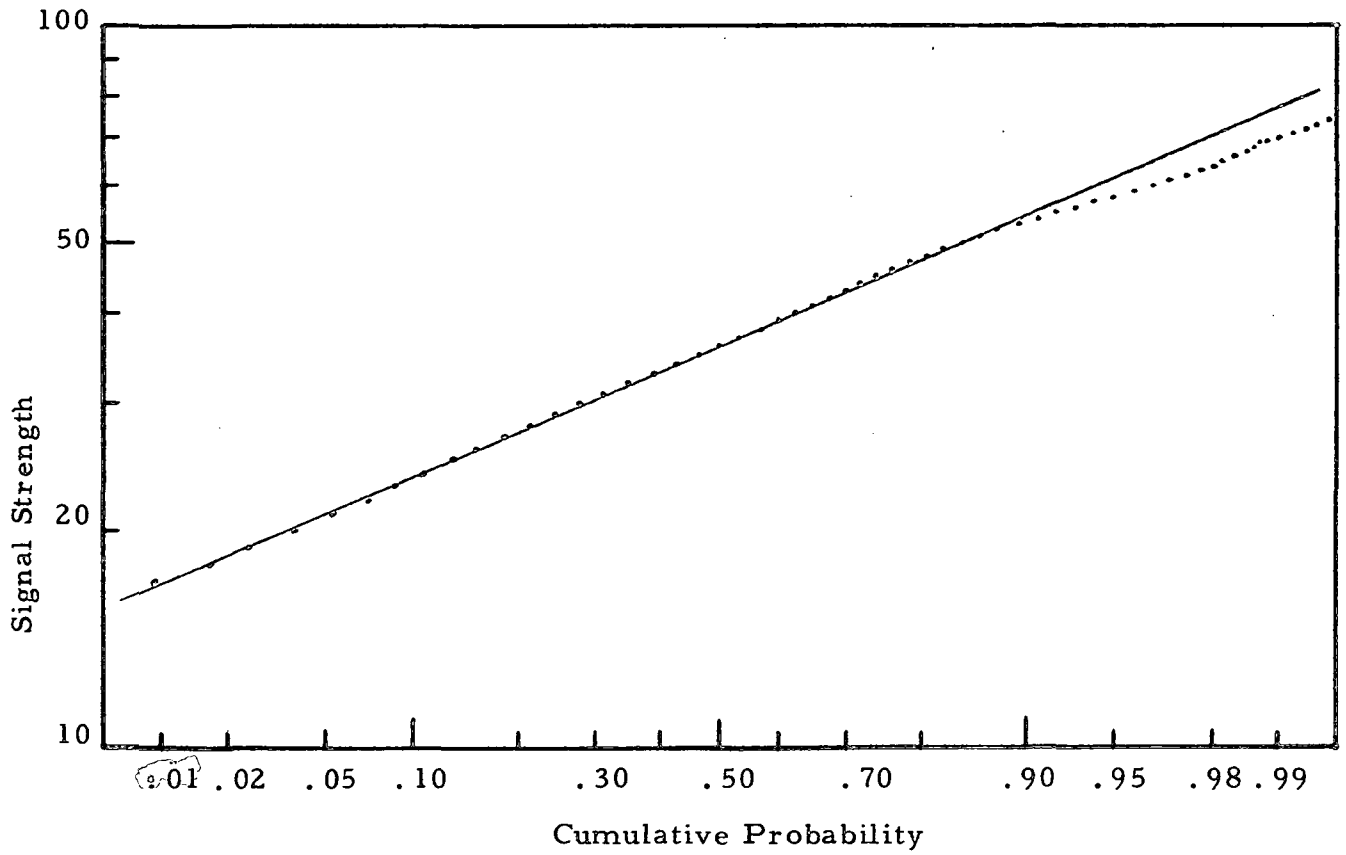

Figure 29. Signal Probability Distribution for Run #2.

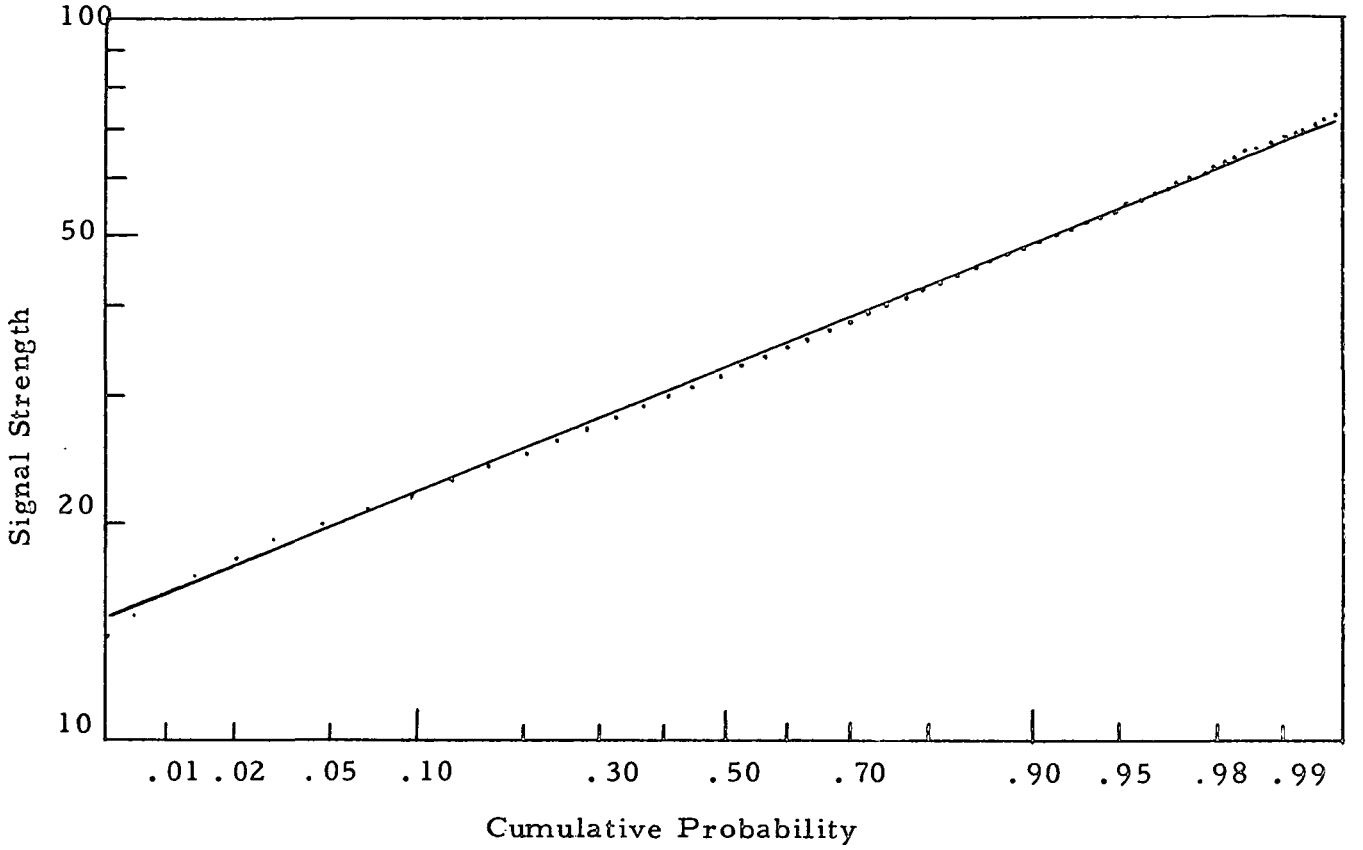

Figure 30. Signal Probability Distribution for Run #3.

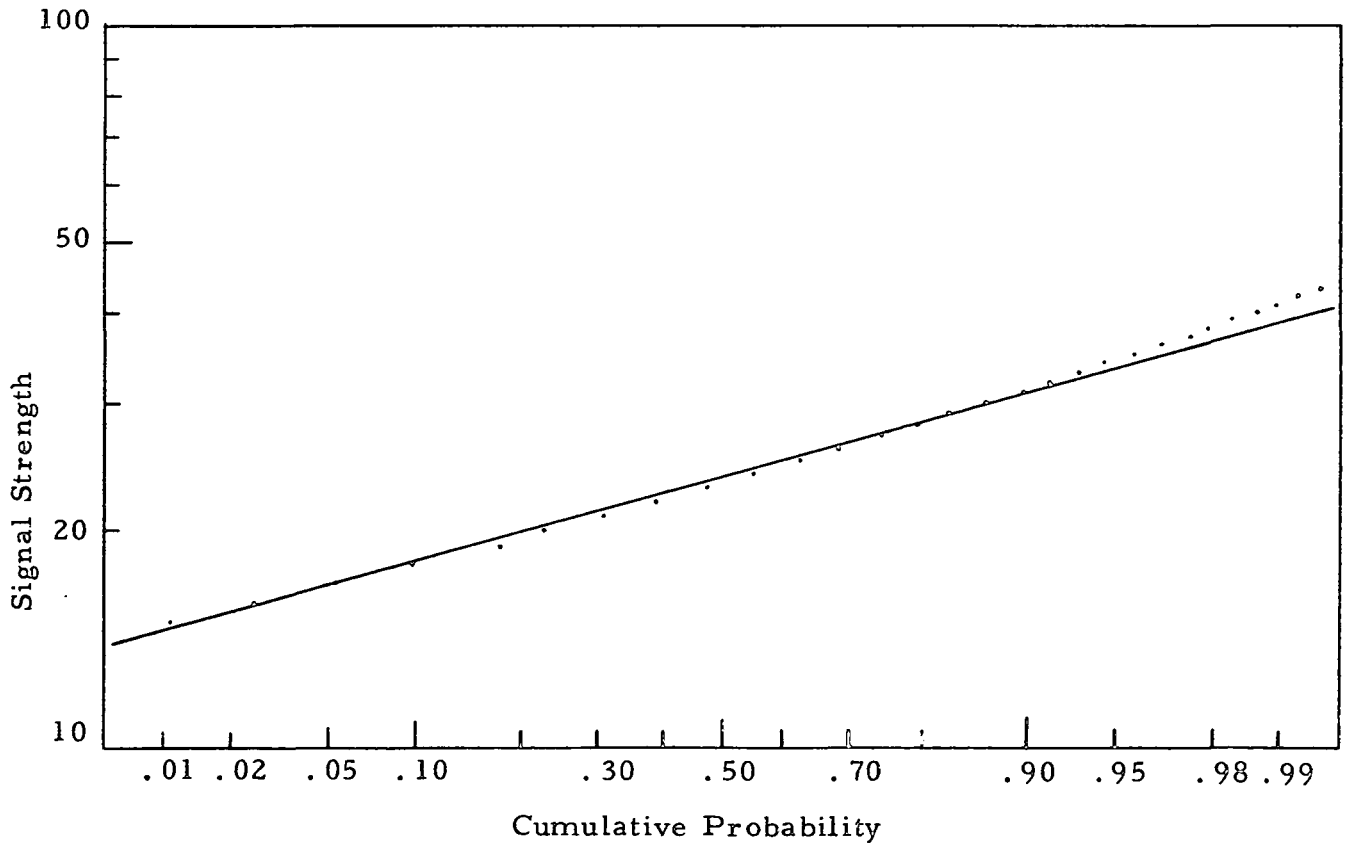

Figure 31. Signal Probability Distribution for Run #4.

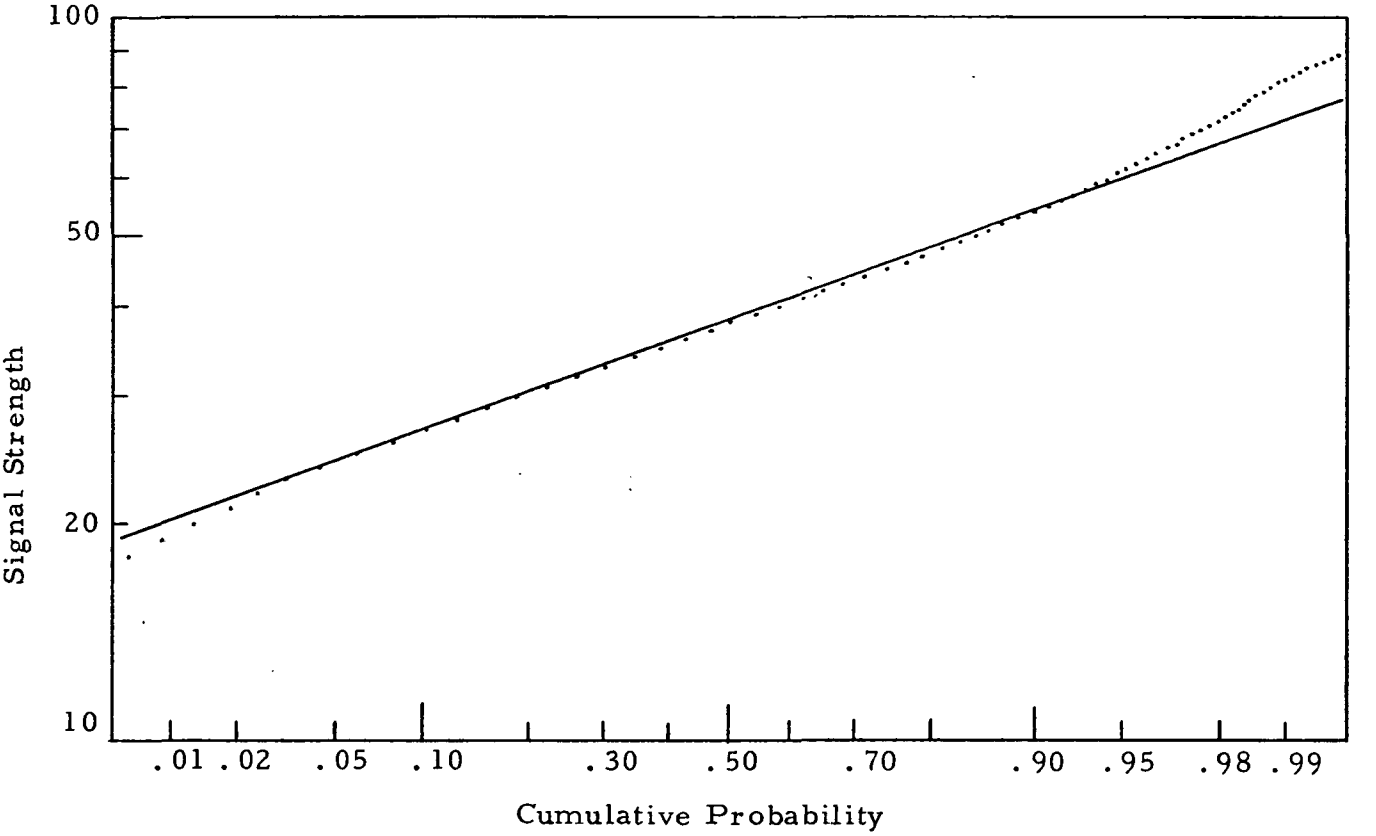

Figure 32. Signal Probability Distribution for Run #8.

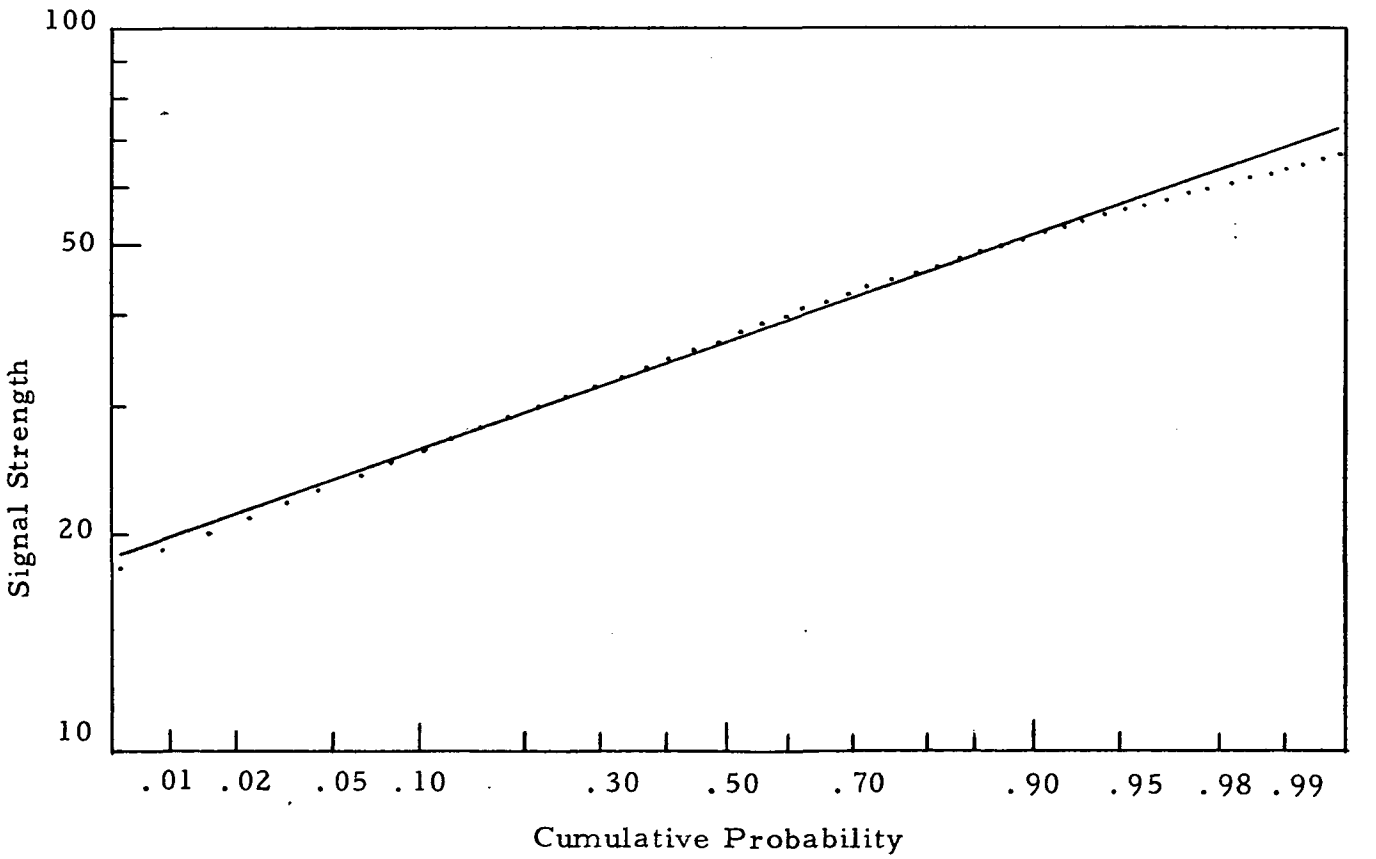

Figure 33. Signal Probability Distribution for Run #9.

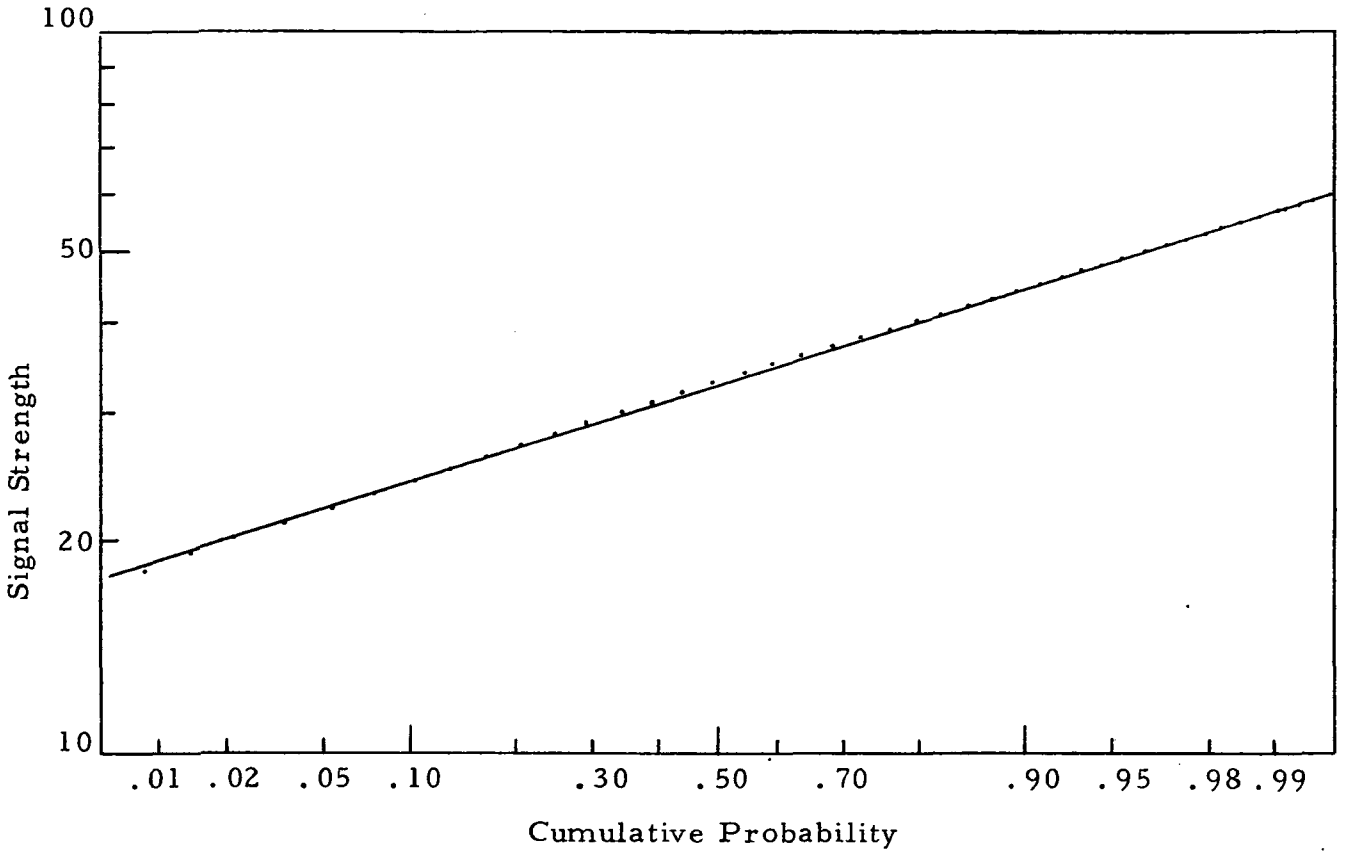

Figure 34. Signal Probability Distribution for Run #10.

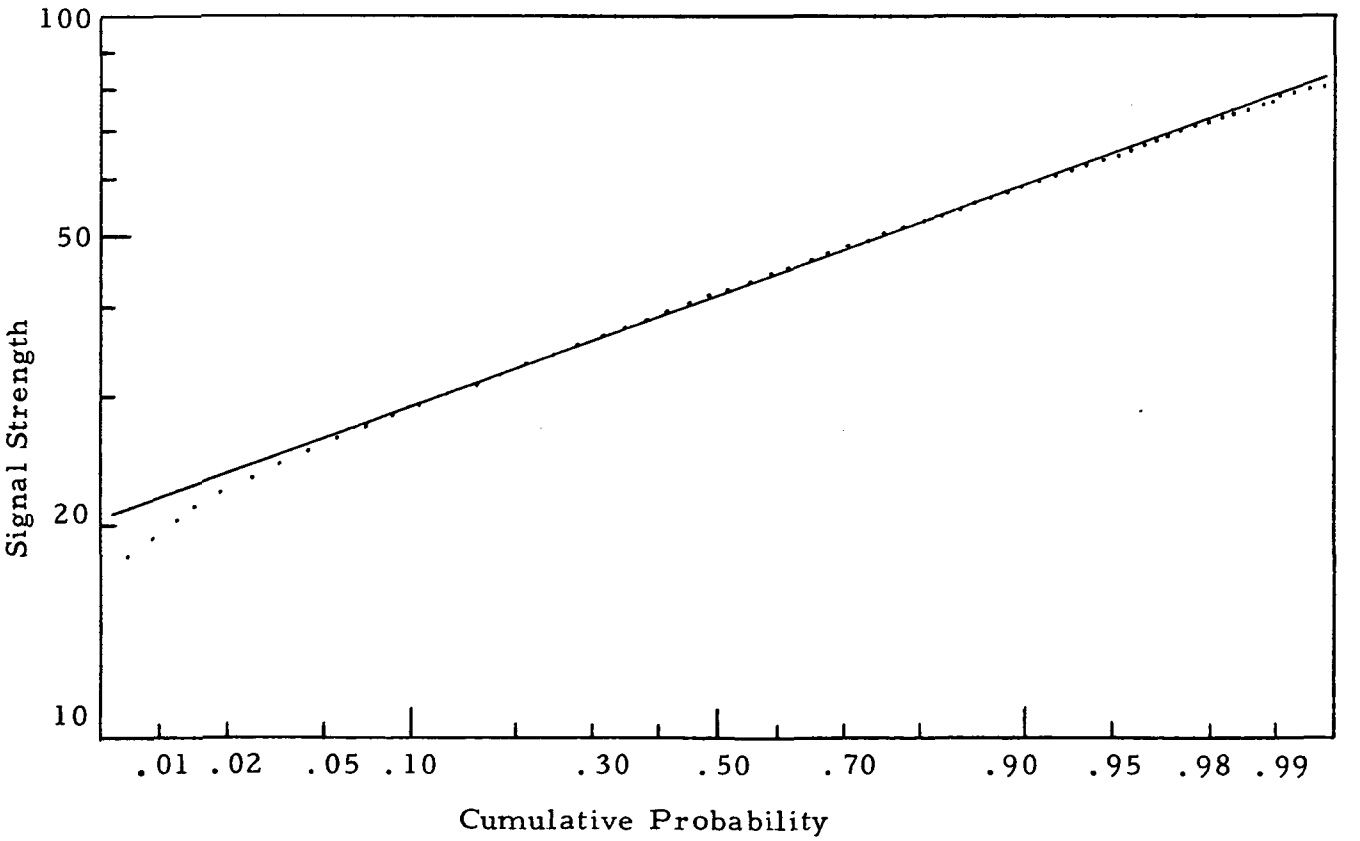

Figure 35. Signal Probability Distribution for Run #12.

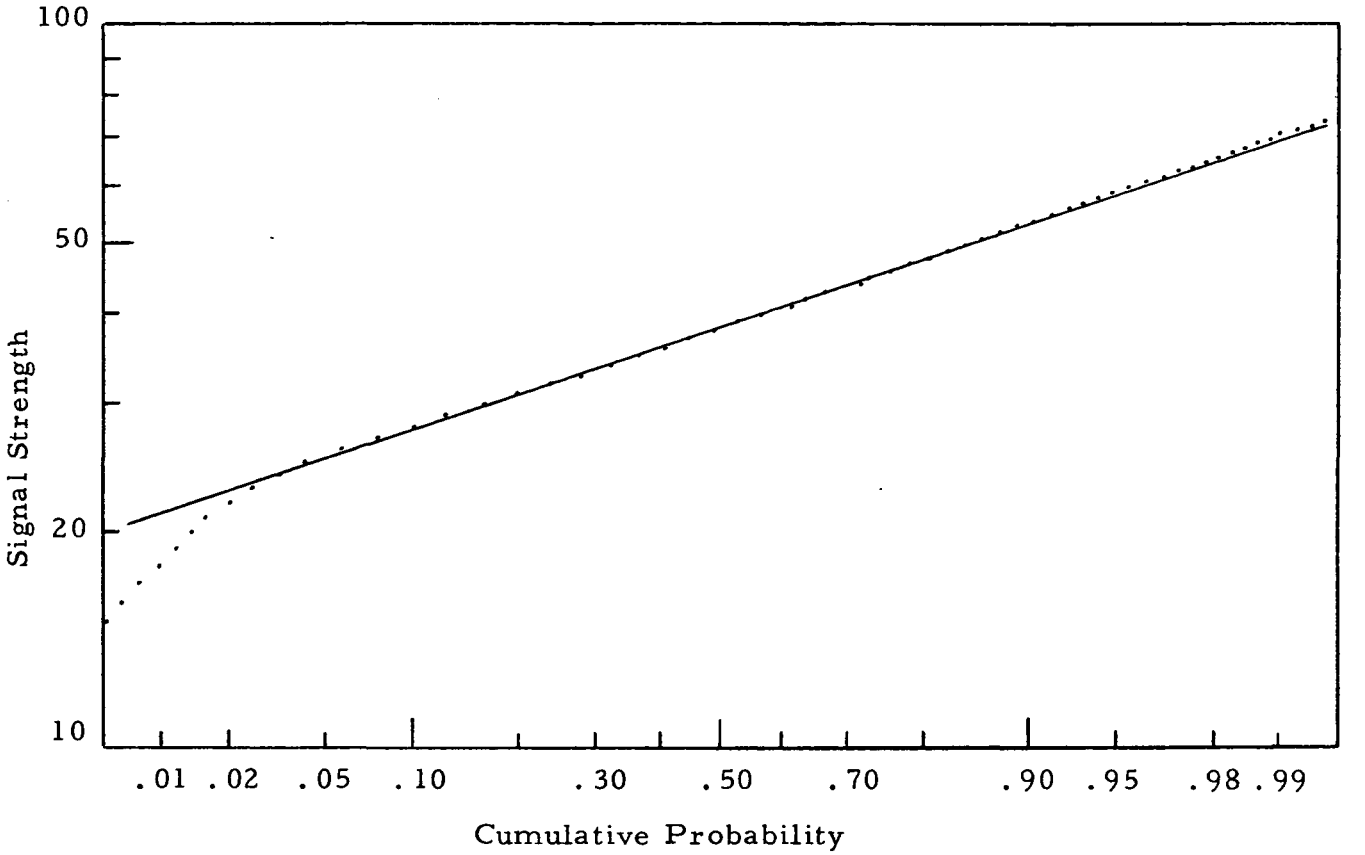

Figure 36. Signal Probability Distribution for Run #13.

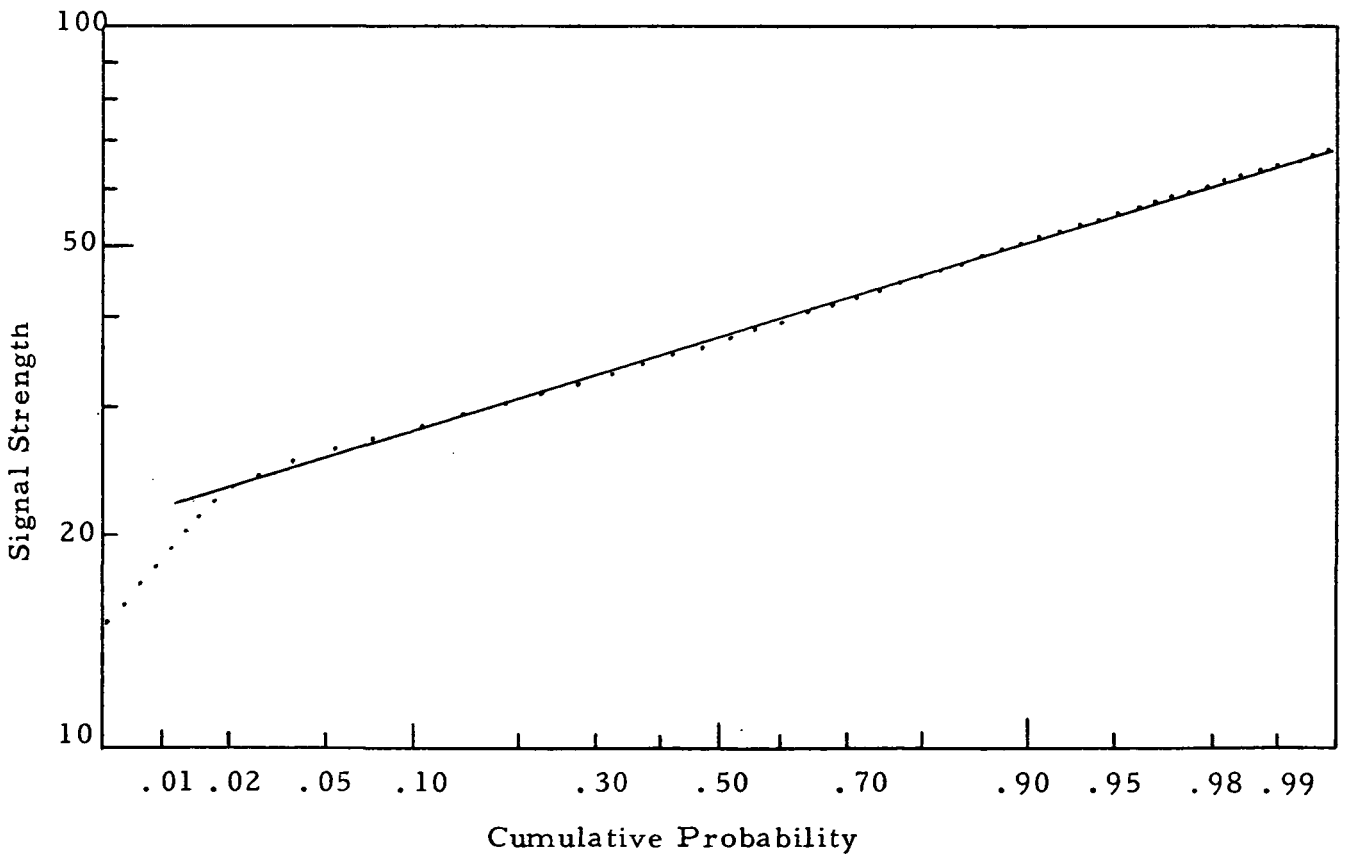

Figure 37. Signal Probability Distribution for Run #14.

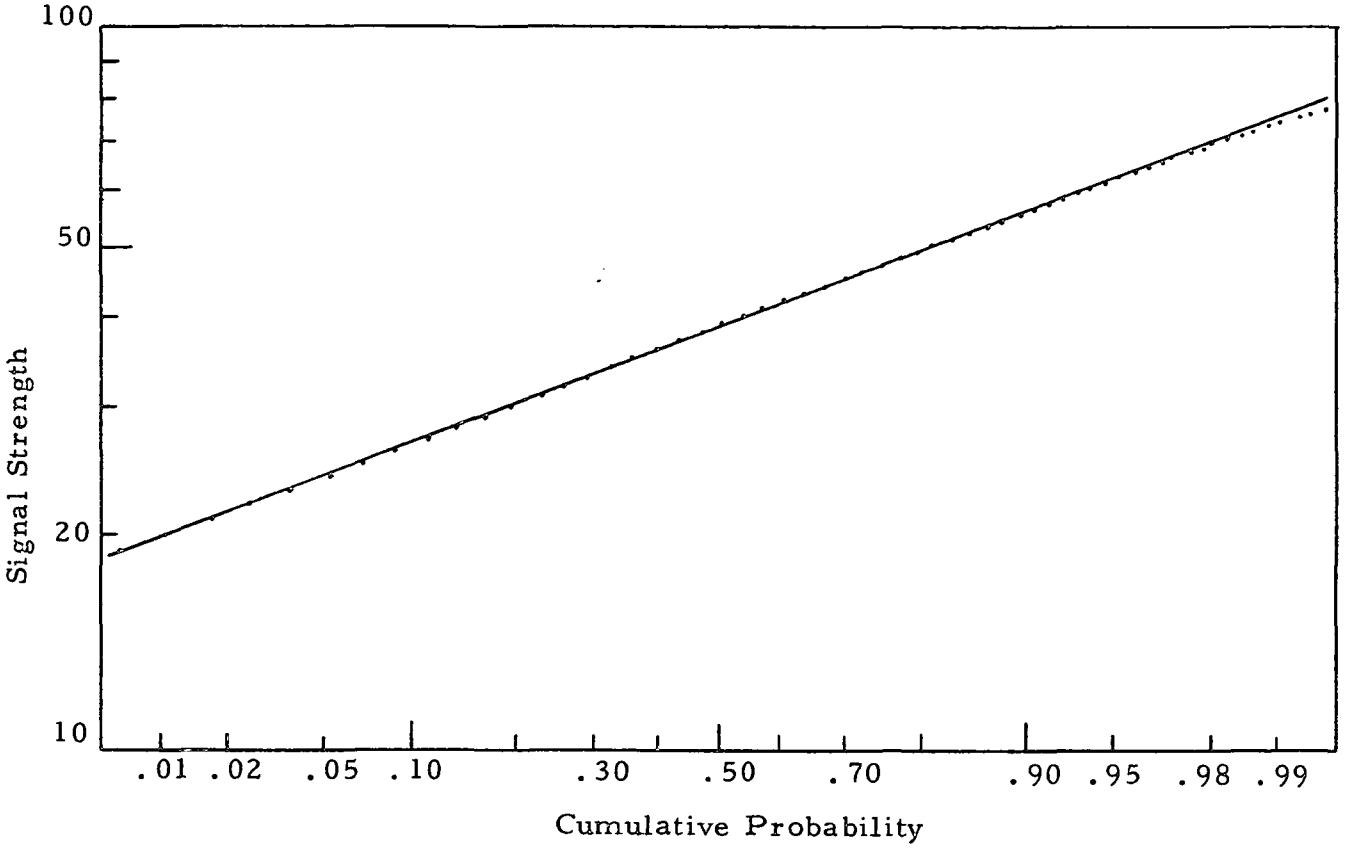

Figure 38. Signal Probability Distribution for Run #17.

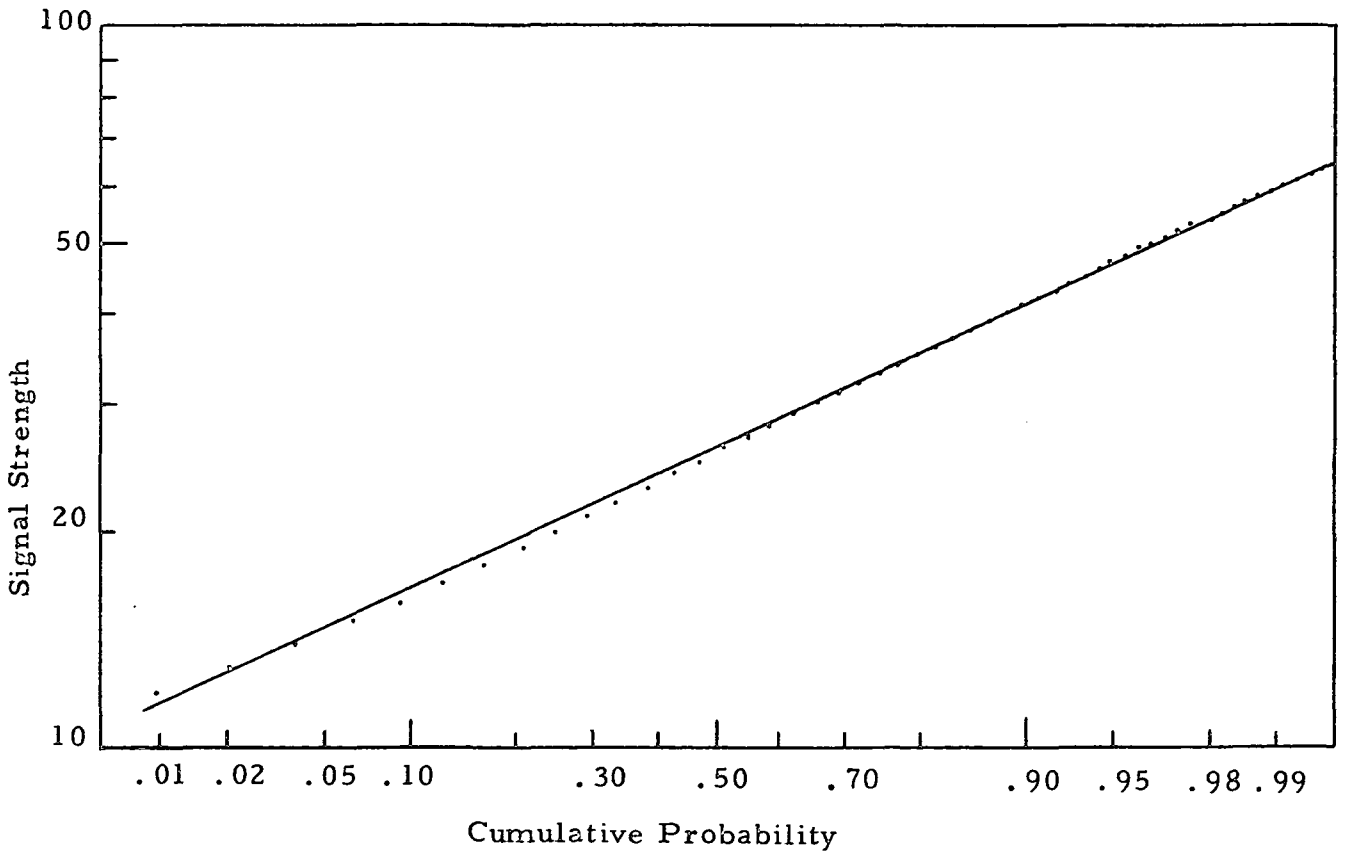

Figure 39. Signal Probability Distribution for Run #18.

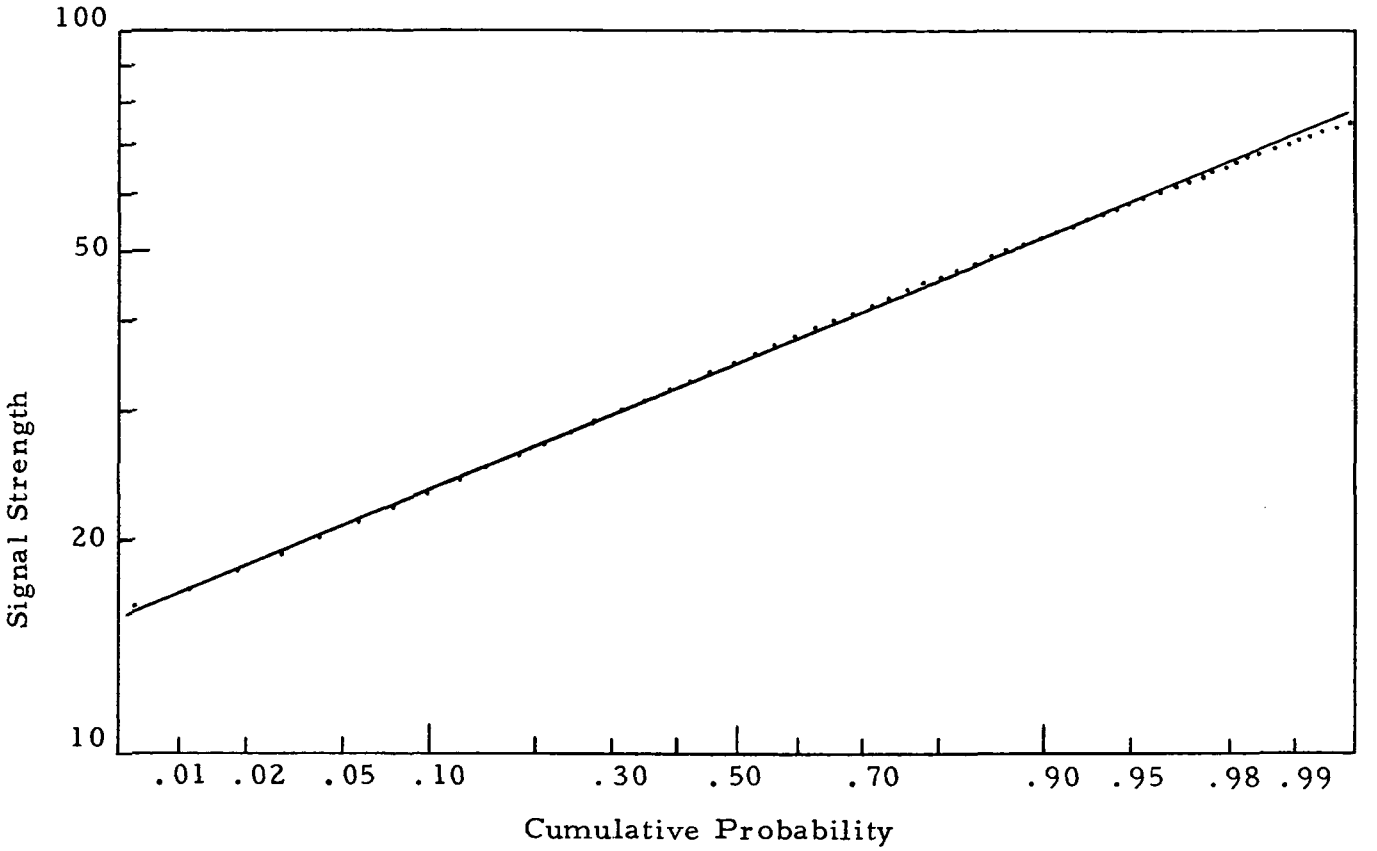

Figure 40. Signal Probability Distribution for Run #19.

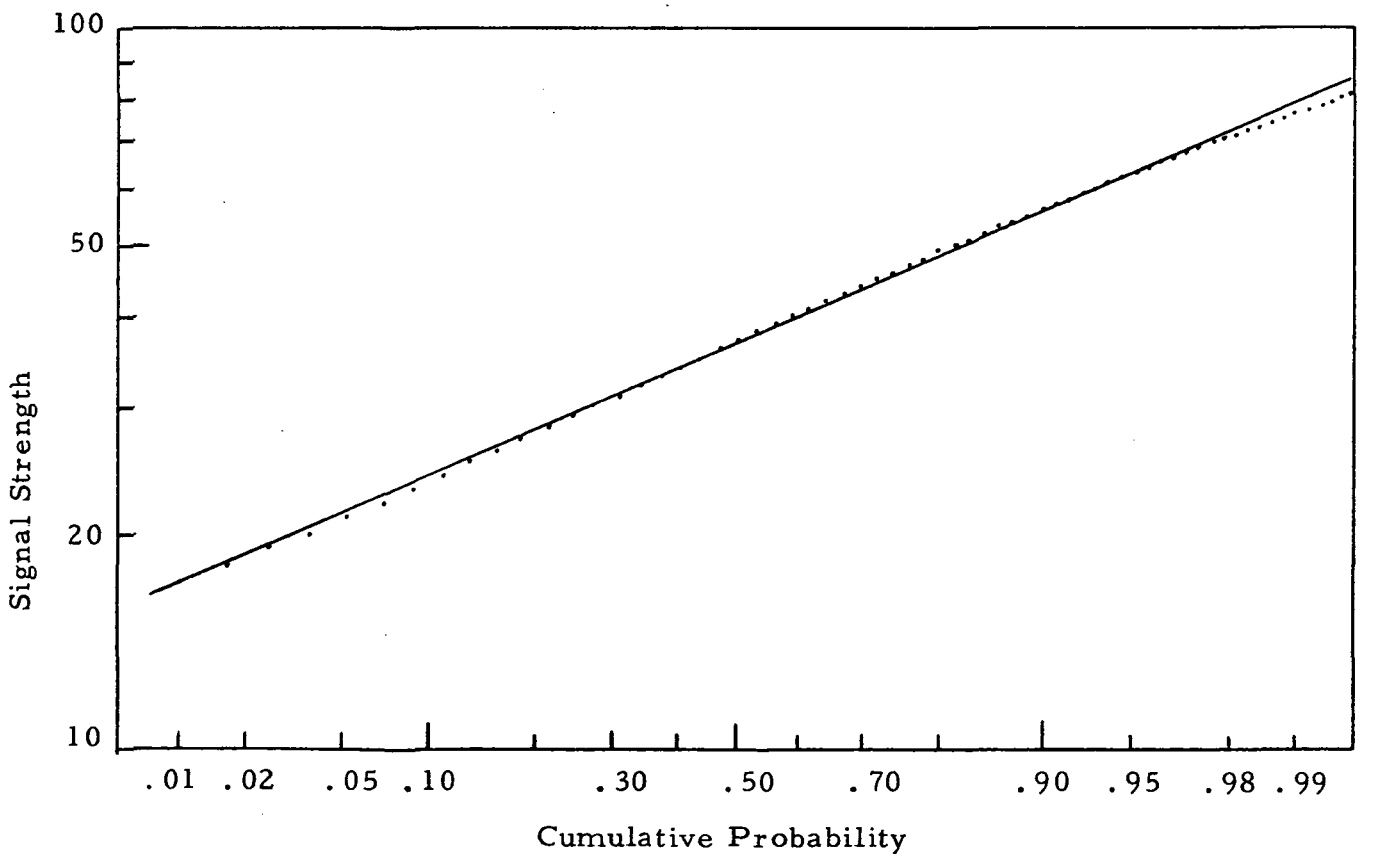

Figure 41. Signal Probability Distribution for Run #20.

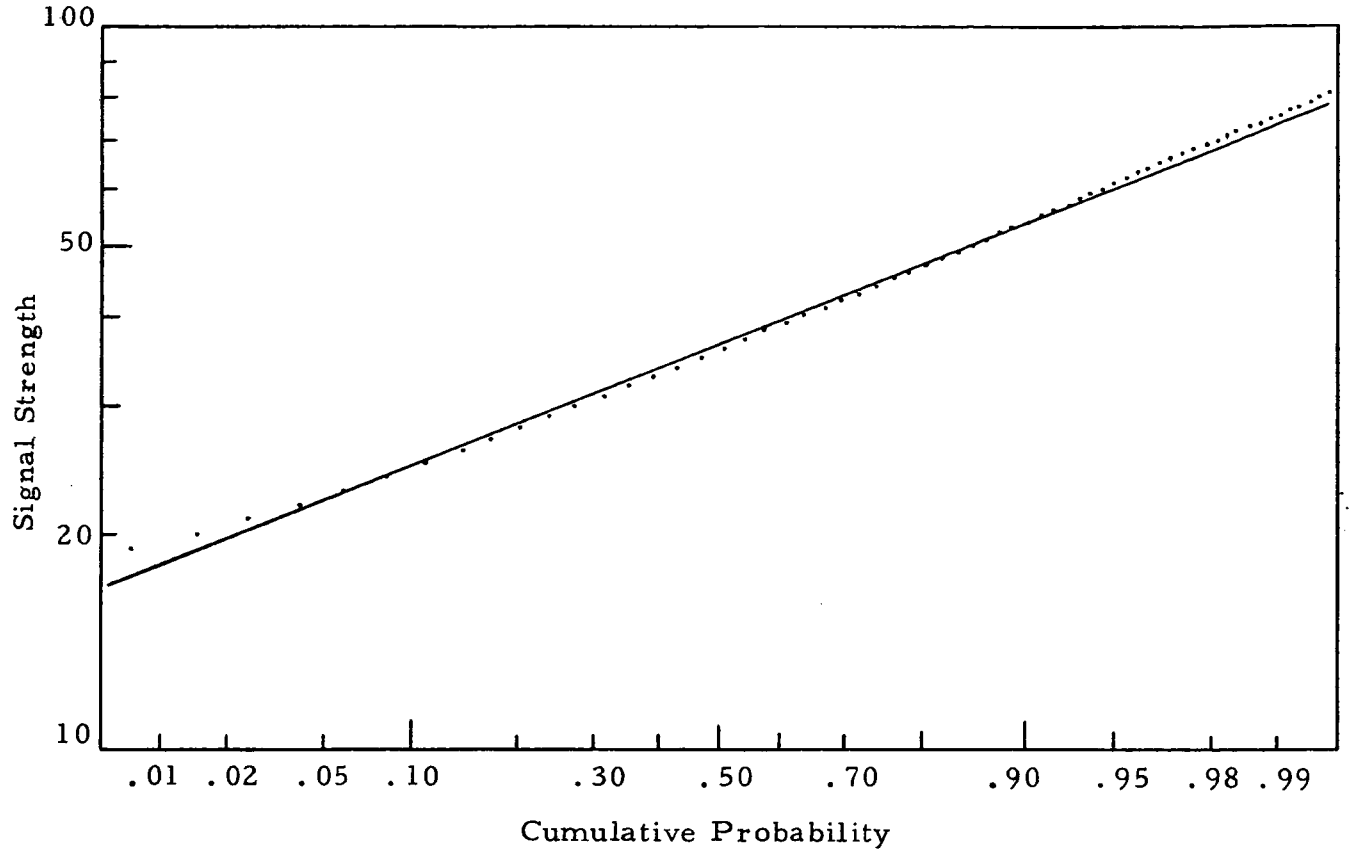

Figure 42. Signal Probability Distribution for Run #23.

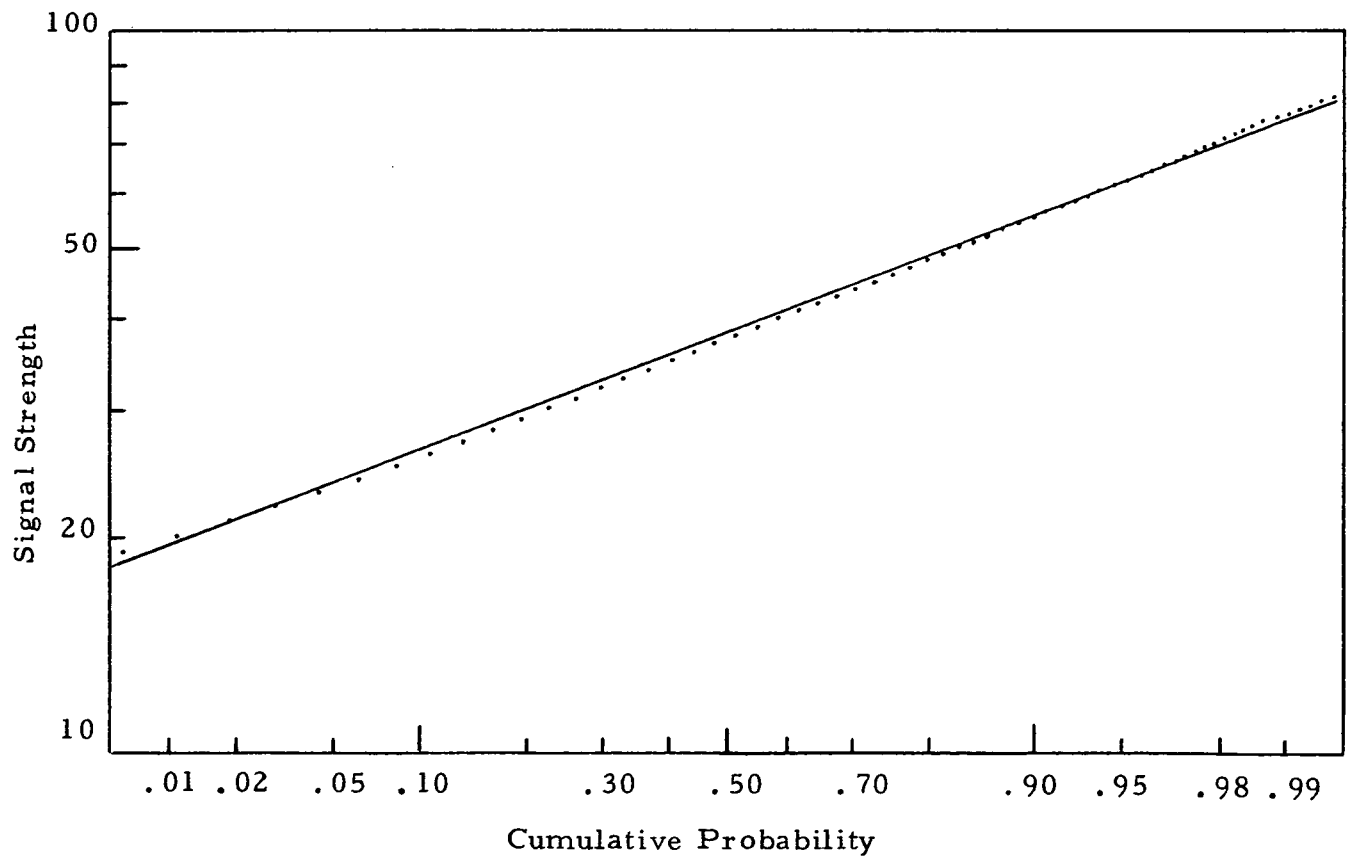

Figure 43. Signal Probability Distribution for Run #24.

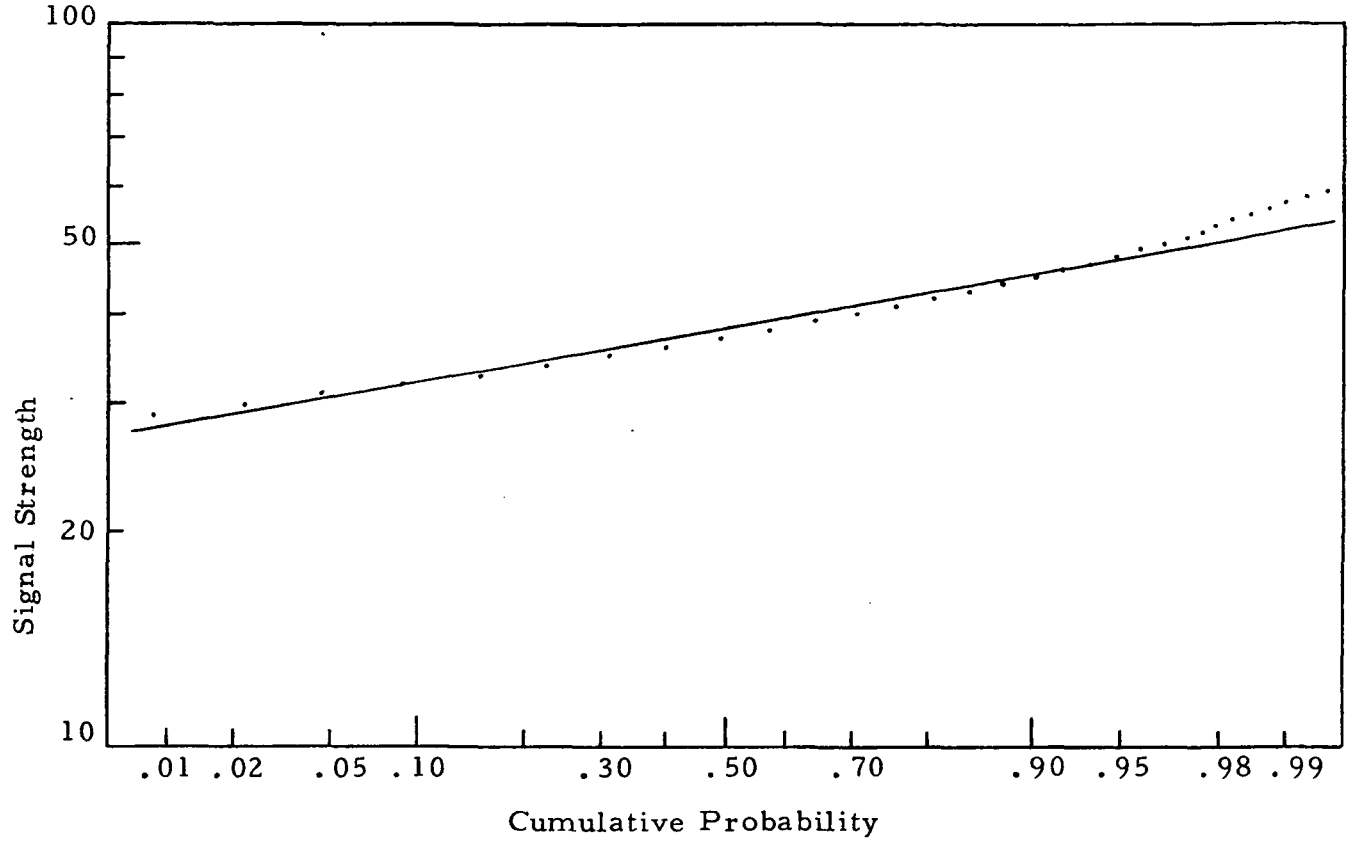

Figure 44. Signal Probability Distribution for Run #27.

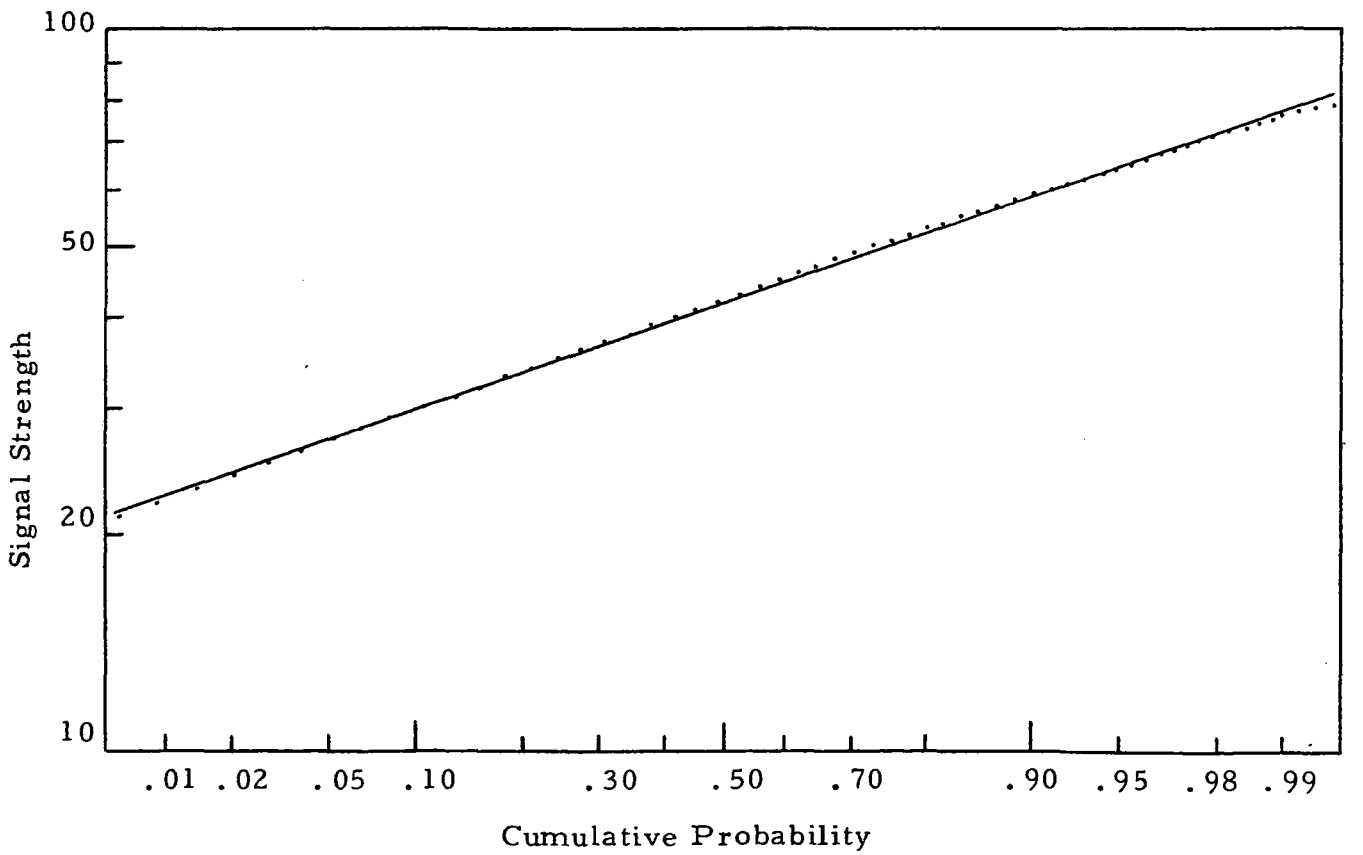

Figure 45. Signal Probability Distribution for Run #29.

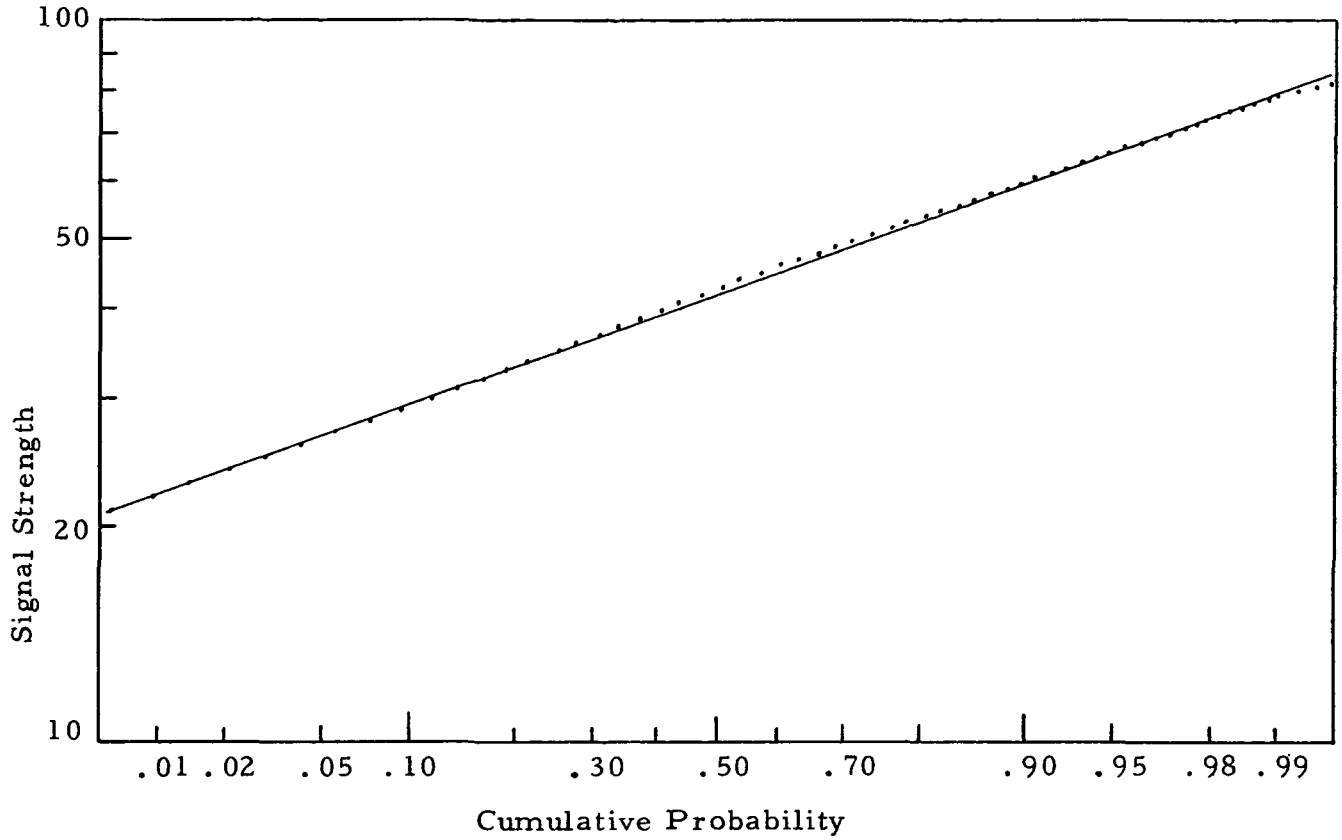

Figure 46. Signal Probability Distribution for Run #30.

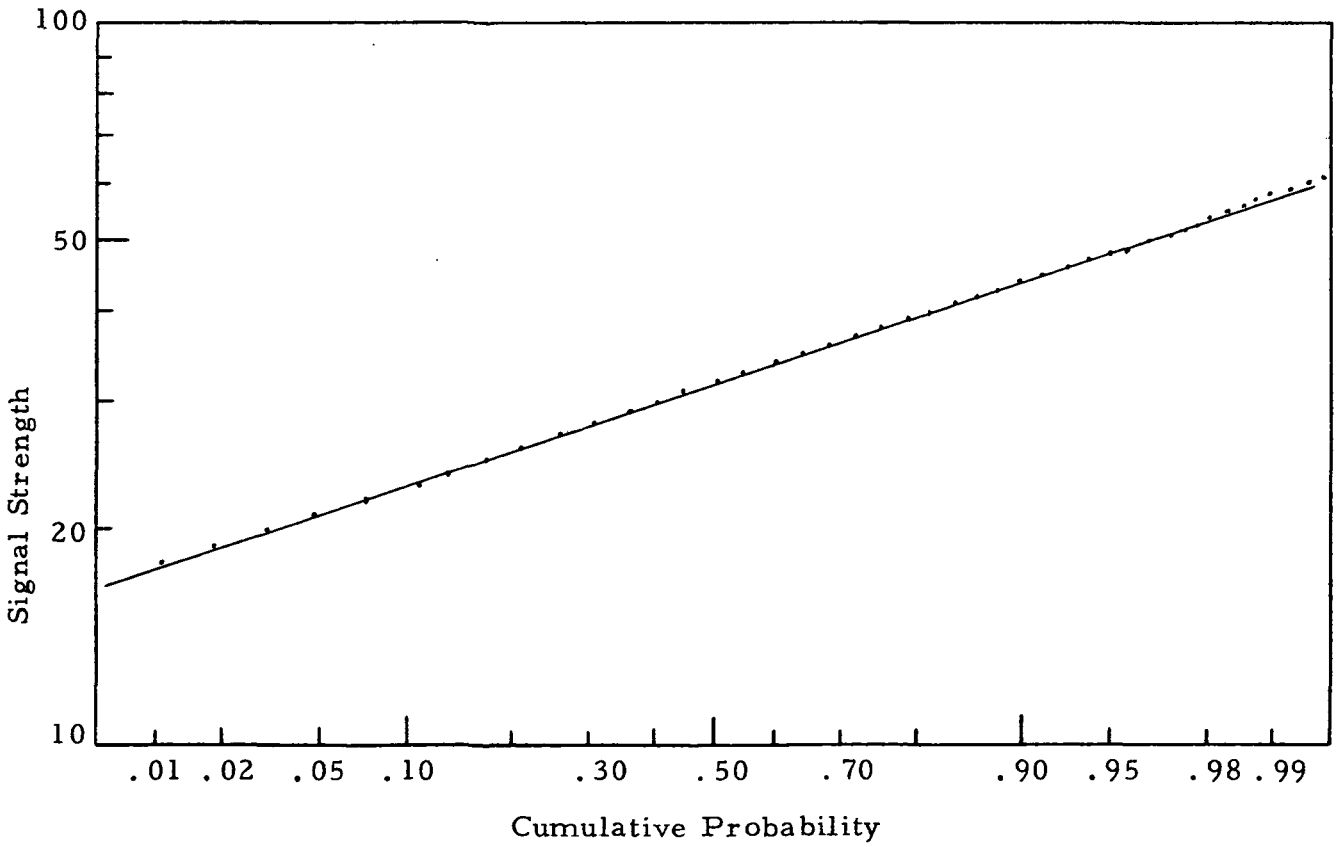

Figure 47. Signal Probability Distribution for Run #31.

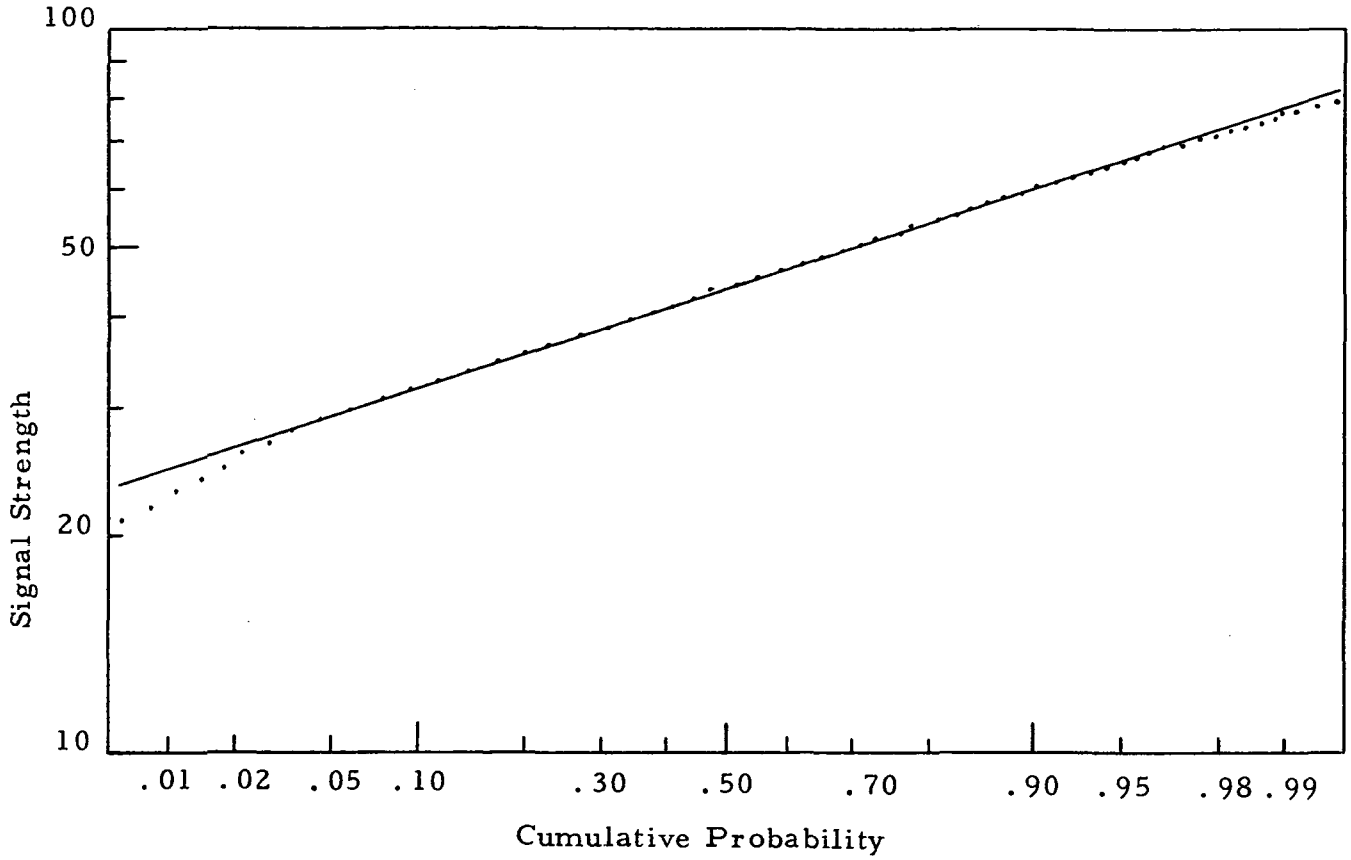

Figure 48. Signal Probability Distribution for Run #33.

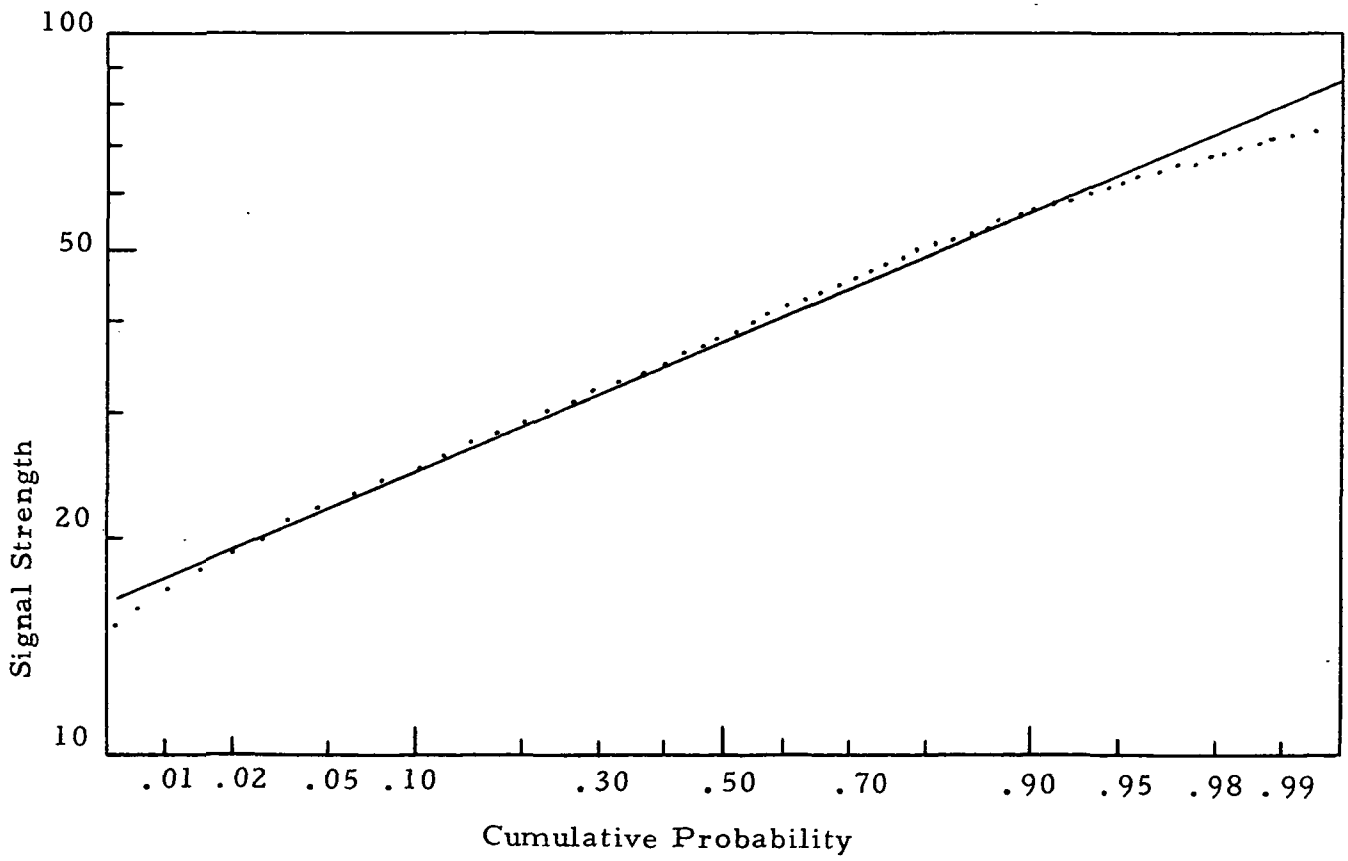

Figure 49. Signal Probability Distribution for Run #38.

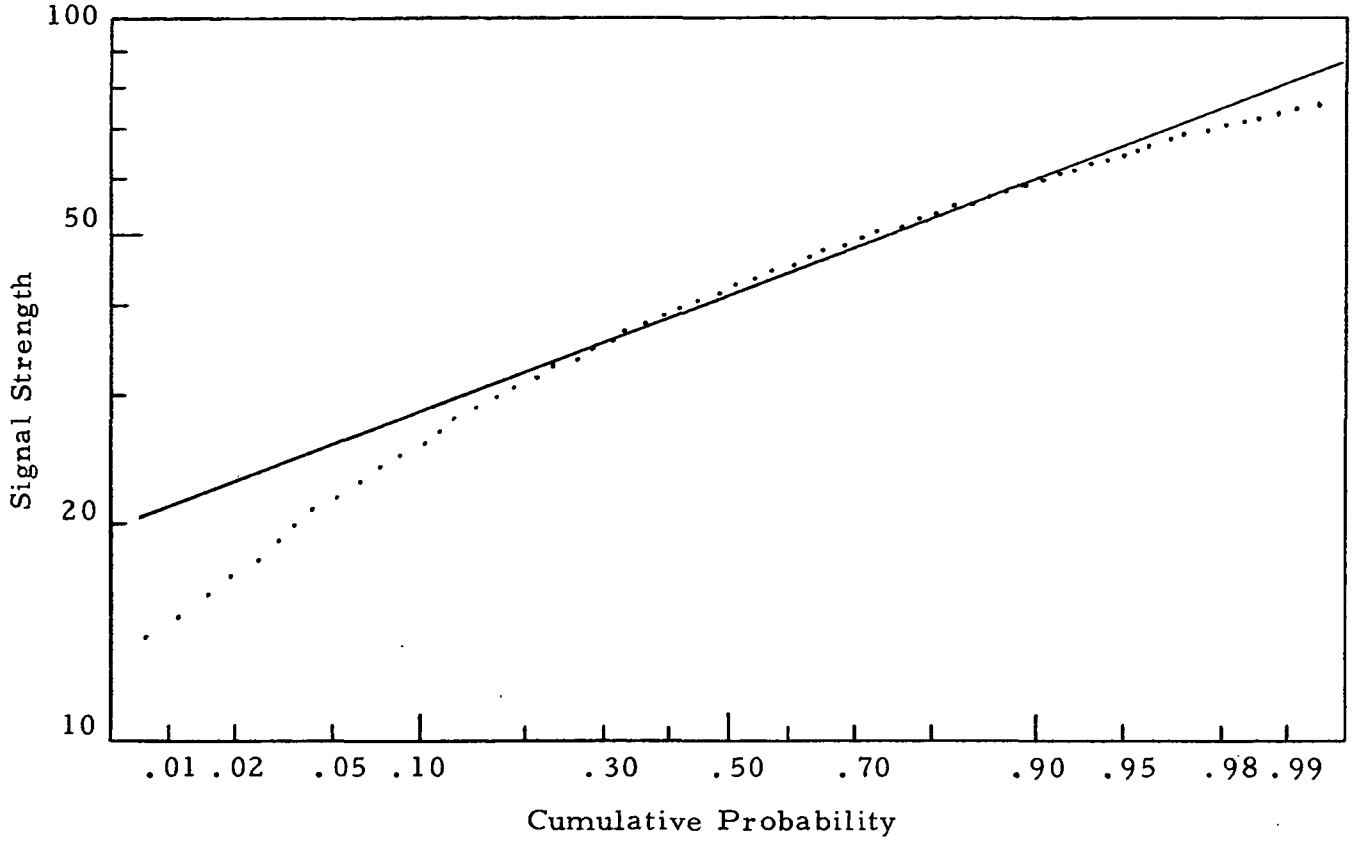

Figure 50. Signal Probability Distribution for Run #39.

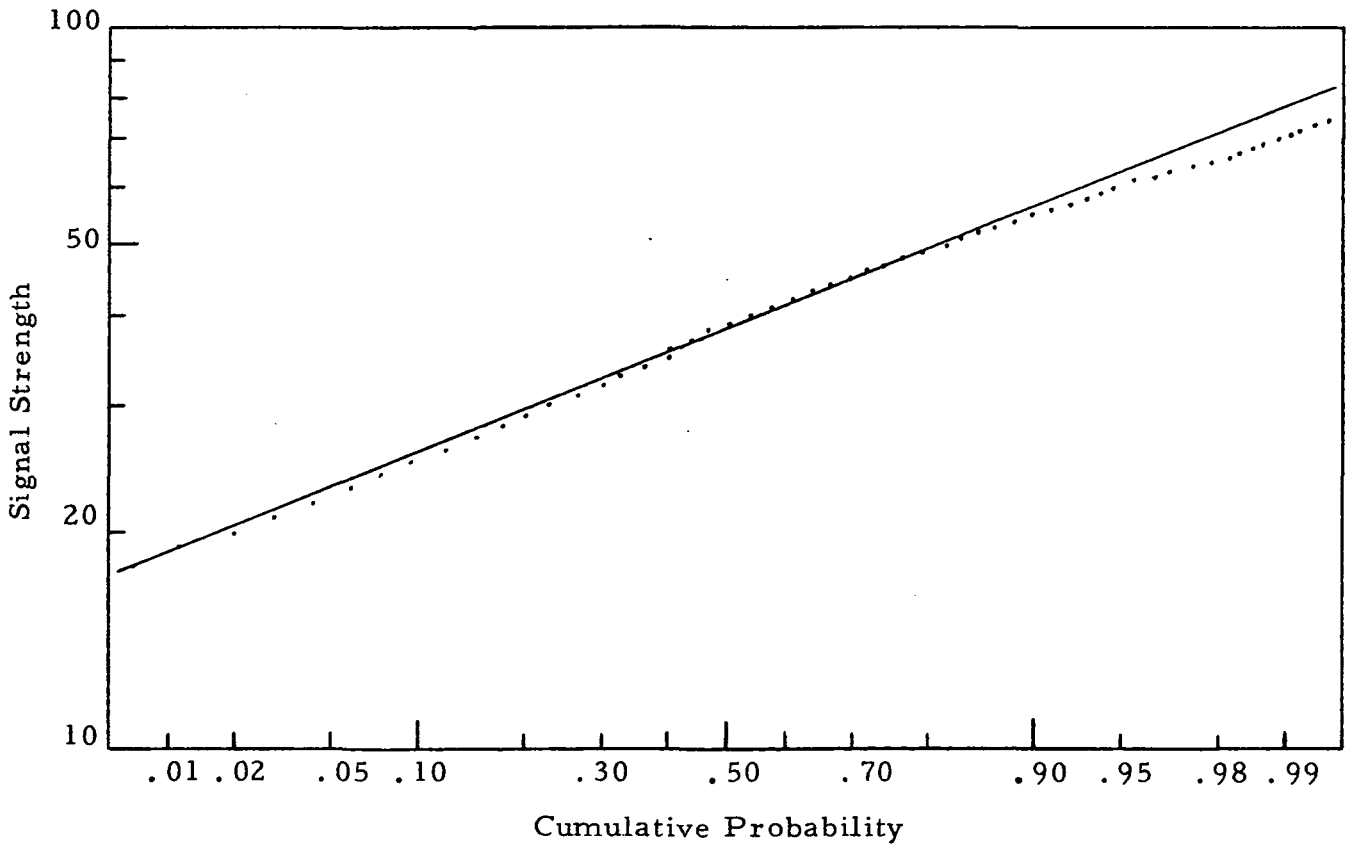

Figure 51. Signal Probability Distribution for Run #42.

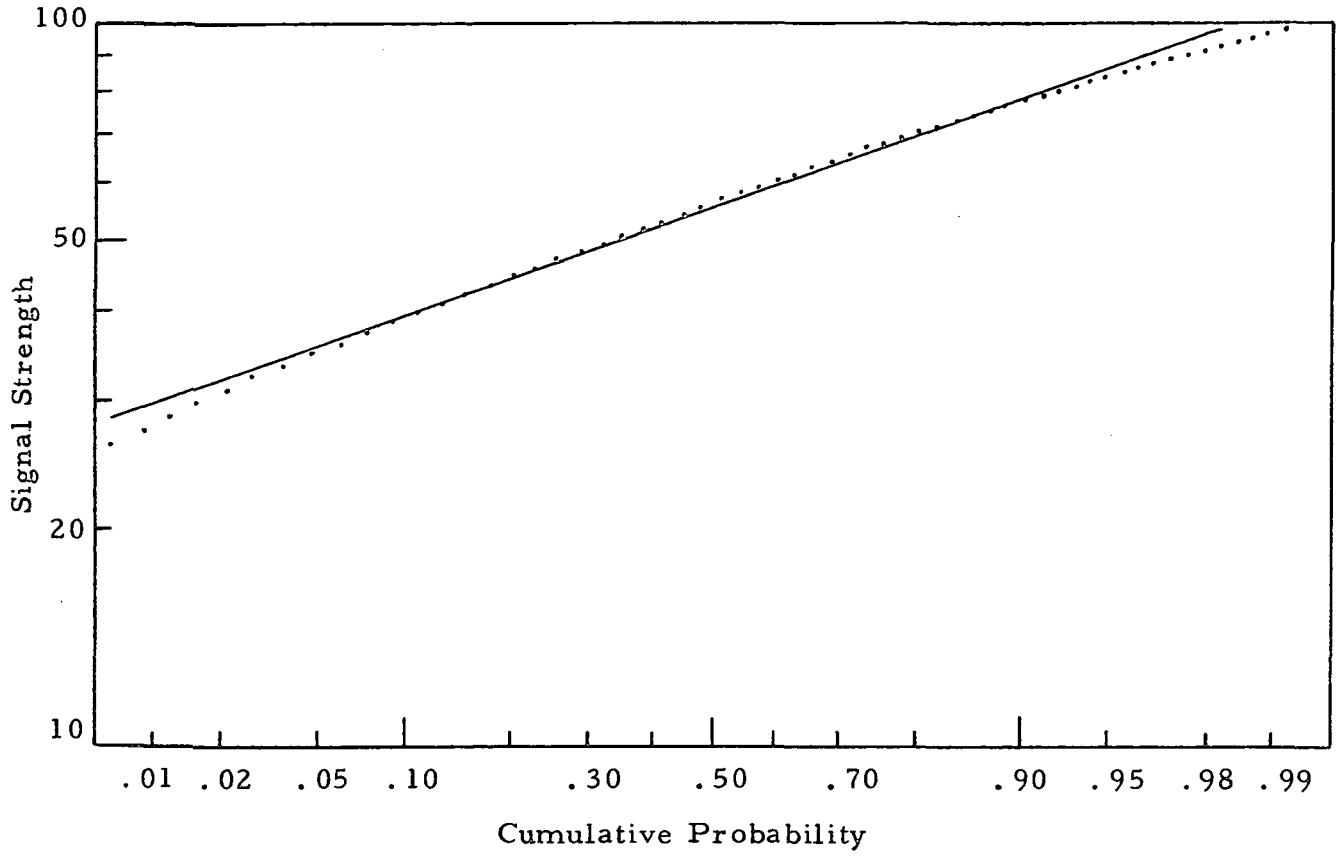

Figure 52. Signal Probability Distribution for Run #46

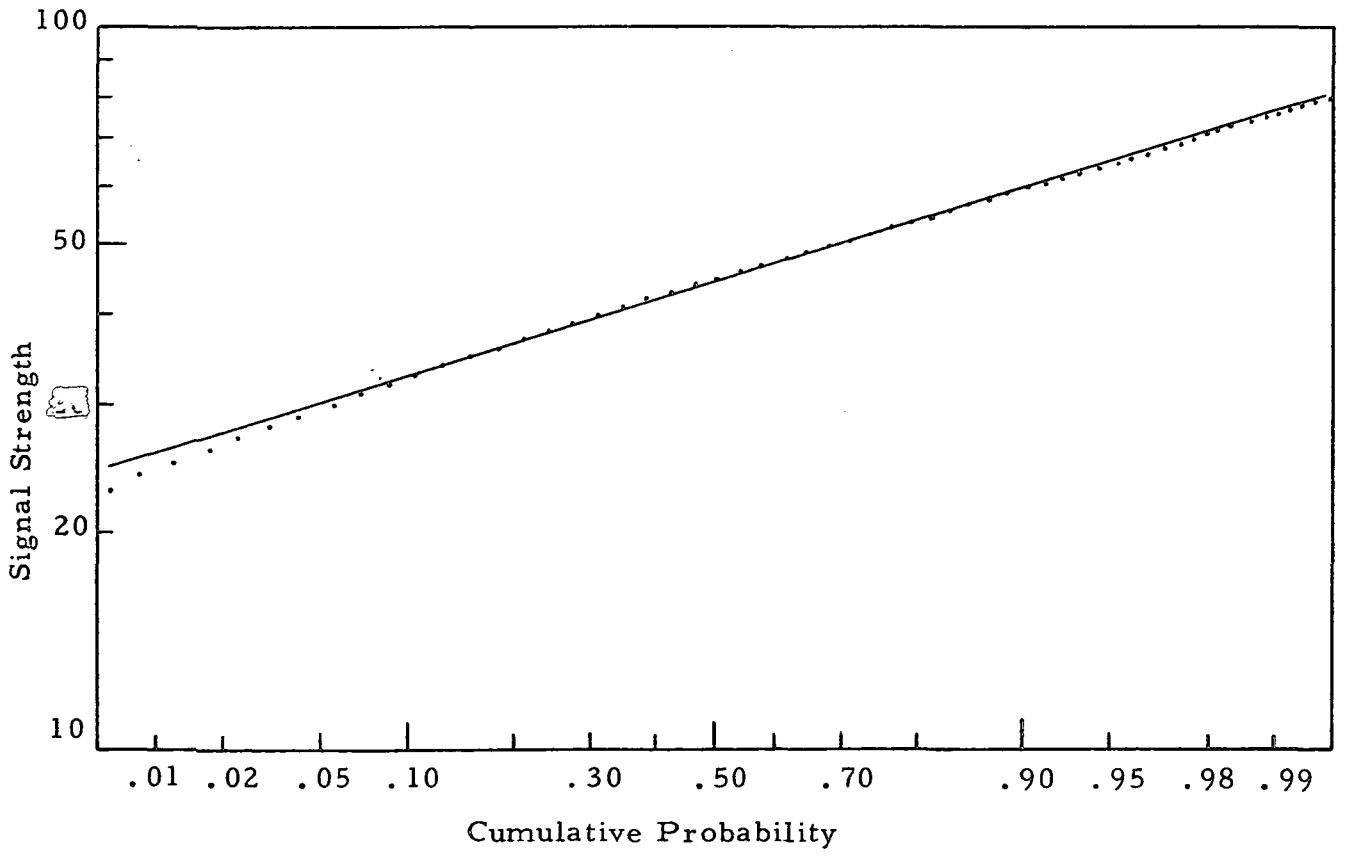

Figure 53. Signal Probability Distribution for Run #47.

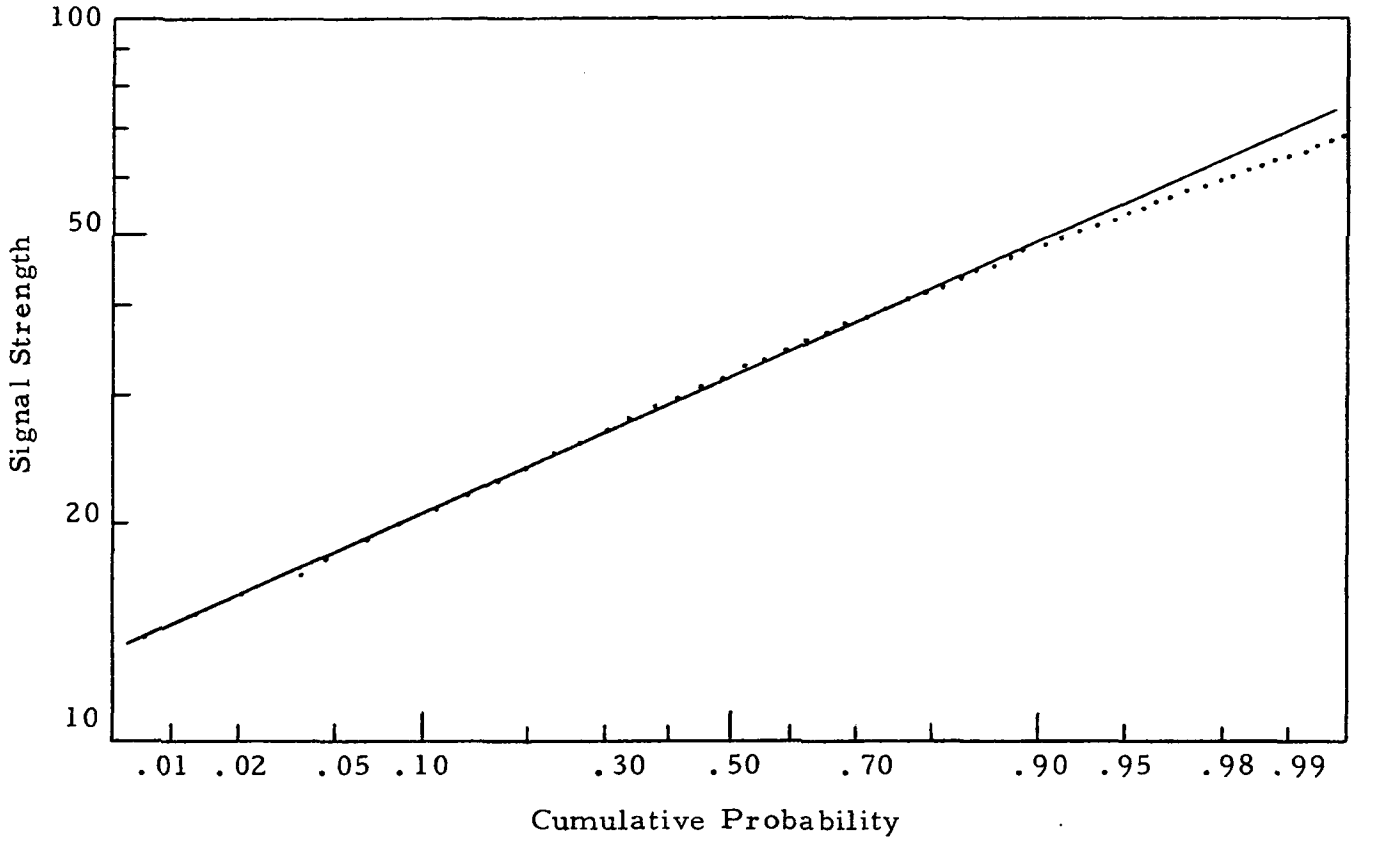

Figure 54. Signal Probability Distribution for Run #48.

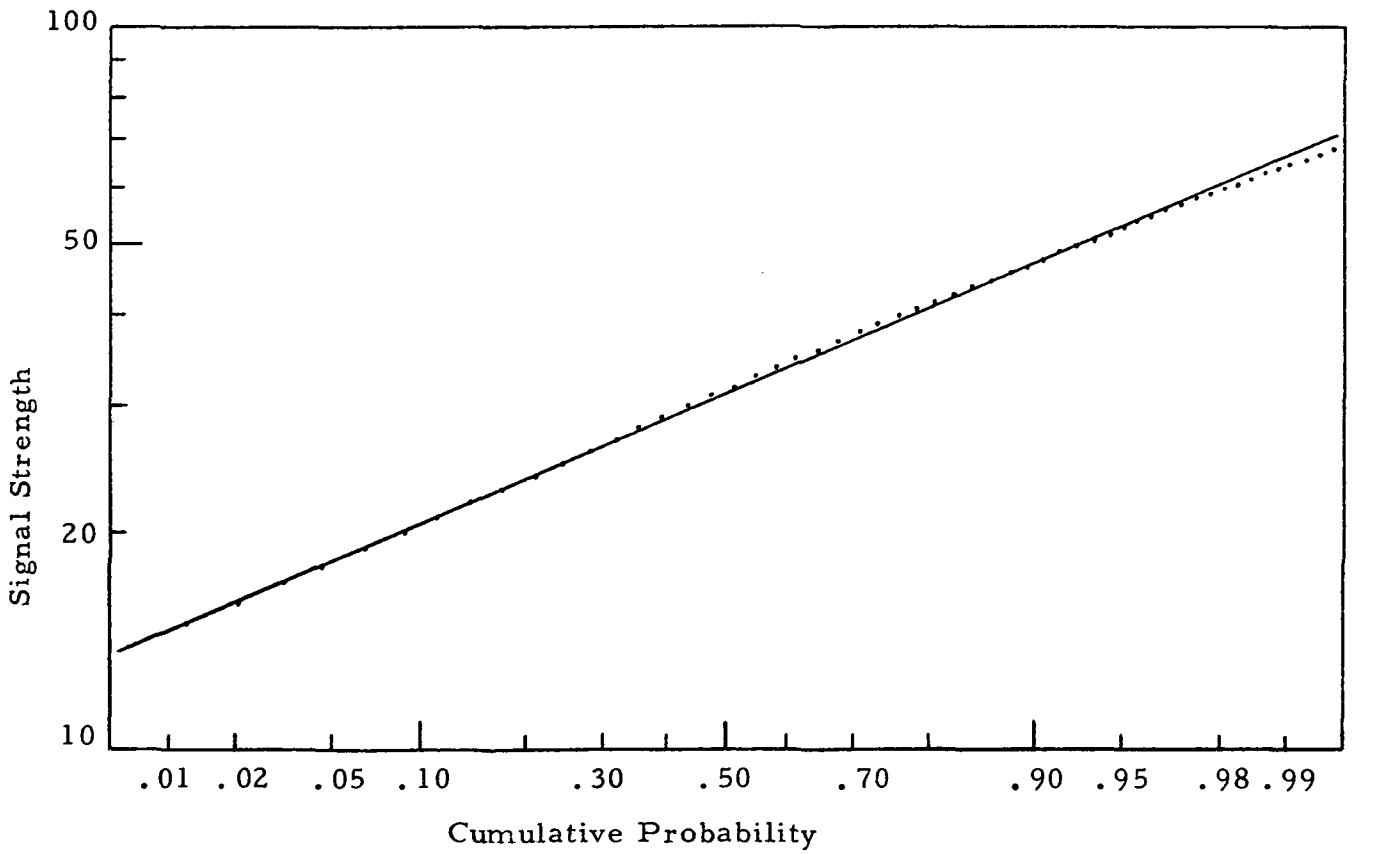

Figure 55. Signal Probability Distribution for Run #49.

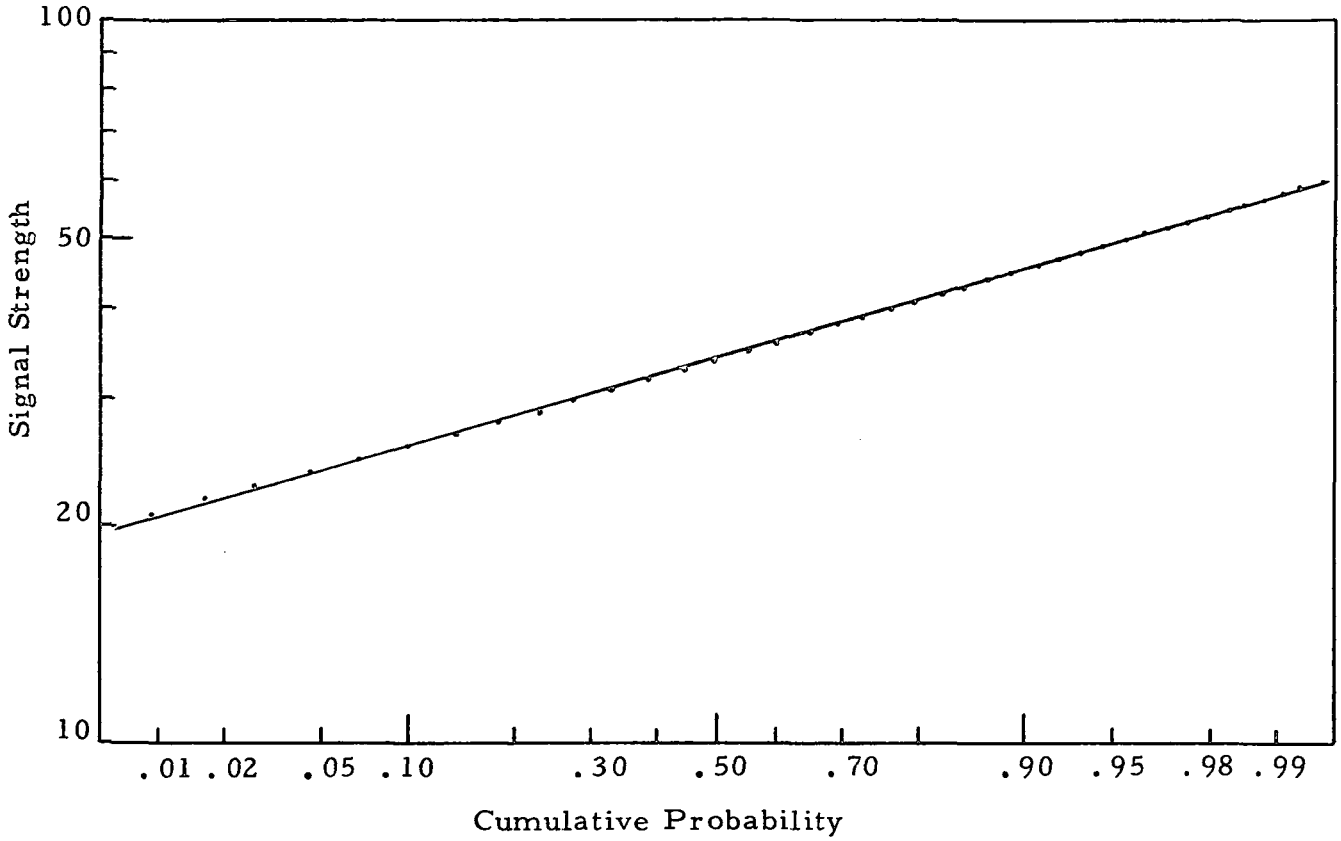

Figure 56. Signal Probability Distribution for Run #52.

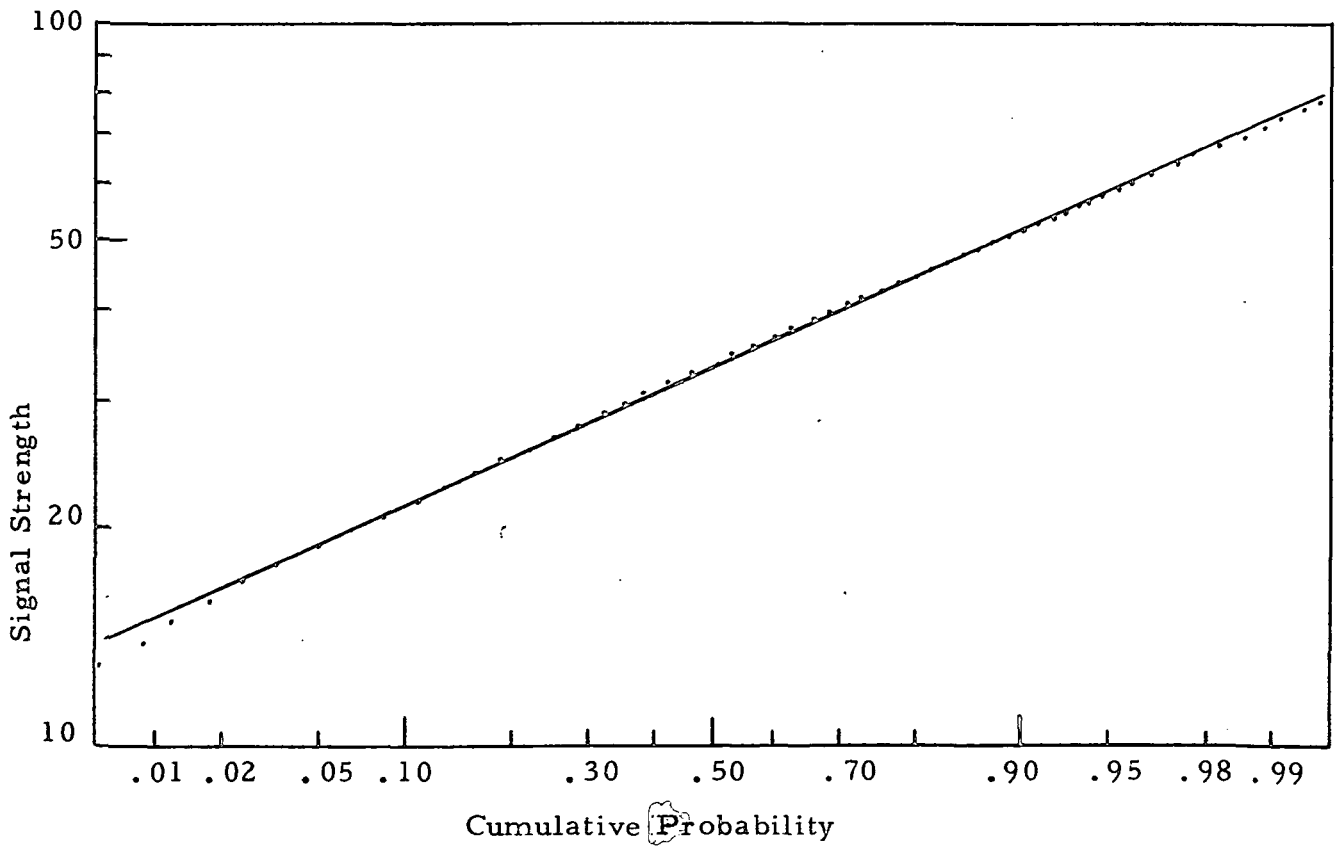

Figure 57. Signal Probability Distribution for Run #53.

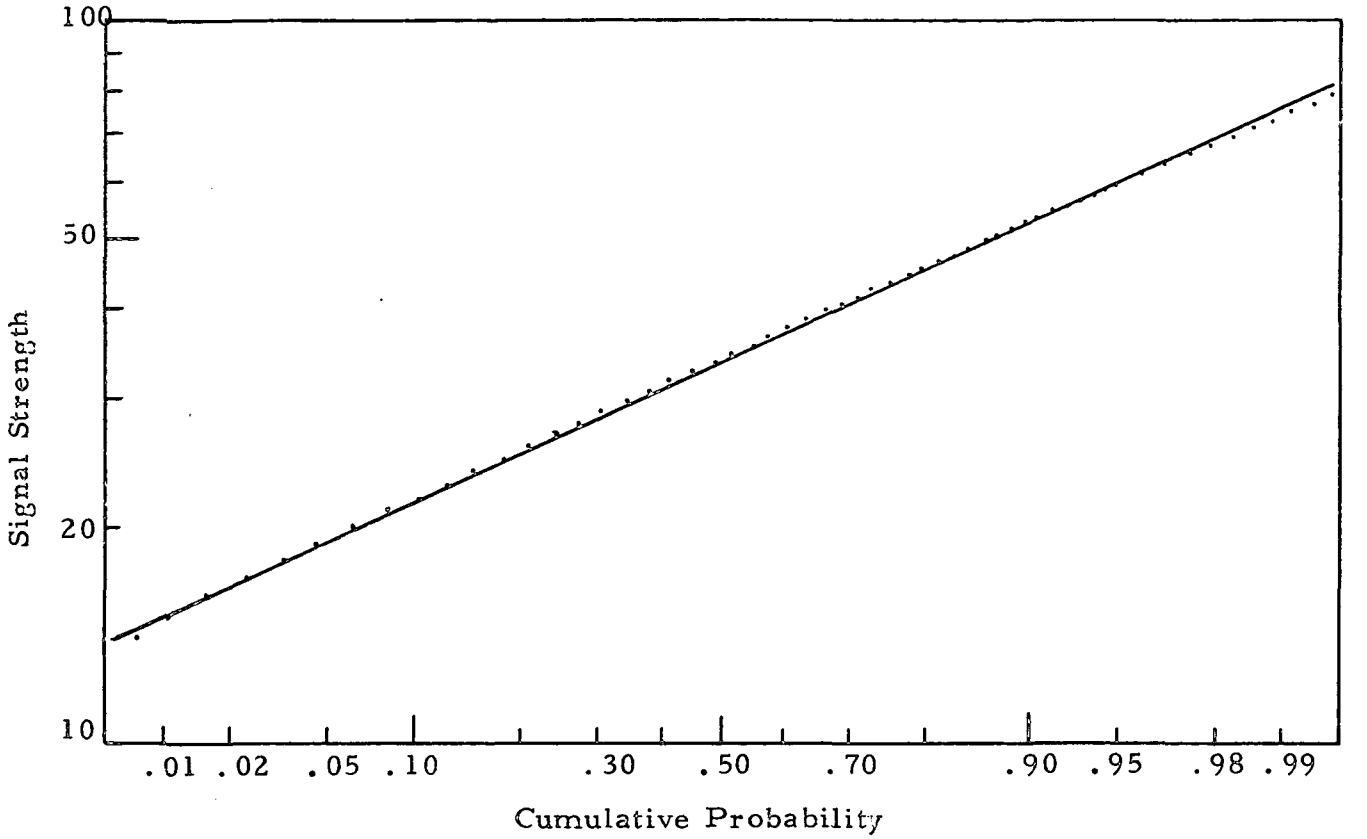

Figure 58. Signal Probability Distribution for Run #54.

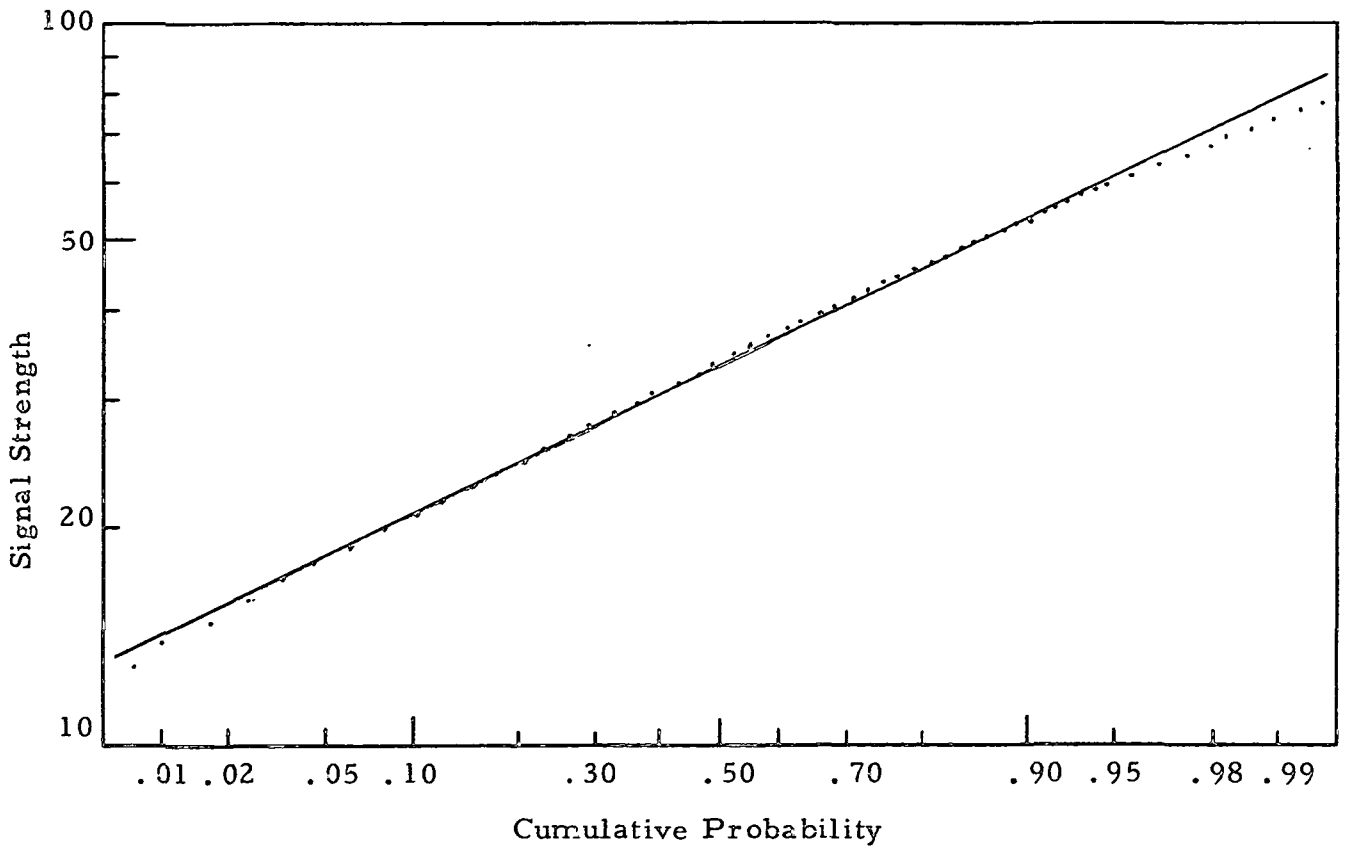

Figure 59. Signal Probability Distribution for Run #57.

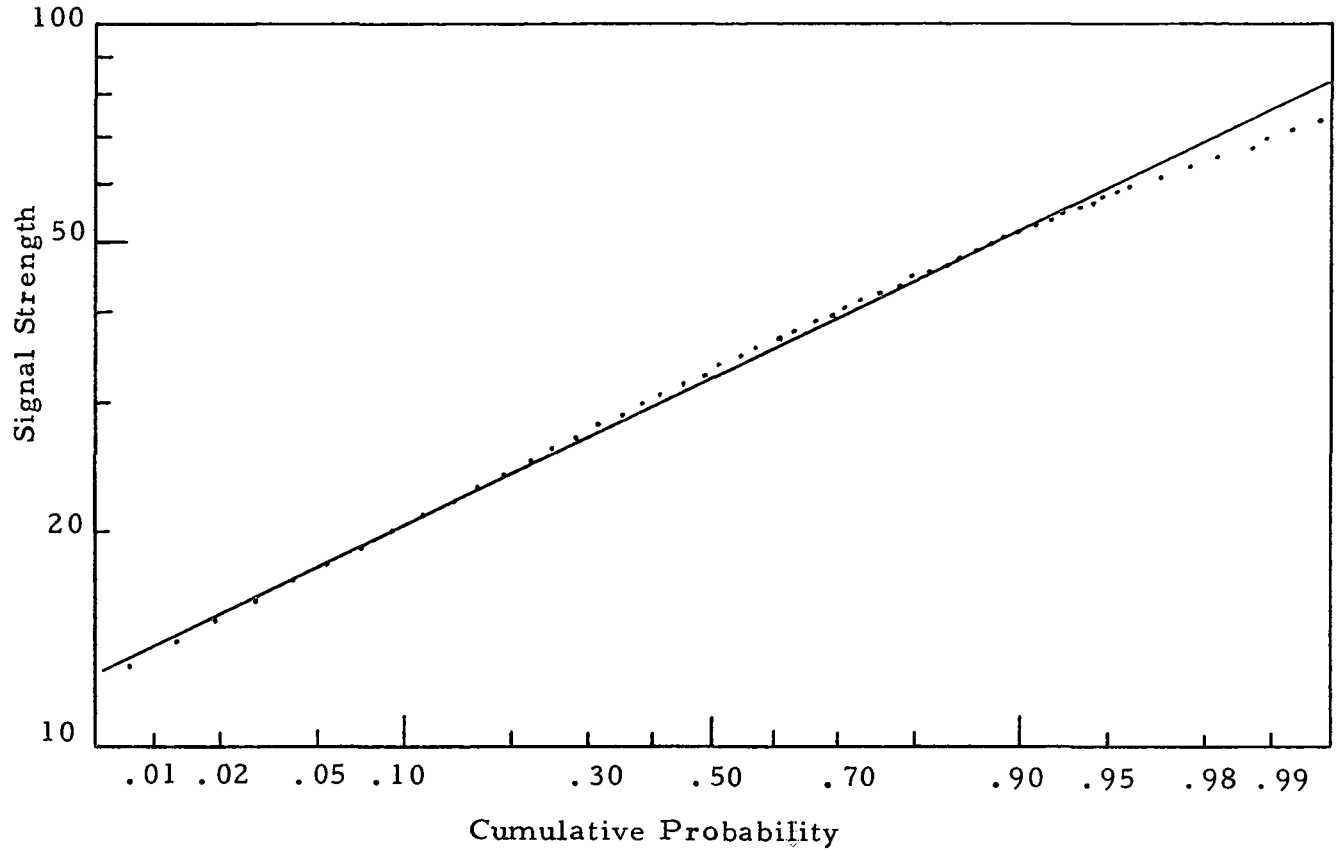

Figure 60. Signal Probability Distribution for Run #58.

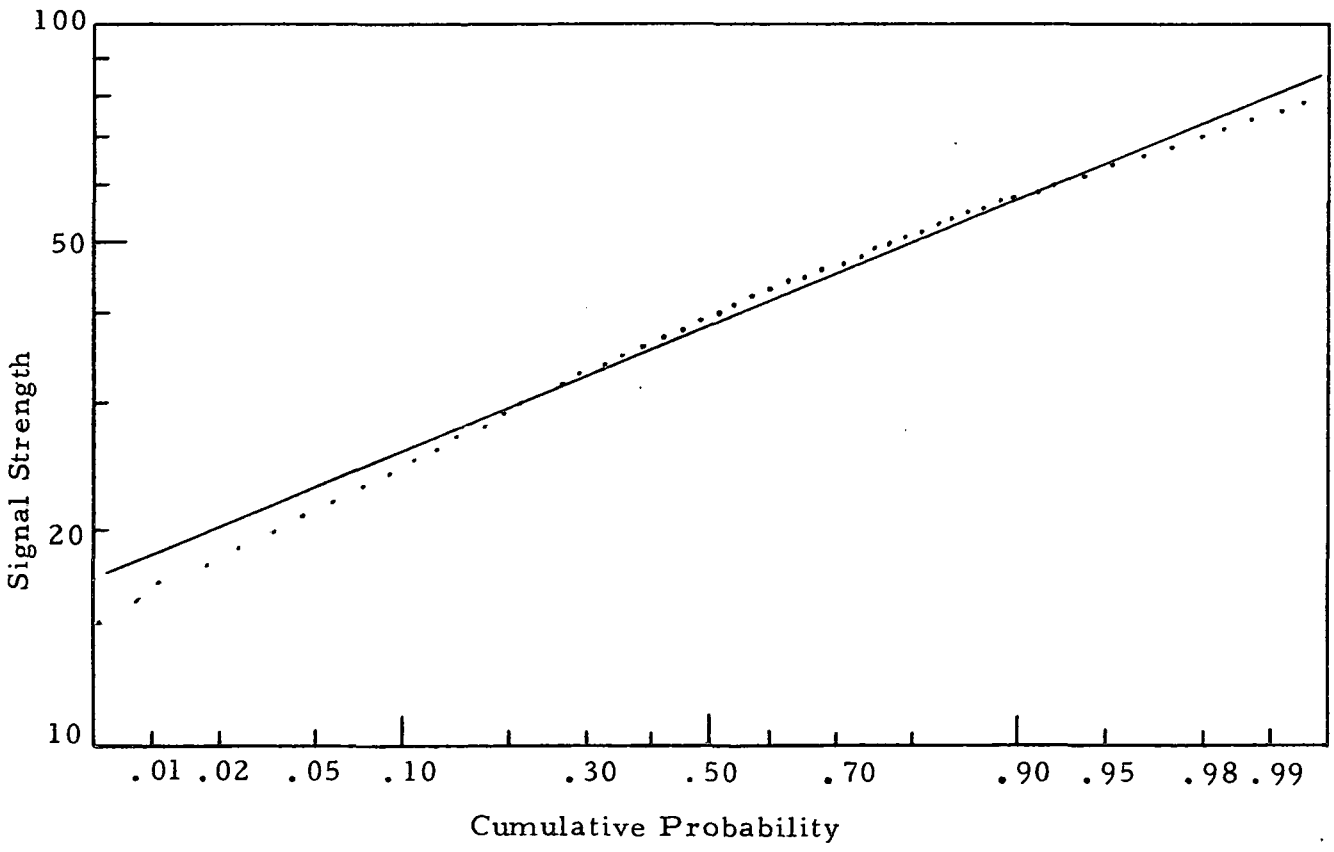

Figure 61. Signal Probability Distribution for Run #59.

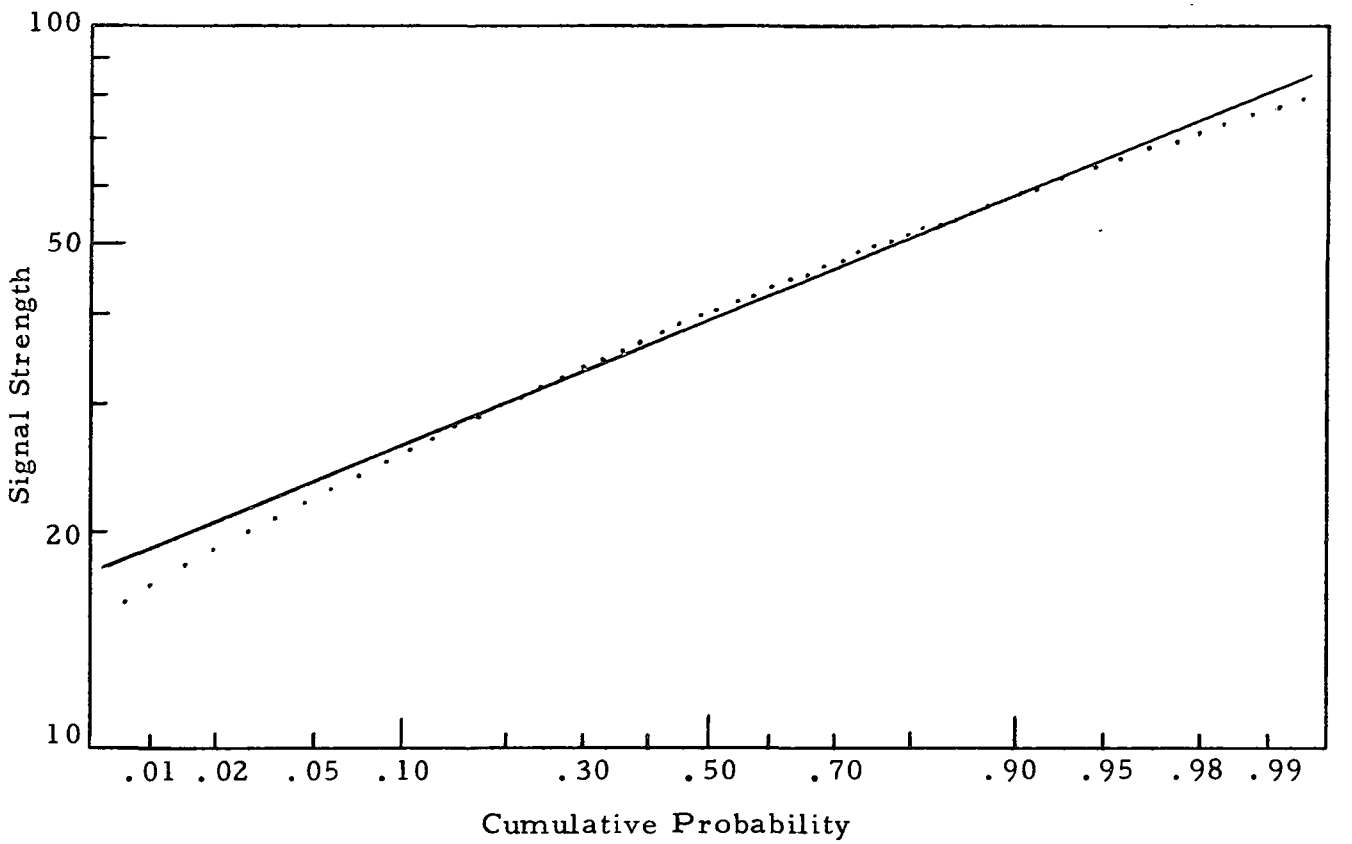

Figure 62. Signal Probability Distribution for Run #61.

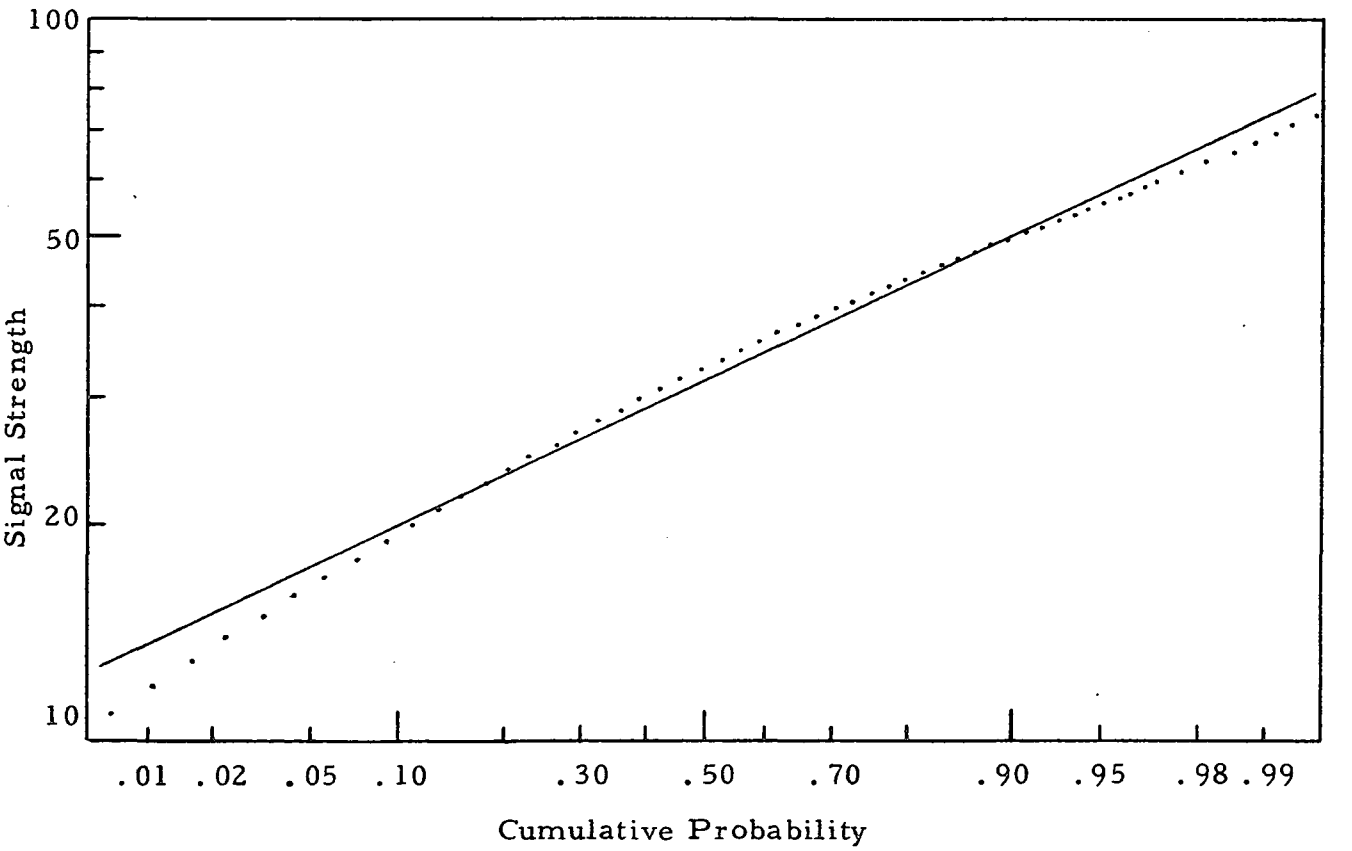

Figure 63. Signal Probability Distribution for Run #62.

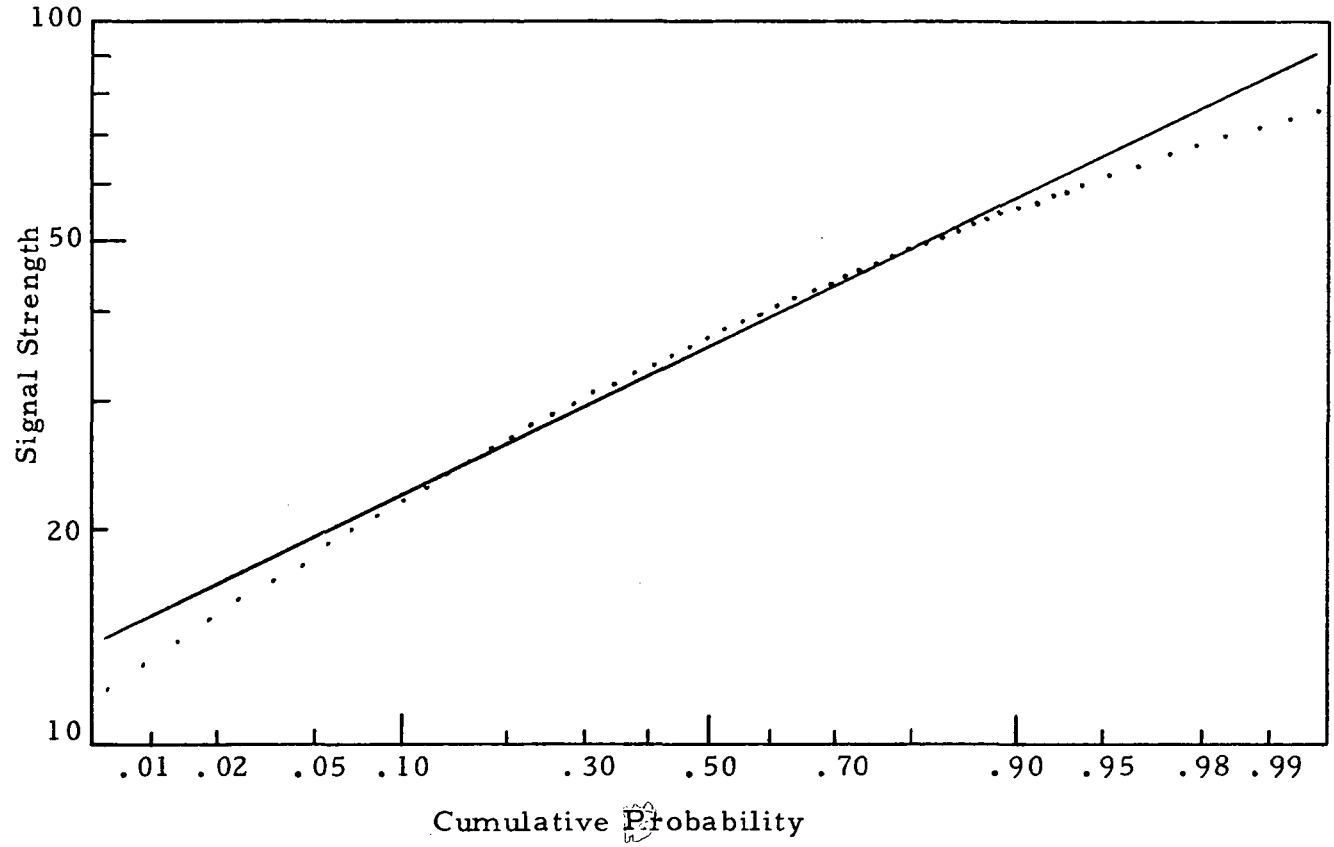

Figure 64. Signal Probability Distribution for Run #64.

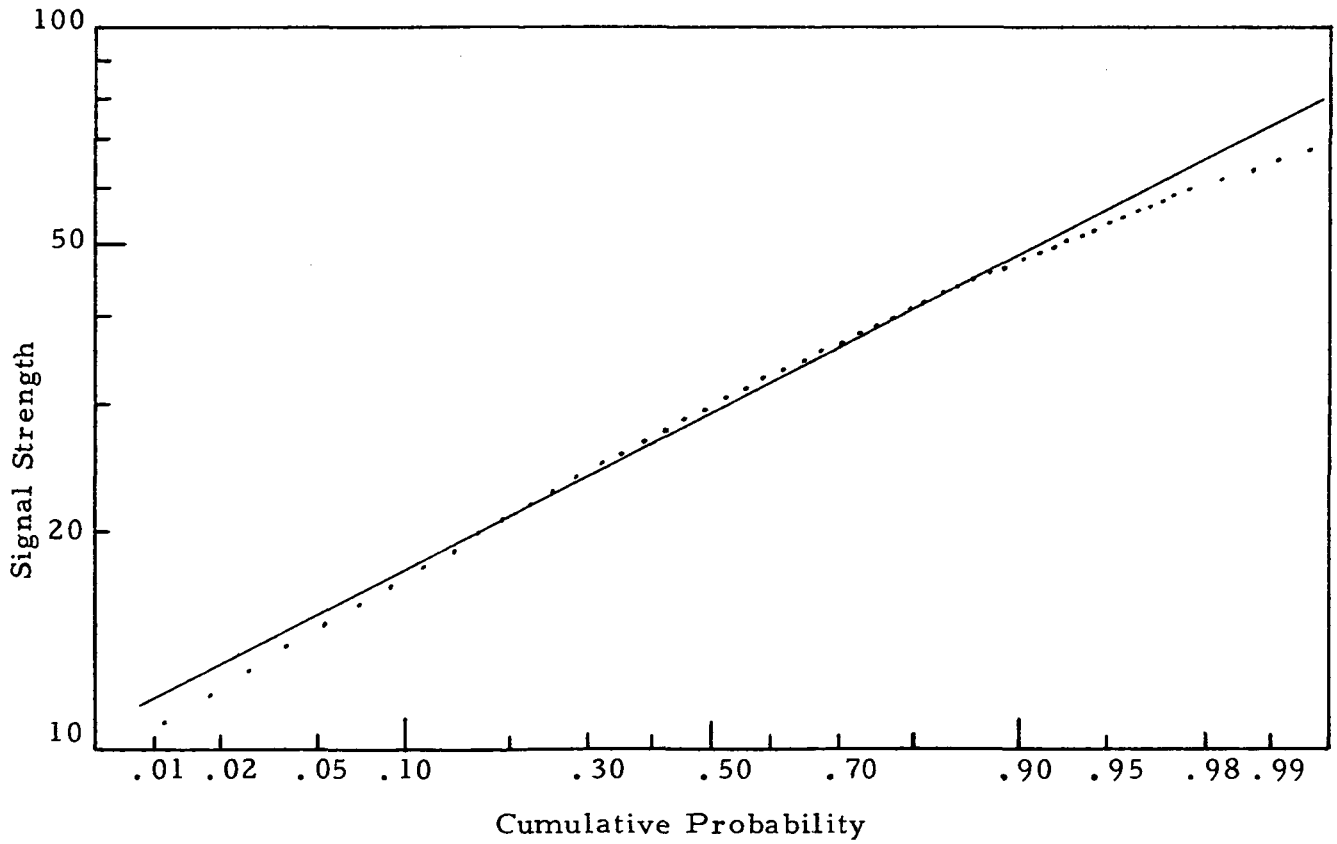

Figure 65. Signal Probability Distribution for Run #66.

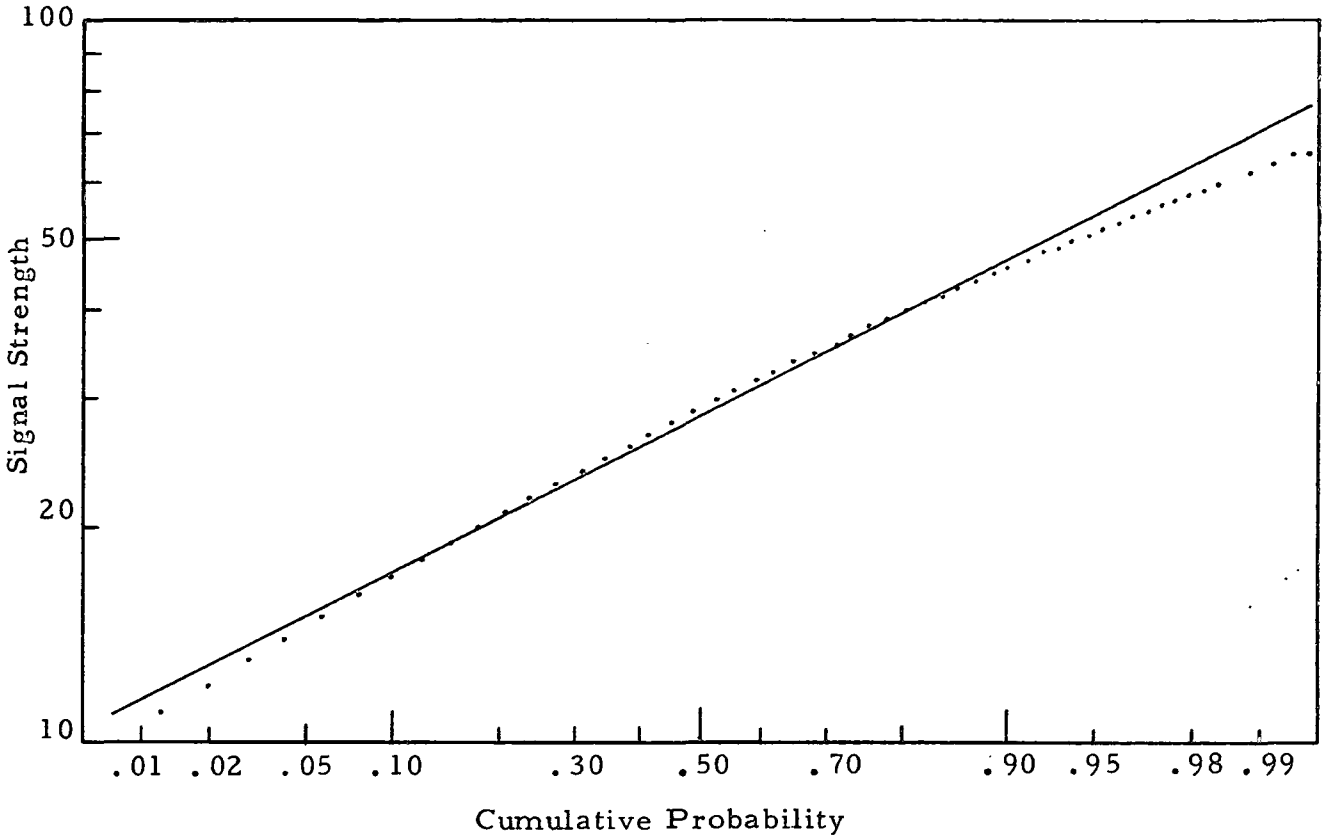

Figure 66. Signal Probability Distribution for Run #67.

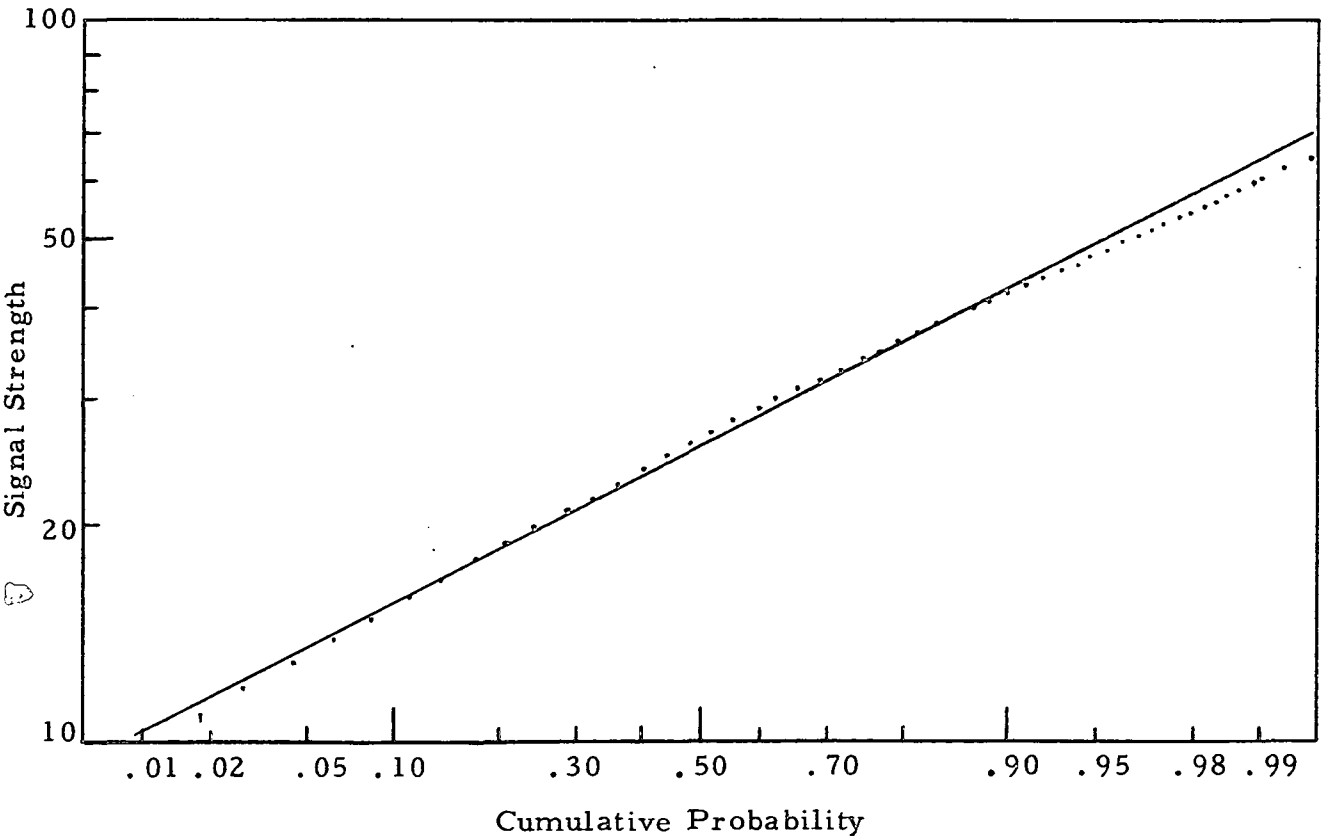

Figure 67. Signal Probability Distribution for Run #69.

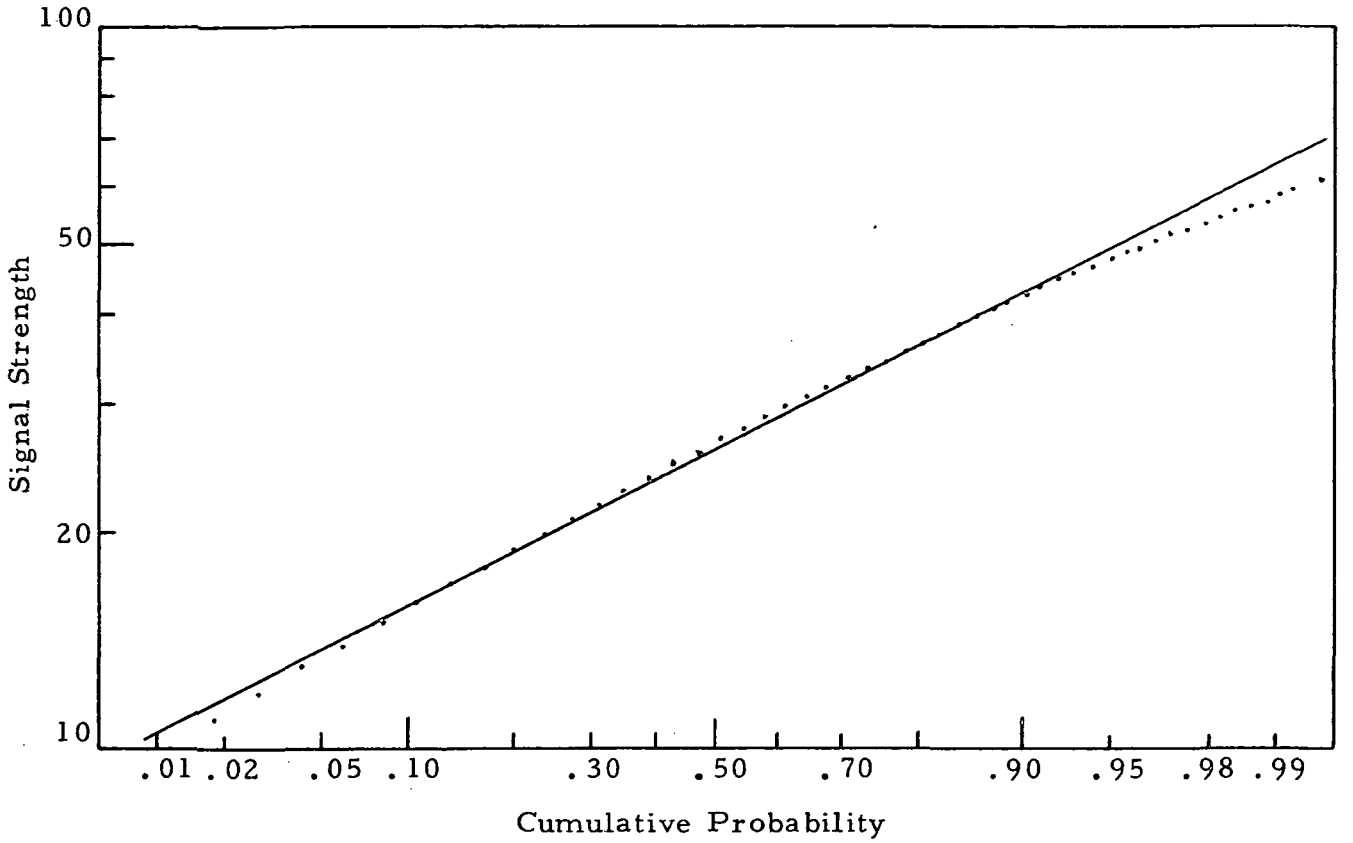

Figure 68. Signal Probability Distribution for Run #70.

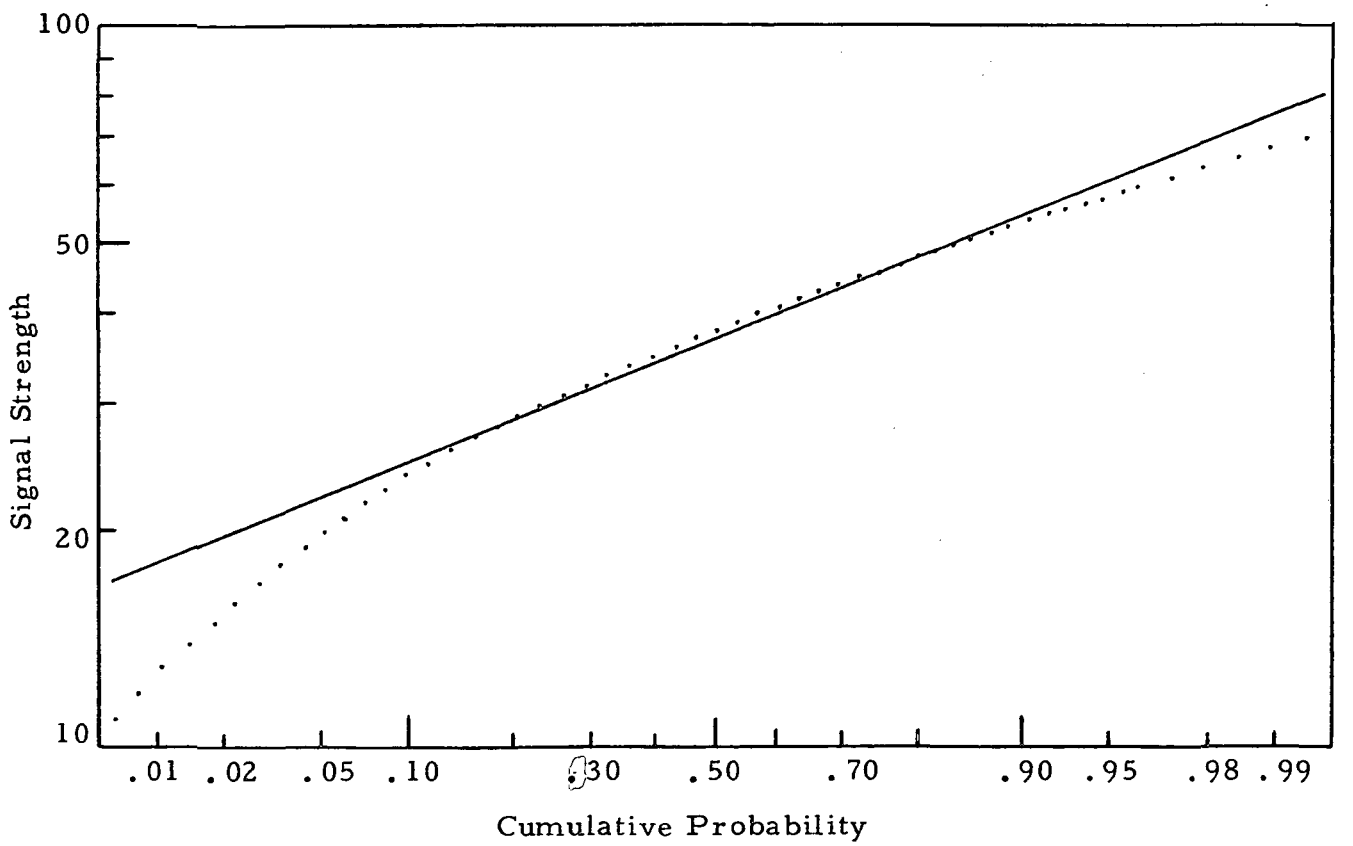

Figure 69. Signal Probability Distribution for Run #71

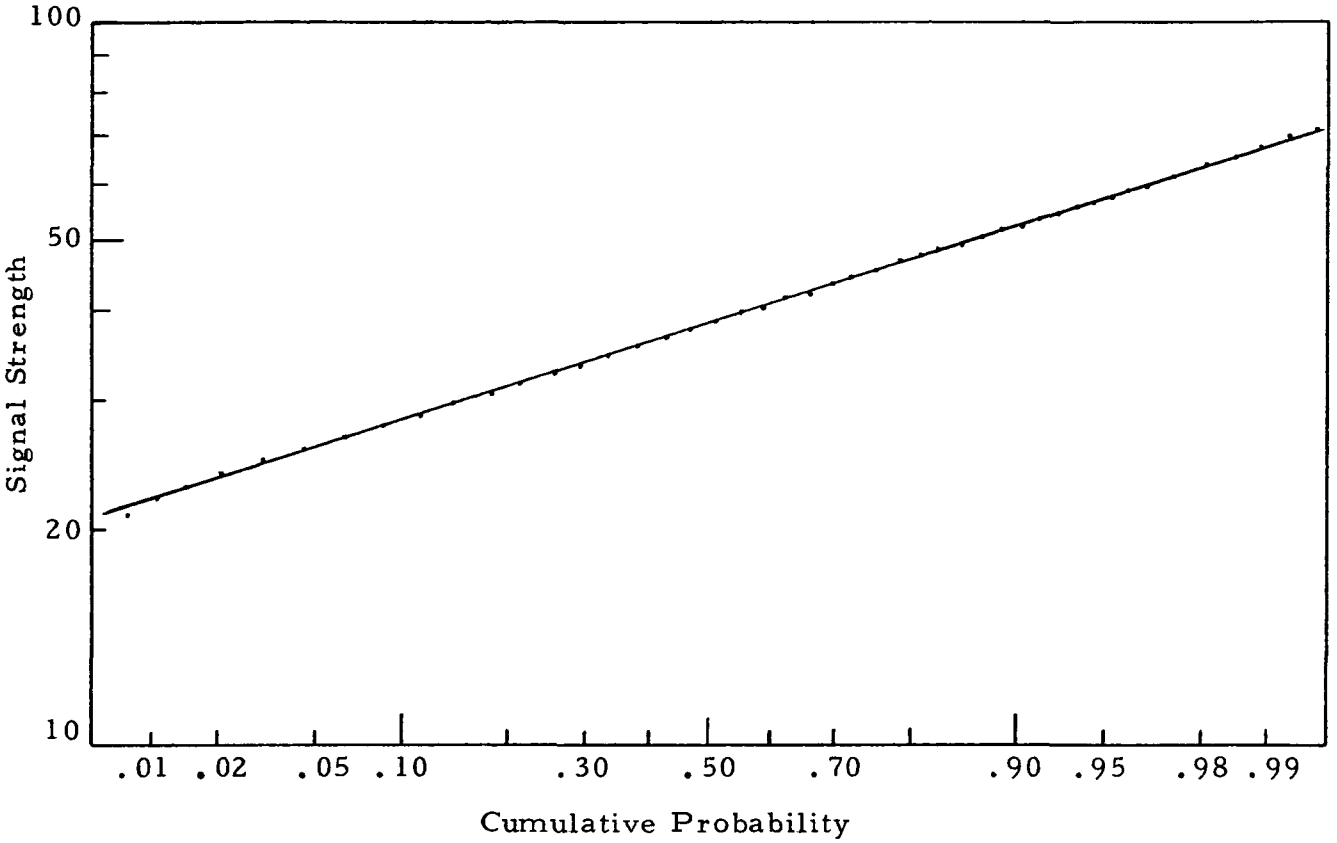

Figure 70. Signal Probability Distribution for Run #75

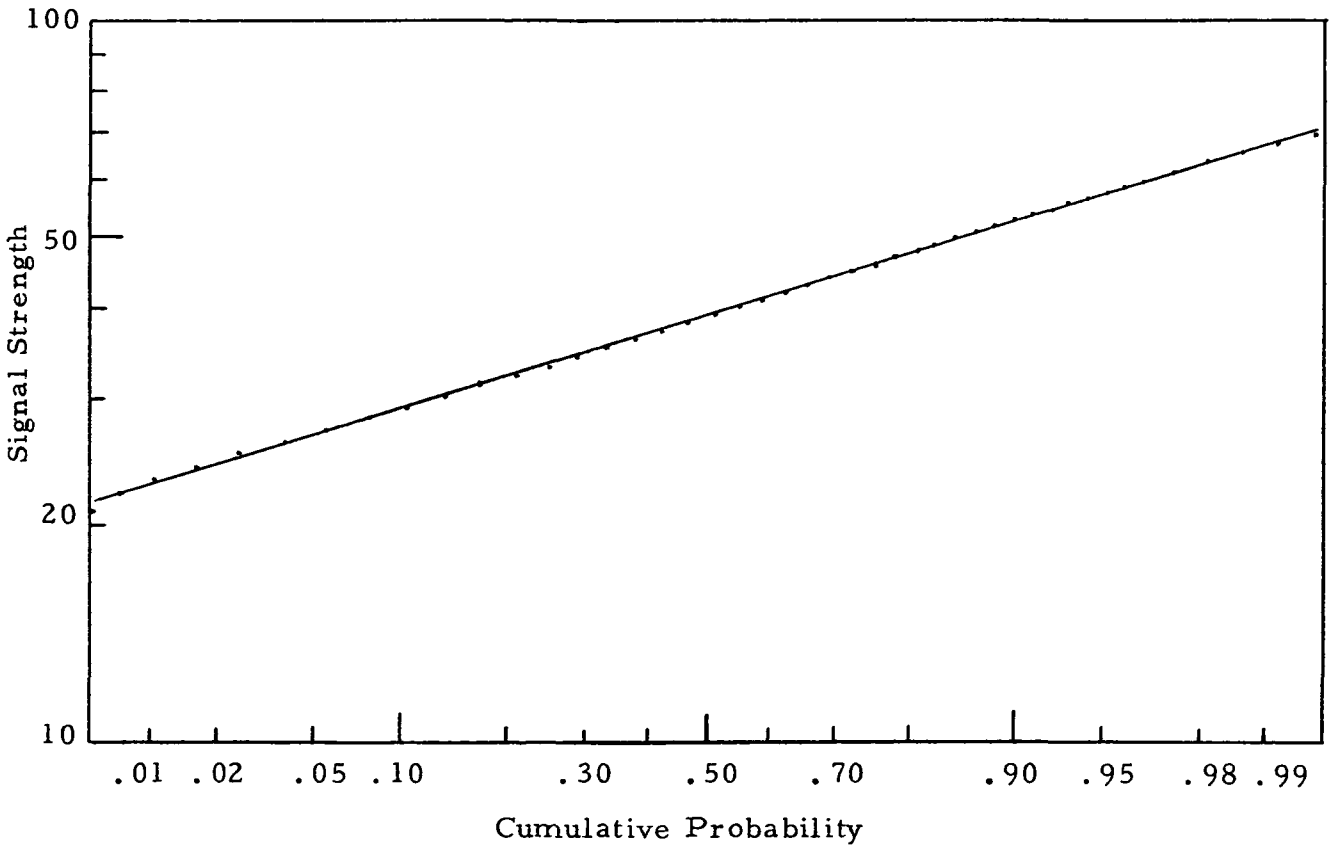

Figure 71. Signal Probability Distribution for Run #76.

on a normal distribution scale.) If the random variable whose cumulative probability is being plotted follows a log-normal distribution, the plot will be a straight line. An examination of each of these figures shows that the measured distribution can be reasonably accurately classified as log-normal, at least between the 10% and 90% cumulative probability levels. In the extremes beyond these limits, other contaminating effects sometimes appear, but they appear to be either too small or too infrequent to significantly affect the main body of the distribution between 10% and 90% -- though lying at the extreme values, they are obviously able to affect the higher moments, as noted in examination of Table 10.

As a method of validating the measured values of the scintillation runs' mean and variance (i.e., second central moment) with background effects removed, which we presented in Table 8 and which we used to calculate the normalized second central moment of the scintillation given in Table 9, we have taken a straight-line fit to the data in Fig.'s 28 to 71 in the 10% to 90% range, and obtained an independent estimate of the mean and second central moment for each scintillation run from this. In Table 11 we show the original measured data as taken from Table 7* and the corresponding straight-line fit data obtained from the figures.

As can be seen from a comparison of the two sets of data in Table 11, the measured data for the first two moments seems to be in good agreement with the straight-line fit data. The discrepancies are all less than 20% and generally are less than 10%. Based on this, we conclude that whatever effects caused the extremes of the probability distribution to deviate from a log-normal distribution, and the third and fourth moments to deviate from the values expected for a log-normal distribution, did not significantly affect

---

* Because the cumulative probability data plotted in Fig.'s 28 to 71 still contains the effect of the background, it is necessary to compare the straight-line fit data to the measured moments in Table 7, i.e., the measured moments without background effects removed, rather than to the data in Table 8 for which the background effects have been removed.

Table 11

Scintillation Data Runs, Mean and Variance

Run Number	Diameter (m)	Measured		Straight-Line Fit	
		Mean	Variance	Mean	Variance
1	0.76	42.37	117.9	41.59	119.1
2	0.76	38.17	135.5	37.95	158.5
3	0.08	34.54	117.8	34.18	113.2
4	0.04	24.70	29.90	24.31	27.25
8	0.76	40.10	141.6	39.59	120.8
9	0.76	38.79	99.36	38.20	109.3
10	0.76	34.33	66.44	33.51	65.53
12	0.08	43.06	140.3	42.51	141.3
13	0.08	40.17	110.4	39.61	104.4
14	0.08	38.42	84.93	38.16	80.35
17	0.16	40.73	133.1	40.06	133.4
18	0.16	28.04	105.9	27.72	101.2
19	0.16	37.32	136.0	36.45	137.7
20	0.16	39.24	168.3	38.69	169.4
23	0.16	38.44	144.0	38.14	137.6
24	0.16	39.82	142.9	39.82	139.7
27	0.04	38.59	29.99	38.48	26.97
29	0.76	44.05	132.8	42.81	134.1
30	0.76	44.56	147.4	43.77	151.2
31	0.32	33.32	70.32	32.61	69.23
33	0.32	46.00	128.8	45.33	130.1
38	0.76	40.22	149.8	39.33	166.5
39	0.76	43.29	169.1	43.25	161.3
42	0.16	39.83	137.3	39.79	151.4

Run Number	Diameter (m)	Measured		Straight-Line Fit	
		Mean	Variance	Mean	Variance
46	0.76	47.11	150.0	46.54	165.0
47	0.76	46.22	117.1	45.76	119.6
48	0.32	34.20	123.1	33.70	135.8
49	0.32	33.61	119.0	32.69	120.1
52	0.08	35.59	61.45	35.36	62.48
53	0.16	36.13	151.7	35.14	155.5
54	0.16	36.87	162.5	36.25	173.3
57	0.32	36.59	172.2	35.89	187.7
58	0.32	35.62	157.0	34.88	177.6
59	0.76	41.23	169.5	40.40	166.7
61	0.76	42.09	170.9	41.22	174.3
62	0.76	34.80	150.3	33.59	157.3
64	0.76	38.70	174.1	38.13	215.2
66	0.76	32.18	144.3	31.95	169.5
67	0.76	31.19	131.0	30.70	156.6
69	0.76	28.39	113.4	27.75	126.5
70	0.76	28.81	115.0	28.13	130.3
71	0.76	39.02	137.7	38.83	148.8
75	0.76	40.41	97.04	39.71	96.65
76	0.76	40.49	93.97	39.80	98.30

the first and second moments. Therefore, we believe that the measured scintillation mean and variance (i.e., second central moment) without background effects removed, as presented in Table 7, can be relied upon. Thus we shall be able to use, without concern for the effects of spurious signal contamination, the normalized second central moment values presented in Table 9 as calculated from the values in Table 7 in our study of the relationship between measured data and aperture averaging theory. We take this up in the next section.

5. Comparison of Experimental Results With Theory

At this point we have, in terms of the normalized second central moment, i.e., the normalized variance for the scintillation runs, as presented in Table 9, a suitable measurement data base for comparison of theory with experiment. The basic theory of aperture averaging is presented in Eq.'s (19) and (20), with the appropriate prior equation providing a definition of the quantities. Because our measurements were taken at different zenith angles, we shall be particularly interested in Eq.'s (11) and (17) as a basis for correcting the data for its zenith angle dependence. We shall take up the matter of zenith angle dependence compensation first, and then go into the question of comparing the data with theory.

5.1 Zenith Angle Dependence Compensation

Ideally, if we had a reliable measure of the vertical distribution of the optical strength of turbulence, C_N^2, during the approximately three-hour measurement period of the data collection portion of flight #5, we could calculate the expected value of the normalized variance of the aperture averaged scintillating laser signal and compare it with the measured values. This would automatically take accoant of the zenith angle dependence and we would not have to devote any special attention to it.

Unfortunately, however, the measured values of C_N^2 , as discussed in Appendix B, do not appear to be reliable, and we have therefore had to relate the measurements to theory through a more indirect process. This causes us to have to consider the zenith angle dependence explicitly.

There are two ways in which zenith angle dependence enters into the value of the normalized variance of the signal. First, we note that in accordance with Eq. (11), the magnitude of the scintillation as measured by a very small diameter receiver with no aperture averaging will vary as the 11/6-power of the cosine of the zenith angle. Actually it is the variance of the logarithm of the signal that varies as $(\cos \theta)^{-11/6}$. Secondly, in accordance with Eq. (17), we note that the length d_o , which is divided into the aperture diameter to provide a dimensionless number from which the aperture averaging factor can be calculated, varies as one over the square-root of the cosine of the zenith angle, i.e., as $(\cos \theta)^{-1/2}$. In our examination of the measured normalized variance of the signal fluctuation, we shall use these two relationships to relate the measured values to the values we would expect if the source had been directly overhead, i.e., of a zenith angle $\theta = 0$.

5.1.1 Aperture Size Compensation

To take account of the fact that d_o varies as $(\cos \theta)^{-1/2}$ and convert our measured values to equivalent values for $\theta = 0$, we note that the aperture averaging factor for an aperture of diameter D is a function of D/d_o . This means that the degree of aperture averaging achieved when $\theta \neq 0$ with an aperture of diameter D is equivalent to the degree of aperture averaging that would have been obtained by an aperture of diameter D_{eff} at $\theta = 0$, where

$$D_{eff} = D (\cos \theta)^{1/2} \quad , \tag{80}$$

since, as a result of Eq. (17)

$$D/d_o = D_{eff}/(d_{o_o})_{zenith} \quad . \tag{81}$$

This means that if we wish to compare our measured normalized variance results with theory for aperture averaging of a source at the zenith, we should plot the normalized variance, or rather an adjusted normalized variance, not against the aperture diameter D, but rather against the aperture averaging equivalent diameter for zenith viewing, i.e., against D_{eff}.

5.1.2 Normalized Variance Compensation

In order to be able to adjust the normalized variance for its zenith angle dependence, we have to be able to separate the aperture averaging factor from the small diameter receiver signal variance, so that we can scale this signal variance for the zenith angle dependence. We recall from Section 1, Eq.'s (13) and (14), that the normalized variance can be written as

$$\Sigma = \frac{\sigma_s^2}{\overline{S}^2}$$

$$= \mathcal{A} \left[\exp\left(\sigma_L^2\right) - 1\right] \quad , \tag{82}$$

and from Eq. (11), we see that this can be written as

$$\Sigma = \mathcal{A} \left\{\exp\left[(\cos\theta)^{-11/6} \left(\sigma_L^2\right)_{zenith}\right] - 1\right\} \quad . \tag{83}$$

If we solve Eq. (83) for the aperture averaging factor, $\mathcal{A}$, we get

$$\mathcal{A} = \frac{\Sigma}{\left\{\exp\left[(\cos\theta)^{-11/6} \left(\sigma_L^2\right)_{zenith}\right] - 1\right\}} \quad . \tag{84}$$

We see that the aperture averaging factor can be calculated from the measured normalized signal variance, $\sigma_s^2/\bar{S}^2$, and the zenith angle θ , but only if we assume that we know the log-intensity variance for propagation from the zenith, i.e., $(\sigma_L^2)_{zenith}$.

Our approach to this zenith angle compensation problem is to assume that we know $(\sigma_L^2)_{zenith}$ and see how a particular value works out in matching the data to the theory. In the next subsection, we present the results of such an effort.

5.2 Data Analysis

Making use of the effective diameter scaling relationship presented in Eq. (80), we have been able to convert the actual receiver diameter for each scintillation data run to an effective diameter. These results are shown in Table 12. Along with the effective diameter results, we have also included in Table 12 the value of the aperture averaging factor computed for various values of $(\sigma_L^2)_{zenith}$. Based on the fact that the normalized small diameter receiver signal variance viewing a source at the zenith angle would be

$$\Sigma^0_{zenith} = \exp\left[(\sigma_L^2)_{zenith}\right] - 1 \quad , \tag{85}$$

we have chosen the four values of $(\sigma_L^2)_{zenith}$ equal to 0.300 , 0.336 , 0.372 , and 0.405 , corresponding to Σ^0_{zenith} equal to 0.35 , 0.40 , 0.45 , and 0.50 , for the aperture averaging values computed in Table 12.

In Fig.'s 72 to 75, we have plotted the aperture averaging factor, Θ , computed for each of these four values of Σ^0_{zenith} as a function of the effective diameter, D_{eff} , using the data in Table 12. The encircled data points correspond to the set of scintillation data runs performed using the 0.76 m diameter aperture with the 0.20 m central obscuration. The shaded circle near the center of each of the large elliptical regions in these

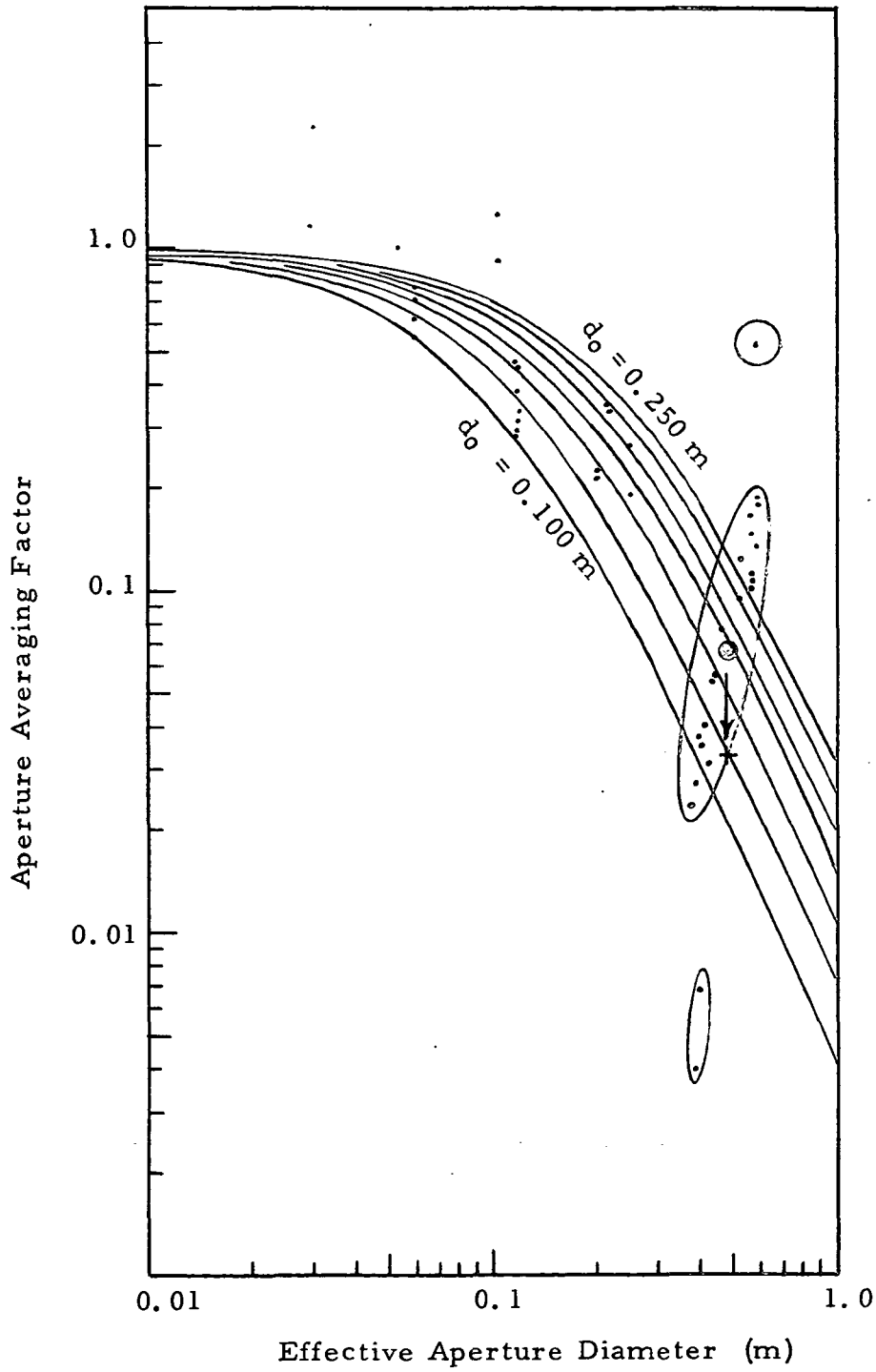

Figure 72. Aperture Averaging Measurements Corrected to Zenith Viewing Using $\Sigma^{o}_{Zenith} = 0.32$. Theoretical predictions are shown for $d_o = 0.100$ m , 0.125 m , 0.150 m , 0.175 m , 0.200 m , 0.225 m , and 0.250 m , as the solid curves. Measured values are indicated by the dots. The encircled data points were taken with a central obstruction in the aperture.

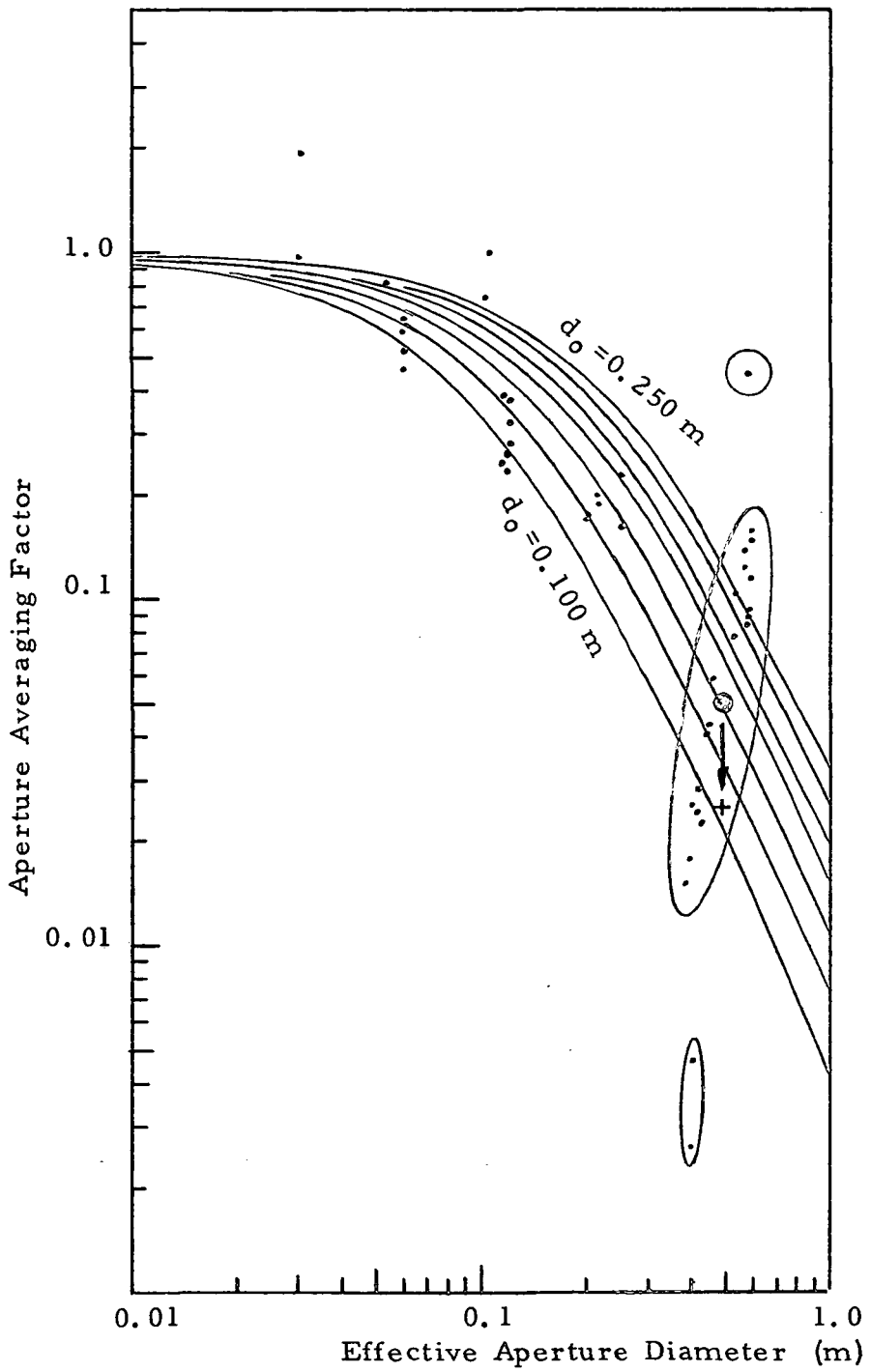

Figure 73. Aperture Averaging Measurements Corrected to Zenith Viewing Using Σ^{o}_{Zenith}=0.40. Theoretical predictions are shown for d_o = 0.100 m , 0.125 m , 0.175 m , 0.200 m , 0.225 m , and 0.250 m, as the solid curves. Measured values are indicated by the dots. The encircled data points were taken with a central obscuration in the aperture. The choice of Σ^{o}_{Zenith}=0.40 and d_o =0.125 m appears to give the best fit to the data of all the possibilities considered.

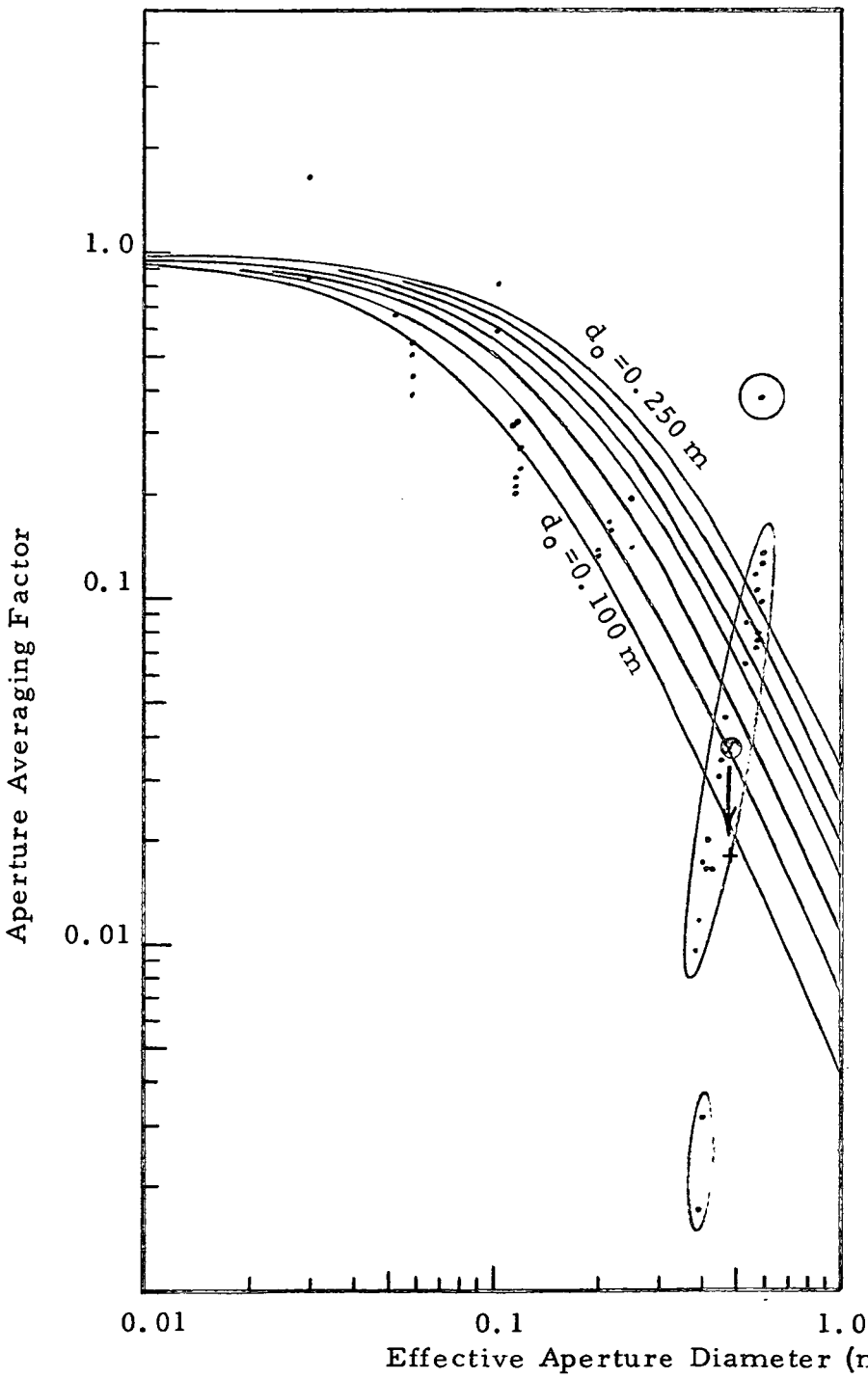

Figure 74. Aperture Averaging Measurements Corrected to Zenith Viewing Using Σ^2_{zenith}=0.45. Theoretical predictions are shown for d_o = 0.100 m , 0.125 m , 0.150 m , 0.175 m , 0.200 m , 0.225 m , and 0.250 m, as the solid curves. Measured values are indicated by the dots. The encircled data points were taken with a central obscuration in the aperture.

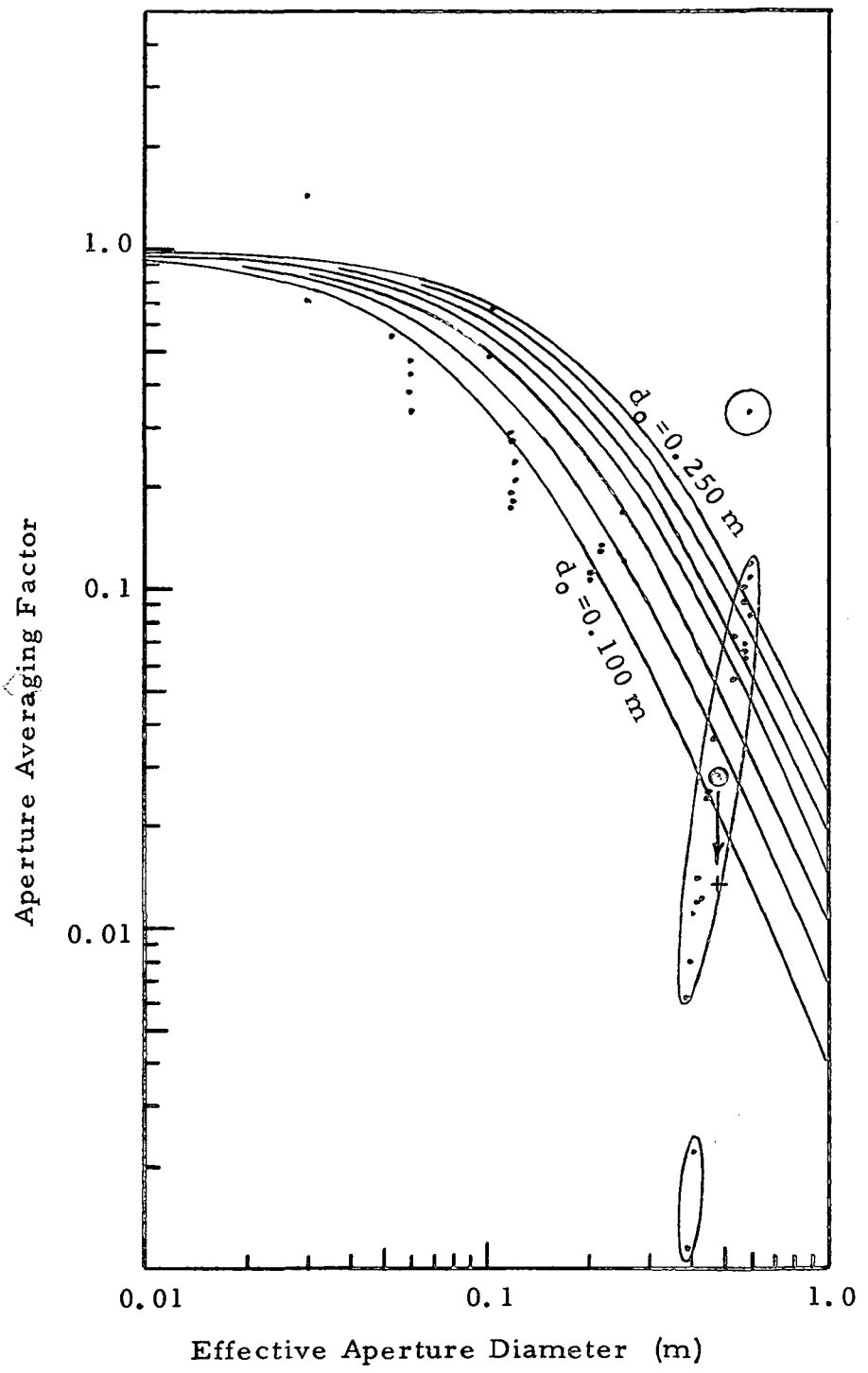

Figure 75. Aperture Averaging Measurements Corrected to Zenith Viewing Using $\Sigma^2_{zenith}=0.50$. Theoretical predictions are shown for $d_o=0.100$ m , 0.125 m , 0.150 m , 0.175 m , 0.200 m , 0.225 m , and 0.250 m , as the solid curves. Measured values are indicated by the dots. The encircled data points were taken with a central obscuration in the aperture.

Table 12

Aperture Averaging Measurement Data Compensated to Zenith Propagation

Uncompensated Values				Compensated Results Corresponding to Zenith Propagation				
Run Number	Diameter (m)	Zenith Angle (deg)	Measured Normalized Variance	Effective Diameter (m)	Aperture Averaging Factor			
					$(\Sigma^{o}_{zenith}=0.35)$	$(\Sigma^{o}_{zenith}=0.40)$	$(\Sigma^{o}_{zenith}=0.45)$	$(\Sigma^{o}_{zenith}=0.50)$
1	0.76	56.56	0.1458	0.564	0.1009	0.08453	0.07199	0.06212
2	0.76	56.56	0.2373	0.564	0.1638	0.1372	0.1169	0.1009
3	0.08	56.57	0.8870	0.0594	0.6126	0.5132	0.4370	0.3771
4	0.04	56.57	1.667	0.0299	1.151	0.9644	0.8214	0.7088
8	0.76	56.57	0.2118	0.564	0.1464	0.1227	0.1045	0.09013
9	0.76	56.58	0.1601	0.564	0.1104	0.09249	0.07877	0.06797
10	0.76	56.63	0.1536	0.564	0.1059	0.08868	0.07551	0.06514
12	0.08	56.84	0.8049	0.0592	0.5450	0.4561	0.3881	0.3346
13	0.08	56.87	1.040	0.0591	0.7025	0.5879	0.5001	0.4311
14	0.08	56.98	1.137	0.0591	0.7637	0.6389	0.5433	0.4682
17	0.16	57.17	0.4240	0.1178	0.2800	0.2341	0.1989	0.1713
18	0.16	56.41	0.6407	0.1190	0.4479	0.3754	0.3199	0.2762
19	0.16	57.16	0.4637	0.1178	0.2868	0.2398	0.2038	0.1755
20	0.16	57.14	0.4688	0.1179	0.3104	0.2595	0.2206	0.1900
23	0.16	56.27	0.6374	0.1192	0.4496	0.3770	0.3214	0.2776
24	0.16	56.02	0.5262	0.1196	0.3780	0.3172	0.2707	0.2340

Table 12 (Continued)

Uncompensated Values				Compensated Results Corresponding to Zenith Propagation				
Run Number	Diameter (m)	Zenith Angle (deg)	Measured Normalized Variance	Effective Diameter (m)	Aperture Averaging Factor			
					$(\Sigma^{o}_{Zenith}=0.35)$	$(\Sigma^{o}_{Zenith}=0.40)$	$(\Sigma^{o}_{Zenith}=0.45)$	$(\Sigma^{o}_{Zenith}=0.50)$
27	0.04	54.67	2.875	0.0304	2.266	1.910	1.636	1.420
29	0.76	53.33	0.1998	0.587	0.1718	0.1453	0.1249	0.1088
30	0.76	53.15	0.2143	0.589	0.1858	0.1572	0.1352	0.1179
31	0.32	52.63	0.2956	0.249	0.2652	0.2247	0.1935	0.1688
33	0.32	52.06	0.2043	0.251	0.1890	0.1603	0.1383	0.1208
38	0.76	53.70	0.6209	0.585	0.5212	0.4404	0.3782	0.3292
39	0.76	53.98	0.1615	0.583	0.1332	0.1124	0.09649	0.08391
42	0.16	55.42	0.4422	0.1205	0.3312	0.2785	0.2381	0.2062
46	0.76	60.96	0.2603	0.530	0.1242	0.1021	0.08533	0.07227
47	0.76	61.50	0.2094	0.525	0.09472	0.7761	0.06467	0.05461
48	0.32	62.55	0.5721	0.217	0.2325	0.1893	0.1567	0.1315
49	0.32	62.88	0.6010	0.216	0.2357	0.1915	0.1582	0.1324
52	0.08	64.26	3.019	0.0527	1.009	0.8112	0.6633	0.5498
53	0.16	65.03	4.091	0.1040	1.240	0.9901	0.8043	0.6624
54	0.16	65.84	3.391	0.1024	0.9208	0.7299	0.5884	0.4809
57	0.32	67.14	0.9853	0.1995	0.2205	0.1723	0.1370	0.1104
58	0.32	67.47	1.034	0.1981	0.2187	0.1702	0.1348	0.1082
59	0.76	68.56	0.4340	0.459	0.07640	0.05857	0.04568	0.03612

Table 12 (Continued)

Uncompensated Values				Compensated Results Corresponding to Zenith Propagation				
Run Number	Diameter (m)	Zenith Angle (deg)	Measured Normalized Variance	Effective Diameter (m)	Aperture Averaging Factor			
					$(\Sigma^{\circ}_{zenith}+0.35)$	$(\Sigma^{\circ}_{zenith}=0.40)$	$(\Sigma^{\circ}_{zenith}=0.45)$	$(\Sigma^{\circ}_{zenith}=0.50$
61	0.76	69.73	0.3993	0.447	0.05597	0.04209	0.03221	0.02499
62	0.76	70.30	0.4379	0.441	0.05438	0.04046	0.03063	0.02352
64	0.76	71.67	0.3453	0.426	0.03078	0.02221	0.01631	0.01215
66	0.76	72.78	0.6110	0.414	0.03975	0.02780	0.01980	0.01431
67	0.76	73.31	0.6286	0.407	0.03454	0.02375	0.01662	0.01181
69	0.76	73.99	0.8526	0.399	0.03690	0.02475	0.01690	0.01173
70	0.76	74.63	0.8004	0.391	0.02695	0.01760	0.01170	0.00791
71	0.76	75.36	0.9597	0.382	0.02347	0.01479	0.00950	0.00621
75	0.76	73.99	0.1584	0.399	0.00683	0.00458	0.00313	0.00217
76	0.76	74.63	0.1168	0.391	0.00394	0.00257	0.00171	0.00115

four figures represents a nominal average of the values encircled by the ellipse. As pointed out in Appendix A, for a 0.20 m central obscuration in a 0.76 m receiver aperture, we expect only about half as much aperture averaging as would be produced by a 0.76 m diameter receiver with no central obscuration. A factor of two below the shaded circle, we have plotted a plus mark (+) which we believe properly represents the average value of all of the enclosed data points after we make allowance for the central obscuration. We would expect the theory for aperture averaging with a clear aperture to match up to this point, i.e., (+), rather than to encircled data points as plotted.

On each of the four figures, i.e., Fig.'s 72 to 75, we have superimposed the prediction of the aperture averaging factor for a clear aperture for various values of $(d_o)_{zenith}$, as calculated from Eq. (19). Examination of all of the figures suggests that the best match to the data is provided by using the values

$$\Sigma^o{}_{zenith} = 0.40 \quad , \quad (\sigma_L{}^2)_{zenith} = 0.336 \quad ,$$

$$(d_o)_{zenith} = 0.125 \text{ m} \quad .$$

These values are in reasonably good agreement with what we would normally expect for daytime propagation, namely, a log-amplitude variance, $\sigma_\ell{}^2 = 0.0841$, and a scintillation correlation distance of the order of 12.5 cm.

5.3 Conclusions

While the spread of the data is too large to tightly bound the conclusions that can be drawn from a comparison of theory and experiment, we can generally conclude that the experimental data are in general agreement with the existing theory of aperture averaging. Most of the deviation between theory and experiment can be attributed to the stochastic nature

of the scintillation phenomena. The few data points that significantly deviate from the theoretical predictions are most likely due to excess noise or some other anomaly in the data channel. The values obtained for the log-amplitude variance, σ_ℓ^2 , for $\lambda = 0.633\ \mu m$ zenith propagation, namely, $\sigma_\ell^2 = 0.084$, is apparently the only available measurement for the scintillation effects of turbulence during daylight hours. We believe the general agreement of the data obtained in this experiment with theoretical predictions of aperture averaging provides a basis for applying that theory in the analysis of the expected performance of a space-to-ground laser communications link.

References

1. P. O. Minott, J. L. Bufton, W. H. Schaefer, and D. A. Grolemund, "Vertical Laser Beam Propagation Through the Troposphere," NASA Preprint X-723-74-123, Goddard Space Flight Center, Greenbelt, Maryland, April 1974

2. D. L. Fried, "Theoretical Analysis of Aperture Averaging," Optical Science Consultants Report No. DR-015, Yorba Linda, CA, October 1973. (Final Report on NASA Contract NAS5-23272.)

3. V. I. Tatarski, "Wave Propagation in a Turbulent Medium," McGraw-Hill, New York, 1961.

4. V. I. Tatarski, "The Effects of the Turbulent Atmosphere on Wave Propagation," National Technical Information Service, Springfield, VA, 1971.

5. J. W. Strohbehn, "Optical Propagation Through the Turbulent Atmosphere," in "Progress in Optics," edited by E. Wolf, American Elsevier, New York, 1971.

6. D. L. Fried, G. E. Mevers, and M. P. Keister, Jr., "Measurements of Laser-Beam Scintillation in the Atmosphere," J. Opt. Soc. Am. 57, 787 (1967).

7. R. L. Mitchell, "Permanence of the Log-Normal Distribution," J. Opt. Soc. Am. 58, 1267 (1968)

8. D. L. Fried, "Aperture Averaging of Scintillation," J. Opt. Soc. Am. 57, 169 (1967).

9. A. T. Young, "Aperture Filtering and Saturation of Scintillation," J. Opt. Soc. Am. 60, 248 (1970).

10. Private communications from Dr. Harold Hance, Lockheed Palo Alto Research Laboratory, Palo Alto, CA.

11. D. L. Fried, "Statistics of Laser Beam Fade Induced by Pointing Jitter," Appl. Opt. 12, 422 (1973).

Appendix A

Aperture Averaging

in the

Presence of a Central Obscuration

Introduction

The theory of aperture averaging of atmospheric turbulence-induced intensity variations was rather extensively treated in a previous work of ours[1] for the case of a circular clear aperture. Here we shall be concerned with assessing the implications of a circular central obscuration on the variance of the aperture averaged signal. As we shall see, the theoretical results for aperture averaging with central obscuration can be obtained directly from our previous results for aperture averaging without any central obscuration. We therefore first briefly review these results, and then proceed with the development of the new results.

Previous Results

It has previously been shown[2] that for propagation over a path of length L, by radiation of wave number k, if the distribution of the refractive-index structure constant over the path is given by $C_N^2(s)$ (where $s = 0$ at the source and $s = L$ at the aperture, i.e., measurement plane), the log-amplitude variance is given by the equation

$$\sigma_\ell^2 = 0.56\, k^{7/6} \int_{\text{Path}} ds\; C_N^2(s)\, s^{5/6}\, \mu^{5/6} \quad , \tag{1}$$

where

$$\mu = \begin{cases} 1 & , \text{ if the source is an infinite plane wave source} \\ s/L & , \text{ if the source is a point source.} \end{cases} \quad . \tag{2}$$

It has been shown[3] that since the fluctuations of intensity are log-normally distributed, if the mean intensity at the measurement plane is denoted by I_o, then the intensity variance can be written as

$$\sigma_I^2 = I_o^2 \left[\exp\left(4\,\sigma_\ell^2\right) - 1\right] \quad . \tag{3}$$

In our previous work on aperture averaging[1] we showed that if we considered a circular clear aperture of diameter D collecting a signal S from the fluctuating intensity signal described above, that signal would have a mean value S_o , and a variance, σ_s^2 given by the expressions

$$S_o = \tfrac{1}{4} \pi D^2 I_o \quad , \tag{4}$$

and

$$\sigma_s^2 = \sigma_I^2 \, (\tfrac{1}{4} \pi D^2)^2 \, \textcircled{A} \tag{5}$$

where $\textcircled{A}$ is what we have called the aperture averaging factor. The value of the aperture averaging factor was developed for the circular clear aperture. It was shown that for an aperture of diameter D , the aperture averaging factor has the value given by the expression

$$\textcircled{A} = \left[1 + \left(\frac{D}{d_o} \right)^{7/6} + \left(\frac{D}{d_o} \right)^{7/3} \right]^{-1} \quad , \tag{6}$$

where the length d_o is a propagation parameter whose value is

$$d_o = 2.399 \, k^{-1/2} \left\{ \frac{\int_{Path} ds \; C_N^2(s) \, (L-s)^2 \, \mu^{-1/3}}{\int_{Path} ds \; C_N^2(s) \, (L-s)^{5/6} \, \mu^{5/6}} \right\}^{3/7} \quad . \tag{7}$$

With these results, it is a straightforward matter to undertake the calculation of the aperture averaged signal for a circular clear aperture of diameter D , given the distribution of the refractive-index structure constant along the propagation path. We now turn our attention to the problem of extending these results to the case of a circular aperture with a central obscuration.

Central Obscuration Considerations

In this section, we shall be concerned with a circular aperture of diameter D with a concentric circular obscuration of diameter d, subject to the constraints that we are dealing with an aperture that is large enough that

$$D \gg d_o \quad , \tag{8}$$

$$\tfrac{1}{2}(D-d) \gg d_o \quad , \tag{9}$$

but for which we shall not be too severe in enforcing the "very much greater than" relationship. Our approach to this problem is by noting that the fluctuations of the aperture averaged signal are not due to variation in the total optical signal power reaching the measurement (i.e., the aperture) plane, but rather are due to redistribution of the energy from one point in the plane to another. Generally speaking, this redistribution of energy takes place over a range of the order of d_o or less. This means that the variations of the aperture averaged signal collected by an unobstructed circular aperture of diameter d are to be associated with variations in the spill over of energy into or out of the region surrounding that aperture. Similarly, the variation in the aperture averaged signal from an unobstructed circular aperture of diameter D are to be associated with the random relocation of energy between inside and outside of the circle. For the obstructed aperture, if we assume that D is sufficiently greater than d, as required by Eq. (9), then the aperture is randomly exchanging optical power with its external surroundings with an exchange variance, σ_D^2, as given by the clear aperture formula for diameter D, and is randomly exchanging optical power with the internal "surroundings" (i.e., the obstruction region), with an exchange variance σ_d^2, as given by the clear aperture formula for diameter d. The signal

variance σ_s^2 is the sum of these two variances, i.e.,

$$\sigma_s^2 = \sigma_D^2 + \sigma_d^2 \quad , \tag{10}$$

where

$$\sigma_D^2 = \sigma_I^2 \left(\tfrac{1}{4}\pi D\right)^2 \left[1 + \left(\frac{D}{d_o}\right)^{7/6} + \left(\frac{D}{d_o}\right)^{7/3}\right]^{-1} \quad , \tag{11}$$

$$\sigma_d^2 = \sigma_I^2 \left(\tfrac{1}{4}\pi d^2\right) \left[1 + \left(\frac{d}{d_o}\right)^{7/6} + \left(\frac{d}{d_o}\right)^{7/3}\right]^{-1} \quad . \tag{12}$$

It now follows that the aperture averaged signal variance for the obstructed aperture case can be written as

$$\sigma_s^2 = \sigma_I^2 \left[\tfrac{1}{4}\pi (D^2 - d^2)\right] \tilde{\Theta} \quad , \tag{13}$$

where $\tilde{\Theta}$ is the modified aperture averaging factor. Its value is given by the expression

$$\tilde{\Theta} = \frac{D^2}{D^2 - d^2} \left\{ \frac{1}{\left[1 + \left(\frac{D}{d_o}\right)^{7/6} + \left(\frac{D}{d_o}\right)^{7/3}\right]} + \frac{d^2/D^2}{\left[1 + \left(\frac{d}{d_o}\right)^{7/6} + \left(\frac{d}{d_o}\right)^{7/3}\right]} \right\} . \tag{14}$$

This, together with Eq. (13), represents our basic result for aperture averaging with central obscuration.

To see the significance of the central obscuration correction factor for aperture averaging, compared to the result for unobstructed aperture averaging, we have calculated the aperture averaging factor for the variety of cases listed in Table 1. As can readily be seen, the correction can be significant -- in the cases shown, the difference represents about a factor of two.

References (for Appendix A)

1. D. L. Fried, "Theoretical Analysis of Aperture Averaging," Report No. DR-015, Optical Science Consultants (Oct. 1973). Final Report on Contract No. NAS5-23272.

2. V. I. Tatarski, "Wave Propagation in a Turbulent Medium," McGraw-Hill (New York, 1961).

3. D. L. Fried, "Aperture Averaging of Scintillation," J. Opt. Soc. Am. 57, 169 (1967).

Table 1A

Aperture Averaging

With and Without Central Obscuration

D = outer diameter

d = central obscuration diameter

d_o = aperture averaging length

d_o (m)	Θ D = 0.76 m	$\tilde{\Theta}$ D = 0.76 m d = 0.20 m	Θ D = 0.64 m	$\tilde{\Theta}$ D = 0.64 m d = 0.20 m
0.100	.007986	.01756	.01166	.02598
0.11	.009857	.02115	.01435	.03127
0.12	.01193	.02500	.01732	.03691
0.13	.01420	.02907	.02055	.04288
0.14	.01667	.03336	.02405	.04914
0.15	.01933	.03785	.02781	.05567
0.16	.02218	.04252	.03181	.06244
0.17	.02521	.04736	.03604	.06944
0.18	.02842	.05236	.04050	.07663
0.19	.03181	.05751	.04518	.08401
0.200	.03536	.06279	.05006	.09156

Appendix B

Thermosonde Balloon Flight #7

Measurements of C_N^2

Introduction

At approximately the same time that laser transmitter balloon flight #5 was being conducted, thermosonde balloon flight #7 was carried out to obtain data on the vertical distribution of the refractive-index structure constant, C_N^2 . The basic plan when the experiment was organized was to obtain data on C_N^2 which could then be used with propagation theory and aperture averaging theory to allow run-by-run comparison of measurements with theory. Unfortunately, as noted in the body of this report, the thermosonde appears to have functioned incorrectly (possibly due to solar heating) and the measured values of C_N^2 appear to be substantially too large. In this appendix we shall briefly present the results associated with the thermosonde data, and explain the basis for considering the derived values of C_N^2 to be too large. We have not been able to develop any plausible method of "correcting" the measured values of C_N^2 .

Measurements

The thermosonde makes measurements of the mean square difference of temperature at two points some fixed distance apart. From this, it is then possible to calculate the temperature structure constant, C_T^2 . From that, and knowledge of the local temperature and pressure, it is then a straightforward matter to calculate the refractive-index structure constant, C_N^2 .

Because of the stochastic nature of turbulence, individual measurements of C_N^2 fluctuate strongly and a great deal of averaging is required to obtain statistically significant results. Because the thermosonde balloon's altitude is continuously changing as the C_N^2 measurements are being made, it is convenient to convert the measurements into an estimate of the integral of C_N^2 over altitude. Such a curve is relatively smooth,

and in fact can usefully be represented by a quite smooth curve. The slope of this smooth curve can then be taken as a well-averages estimate of the value of C_N^2 at each altitude.

In Fig. B-1, we show a plot of the integral of C_N^2 with altitude starting at 1.5 km. The smooth curve has been drawn so as to represent what we identify as the general trends of the integral. However, it does not follow the point-by-point irregularities which we identify with the stochastic aspects of the measurement data. Working with the slope of this curve, we have prepared estimates of the mean value of C_N^2 in each of the one-kilometer intervals centered about the altitudes 2 km , 3 km , . . ., 25 km. These results are shown in Table B-1.

Calculations and Conclusions

We have utilized the turbulence mode presented in Table B-1 to calculate the expected log-amplitude variance, σ_ℓ^2 , and the scintillation averaging length, d_o , for $\lambda = .633$ μm radiation viewed at the zenith. Using this turbulence model, we obtain $\sigma_\ell^2 = 0.474$ nepers^2 , and $d_o = 0.0889$ m . We note first of all that these results are in significant disagreement with the measurements of scintillation which we found were best explained by the values $\sigma_\ell^2 = 0.0841$ nepers^2 and $d_o = 0.125$ m . The value of d_o obtained from the thermosonde data is only 70% as large as the value obtained from the optical measurements, a discrepancy large enough to raise questions, but not large enough to base a firm conclusion on. However, the value of σ_ℓ^2 calculated from the thermosonde data is 564% larger than the value obtained from the optical measurements. This is much too large an error to be attributed to the stochastic nature of the data. Moreover, the value of σ_ℓ^2 obtained from the thermosonde data is so large as to put the propagation into the saturation of scintillation regime -- a condition which we consider highly unlikely for this propagation

path. We note that this value of σ_ℓ^2 , i.e., $\sigma_\ell^2 = 0.474$, corresponds to an rms intensity fluctuation of 237% . This large an intensity scintillation would be clearly visible as a very distinct phenomena for all high altitude optical sources during the daytime. Since no such striking intensity scintillation is observed, and because $\sigma_\ell^2 = 0.474$ is so at variance with what we expect for this propagation path, we resolve the discrepancy between the thermosonde data and the optical data by concluding that the thermosonde data should be considered unreliable. We have been unable to discover any simple and credible correction to the thermosonde data which would remove the discrepancy, and therefore consider the thermosonde data as not being part of the data base of this experiment.

Table B-1

Estimates of C_N^2 From Thermosonde Balloon Flight #7

Altitude (km)	C_N^2 ($m^{-2/3}$)	Altitude (km)	C_N^2 ($m^{-2/3}$)
2	3.23×10^{-16}	16	1.13×10^{-16}
3	2.27	17	0.79
4	1.67	18	0.79
5	1.28	19	0.62
6	1.27	20	0.48
7	0.97	21	0.59
8	0.86	22	0.52
9	1.08	23	0.45
10	1.40	24	0.36
11	1.39	25	0.17
12	1.60		
13	1.80		
14	2.19		
15	1.49		

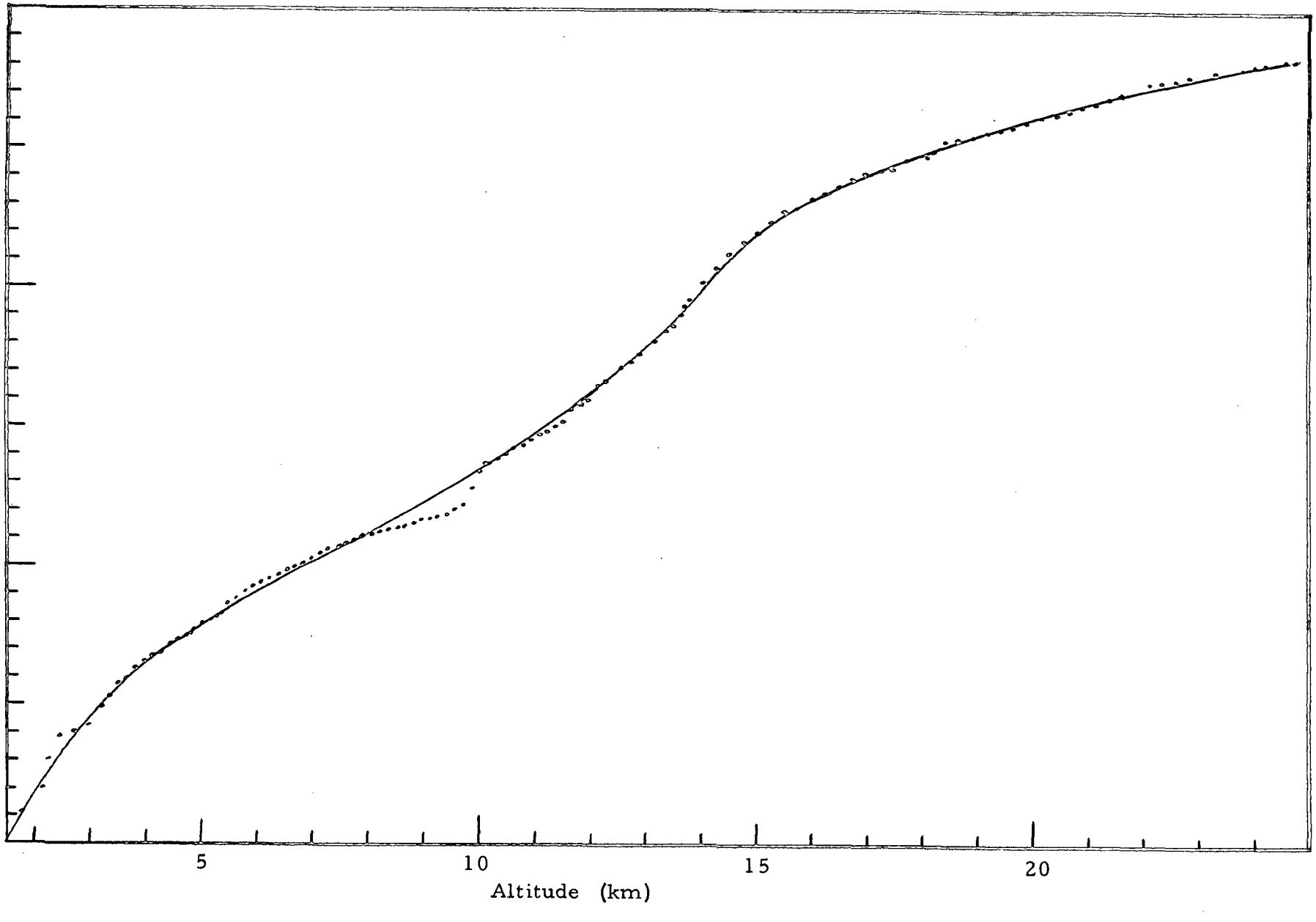

Figure B-1. Altitude Integral of the Refractive-Index Structure Constant Measured by Thermosonde Balloon Flight #7.

Appendix C

Temporal Power Spectra

This appendix is in the nature of an addendum to the body and principal concerns of this report, which was to study aperture averaging. Having had the recordings of the various data runs, it has been convenient to Fourier analyze some of that data and study the resulting spectra. Our objective in doing this has been two-fold. First, we wish to assure ourselves that there is no noise entering into our data as a single frequency, such as 60 Hz ripple. Secondly, we wish to see if we can say anything useful about the temporal nature of the aperture averaged signal fluctuations.

In Fig.'s C-1 to C-16, we show the Fourier transform of various of the background runs. In none of the background run spectra do we see any evidence of a serious amount of single frequency noise. In this sense, the experimental apparatus was apparently free of spurious noise problems. We note, however, the rather peculiar and not particularly consistent set of shapes for the background run spectra. We take this as an indication of some excess low frequency noise. Fortunately, the variances of the background runs were generally low enough that we can conclude that this excess noise was not significant.

In Fig.'s C-17 to C-32, we show plots of the power spectra obtained from 16 scintillation runs taken with various aperture diameters and when viewing at various zenith angles. Here again we note the absence of any single frequency noise, which assures us of such things as that there was no significant ripple in the laser output -- a matter which was not tested in our examination of the background run power spectra.

We note that for these power spectra, with the single exception of Run #4, Fig. C-17, which was for a 0.04 m diameter aperture, all of the scintillation power spectra appear to exhibit a relatively well defined decline starting at very low frequencies. It is not clear what

is the origin of this low frequency strength in the power spectra. We have calculated a nominal transition frequency for each of these figures based on an estimated effective wind velocity of $v = 15$ m/sec , and a linear dimension equal to either the projected aperture diameter, $D \cos \theta$ or $d_o = 0.125$ m , whichever is larger. Our nominal transition frequency is

$$f_T = \left\{ \begin{array}{l} v/(2\ D \cos \theta) \\ \\ v/(2\ d_o) \end{array} \right\}_{\substack{\text{whichever} \\ \text{is greater}}} \qquad (1)$$

At frequencies below f_T we expect the power spectrum to be relatively constant or decreasing. In each of the scintillation data run power spectra figures, we have indicated this transition frequency by an arrow. As can be seen, in general the power spectra continues to rise as frequency decreases below f_T . We have not been able to identify this source of extra low frequency power. The possibility exists that it may be related to turbulence effects interacting with the small diameter laser beam in the atmosphere. However, this is only conjecture, and further study of this question is required.

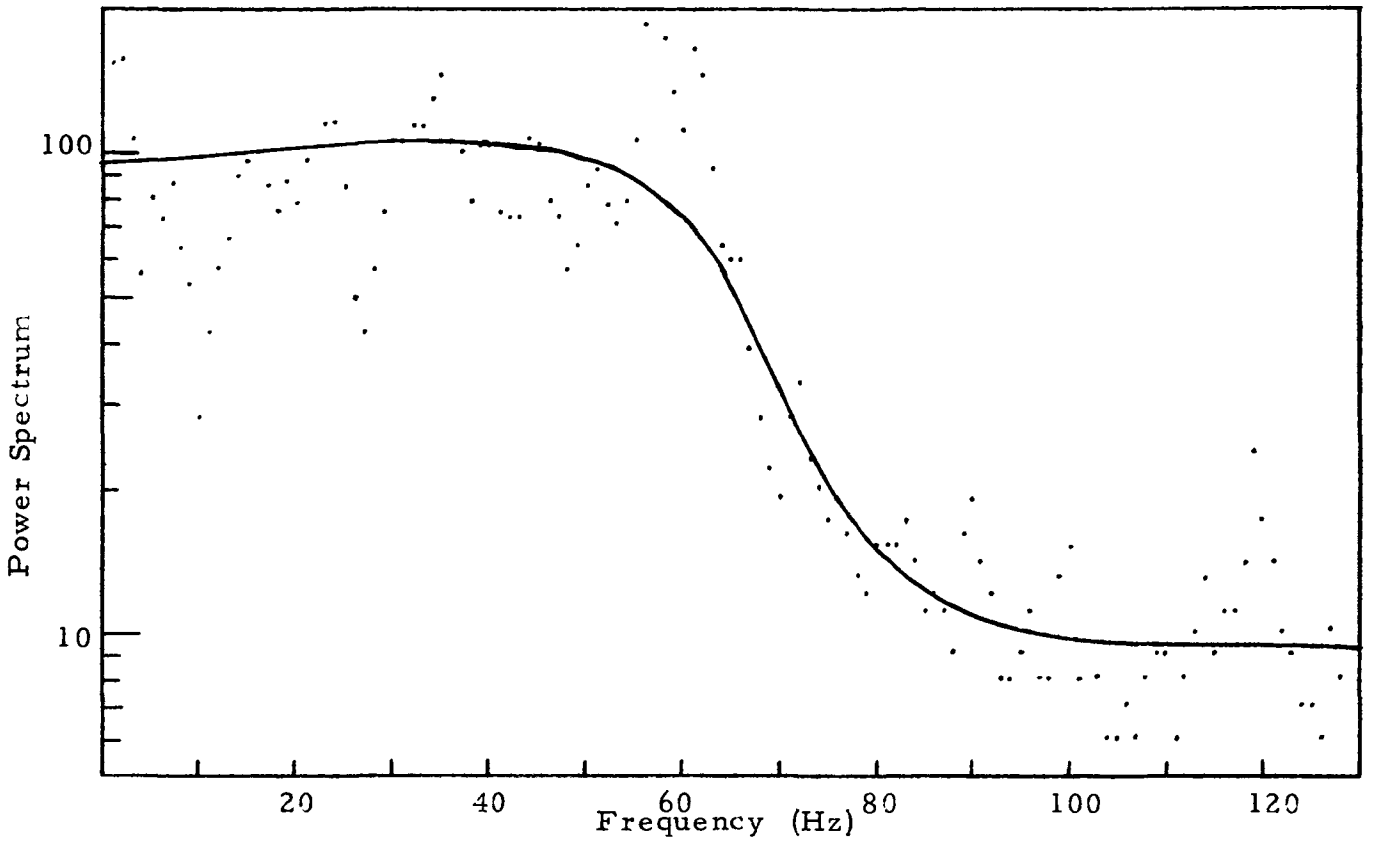

Figure C-1. Power Spectrum for Background Run #5.

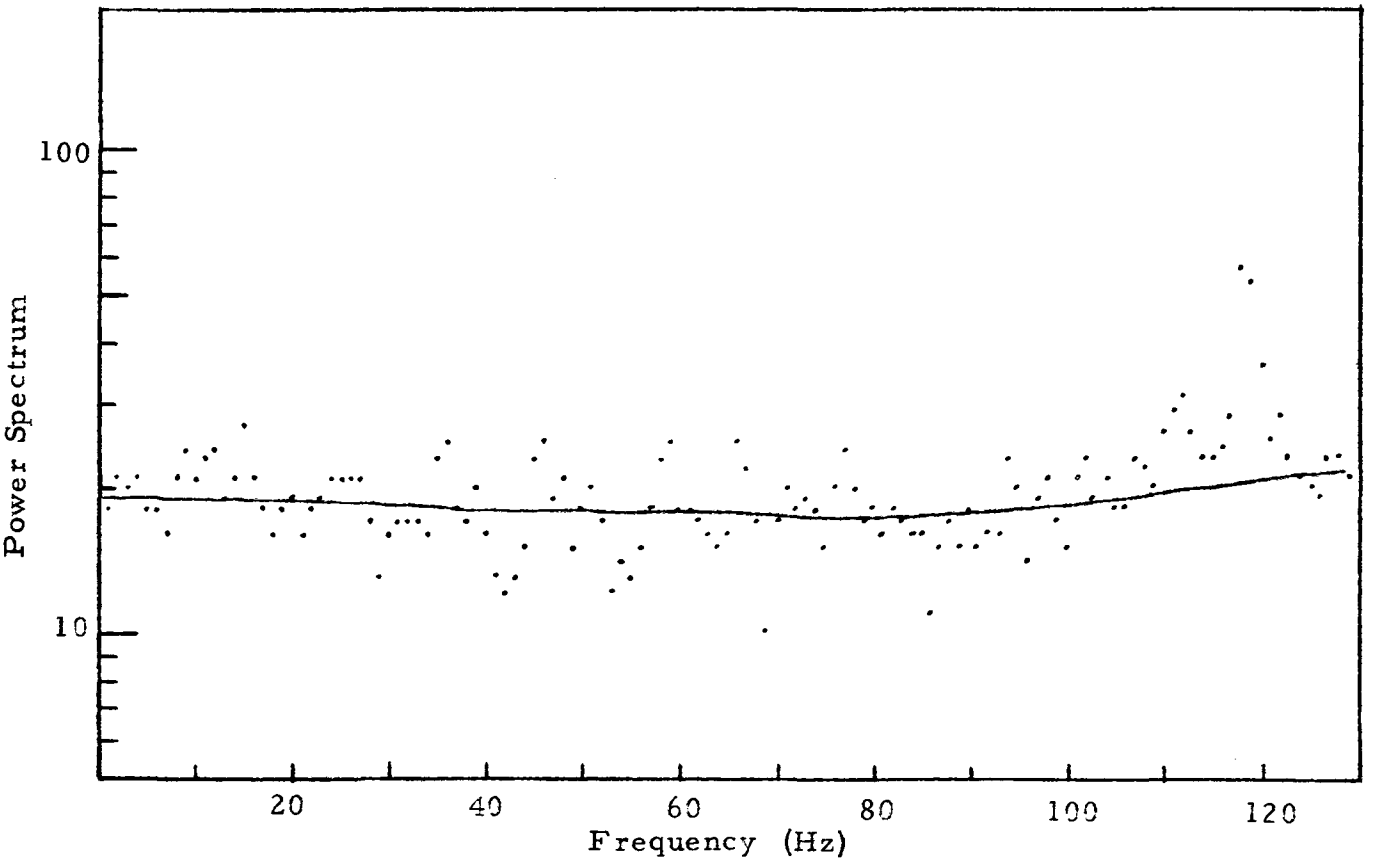

Figure C-2. Power Spectrum for Background Run #28.

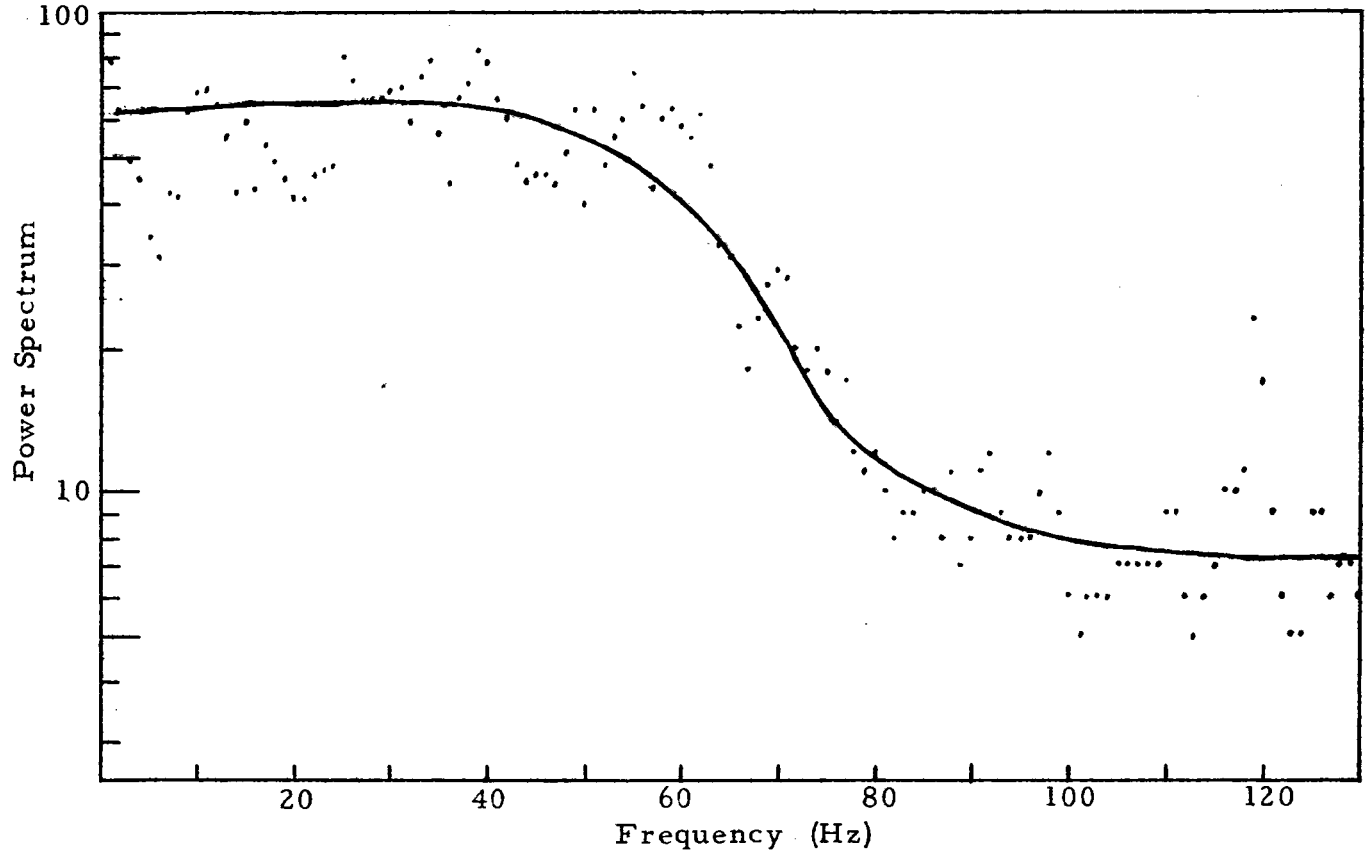

Figure C-3. Power Spectrum for Background Run #6

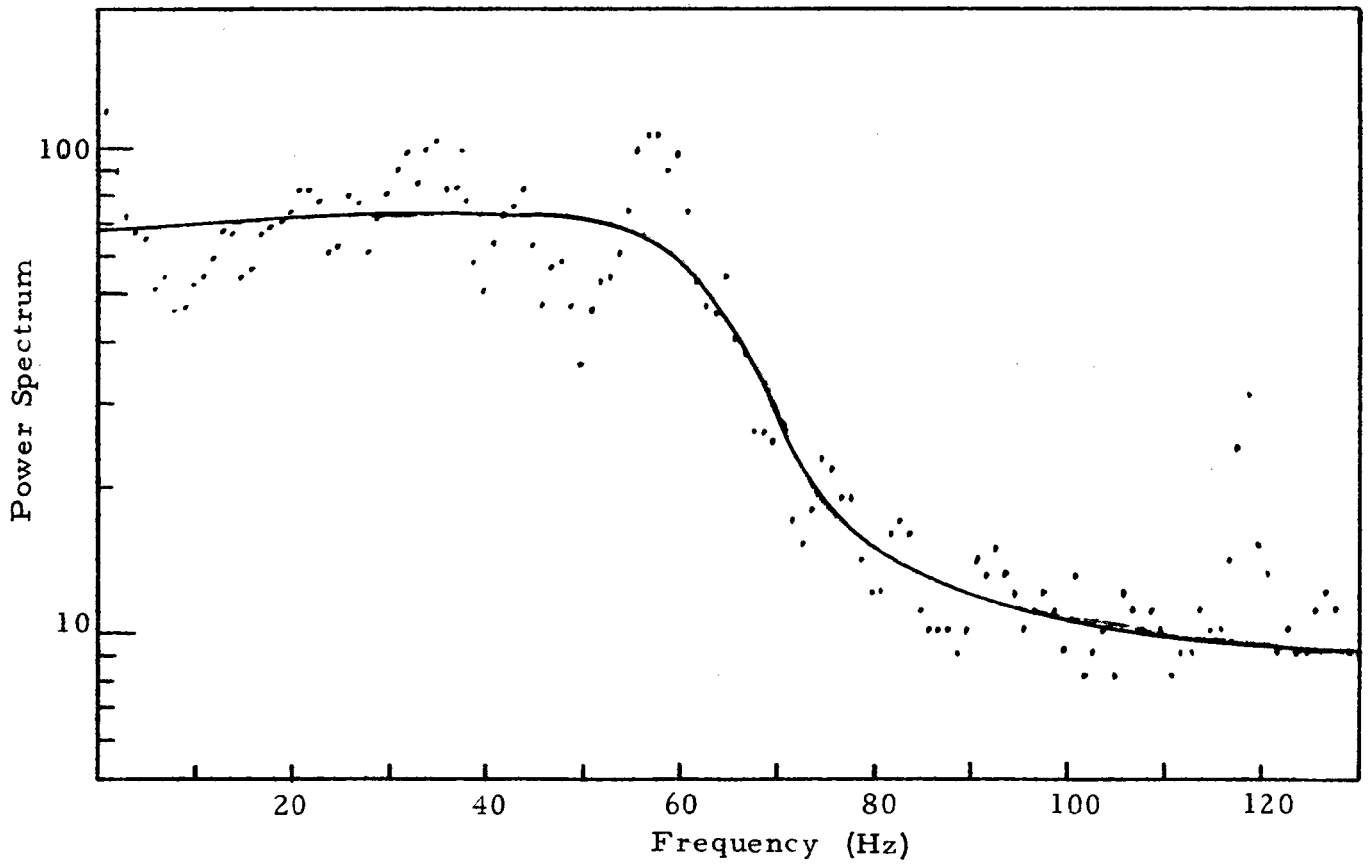

Figure C-4. Power Spectrum for Background Run #15.

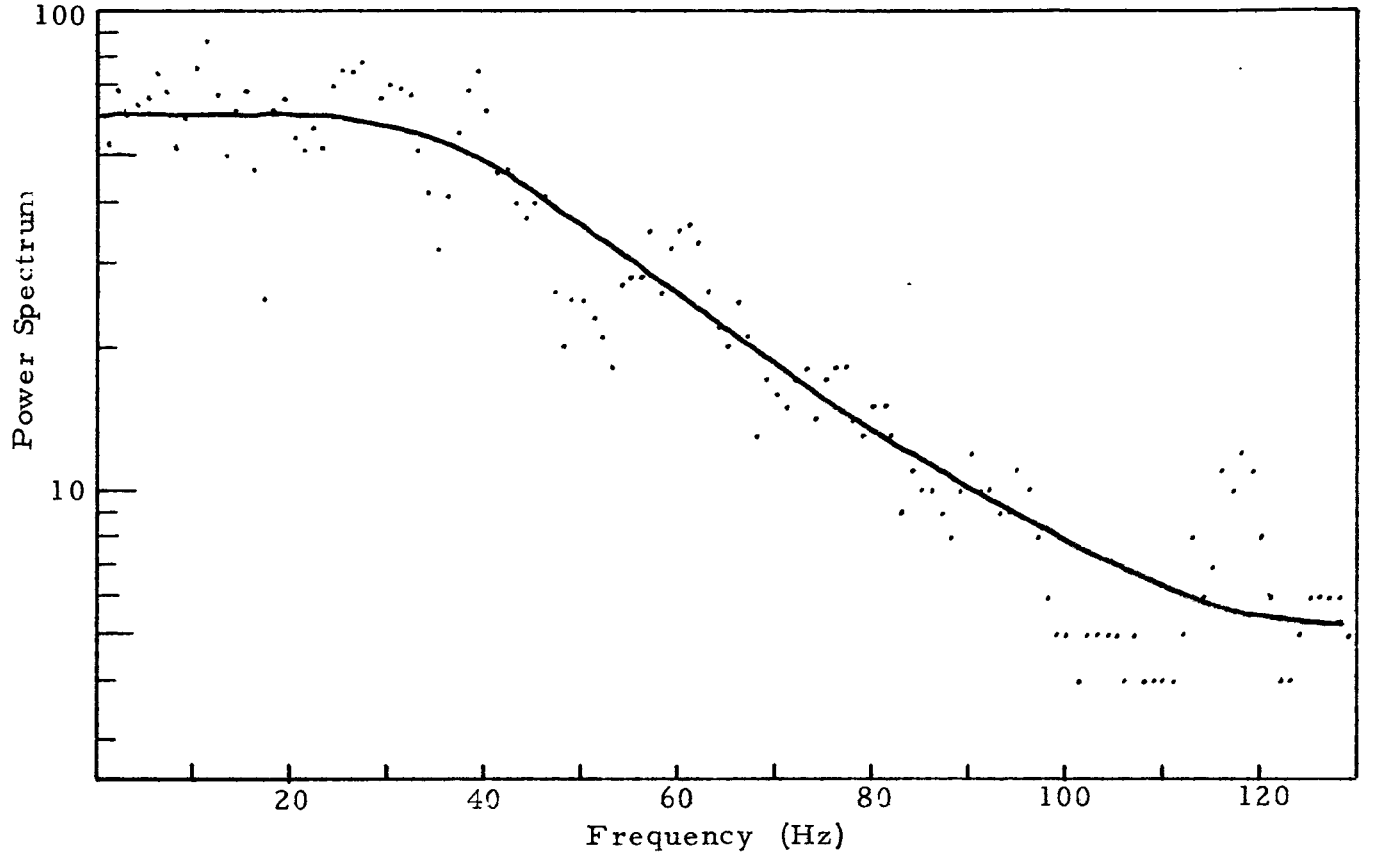

Figure C-5. Power Spectrum for Background Run #25.

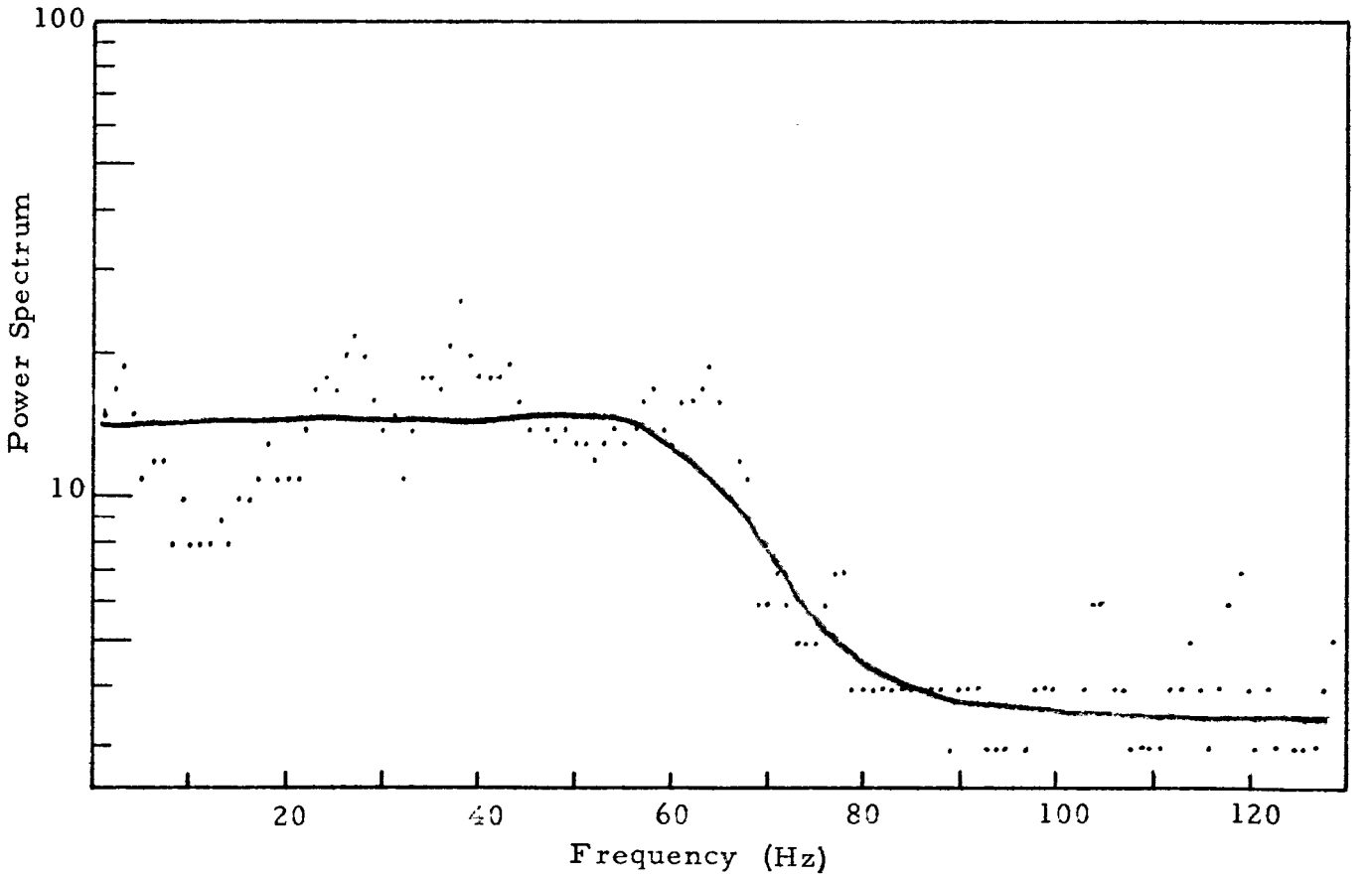

Figure C-6. Power Spectrum for Background Run #21.

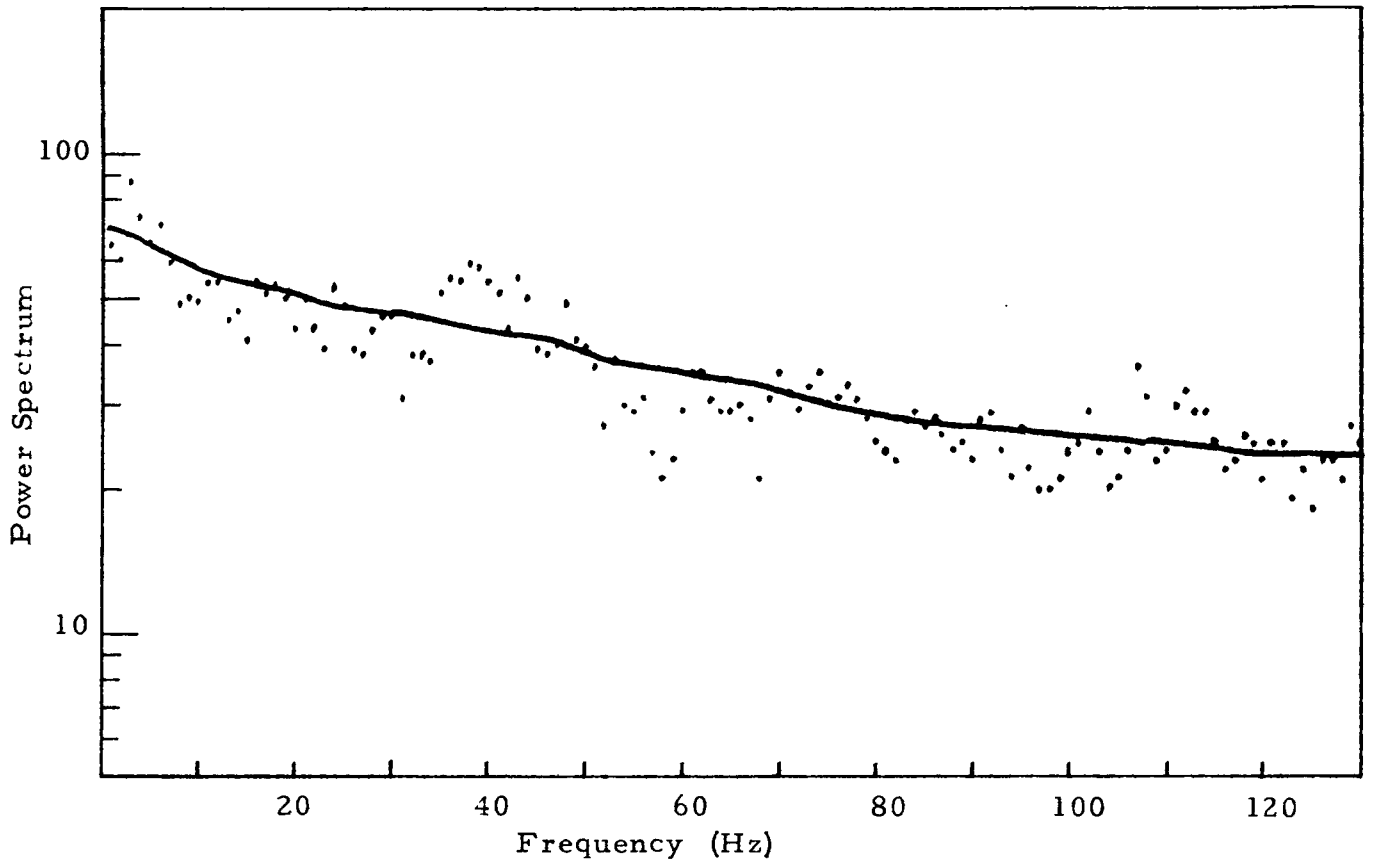

Figure C-7. Power Spectrum for Background Run #55.

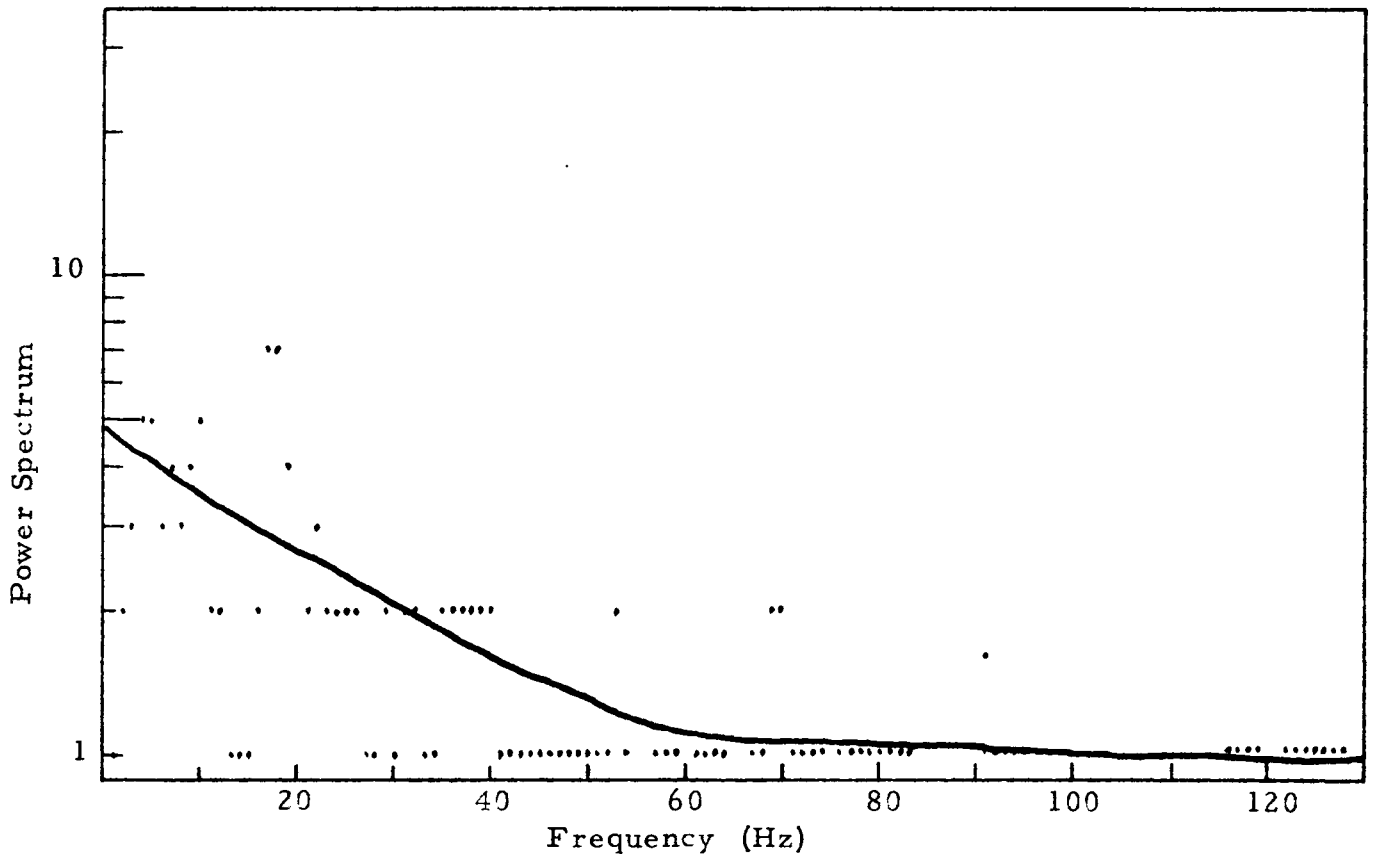

Figure C-8. Power Spectrum for Background Run #35.

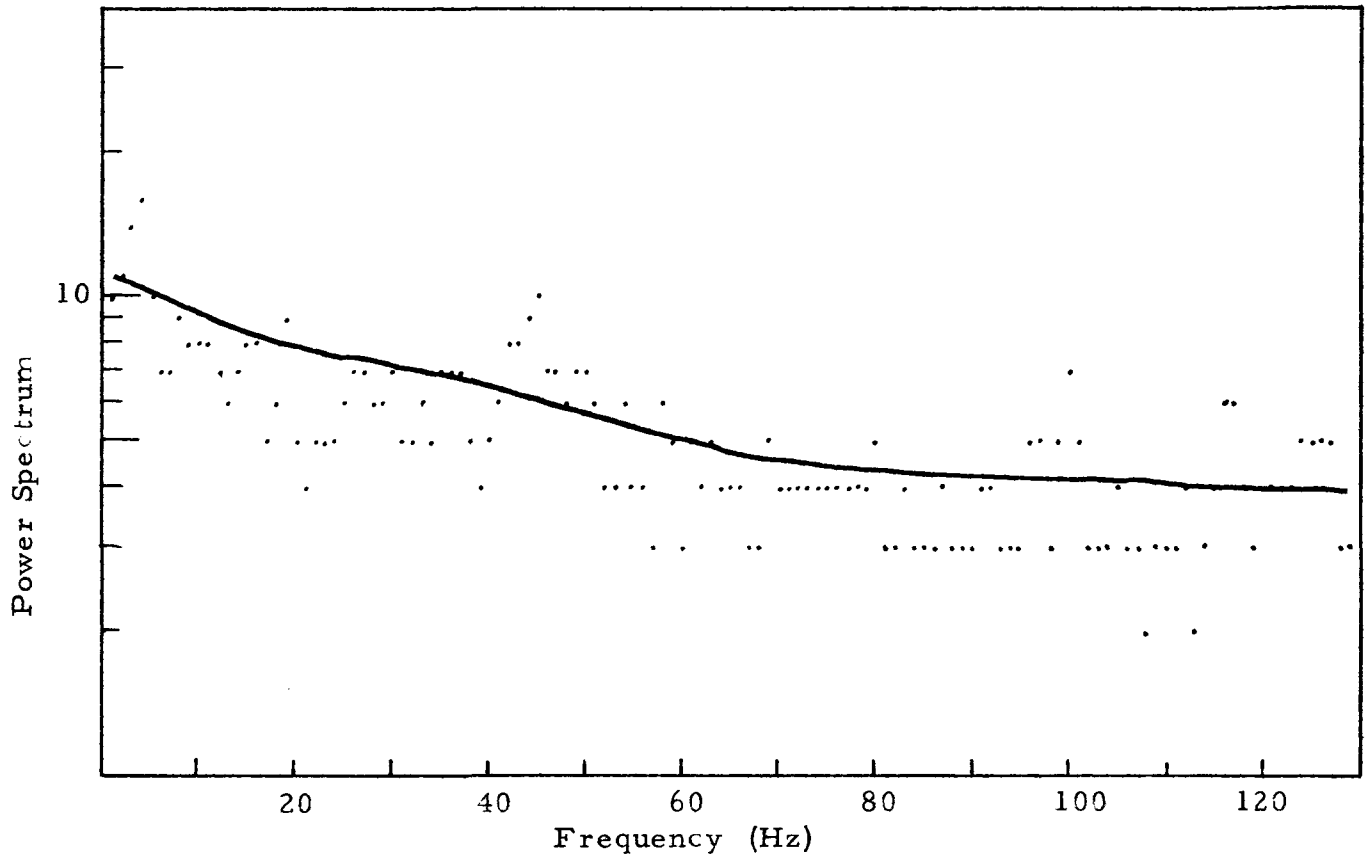

Figure C-9. Power Spectrum for Background Run #50.

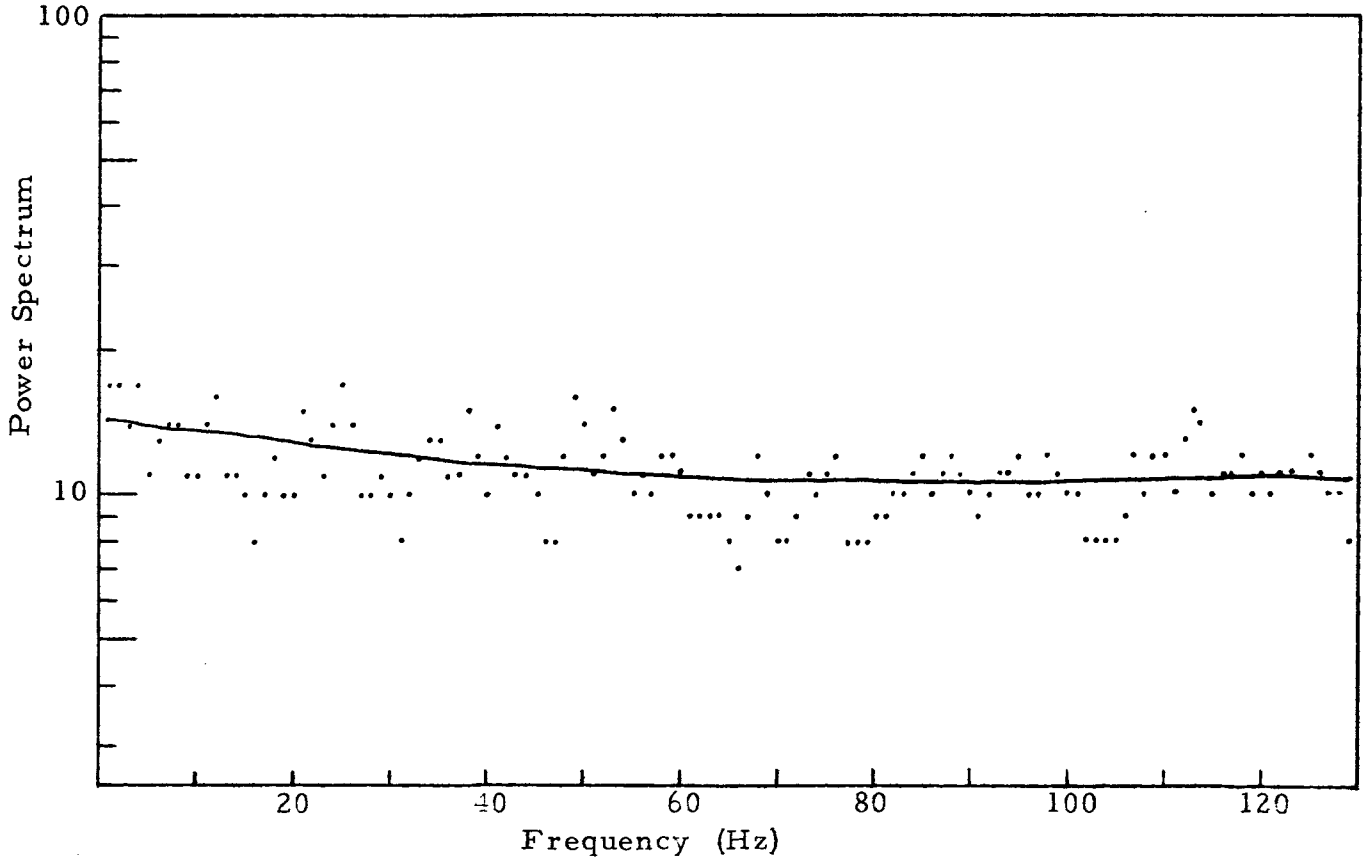

Figure C-10. Power Spectrum for Background Run #56.

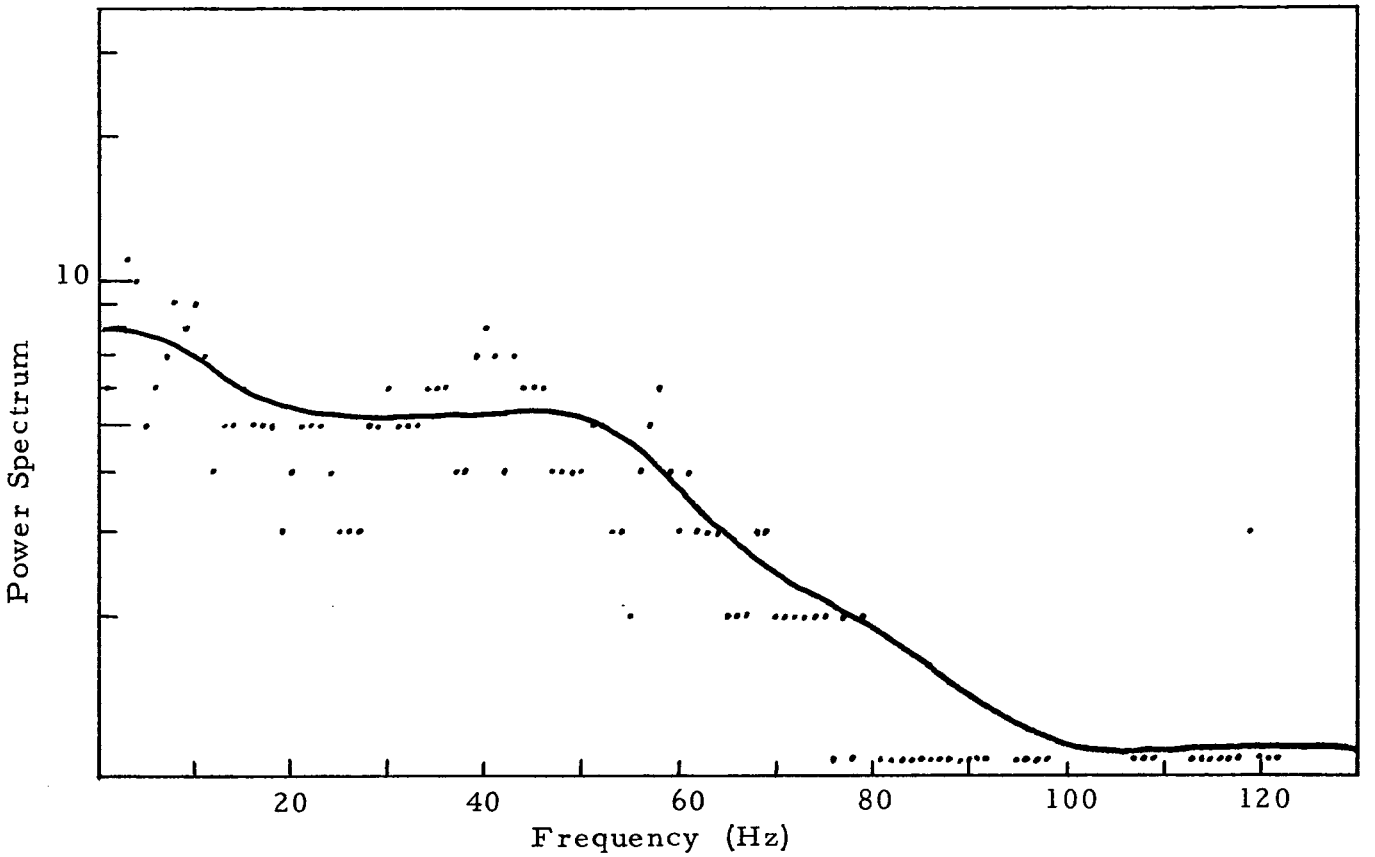

Figure C-11. Power Spectrum for Background Run #7.

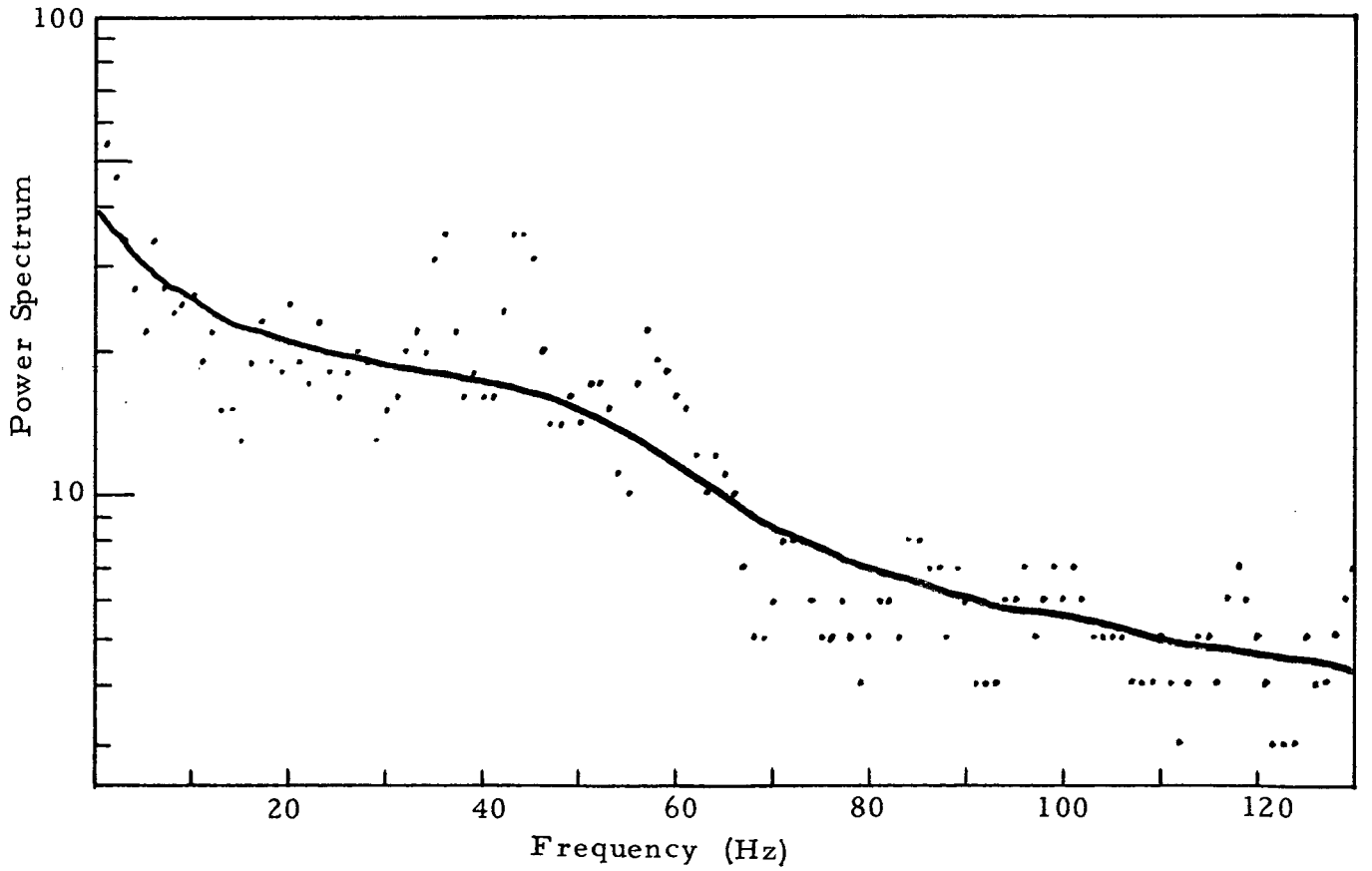

Figure C-12. Power Spectrum for Background Run #63.

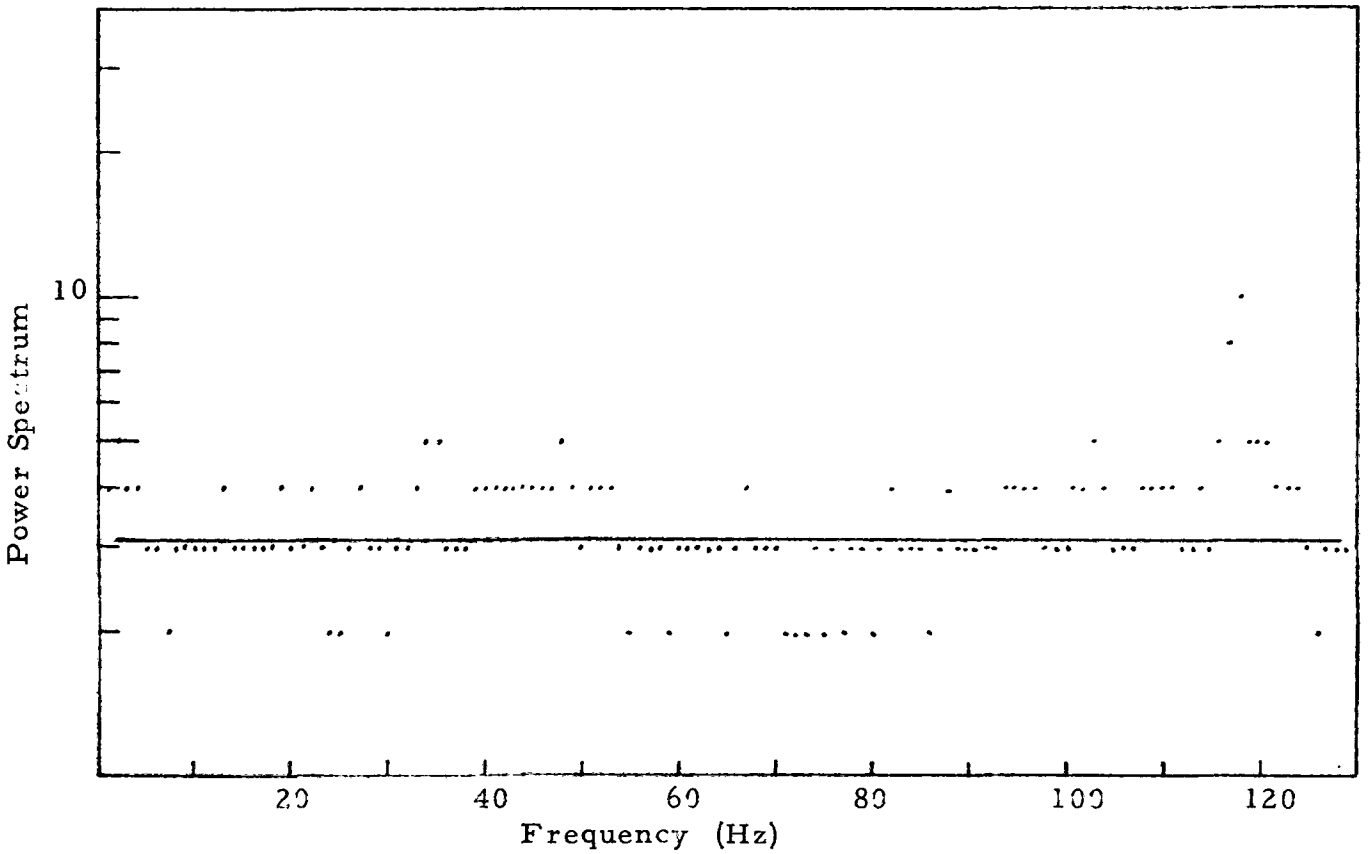

Figure C-13. Power Spectrum for Background Run #65.

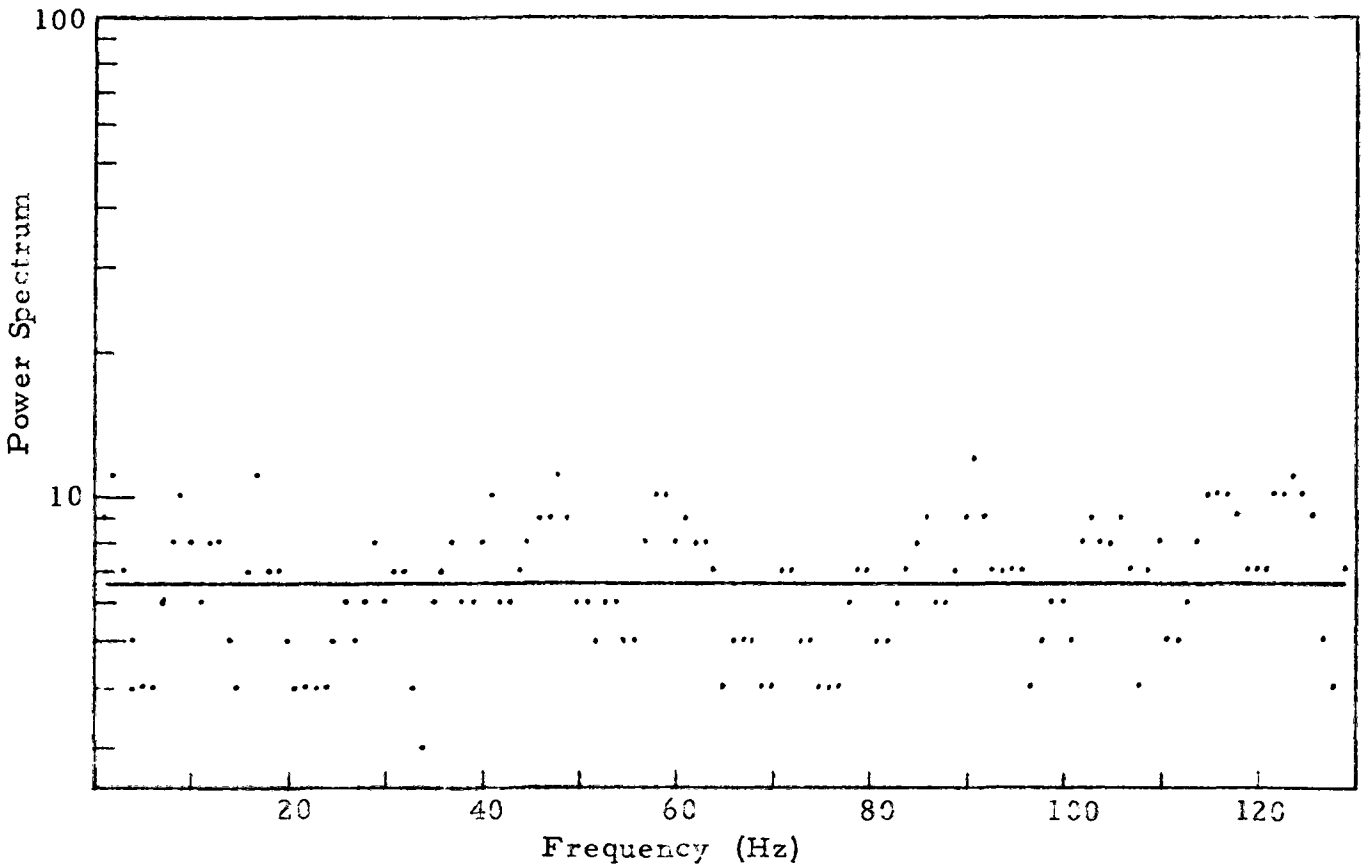

Figure C-14. Power Spectrum for Background Run #68.

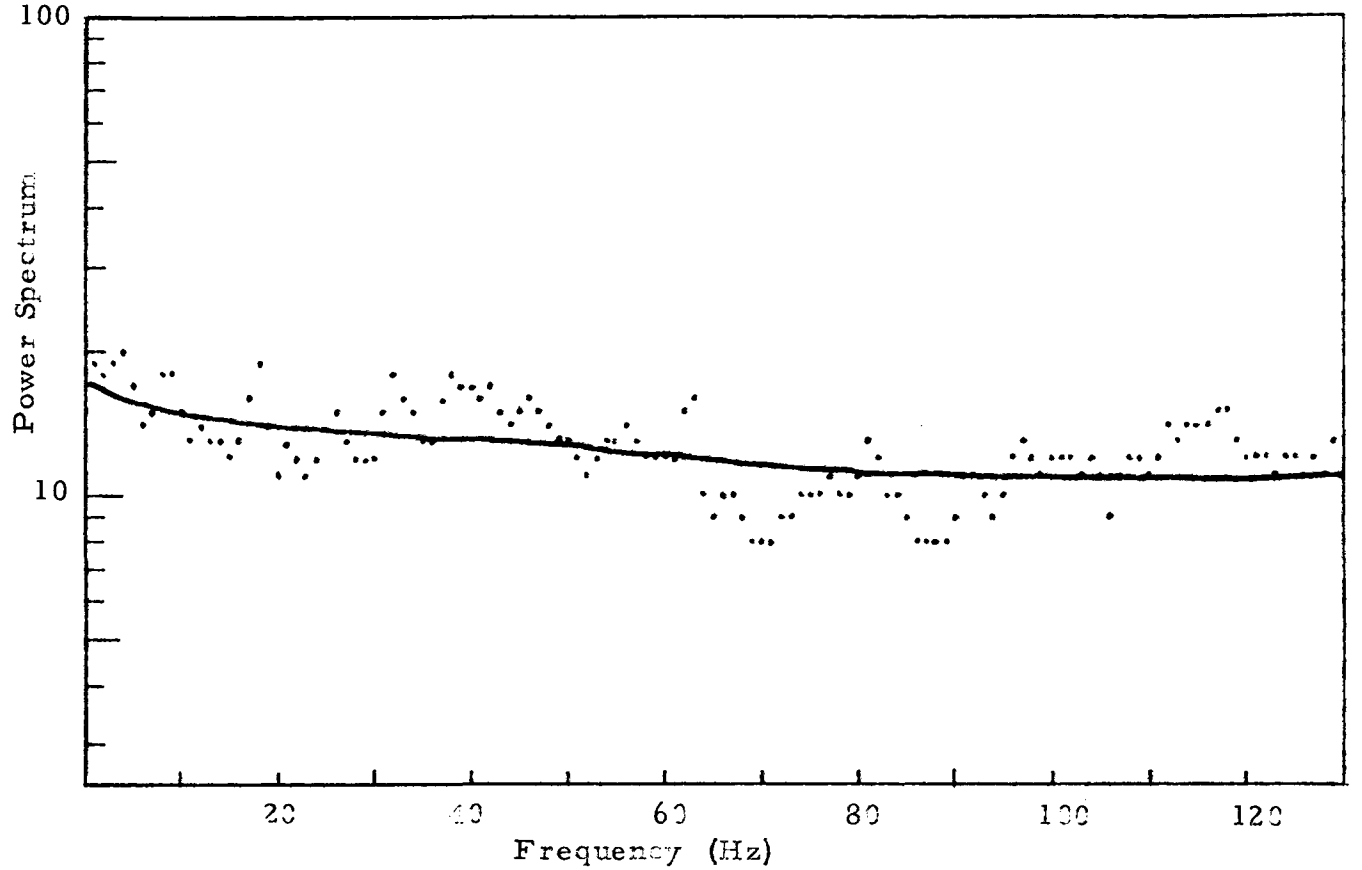

Figure C-15. Power Spectrum for Background Run #72.

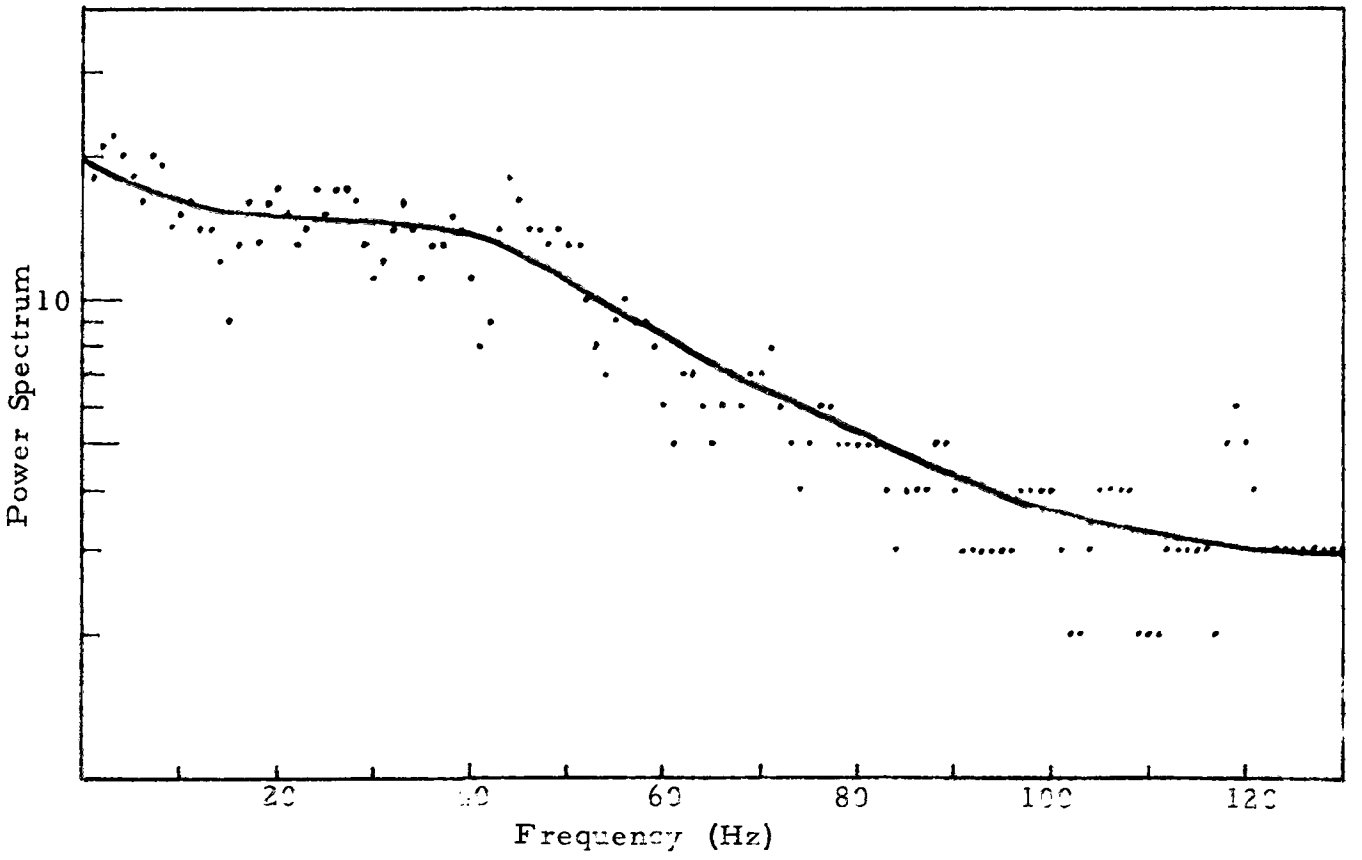

Figure C-16. Power Spectrum for Background Run #73.

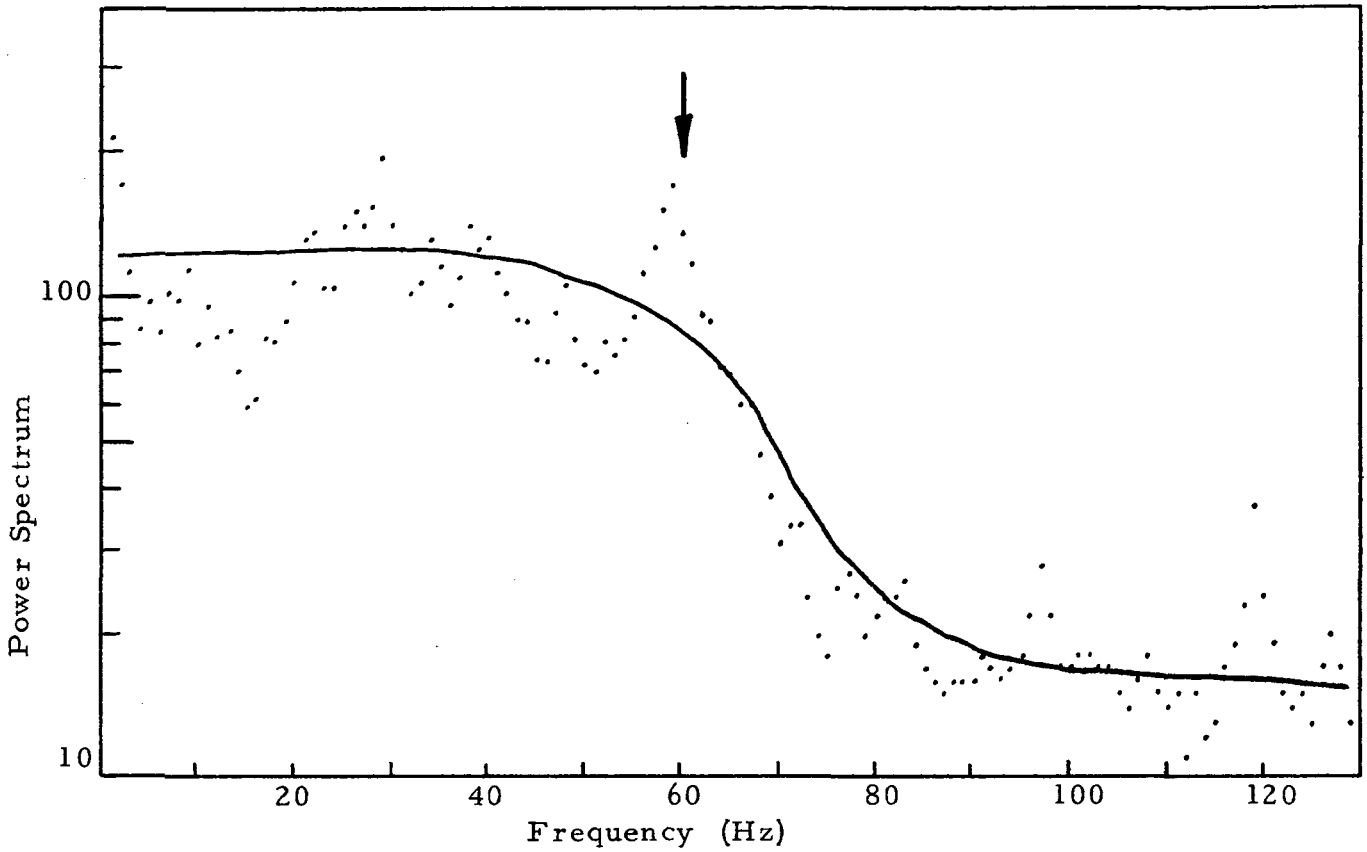

Figure C-17. Power Spectrum for Scintillation Run #4.

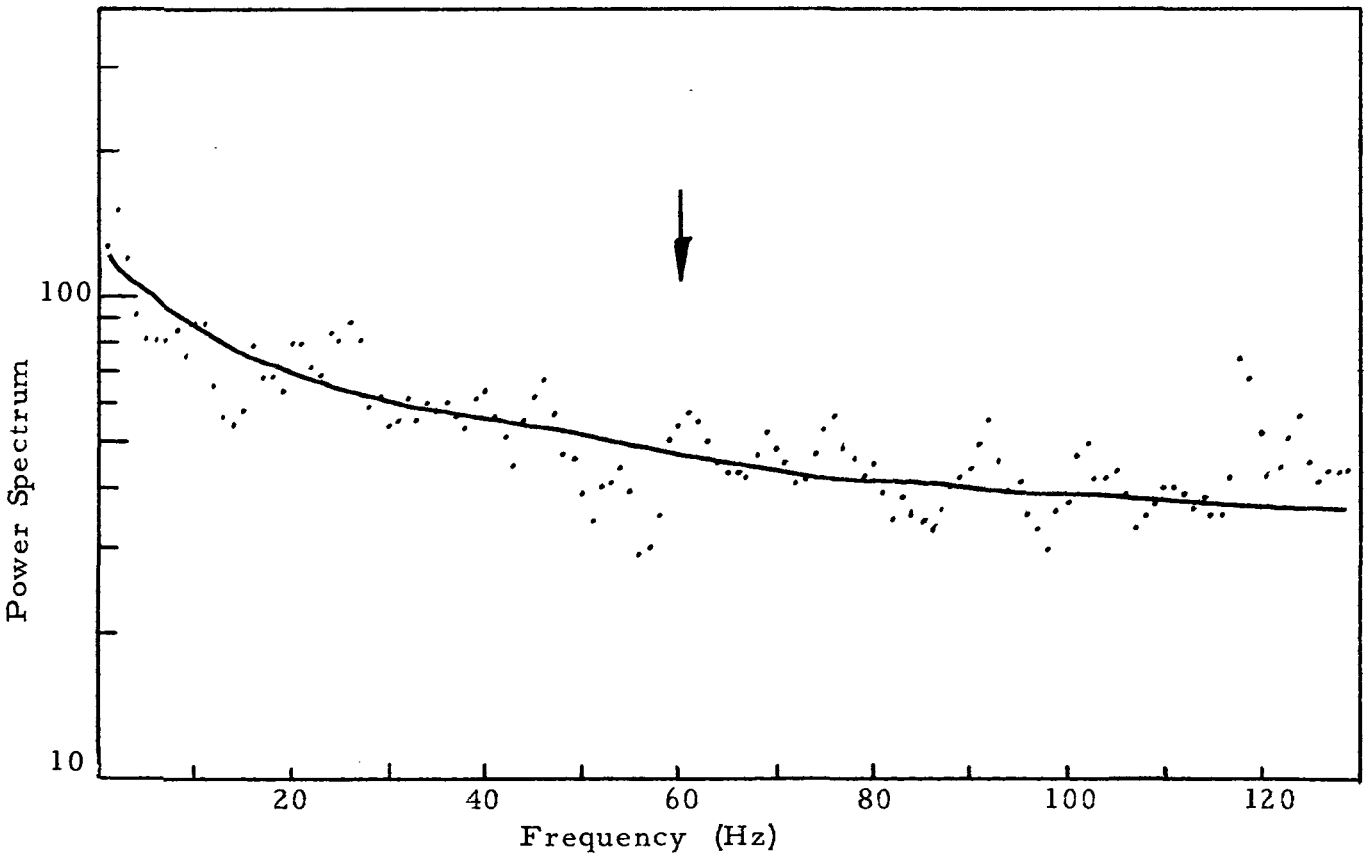

Figure C-18. Power Spectrum for Scintillation Run #27.

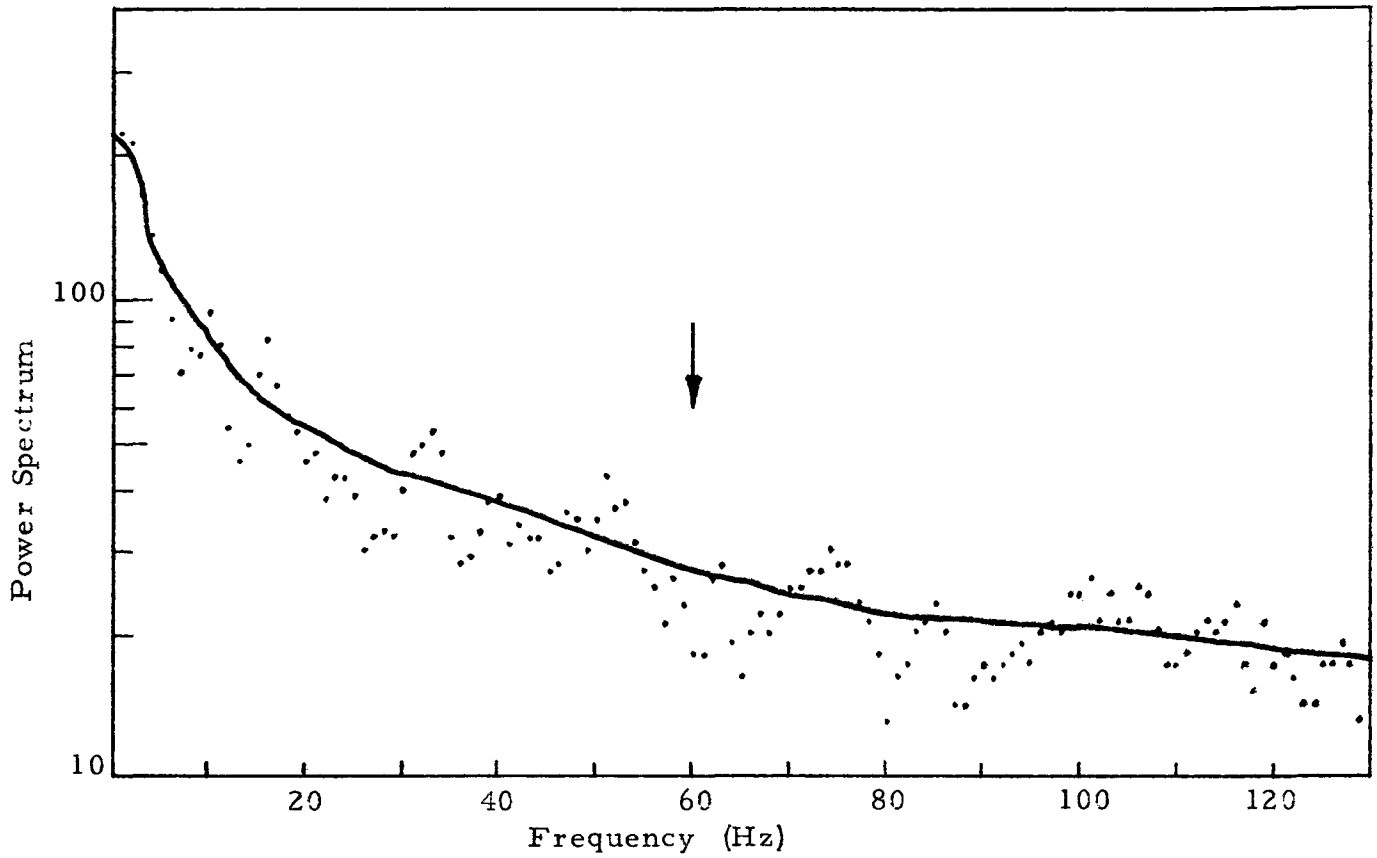

Figure C-19. Power Spectrum for Scintillation Run #3.

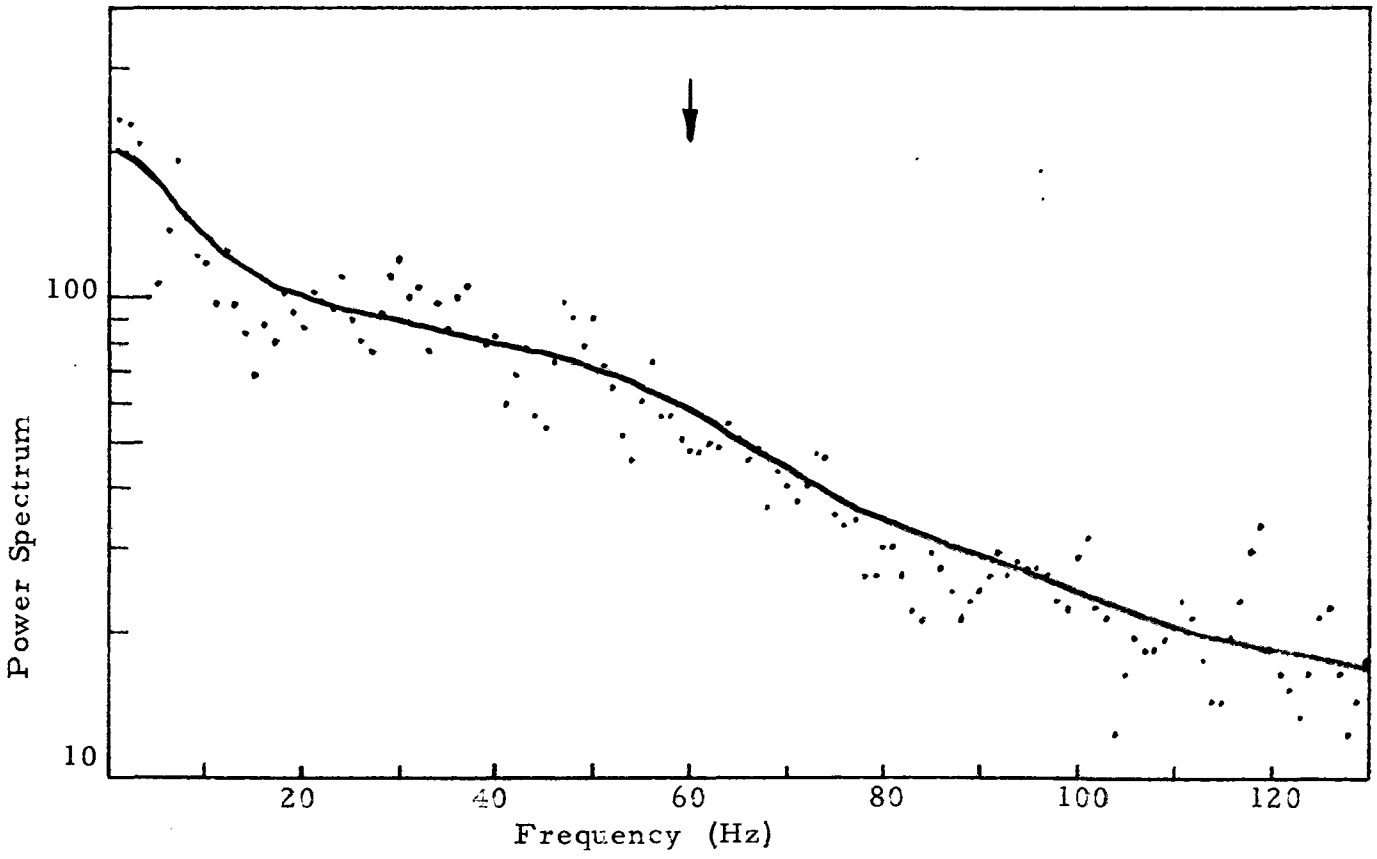

Figure C-20. Power Spectrum for Scintillation Run #14.

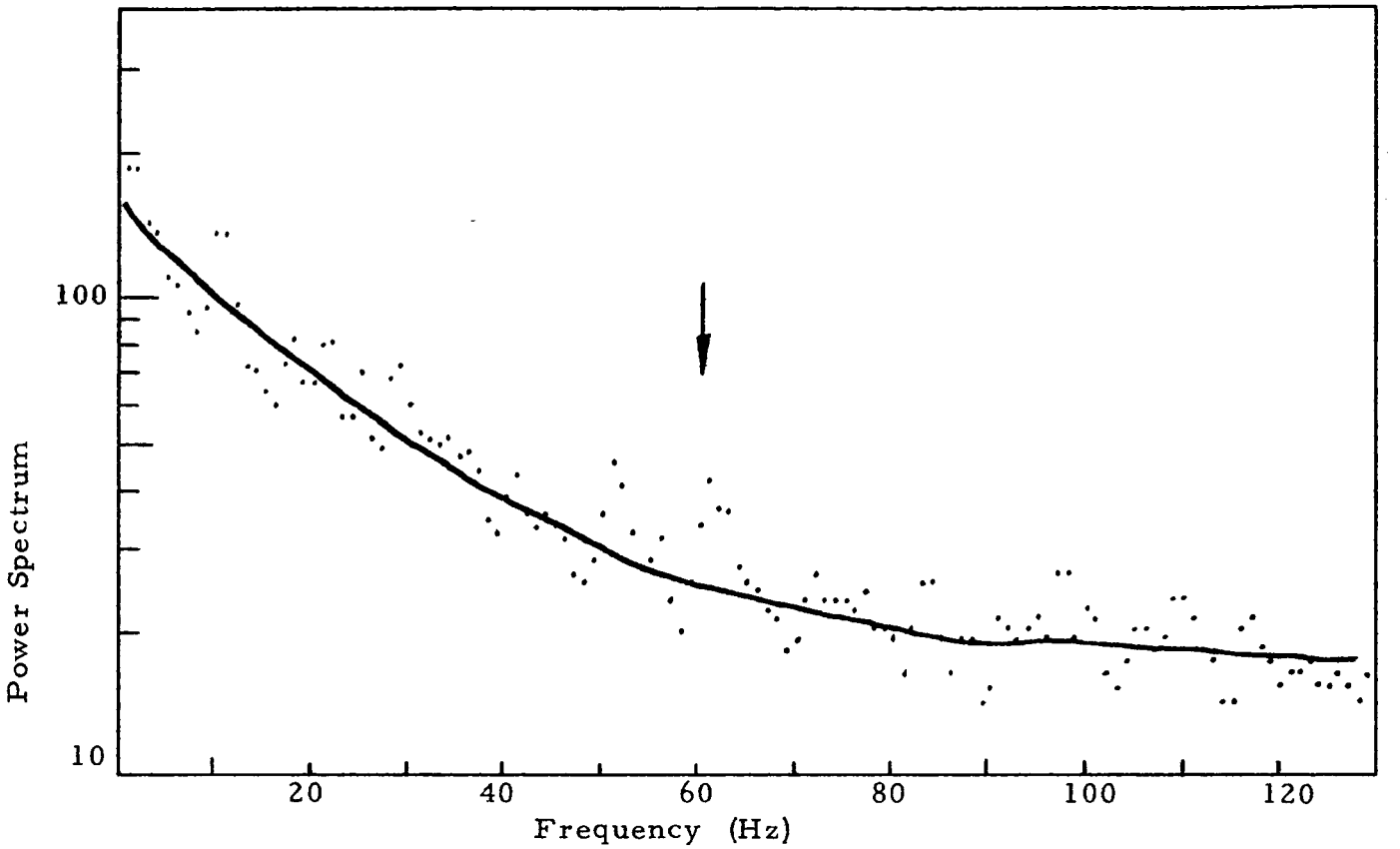

Figure C-21. Power Spectrum for Scintillation Run #18.

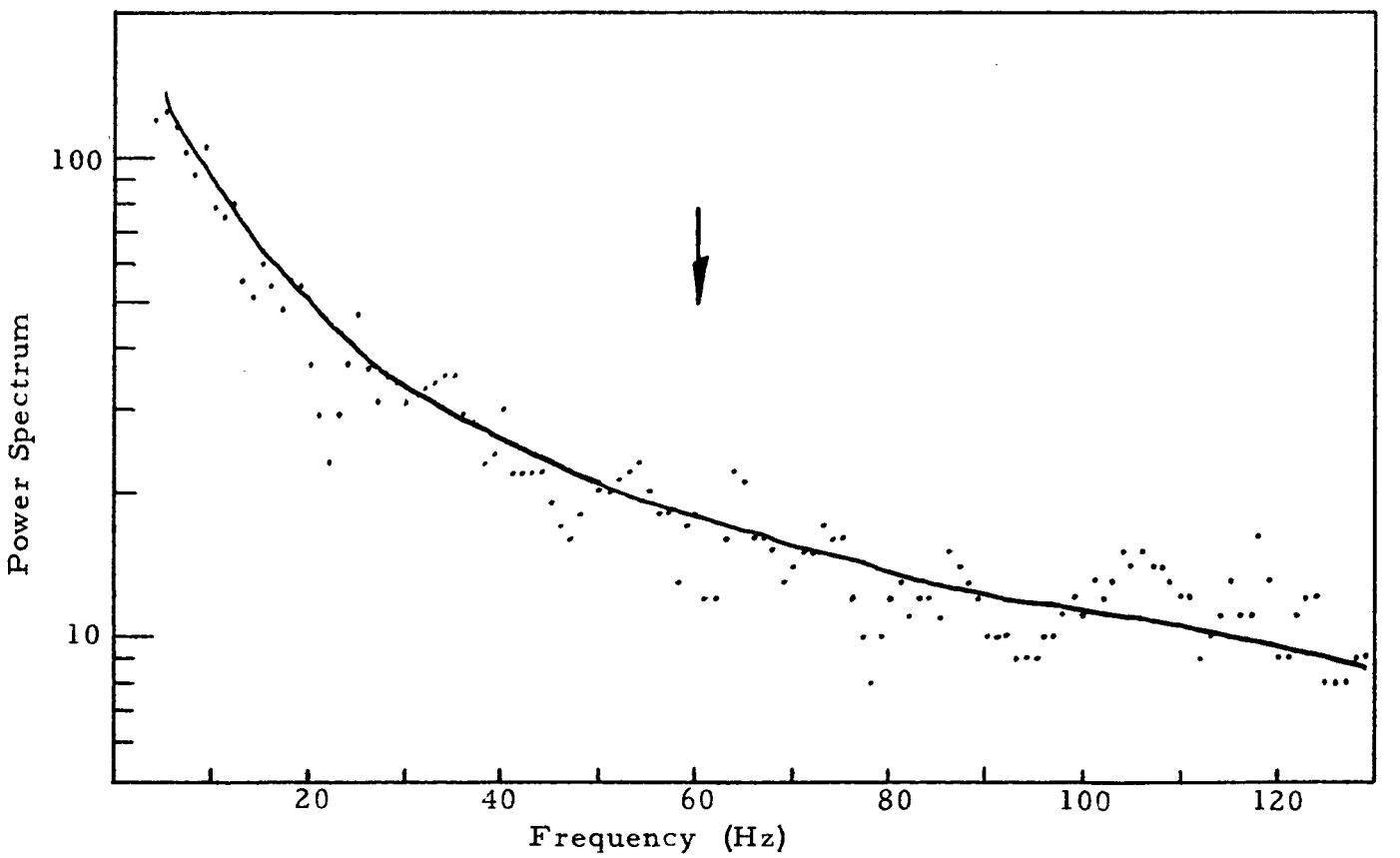

Figure C-22. Power Spectrum for Scintillation Run #19.

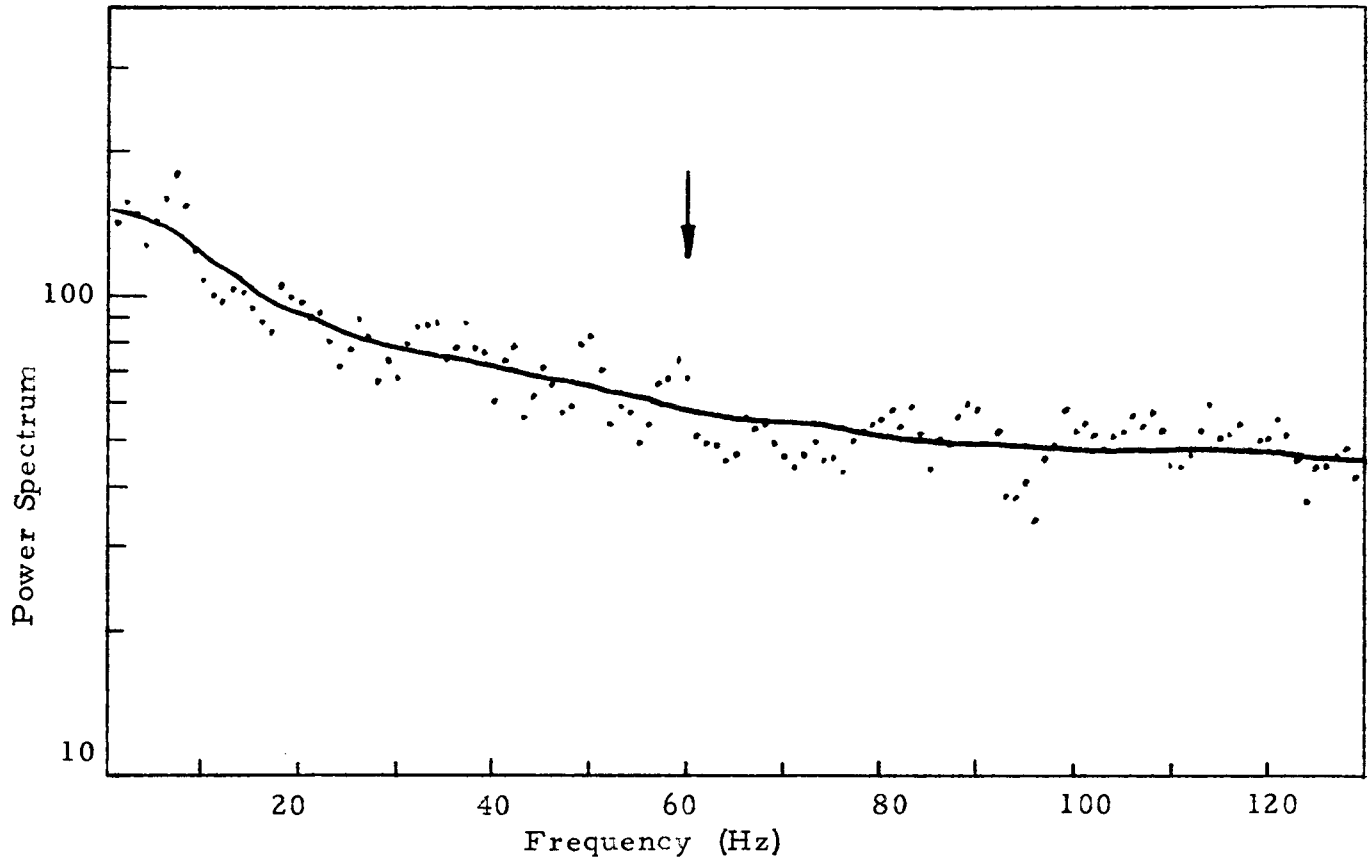

Figure C-23. Power Spectrum for Scintillation Run #54.

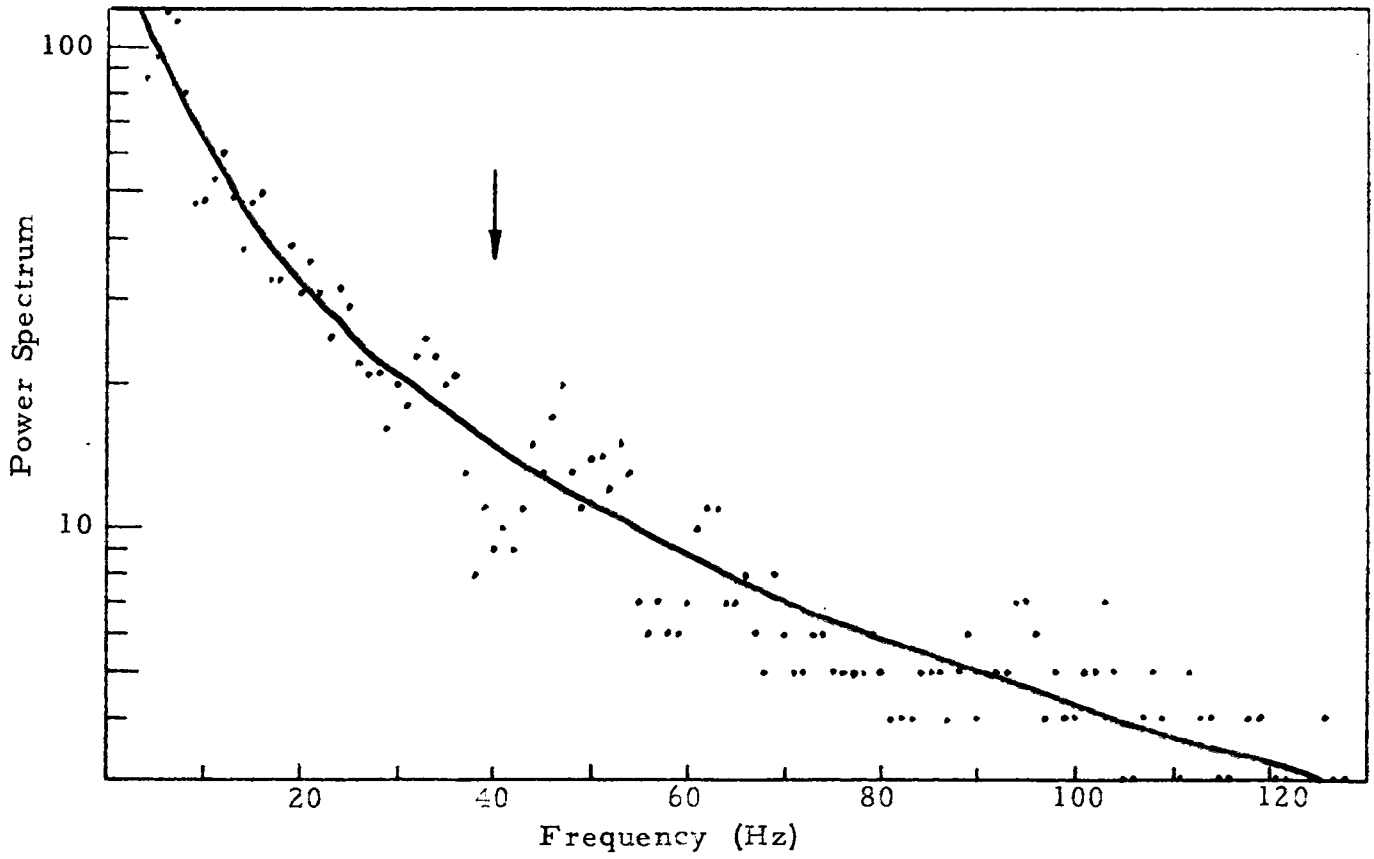

Figure C-24. Power Spectrum for Scintillation Run #33.

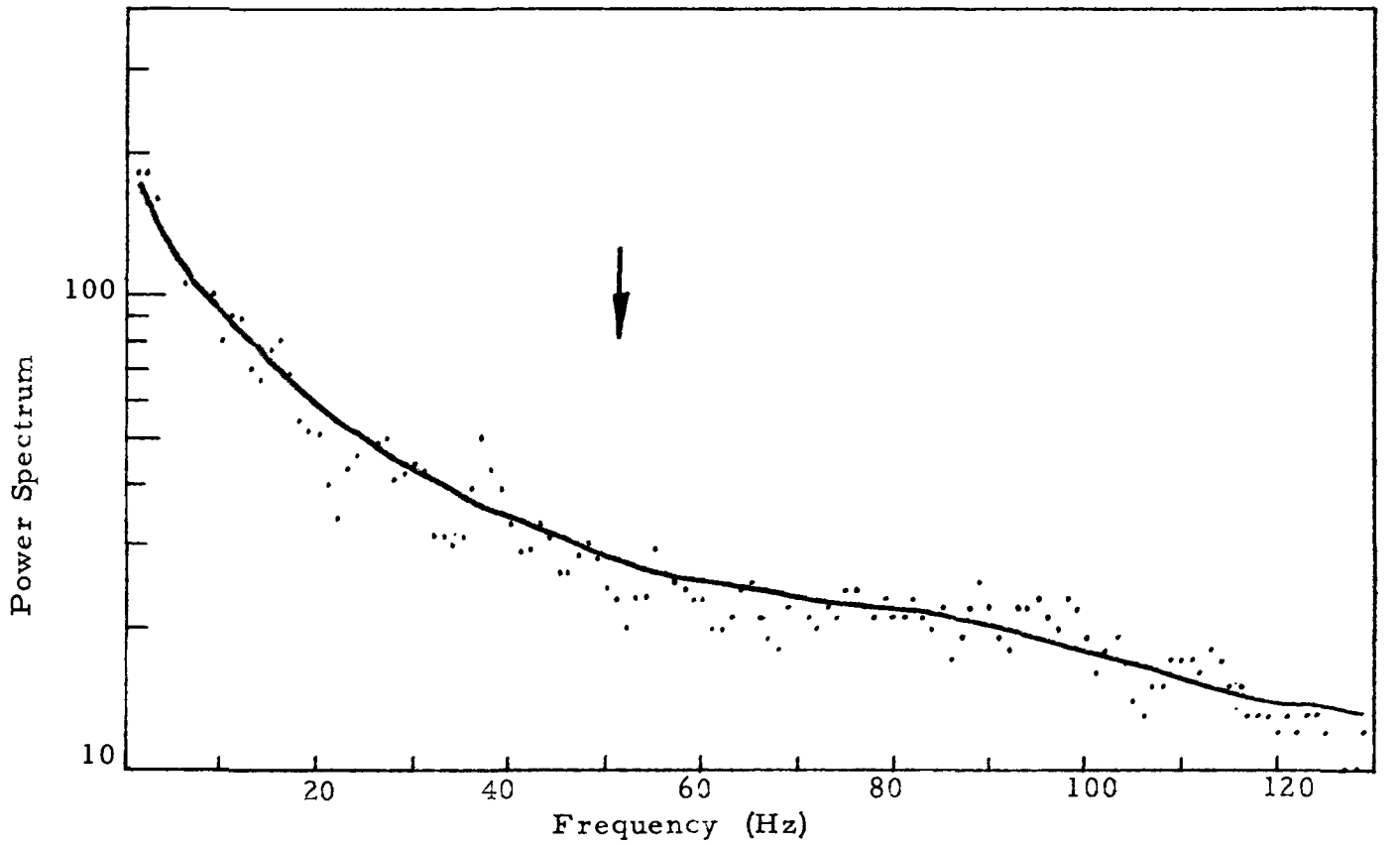

Figure C-25. Power Spectrum for Scintillation Run #48.

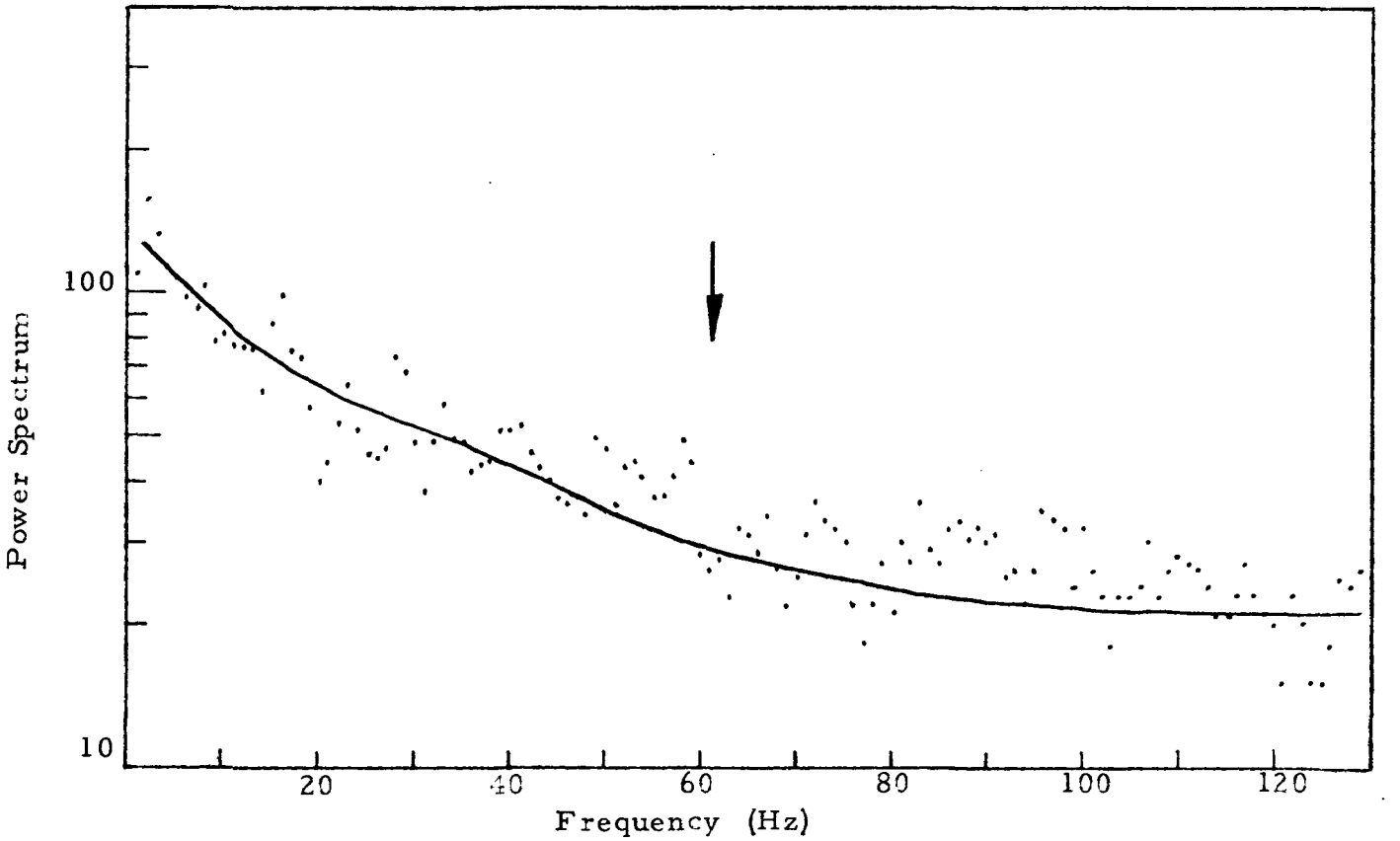

Figure C-26. Power Spectrum for Scintillation Run #58.

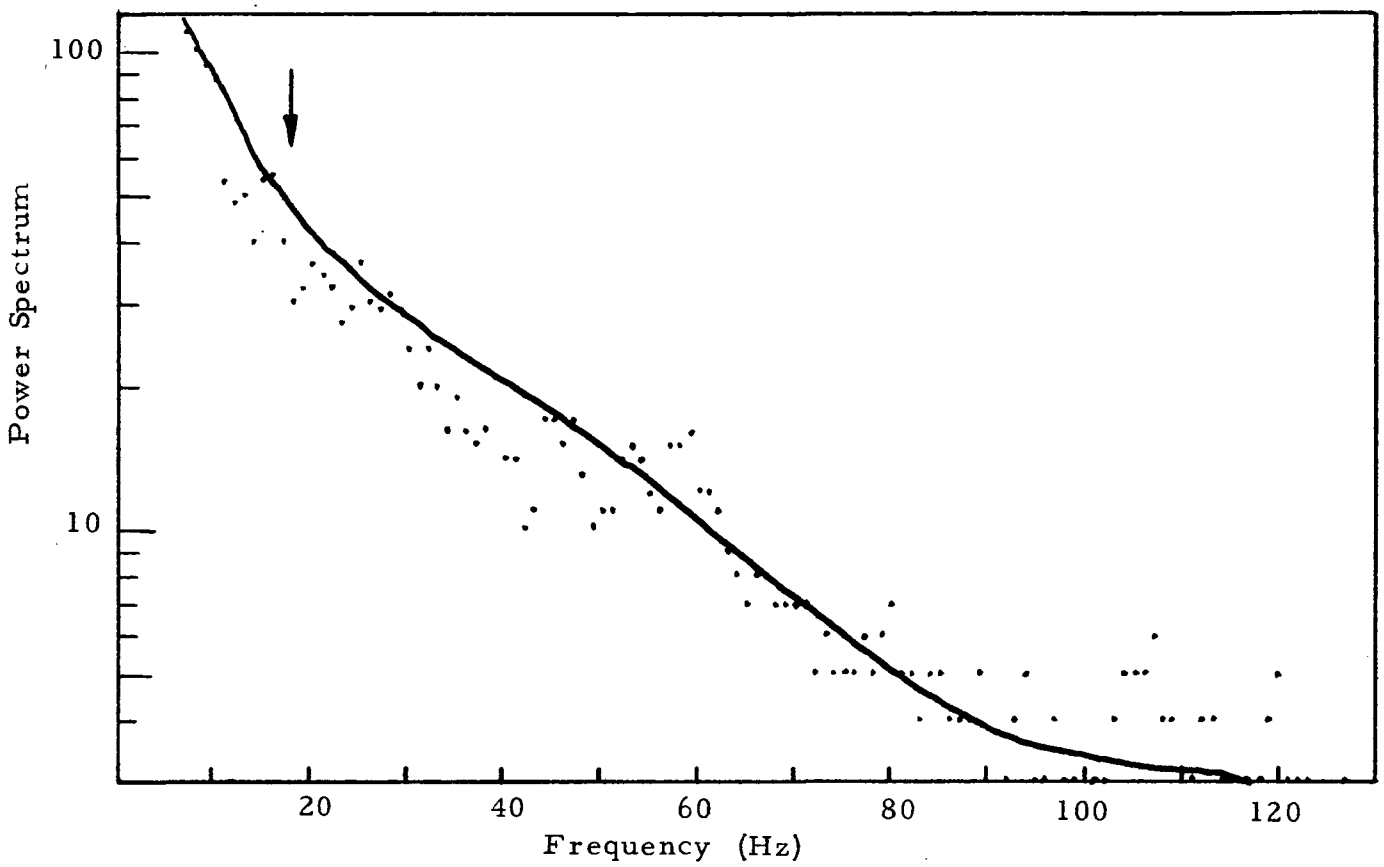

Figure C-27. Power Spectrum for Scintillation Run #10.

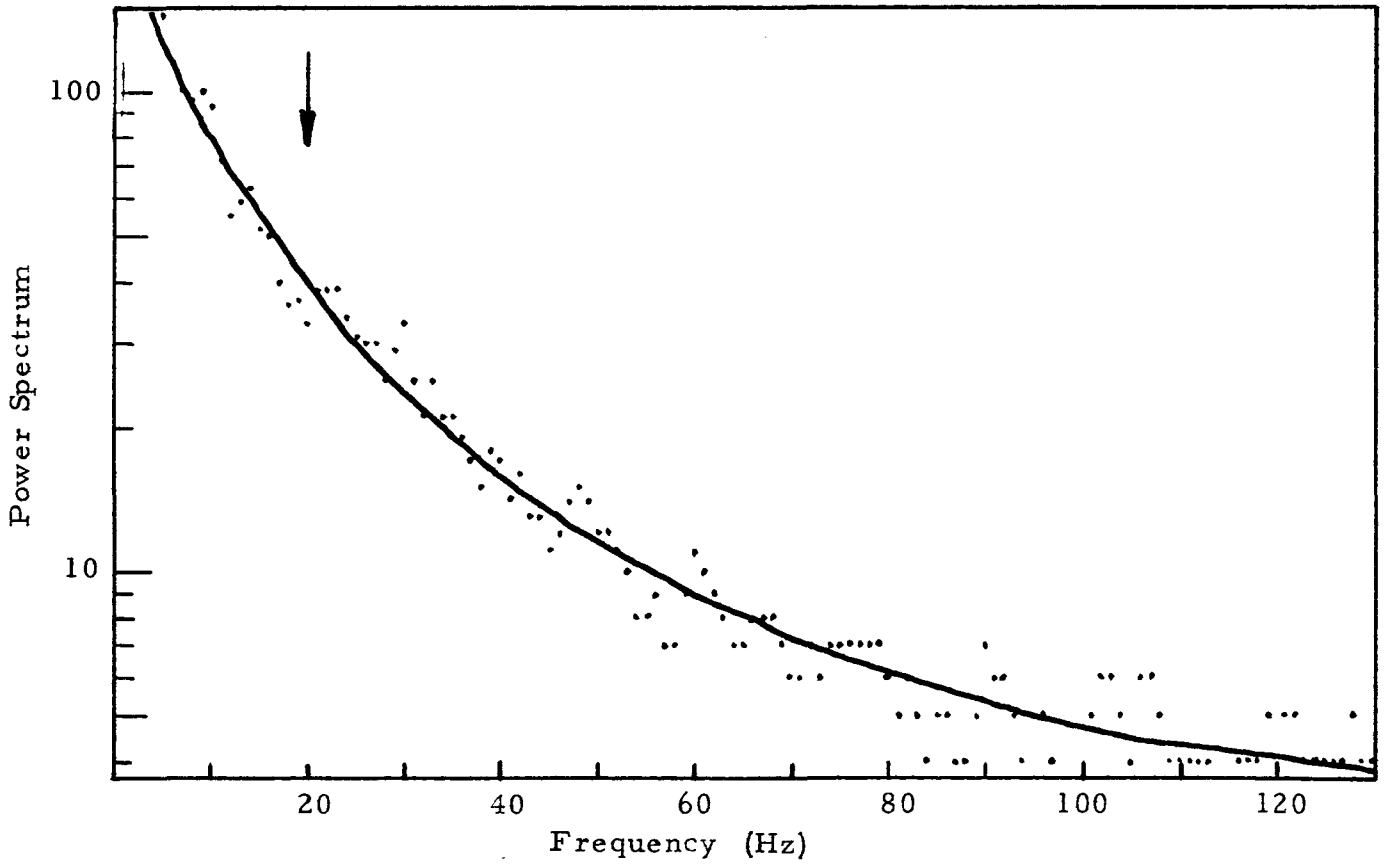

Figure C-28. Power Spectrum for Scintillation Run #46.

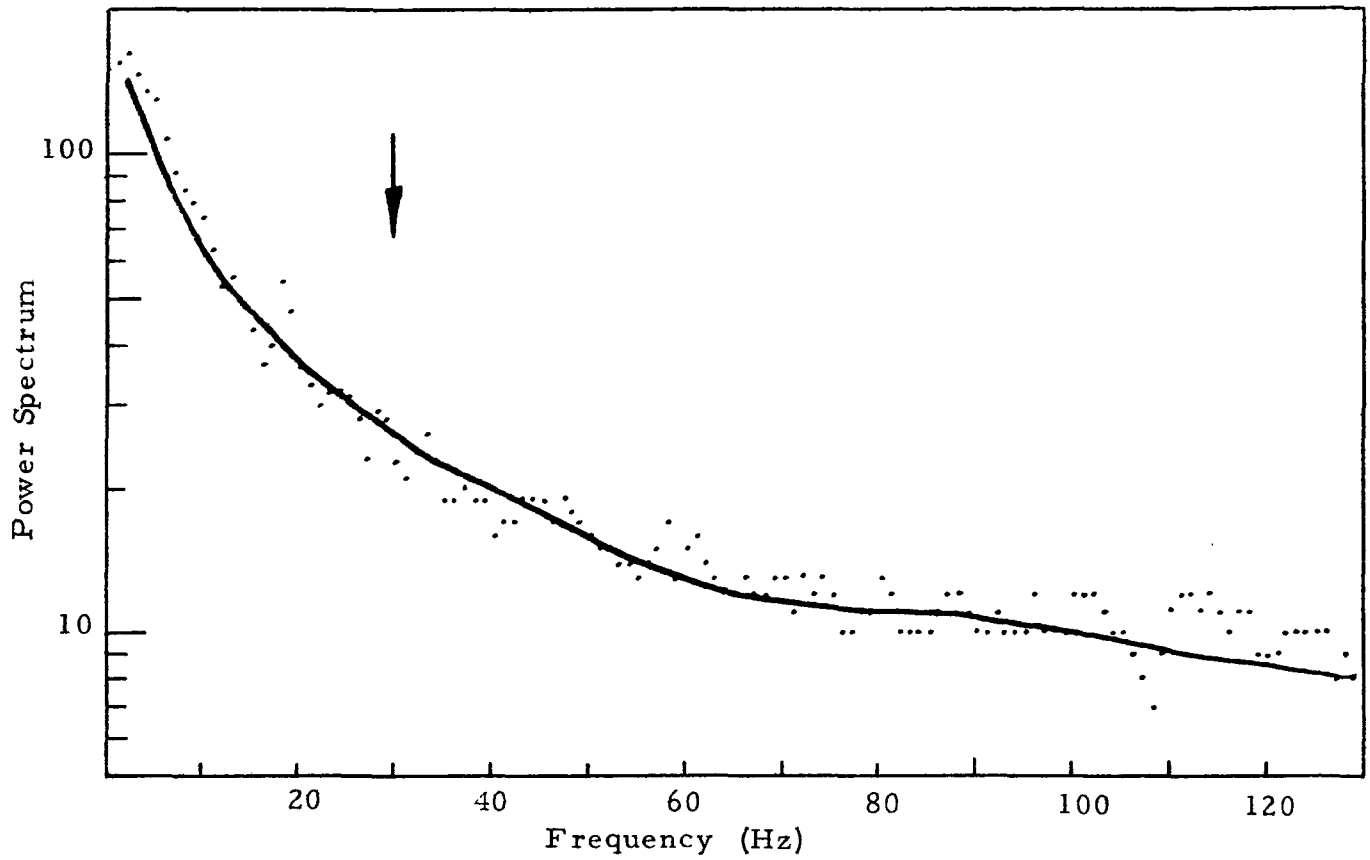

Figure C-29. Power Spectrum for Scintillation Run #62.

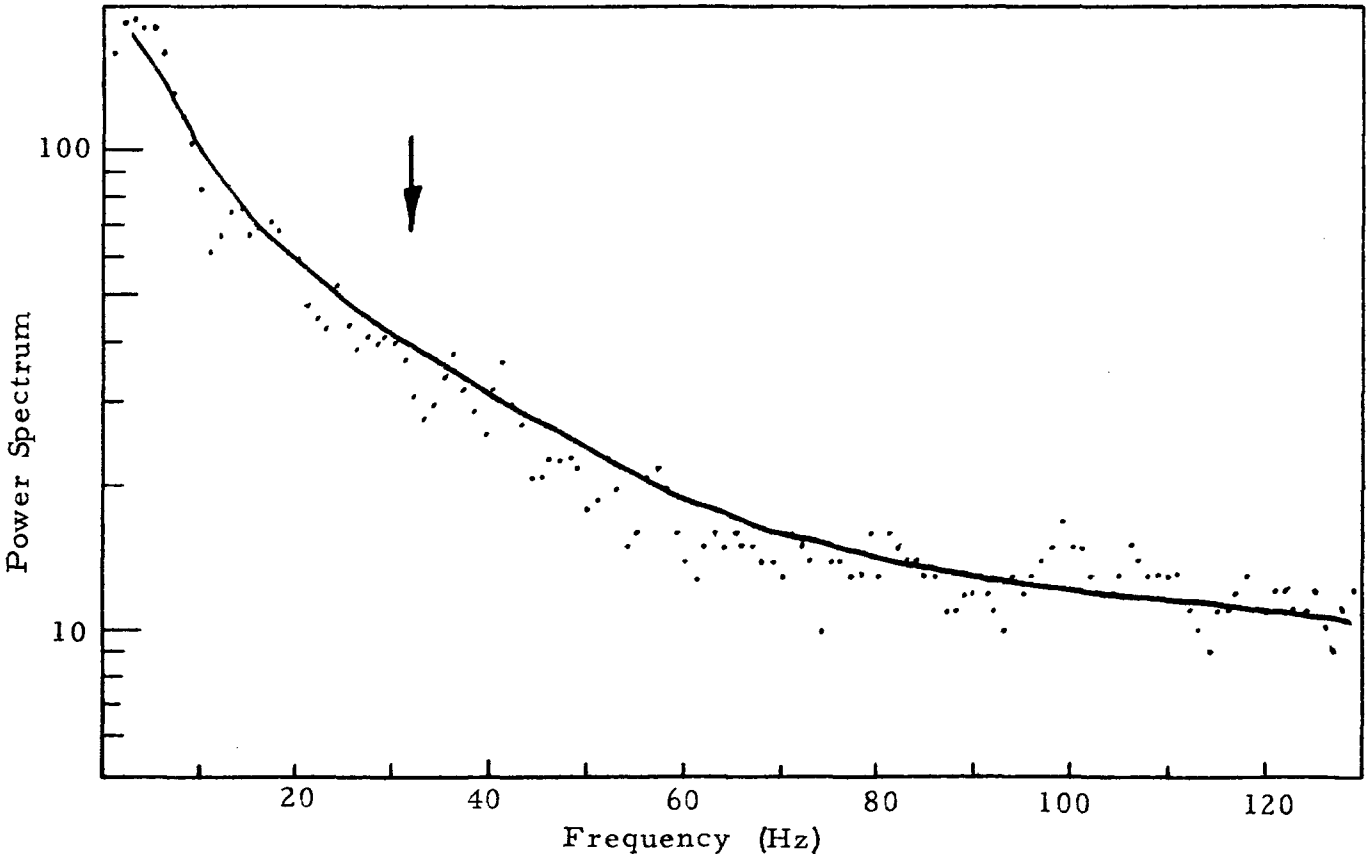

Figure C-30. Power Spectrum for Scintillation Run #64.

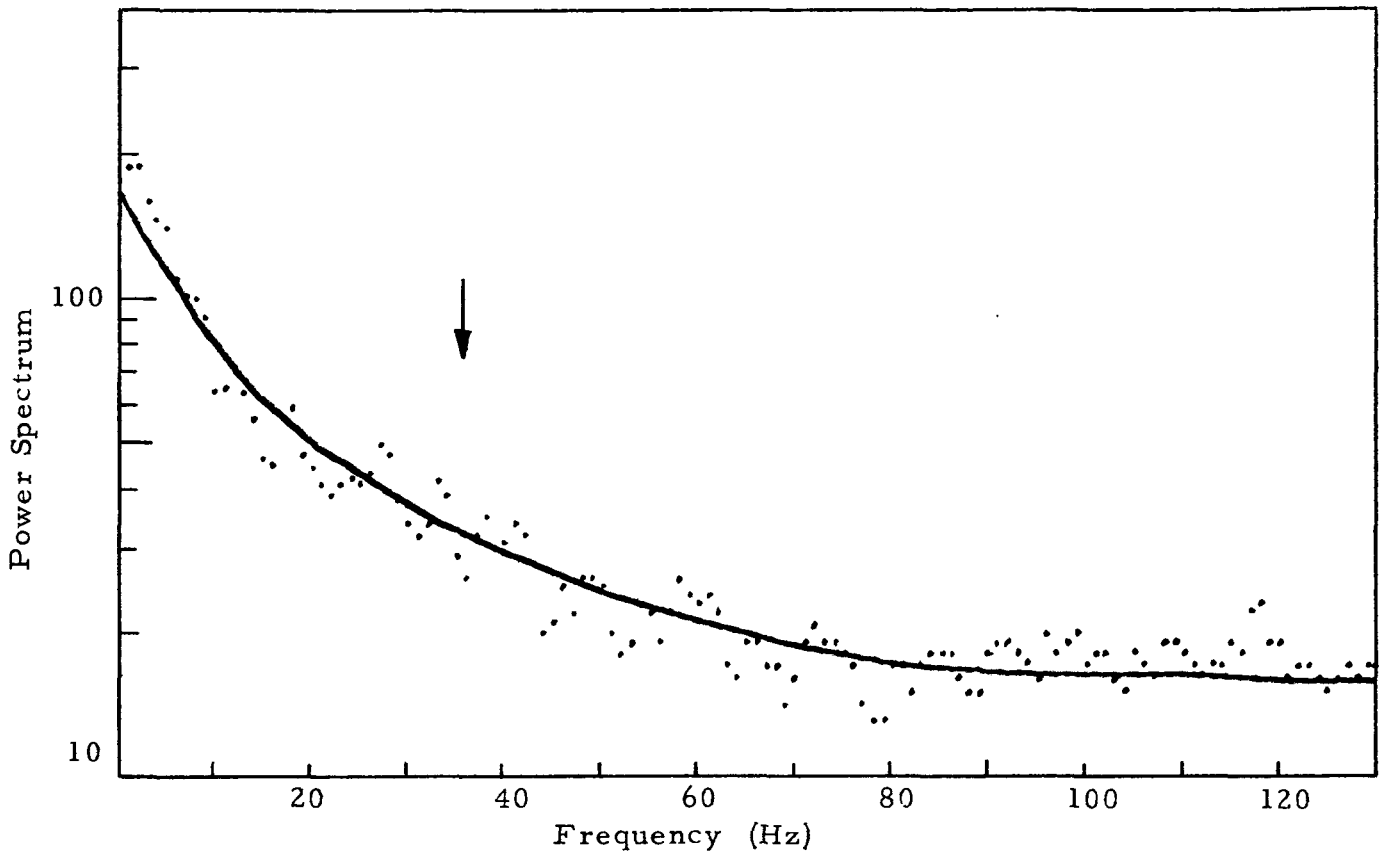

Figure C-31. Power Spectrum for Scintillation Run #69.

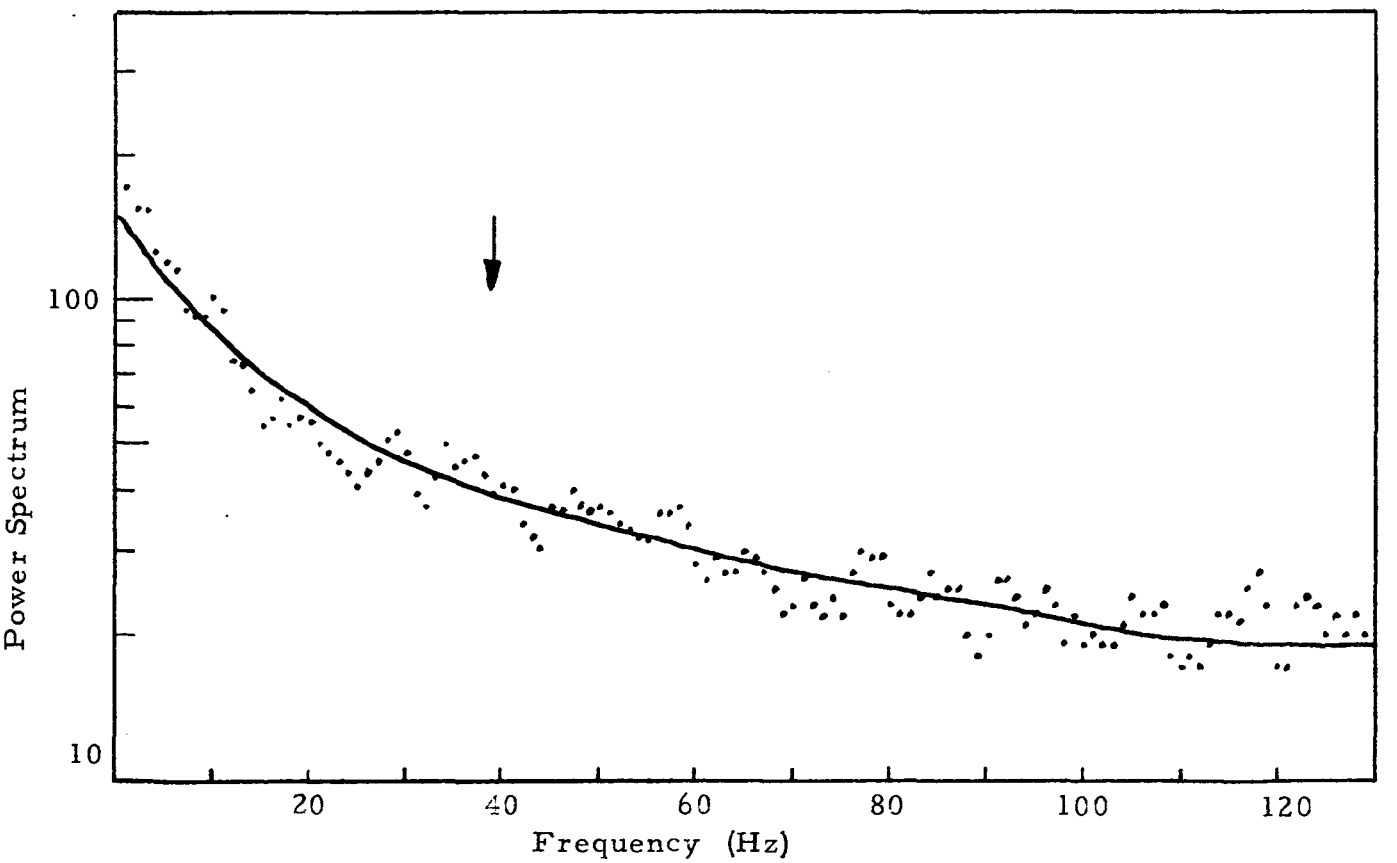

Figure C-32. Power Spectrum for Scintillation Run #71.